

DISSERTATION

DYNAMICS AND PARAMETERIZATION OF STABLY STRATIFIED TURBULENCE:
IMPLICATIONS FOR ESTIMATES OF MIXING IN GEOPHYSICAL FLOWS

Submitted by

Benjamin D. Mater

Department of Civil and Environmental Engineering

In partial fulfillment of the requirements

For the Degree of Doctor of Philosophy

Colorado State University

Fort Collins, Colorado

Summer 2014

Doctoral Committee:

Advisor: Subhas K. Venayagamoorthy

Brian P. Bledsoe

Lakshmi P. Dasi

Pierre Y. Julien

Copyright by Benjamin D. Mater 2014

All Rights Reserved

ABSTRACT

DYNAMICS AND PARAMETERIZATION OF STABLY STRATIFIED TURBULENCE: IMPLICATIONS FOR ESTIMATES OF MIXING IN GEOPHYSICAL FLOWS

This research focuses on the relationship between the observed length scales of overturns in stably-stratified shear-flow turbulence and the fundamental length scales constructed from dimensional analysis of basic physical quantities. In geophysical flows such as the ocean, overturns are relatively easy to observe while the basic quantities are not. As such, overturns provide a means of inferring basic quantities if the relationship between the observed and fundamental scales are known. In turn, inferred values of the basic quantities, namely the turbulent kinetic energy k , and the dissipation rate of turbulent kinetic energy ϵ , can be used to estimate diapycnal diffusivity (i.e. turbulent mixing). Most commonly, the observed Thorpe length scale, L_T , is assumed to scale linearly with the fundamental Ozmidov scale, $L_O = (\epsilon/N^3)^{1/2}$, so that inferred values of ϵ can be obtained and used to estimate mixing from the Osborn formulation for diapycnal diffusivity. A major goal of this research is to re-examine this and other possible scalings using dimensional analysis, direct numerical simulation (DNS), laboratory data, and field observations.

The preliminary chapters constitute a fresh approach at dimensional analysis that presents the fundamental length scales, time scales, and dimensionless parameters relevant to the problem. The relationship between L_T and the fundamental length scales is then examined for the simple case of homogeneously stratified turbulence (without shear) using DNS. A key finding is that the common practice of inferring ϵ from $L_T \sim L_O$, is valid at the transition between a buoyancy-dominated regime and an inertia-dominated regime where the time scale of the buoyancy oscillations, N^{-1} , roughly matches that of the inertial motions, $T_L = k/\epsilon$. Regime definition is made possible using a non-dimensional buoyancy strength parameter $NT_L = Nk/\epsilon$.

Next, the problem is generalized to consider mean shear, and thus, a shear strength parameter, $ST_L = Sk/\epsilon$, and the gradient Richardson number, $Ri = N^2/S^2$, are considered along with NT_L to define three regimes available to high Reynolds number stratified shear-flow turbulence: a buoyancy-dominated regime ($NT_L \gtrsim 1.7$, $Ri \gtrsim 0.25$), a shear-dominated regime ($ST_L \gtrsim 3.3$, $Ri \lesssim 0.25$), and an inertia-dominated regime ($NT_L \lesssim 1.7$, $ST_L \lesssim 3.3$). The regimes constitute a multi-dimensional parameter space which elucidates the independent influences that shear and stratification have on the turbulence. Using a large database of DNS and laboratory results, overturns are shown to have unique scalings in the various regimes. Specifically, $L_T \sim k^{1/2}N^{-1}$, $L_T \sim k^{1/2}S^{-1}$, and $L_T \sim k^{3/2}\epsilon^{-1}$ in the buoyancy-, shear-, and inertia-dominated regimes, respectively. $L_T \sim L_O$ is found only for the case of $NT_L = O(10^0)$ and $ST_L \lesssim 3.3$, or for $NT_L = O(10^0)$, $ST_L \approx 3.3$ and $Ri \approx 0.25$ when shear is present. In all three regimes, L_T is found to generally indicate k rather than ϵ . An alternative parameterization of turbulent diffusivity is developed based on inferred values of k with a practical eye toward field applications. When tested with DNS and laboratory data, the new model is shown to be more accurate than estimates based on inferred values of ϵ .

The multi-parameter framework is broadened with consideration for the turbulent Reynolds number, Re_L , thus allowing for an evaluation of existing parameterizations of diapycnal mixing efficiency, R_f^* . Select DNS and laboratory data sets are used in the analysis. A key finding is that descriptions of R_f^* based on a single-parameter are generally insufficient. It is found that Ri is an accurate parameter in the shear-dominated regime but fails in the inertia-dominated regime where turbulence is generated by external forcing (rather than mean shear). In contrast, the turbulent Froude number, $Fr_T = (L_O/L_T)^{2/3}$, is an accurate parameter in the inertia-dominated regime but loses accuracy in the shear-dominated regime. Neither Ri or Fr_T sufficiently describe R_f^* in the buoyancy-dominated regime where additional consideration for Re_L is needed. Another key finding is that the popular buoyancy Reynolds number, $Re_b = Re_L(NT_L)^{-2}$, is a particularly misleading parameter for describing

R_f^* because it fails to distinguish between (i) a low-Reynolds number, weakly stratified regime of low efficiency (low Re_L , low NT_L , low R_f^*) typical of DNS flows and (ii) a high-Reynolds number, strongly stratified regime of high efficiency (high Re_L , high NT_L , high R_f^*) typical of geophysical flows.

Finally, oceanic observations from Luzon Strait and the Brazil Basin are featured to examine the relationship between L_T and L_O in geophysical flows where turbulence is driven by overturns that are very large by open ocean standards. L_T is found to increase with respect to L_O as a function of the normalized overturn size $\widehat{L}_T = L_T N^{1/2} \nu^{-1/2}$. When large overturns are present, dissipation rates inferred from $L_T \sim L_O$ are generally larger than measured values on average. The overestimation is quantified over a spring tidal period at Luzon Strait where depth- and time-integration of inferred and measured values show that inferred energy dissipation is four times too large.

ACKNOWLEDGEMENTS

I sincerely thank my advisor, Dr. Karan Venayagamoorthy for his supportive and indefatigable enthusiasm throughout my PhD studies at CSU. His encouragement, imparted knowledge, and the life he brings to research have made this dissertation possible and have enriched my experience at CSU beyond expectation. Moreover, I am grateful for Karan's willingness to promote and 'go to bat' for his students — a quality that has allowed for my funding through the U.S. Office of Naval Research as well as various opportunities to travel around the world to experience science and scientists beyond the CSU campus.

I deeply thank Dr. Brian Bledsoe for his advice and mentorship that largely led to me choosing to pursue my doctorate at CSU in the first place. Thanks also to Dr. Pierre Julien for his insightful suggestions and exceptional courses. Also, I thank Dr. Prasad Dasi for his helpful comments, his willingness to serve as an out-of-department committee member, and his contributions to the ideas of this dissertation regarding unstratified turbulence. Thanks also to Drs. Jim Moum and Lou St. Laurent for their oceanographic insights.

I thank my officemates with special thanks to my fellow PhD students, Dr. Farid Karimpour and Jordan Wilson. Our various conversations — be they scientific, philosophical, or otherwise — have fostered a camaraderie and friendship I will always cherish. Thanks also to my friend and former officemate, Simon Schaad, who contributed greatly to the DNS work shown in this dissertation and with whom I have had many inspiring conversations.

Thanks also to my dog Wendell for his loyal companionship, kind heartedness, and constant reminders of the health benefits of getting out from behind a desk.

Of course, thanks for the loving support of my family. I especially thank my parents Bruce and Betty Mater for their encouragement, instilled ethics, imparted wisdom, and love.

Most importantly, I thank my partner and fiancée Lindsey Christensen for her commitment, encouragement and support when I need it most, her willingness to move to Colorado, her sacrifices, and her unconditional love.

TABLE OF CONTENTS

ABSTRACT	ii
ACKNOWLEDGMENTS	v
LIST OF TABLES	xi
LIST OF FIGURES	xii
1 Introduction	1
1.1 Motivation	1
1.2 Objectives	4
1.3 Dissertation Layout	5
2 Governing Equations	7
2.1 Conservation of Mass	7
2.2 Conservation of Momentum	8
2.3 Conservation of Energy	9
2.4 Boussinesq Approximations	10
2.5 Reynolds Decomposition: The Turbulence Framework	12
2.6 Turbulent Kinetic Energy Budget	14
2.7 Turbulent Potential Energy Budget	16
3 Literature Review	19
3.1 Length and Time Scales of Turbulence	19
3.1.1 The Energy Cascade	19
3.1.2 Unforced Turbulence	20
3.1.2.1 Kolmogorov’s Hypotheses	20
3.1.2.2 Taylor Microscale	23
3.1.3 Scales of Shear-flow Turbulence	24
3.1.4 Scales of Stratified Turbulence	26
3.1.5 Scales of the Turbulent Scalar Field	27
3.2 Dimensionless Parameters	29
3.2.1 Turbulent Reynolds Number	29
3.2.2 Turbulent Shear Parameter	30

3.2.3	Turbulent Froude Number	31
3.2.4	Gradient Richardson Number	33
3.2.5	Buoyancy Reynolds Number	35
3.2.6	Shear Reynolds Number	37
3.3	Mixing	38
3.3.1	Relevance to Numerical Modeling	38
3.3.2	Diapycnal Mixing	39
3.3.3	Mixing Efficiency	41
3.4	Parameterizations of Mixing	42
3.4.1	Oceanic Observations	43
3.4.2	Experimental and Numerical Studies	45
3.5	Overturning	49
3.6	Basis for Study	50
4	Dimensional Analysis	52
4.1	Unstratified Shear-Flow Turbulence	52
4.1.1	Isotropic Scales Revisited	53
4.1.1.1	Classical large scales, $L_{k\epsilon} = k^{3/2}/\epsilon$ & $T_L = k/\epsilon$	53
4.1.1.2	Classical small scales, $\eta = (\nu^3/\epsilon)^{1/4}$ & $T_\eta = (\nu/\epsilon)^{1/2}$	54
4.1.1.3	New sub-Kolmogorov scales, $L_{k\nu} = (\nu^2/k)^{1/2}$ & $T_{k\nu} = \nu/k$	55
4.1.2	Shear Scales Revisited	56
4.1.2.1	Large shear scales, $L_{kS} = (k/S^2)^{1/2}$ & S^{-1}	56
4.1.2.2	Corrsin scale, $L_C = (\epsilon/S^3)^{1/2}$	56
4.1.2.3	Small shear scale, $L_{\nu S} = (\nu/S)^{1/2}$	57
4.1.3	Dimensionless Parameters	57
4.2	Stratified (shear-free) Turbulence	59
4.2.1	Buoyancy Scales Revisited	59
4.2.1.1	Large buoyancy scales, $L_{kN} = (k/N^2)^{1/2}$ & N^{-1}	59
4.2.1.2	Ozmidov scale, $L_O = (\epsilon/N^3)^{1/2}$	60
4.2.1.3	Small buoyancy scale, $L_{\nu N} = (\nu/N)^{1/2}$	60
4.2.2	Dimensionless Parameters	61
4.3	Summary	63
5	Overturning in Stably Stratified Turbulence	64
5.1	Introduction	64

5.2	Relevant Length and Time Scales	66
5.2.1	Thorpe Length Scale	66
5.2.2	Fundamental Scales	67
5.3	Numerical Approach	70
5.3.1	Set-up	70
5.3.2	Parameter Values	71
5.3.3	Thorpe Sorting	72
5.4	DNS Results	75
5.4.1	Thorpe vs. Ellison Scales	75
5.4.2	Thorpe vs. Ozmidov Scales	75
5.4.3	Thorpe vs. Turbulent Kinetic Energy Scale	76
5.4.4	Thorpe vs. Isotropic Large Scale	77
5.5	Discussion	78
5.5.1	Physical Interpretations	78
5.5.2	Implications	79
5.5.3	Comparisons with Previous Studies	82
5.6	Conclusions	84
6	A Unifying Framework	87
6.1	Introduction	87
6.2	Dimensional Analysis	91
6.2.1	A Conceptual Framework	91
6.2.2	Relevant Length Scales	94
6.2.3	A Note on Anisotropy	98
6.2.4	Observed Length Scales	99
6.3	Data Sources	99
6.4	Observed vs. Fundamental Length Scales	104
6.5	Discussion	105
6.5.1	Relevancy to Conceptual Interpretations of Length Scales	105
6.5.2	Relevancy to Oceanic Measurements	109
6.6	Conclusions	117
7	Parameterizations of Mixing Efficiency	119
7.1	Introduction	119
7.2	A Unifying Framework	121

7.3	Ambiguities of Single-Parameter Approaches	124
7.3.1	Ri -based Approaches	124
7.3.1.1	$Ri < 0.25$	124
7.3.1.2	$Ri > 0.25$	126
7.3.2	Fr -based Approaches	127
7.3.2.1	$Fr_T > 1$	127
7.3.2.2	$Fr_T < 1$	129
7.3.3	Re_b -based Approaches	129
7.4	Relevance to Field Observations	132
7.5	Concluding Remarks	133
8	Oceanic Observations of Overturning and Dissipation	136
8.1	Introduction	136
8.2	Fundamentals of the Thorpe-Ozmidov relation	138
8.3	Data Sets	140
8.3.1	Luzon Strait (IWISE)	141
8.3.2	Brazil Basin (BBTRE)	143
8.3.3	North Atlantic (NATRE)	144
8.4	Methods	146
8.4.1	Thorpe scale calculations for turbulent patches	146
8.4.2	Temperature-salinity relationships	147
8.4.3	Calculation of buoyancy frequency	149
8.4.4	Estimation of dissipation	149
8.5	Direct comparisons	150
8.6	Mean profiles	159
8.7	Time integration: energy budgets	165
8.8	Conclusion	168
9	Summary & Conclusions	170
9.1	Summary of Investigation	170
9.2	Conclusions on Key Findings	171
9.3	Suggestions for Further Research	174
	References	176

Appendix A Length Scales of the Unstratified Boundary Layer	185
Appendix B Select Field Observations	191
B.1 IWISE M profiles (spring tidal period)	191
B.2 IWISE N2 profiles (spring tidal period)	193
B.3 BBTRE profiles	195
B.4 NATRE profiles	197
B.5 Additional figures	199

LIST OF TABLES

6.1	Summary of DNS and laboratory data sources	103
8.1	Patch-wise statistics for field data	150

LIST OF FIGURES

4.1	Schematic energy cascade for shear-flow	59
4.2	Schematic energy cascade for stratified shear-flow	62
5.1	Re_b - NT_L regime diagram for DNS results	72
5.2	Sample density profiles from DNS results	73
5.3	Comparison of L_T , L_{T3D} , and L_E from DNS results	74
5.4	Comparison of L_O and L_T from DNS results	76
5.5	Comparison of L_{kN} and L_T from DNS results	77
5.6	Comparison of $L_{k\epsilon}$ and L_T from DNS results	78
5.7	Comparison of E_{PE} and k from DNS results	80
5.8	Comparison of L_O , L_{kN} , $L_{k\epsilon}$ and L_E for a classic laboratory experiment	83
6.1	Conceptual three-dimensional parameter space	90
6.2	$NT_L - ST_L$ parameter space for interpretation of high-Reynolds number stratified shear-flow turbulence	95
6.3	Schematic of energy cascade with large length scales	97
6.4	Comparisons of the fundamental shear length scales, L_{kS} and L_C , to L_E	106
6.5	Comparisons of the fundamental buoyancy length scales, L_{kN} and L_O , to L_E	107
6.6	Comparisons of the fundamental isotropic length scale, $L_{k\epsilon}$, to L_E	108
6.7	Comparisons of estimated and actual density diffusivity, K_d^* , normalized by ν	115
6.8	Comparisons of estimated and actual momentum diffusivity, K_m^* , normalized by ν	116
7.1	$NT_L - ST_L$ parameter space with data from Shih et al. (2005)	123
7.2	$NT_L - Re_L$ parameter space for interpretation of stratified turbulence	123
7.3	Diapycnal mixing efficiency, R_f^* , versus the gradient Richardson number, Ri	125
7.4	Diapycnal mixing efficiency, R_f^* , versus the overturn Froude number, Fr_T	128
7.5	Diapycnal mixing efficiency, R_f^* , versus the buoyancy Reynolds number, Re_b	130
8.1	Study site locations	140
8.2	Bathymetry and profile locations for IWISE	141
8.3	Bathymetry and profile locations for BBTRE	143
8.4	Bathymetry and profile locations for NATRE	145
8.5	Example of a turbulent patch identified by the top-down cumulative sum of Thorpe displacements, $\sum \delta_T$	147

8.6	Temperature-salinity (T-S) diagram for IWISE, BBTRE, and NATRE data . . .	148
8.7	Scatter plot comparison of the Thorpe, L_T , and Ozmidov, L_O , scales	151
8.8	Scatter plot comparison of the Thorpe-inferred dissipation, ϵ_T , and the patch-averaged measured dissipation, ϵ_O	152
8.9	Comprison of L_T/L_O with the normalized overturn scale, $\widehat{L}_T = L_T/L_{\nu N}$	154
8.10	Comprison of ϵ_T/ϵ_O with the normalized overturn scale, $\widehat{L}_T = L_T/L_{\nu N}$	155
8.11	Example turbulent patch from BBTRE station 68	157
8.12	Example turbulent patch from BBTRE station 80	158
8.13	Mean values as a function of depth for IWISE M stations	160
8.14	Mean values as a function of depth for IWISE station N2	161
8.15	Mean values as a function of height above bottom for BBTRE	162
8.16	Mean values as a function of depth for NATRE	163
8.17	Time series of dissipation rates for profiles taken at IWISE M stations	166
8.18	Unit power and time-integrated energy for IWISE M stations	167
A.1	Wall-normal profiles of length scales in unstratified channel flow	187
A.2	Wall-normal profiles of dimensionless parameters in unstratified channel flow . .	187
A.3	Mean velocity profile from DNS of unstratified channel flow	190
A.4	Wall normal profile of L_{kS} and L_C from DNS of unstratified channel flow	190
B.1	IWISE profile 8042 from station M2 during the spring tidal period	191
B.2	IWISE profile 10013 from station M4 during the spring tidal period	192
B.3	IWISE profile 10023 from station N2 during the spring tidal period	193
B.4	IWISE profile 10030 from station N2 during the spring tidal period	194
B.5	BBTRE profile 68 for the lower ≈ 2000 m	195
B.6	BBTRE profile 80 for the lower ≈ 2000 m	196
B.7	NATRE profile 39 from 200 m to 600 m	197
B.8	NATRE profile 40 from 200 m to 600 m	198
B.9	Comparison L_T and L_O for IWISE M stations during the spring tidal period . .	199
B.10	Time series of dissipation rates for NATRE profiles	199

Chapter 1

Introduction

1.1 Motivation

Turbulence is characterized as the small-scale motions within a flow that are seemingly random and chaotic. In geophysical flows, such as those of the ocean and atmosphere, turbulence is influenced by the competing effects of larger-scale shear and stratification; shearing of the mean flow acts to promote turbulence while mean stratification generally has a dampening effect since most geophysical flows are stably-stratified. The resulting turbulence feeds back into the mean flow through the mixing of momentum and density. This dynamic interaction between small- and larger-scale motions makes turbulent mixing in the ocean and atmosphere critically relevant to global-scale, geophysical processes that govern Earth's climate. The dramatic range of scales characterizing this phenomenon precludes full resolution of the rich dynamics of turbulence in numerical ocean or climate models; therefore, the role of turbulent mixing must be parameterized, or approximated, in terms of more readily observed or computed quantities. The overarching goal of this research is to improve the fundamental understanding of stratified shear-flow turbulence so that dynamically appropriate, physically-based parameterization schemes can be developed for describing turbulent mixing in geophysical settings. Of particular focus will be the use of observed overturning motions to infer basic, but difficult to measure, quantities necessary for estimates of diapycnal diffusivity (i.e. turbulent mixing of density) in the ocean. The spatial scales of interest will be considered sufficiently small so that planetary rotational effects can be ignored (i.e., large Rossby number, $Ro \gg 1$).

It is through dimensional analysis that the relationship between overturning and mixing will be examined. Dimensional analysis is a powerful tool for gaining fundamental insight into turbulence wherein the basic physical quantities (e.g., characteristic length, velocity, or time scales, molecular viscosity, kinetic energy, etc.) are grouped into dimensionless parameters that explain some aspect of flow behavior. Physically, these parameters represent competing forces or processes within a flow. For example, the Reynolds number, $Re = UL/\nu$, is a widely used parameter expressing the competition of inertial forces, $\rho U^2 L^2$, to viscous forces, μUL . Here, U and L are characteristic velocity and length scales for the motions of interest, ν is the kinematic viscosity of the fluid, ρ is fluid density, and $\mu = \rho\nu$ is the fluid's dynamic viscosity. In this sense, motions with $Re \gg 1$ are influenced by their own inertia and are relatively free from the dampening effects of viscosity. This is, thus, a necessary (although not sufficient, as will be shown) condition for the existence turbulence. Other equally important dimensionless parameters relevant to overturning and mixing will be discussed as part of the current work.

Dimensional analysis also facilitates an understanding of turbulence through the formulation of fundamental time and length (or velocity) scales. Like dimensionless parameters, such scales are groupings of the basic physical quantities characterizing the flow. These groupings carry the units of either time or length. Because fundamental scales and dimensionless parameters are constructed from the same quantities, the latter is often expressed as a ratio of the former. Depending of the constituent quantities, a particular time or length scale may have a physical analogue in the flow and, thus, may denote a point in the spatio-temporal spectrum of motion where something of fundamental importance is occurring. For example, a length scale grouping involving ν might indicate the eddy size below which viscous dissipation of turbulence is important. In this dissertation, particular focus will be on the largest turbulent eddies of the flow that are readily observed in field studies. Since these eddies are strongly influenced by shear and stratification, fundamental length scales involving the mean shear rate, S , and the mean buoyancy frequency, N (defined later) will be featured. A comparison of observed and fundamental scales is central to the discussion, and relevant

dimensionless parameters are used to describe regimes of correlation or lack thereof. Agreement between observed and fundamental scales allows for inference of the basic quantities that can then be used to estimate diapycnal diffusivity.

Theoretically, a holistic picture of overturning and the related mixing is complete if the influences of shear, stratification, inertia, viscosity, and scalar diffusivity are all considered using a comprehensive set of parameters and fundamental scales. It is with this holistic mindset that the current research seeks to better understand stably-stratified shear-flow turbulence.

Specific motivators for this research are

- *A need to parameterize turbulent mixing:* Turbulent mixing of momentum and density are typically represented as diffusivity coefficients. As will be discussed, these coefficients are important for (1) characterizing and communicating the “state” of turbulence in environmental flows and (2) numerical modeling of such flows. Various parameterizations for turbulent diffusivity exist, however, none have been universally accepted due to a lack of a unified description of stably-stratified shear-flow turbulence.
- *A need for practical methods of inferring turbulent quantities:* Quantities such as turbulent kinetic energy, k , or turbulent dissipation rate, ϵ , are fundamental to flow behavior such as mixing but remain very difficult and expensive to measure in environmental flows. In oceanography, correlations are often assumed to exist between observed scales of motion and fundamental scales constructed through dimensional analysis. These assumed correlations allow for inferences on the turbulent quantities. The validity of these assumptions has yet to be assessed from a fundamental, holistic viewpoint.
- *A need to link laboratory and numerical findings to geophysical flows:* Much of what is known about stratified shear-flow turbulence comes from well controlled laboratory or numerical experiments. These experiments, however, are performed at relatively low Reynolds numbers when compared to the geophysical flows they are intended to

represent. Thus, parameterizations of flow behavior based on these experiments should be applied with caution to larger scale flows. A holistic understanding of the relevant length and time scales and dimensionless parameters is needed to properly scale-up experimentally based parameterizations.

1.2 Objectives

As stated above, the overarching goal of this research is to improve our fundamental understanding of stably-stratified shear-flow turbulence in an effort to better understand and improve parameterizations of turbulent mixing in geophysical settings. The key tool for doing so will be dimensional analysis tempered by physical reasoning so that relevant dimensionless parameters and fundamental length and time scales of the turbulence can be relied upon to describe the overturns that drive mixing. Data used in the analysis will include a combination of results from direct numerical simulations (DNS), laboratory data of classic studies, and oceanic field data. The main objectives of this research are as follows:

1. **To determine the fundamental scaling relationships for overturns in stably-stratified shear-flow turbulence.** The first major contribution of this dissertation is an analysis of the length scales of overturning in stably-stratified turbulence for the simple case of decaying, shear-free turbulence discussed in chapter 5. The analysis is then broadened to include mean shear, and thus growing turbulence, in chapter 6. In both chapters, correlations between the overturn size and the relevant fundamental length scales are determined and discussed in terms of the non-dimensional parameters of chapter 4. This objective is motivated by the common, yet insufficiently validated, practice of inferring the dissipation rate of turbulent kinetic energy, ϵ , from oceanic observations of overturns, where ϵ is a basic quantity used to estimate diapycnal diffusivity. The findings of chapters 5 and 6 have important implications with regard to this common practice.

2. **To develop a multi-parameter framework for parameterizing overturning and mixing in stably-stratified shear-flow turbulence.** Herein lies the crux of this dissertation: a multi-parameter, multi-regime parameter space is developed in chapter 6 to describe the fundamental scaling relationships of overturning in the presence of both shear and stratification. To date, no such parameter space has been presented that explicitly and independently considers both of these influences. The parameter space serves as a framework to generally conceptualize turbulence and, in chapter 7, is used successfully to describe the efficiency of mixing in DNS and geophysical flows.
3. **To compare the Thorpe and Ozmidov length scales using oceanic data.** In chapter 8, the fundamental groundwork laid by the bulk of this research will be called upon in an analysis of various oceanic data sets. Emphasis will be on data sets featuring overturns that are large by open ocean standards. Using this data, the Thorpe length scale (an observable measure of overturn size) will be compared to the Ozmidov length scale (a fundamental scale involving ϵ) to evaluate the validity of the common practice of inferring ϵ from overturns (mentioned in objective 1). To date, this practice is largely unvalidated in regions of large overturns. This objective serves to partially bridge the gap between theory, experiments, and field observations.

1.3 Dissertation Layout

The chapters of this dissertation each include brief discussions of background material so that the chapters may be read as stand-alone works. As such, some concepts and definitions found in the literature review and elsewhere will be repeated in later chapters. The layout of the dissertation is as follows:

- Chapter 2 represents a review of the full set of governing equations and the approximations typically used in the context of small-scale geophysical flows.

- Chapter 3 represents a review of classical literature pertaining to the dimensional analysis of sheared and/or stratified turbulence. More recent literature regarding the use of dimensionless ratios and fundamental scales to parameterize ocean turbulence will also be discussed.
- Chapter 4 presents the fundamental scales and parameters relevant to the rest of the dissertation.
- Chapter 5 is an analysis of the size of overturns in shear-free stratified turbulence using DNS. This chapter is directly motivated by objective 1 above.
- Chapter 6 addresses objectives 1, and 2 and is the centerpiece of the dissertation. A wide array of numerical and laboratory data is considered in constructing a conceptual framework and a parameterization scheme for ocean mixing is suggested.
- Chapter 7 addresses objective 2 and extends the framework to an analysis of mixing efficiency.
- Chapter 8 directly addresses objective 3 using data from regions of the world's oceans where turbulent mixing by overturning is intense.
- Finally, chapter 9 briefly summarizes the main findings and relevant contributions of the dissertation.

Chapter 2

Governing Equations

In any environment, the behavior of fluid flow (and turbulent motions) is governed by conservation laws. Specifically the conservation of mass, momentum (Newton's second law), and energy (first law of thermodynamics). These laws compose a closed set of equations that can theoretically be solved for an exact description the flow. However, to completely resolve a highly turbulent field becomes practically impossible due to the fine-scale structure of turbulence - hence the need for parameterizations. Nevertheless, the governing conservation laws are presented in this section to lay the fundamental groundwork for further discussion.

2.1 Conservation of Mass

Taking a system to be a set of fluid particles that constitute a deformable volume, $\mathcal{V}(t)$, the derivation of any conservation equation for some extensive variable, B (the total amount of some quantity contained within the volume), begins with the Reynolds transport theorem,

$$\left(\frac{DB}{Dt}\right)_{SYS} = \iiint_{\mathcal{V}} \frac{\partial(\rho\beta)}{\partial t} d\mathcal{V} + \oiint_S \rho\beta(\mathbf{U} \cdot \mathbf{n})dS, \quad (2.1)$$

where β is the intensive (per unit mass) representation of B , ρ is the density of the fluid, \mathbf{U} is the velocity of the system boundary, and \mathbf{n} is the unit vector normal (outward positive) to the control volume surface¹. The left hand side of (2.1) is the material derivative of the property B following the system. The first term on the right hand side is the time rate of change of B within \mathcal{V} at the instant of consideration, t . The second term on the right hand side is the time rate of change due to deformations in the system volume. Alternatively, with

¹ $B = \rho\mathcal{V}\beta$ only if ρ and β are uniform over the control volume.

a flux-based perspective, the first and second right hand terms are the change while the fluid is within a *fixed* control volume and the change due to a net flux through a non-deformable control surface, respectively. With the Gauss divergence theorem and an infinitesimal system volume, (2.1) becomes

$$\rho \frac{D\beta}{Dt} = \frac{\partial(\rho\beta)}{\partial t} + \nabla \cdot (\rho\beta\mathbf{U}). \quad (2.2)$$

When considering mass as the property of interest, $\beta = 1$ and the left hand side of (2.2) goes to zero (i.e., mass cannot be created or destroyed within the system). The conservation of mass can then be written in non-conservative form as

$$\frac{1}{\rho} \frac{D\rho}{Dt} + \nabla \cdot \mathbf{U} = 0, \quad (2.3)$$

where $D\rho/Dt = \partial\rho/\partial t + \mathbf{U} \cdot \nabla\rho$ is the material change in density following a fluid particle and can be nonzero due to changes in pressure, temperature, or salinity.

2.2 Conservation of Momentum

For a system of fluid particles, momentum is conserved in the sense of Newton's second law. That is, the change in system momentum, $D\mathbf{P}/Dt$, equals the sum of the forces acting on the system. In integral form, this may be written as

$$\left(\frac{D\mathbf{P}}{Dt} \right)_{SYS} = \iiint_{\mathcal{V}} \frac{\partial(\rho\mathbf{U})}{\partial t} d\mathcal{V} + \iint_S \rho\mathbf{U}(\mathbf{U} \cdot \mathbf{n}) dS = - \iint_S p\mathbf{n} dS + \iiint_{\mathcal{V}} \rho\mathbf{f} d\mathcal{V} + \iint_S \mathbf{n} \cdot \boldsymbol{\tau}_{ij} dS, \quad (2.4)$$

where the left half of the equation follows from (2.1) with $\beta = \mathbf{U}$ and the three right hand terms are the net forces from pressure (normal), p , body forces, $\rho\mathbf{f}$ (per unit volume), and viscous shear stress, represented by the second rank tensor τ_{ij} . Evoking the Gauss divergence

theorem and (2.3) This can be written in differential form as

$$\rho \frac{D\mathbf{U}}{Dt} = -\nabla p + \rho \mathbf{f} + \nabla \cdot \boldsymbol{\tau}_{ij}, \quad (2.5)$$

which is essentially a restatement of Newton's second law per unit volume of the fluid.

If density is assumed constant (for the time being), (2.3) and (2.5) represent four equations involving ten unknowns (i.e., \mathbf{U} , p , τ_{11} , τ_{22} , τ_{33} , $\tau_{12} = \tau_{21}$, $\tau_{13} = \tau_{31}$, and $\tau_{23} = \tau_{32}$). Closure to the system is provided by a constitutive relationship relating stress to strain in the fluid. Stokes hypothesis provides the needed closure, which for incompressible Newtonian fluids (i.e., those of the flows considered here) is:

$$\tau_{ij} = 2\mu S_{ij}, \quad (2.6)$$

where μ is the dynamic viscosity of the fluid and $S_{ij} = \frac{1}{2} \left(\frac{\partial U_i}{\partial x_j} + \frac{\partial U_j}{\partial x_i} \right)$ is the strain rate tensor. Substitution of (2.6) into (2.5) yields the Navier-Stokes equations for an incompressible fluid of nearly constant viscosity and a body force due solely to gravity (i.e., $\mathbf{f} = \mathbf{g} = -\mathbf{k}g$, where g is the acceleration due to gravity):

$$\rho \frac{D\mathbf{U}}{Dt} = -\nabla p + \rho \mathbf{g} + \mu \nabla^2 \mathbf{U}. \quad (2.7)$$

2.3 Conservation of Energy

In general, (2.3) and (2.7) do not constitute a closed system even with Stokes hypothesis because density is not necessarily a known constant. The thermodynamic equation and an equation of state are then needed to complement (2.3) and (2.7).

The first law of thermodynamics states that changes in the total energy of a system are due to heat transfer with the surroundings and work done by/to the system on/by the surroundings. For a system of fluid particles, the specific total energy is $\mathcal{E} = e + \frac{1}{2} \mathbf{U} \cdot \mathbf{U} + \Phi$,

where the constituent terms represent internal, kinetic, and potential (i.e., $-g\mathbf{k} = -\nabla\Phi$) energy, in that order. Thus, the net change in a system's energy is represented by (2.1) with $\beta = \mathcal{E}$. To satisfy energy conservation, this is then set equal to terms describing work done by surface forces and net heat transfer. In differential form this is

$$\rho \frac{D\mathcal{E}}{Dt} = -\nabla \cdot (\mathbf{q} + p\mathbf{U} - \tau_{ij} \cdot \mathbf{U}), \quad (2.8)$$

where \mathbf{q} is the heat flux per unit area, $p\mathbf{U}$ and $-\tau_{ij} \cdot \mathbf{U}$ are the pressure and viscous work done by the surroundings on the system. For the purposes here, we will neglect viscous work. Through consideration for enthalpy, energy conservation can then be written in terms of temperature, T :

$$\frac{DT}{Dt} = \kappa_T \nabla^2 T, \quad (2.9)$$

where κ_T is the coefficient of thermal diffusivity (see Kundu, 1990). Using an equation of state of the form $\rho = \rho(T)$, this can be rewritten in terms of density. Generally, however, the density can also be affected by changes in salinity, \mathcal{S} , so that $\rho = \rho(T, \mathcal{S})$. In this case, the conservation of energy in terms of density is

$$\frac{D\rho}{Dt} = \kappa_\rho \nabla^2 \rho, \quad (2.10)$$

where κ_ρ is a bulk molecular diffusivity of density that considers diffusion of density due to diffusion of both temperature and salinity. In the ocean, however, heat diffuses roughly 100 times faster than salt so that $\kappa_\rho \approx \kappa_T$ is often assumed.

2.4 Boussinesq Approximations

The governing equations can be simplified if it is assumed that density changes due to pressure, temperature, or salinity are small. First consider the equation for the conservation of mass. In many geophysical applications, the fluid of interest can be considered incom-

compressible so that $\nabla \cdot \mathbf{U} \approx 0$. Furthermore, typical coefficients of thermal or haline expansion are small enough so that $\rho^{-1}D\rho/Dt \ll \nabla \cdot \mathbf{U}$. In this case, (2.3) can be written as

$$\nabla \cdot \mathbf{U} = 0. \quad (2.11)$$

Now consider conservation of momentum. Both density and pressure can be decomposed into background and perturbation components: $\rho(\mathbf{x}, t) = \rho_0 + \delta\rho(\mathbf{x}, t)$ and $p(\mathbf{x}, t) = p_0(z) + \delta p(\mathbf{x}, t)$, where the background pressure is assumed hydrostatic (i.e., $\nabla p_0 = \rho_0 \mathbf{g}$). Here it is assumed that density perturbations, $\delta\rho$, are due to changes in temperature or salinity (not pressure). Perturbations in pressure are interpreted as any departures from the reference hydrostatic pressure. In most geophysical applications, $\delta\rho \ll \rho_0$, so that (2.7) can be rewritten as

$$\frac{D\mathbf{U}}{Dt} = -\frac{1}{\rho_0}\nabla\delta p + \frac{\delta\rho}{\rho_0}\mathbf{g} + \nu\nabla^2\mathbf{U}. \quad (2.12)$$

Herein lies the most profound tenet of the Boussinesq approximation. That is, variations in density can be neglected except when multiplying gravity. The resultant term, $(\delta\rho/\rho_0)\mathbf{g}$, is known as the buoyancy term or reduced gravity and embodies the role of density as an “active” scalar.

Finally, decomposition and simplification of the density equation (2.10) yields

$$\frac{D\delta\rho}{Dt} = \kappa_\rho\nabla^2\delta\rho. \quad (2.13)$$

Here we see that, although the material change in density may be small, $D\delta\rho/Dt \neq 0$ due to the possibility of adiabatic heat exchange or small changes in salinity.

(2.11), (2.12), and (2.13) represent the complete set of governing equations under the Boussinesq approximations. These constitute the equation set typically referenced in many geophysical flow applications - especially ocean applications where the density perturbations within seawater are relatively small. At larger scales where the earth’s rotation is influential,

Coriolis terms must be included in the momentum equation to account for the apparent forces.

The Boussinesq approximations break down if pressure changes are strong enough to affect density. This can occur if the speed of the fluid is large compared to the speed of shock waves (i.e., large Mach number, $Ma \gg 1$) or if hydrostatic pressures are very large. In the ocean, typical flow velocities are on the order of $U \approx 1 \text{ ms}^{-1}$ while the speed of sound corresponding to shock wave velocity is $c \approx 1470 \text{ ms}^{-1}$. This gives $Ma = U^2/c^2 \sim 10^{-7}$. This value is significantly smaller than $Ma = 0.3$, which is the minimum value required for compressibility effects to be important (see Kundu 1990). For variations in density due to hydrostatic pressure to be negligible, the vertical scale of consideration must be less than c^2/g , where g is the acceleration due to gravity (see Kundu 1990). In the ocean, $c^2/g \approx 200 \text{ km}$, which is much larger than the scales considered here so the Boussinesq approximations hold.

2.5 Reynolds Decomposition: The Turbulence Framework

Turbulent flows are instantaneously satisfied by (2.11)-(2.13) so long as the assumptions of the Boussinesq approximations are appropriate (usually so in geophysical flows). Even with these approximations, however, the detail of turbulent length and time scales make direct solution of the equations impractical for all but simple, weakly turbulent examples. The practical solution is thus to decompose the velocity, pressure, and scalar (i.e., density) fields into mean and fluctuating components and then solve only for the mean field. The so called “Reynolds decompositions” are

$$\mathbf{U}(\mathbf{x}, t) = \langle \mathbf{U}(\mathbf{x}, t) \rangle + \mathbf{u}(\mathbf{x}, t), \quad (2.14)$$

$$p(\mathbf{x}, t) = \langle p(\mathbf{x}, t) \rangle + p'(\mathbf{x}, t), \quad (2.15)$$

$$\rho(\mathbf{x}, t) = \langle \rho(\mathbf{x}, t) \rangle + \rho'(\mathbf{x}, t), \quad (2.16)$$

where $\langle \rangle$ indicates temporal averaging for a point in space, and \mathbf{u} , p' , and ρ' are the fluctuating (i.e., turbulent) velocity pressure, and density. The δ -notation of 2.4 has been dropped from pressure and density for convenience but both still indicate departure from a static background reference condition.

Substituting these decompositions into (2.11)-(2.13) and time averaging yields equations for the mean field (shown here in tensor notation):

$$\frac{\partial U_i}{\partial x_i} = 0, \quad (2.17)$$

$$\frac{D\langle U_i \rangle}{Dt} = -\frac{1}{\rho_0} \frac{\partial \langle p \rangle}{\partial x_i} - \frac{\langle \rho \rangle}{\rho_0} g \delta_{i3} + \frac{\partial}{\partial x_j} \left[\nu \frac{\partial \langle U_i \rangle}{\partial x_j} - \langle u_i u_j \rangle \right], \quad (2.18)$$

$$\frac{D\langle \rho \rangle}{Dt} = \frac{\partial}{\partial x_j} \left[\kappa_\rho \frac{\partial \langle \rho \rangle}{\partial x_j} - \langle u_j \rho' \rangle \right], \quad (2.19)$$

where j is the repeated index for a given direction, i (e.g., for an equation evaluated in the x -direction, $i = 1$ and $j = 1, 2, 3$), and δ_{i3} is the third column of the 3x3 Kronecker tensor (i.e., $\delta_{13} = \delta_{23} = 0$, $\delta_{33} = 1$, where $i = 3$ indicates the vertical direction). These equations are the direct analogues to (2.11)-(2.13), with the exception of the additional turbulent fluctuation terms in (2.18) and (2.19). These new terms are the Reynolds stress tensor, $-\langle u_i u_j \rangle$, and the turbulent density flux, $-\langle u_j \rho' \rangle$. The Reynolds stresses are “apparent” stresses felt by the mean flow due to the transfer of mean momentum by the turbulent motions. The turbulent density flux is the flow rate per unit area of density due to turbulent motions. These two terms create a closure problem for solving the mean equations - the ultimate “turbulence closure problem”. The Reynolds stress tensor introduces six new variables, and the turbulent density flux introduces three.

Common parameterizations of the Reynolds stresses and turbulent density fluxes involve evoking turbulent diffusivities that essentially describe turbulent transport as analogous to

molecular transport. That is,

$$-\langle u_i u_j \rangle = K_m \left(\frac{\partial \langle U_i \rangle}{\partial x_j} + \frac{\partial \langle U_j \rangle}{\partial x_i} \right) - \frac{2}{3} k \delta_{ij}, \quad (2.20)$$

where k is the turbulent kinetic energy (see next section), and

$$-\langle u_j \rho' \rangle = K_d \frac{\partial \langle \rho \rangle}{\partial x_j}. \quad (2.21)$$

These equations embody the turbulent-viscosity and gradient diffusion hypotheses, respectively, and represent the nine additional equations required to close the system. It is important to note, however, that the “eddy viscosity”, K_m , and the turbulent density diffusivity, K_d , are properties of the *flow*, not the *fluid*. Therefore, it is possible that they are directionally dependent. With these hypotheses, the task of closure is now simplified to prescribing K_m and K_d .

2.6 Turbulent Kinetic Energy Budget

Reynolds decomposition of the governing equations has created a user-defined framework to study turbulent flows. Namely, the instantaneous motions have been filtered into mean and turbulent fields so that the turbulent field can be modeled with some parameterization such as through turbulent diffusivities. As such, accurate parameterizations rely on an understanding of the fundamental nature of the turbulent field. The key tool for gaining such an understanding is the kinetic energy budget of the turbulent motions, where turbulent kinetic energy per unit mass is half the trace of the Reynolds stress tensor:

$$k \equiv \frac{1}{2} \langle u_i u_i \rangle. \quad (2.22)$$

The budget, or evolution, equation for k is obtained by first subtracting the mean equation (2.18) from the instantaneous equation (2.12) to get an equation for the turbulent velocity, u_i . Multiplication by u_i and then averaging yields the kinetic energy equation:

$$\frac{Dk}{Dt} = \frac{\partial k}{\partial t} + \langle U_j \rangle \frac{\partial k}{\partial x_j} = \mathcal{T} + P + B - \epsilon, \quad (2.23)$$

where \mathcal{T} , P , B , and ϵ are the transport, production, buoyancy flux, and dissipation of turbulent kinetic energy as defined by:

$$\mathcal{T} \equiv -\frac{\partial}{\partial x_j} \left[\frac{1}{\rho_0} \langle p' u_j \rangle + \langle k u_j \rangle - 2\nu \langle u_i s_{ij} \rangle \right] \quad (2.24)$$

$$P \equiv -\langle u_i u_j \rangle \frac{\partial \langle U_i \rangle}{\partial x_j} \quad (2.25)$$

$$B \equiv -\frac{g}{\rho_0} \langle u_i \rho' \rangle \delta_{i3} \quad (2.26)$$

$$\epsilon \equiv 2\nu \langle s_{ij} s_{ij} \rangle = \nu \left\langle \frac{\partial u_i}{\partial x_j} \frac{\partial u_i}{\partial x_j} + \frac{\partial u_i}{\partial x_j} \frac{\partial u_j}{\partial x_i} \right\rangle, \quad (2.27)$$

where $s_{ij} = \frac{1}{2} \left(\frac{\partial u_i}{\partial x_j} + \frac{\partial u_j}{\partial x_i} \right)$ is the fluctuation strain rate tensor. The transport term, \mathcal{T} , describes the transport of k due to pressure fluctuations, turbulent advection, and viscous diffusion, but is often small and, in fact, zero for homogeneous turbulence.

The remaining three terms are relatively more interesting. The production term, P , represents the transfer of kinetic energy from the mean field by way of the Reynolds stress working against the mean shear. This term is usually positive, indicating a “production” of turbulent kinetic energy and a loss of kinetic energy from the mean field.

The buoyancy flux term, B , represents the conversion between turbulent kinetic and turbulent potential energy (defined in section 2.7) and can generally be positive or negative. For stably-stratified flows (i.e., $\partial \langle \rho \rangle / \partial x_3 < 0$, where x_3 is the vertical spatial coordinate), a negative buoyancy flux indicates a positive density flux and a “loss” of kinetic energy. In this case, kinetic energy is expended on the mixing of density against the influence of

gravity. It is important to note, though, that the process is reversible. That is, turbulent potential energy can convert back into kinetic form if a negative density flux occurs before molecular diffusion of density fluctuations can occur. Such is the case with counter-gradient fluxes associated with linear internal gravity waves.

Finally, the dissipation term, ϵ , represents the *irreversible* loss of turbulent kinetic energy to internal energy due to the viscosity of the fluid. This term is always positive, and $-\epsilon$ is, therefore, always a sink term in (2.23). The second term in braces on the right hand side of (2.27) is typically negligible so that ϵ is often approximated as

$$\tilde{\epsilon} = \nu \left\langle \frac{\partial u_i}{\partial x_j} \frac{\partial u_i}{\partial x_j} \right\rangle, \quad (2.28)$$

where $\tilde{\epsilon}$ is known as “pseudo-dissipation”.

2.7 Turbulent Potential Energy Budget

As stated in the previous section, turbulent kinetic energy is typically introduced from the mean field through P , and lost to internal energy through ϵ or to turbulent potential energy through B . It was also stated that the loss through B is reversible since turbulent potential energy can convert back into kinetic form. In that sense turbulent potential energy is often referred to as “available” potential energy, or simply APE, in that it is available to the turbulence. To better understand this phenomenon an evolution equation for turbulent potential energy will now be introduced.

Turbulent potential energy occurs in a stratified flow when turbulent motions act to lift heavy fluid over light, but only exists during the time prior to irreversible molecular mixing of density or motions leading to counter-gradient flux (i.e., net negative density flux). The definition (per unit mass) is given by

$$E_{PE} \equiv \left\langle \frac{1}{\rho_0} \int \rho' g dz' \right\rangle = \frac{g}{\rho_0} \left\langle \int \left(-\frac{\partial \langle \rho \rangle}{\partial z} z' \right) dz' \right\rangle = -\frac{1}{2} \frac{g}{\rho_0} \left(\frac{\partial \langle \rho \rangle}{\partial z} \right)^{-1} \langle \rho'^2 \rangle, \quad (2.29)$$

where the turbulent average density fluctuation of a given fluid parcel is a function of its vertical turbulent departure, z' , from an otherwise stable density profile: $\rho' = -(\partial\langle\rho\rangle/\partial z)z'$. In the absence of molecular mixing or viscous effects, a parcel displaced as such would oscillate vertically about its original (i.e., stable) position with a frequency, N . This so-called buoyancy frequency is defined by

$$N^2 \equiv -\frac{g}{\rho_0} \frac{\partial\langle\rho\rangle}{\partial z}, \quad (2.30)$$

where $z \equiv x_3$ is the vertical spatial coordinate. Turbulent potential energy can then be redefined as

$$E_{PE} = N^2 \left(\frac{\partial\langle\rho\rangle}{\partial z} \right)^{-2} \langle \frac{1}{2}\rho'^2 \rangle. \quad (2.31)$$

It is now obvious that an equation for E_{PE} is essentially an equation for half the density variance, $\langle\rho'^2/2\rangle$. Such an equation is the scalar analogue to the turbulent kinetic energy equation, (2.23), and is derived similarly. First, an equation for the density fluctuations is derived by subtracting the mean equation, (2.19), from the instantaneous equation, (2.13). The variance equation is then achieved by multiplying by $\rho'/2$ and taking the mean:

$$\frac{D\langle\frac{1}{2}\rho'^2\rangle}{Dt} = \frac{\partial\langle\frac{1}{2}\rho'^2\rangle}{\partial t} + \langle U_j \rangle \frac{\partial\langle\frac{1}{2}\rho'^2\rangle}{\partial x_j} = \frac{1}{2} \left(\kappa_\rho \frac{\partial^2\langle\rho'^2\rangle}{\partial x_j \partial x_j} - \frac{\partial\langle u_j \rho'^2 \rangle}{\partial x_j} \right) - \langle u_j \rho' \rangle \frac{\partial\langle\rho\rangle}{\partial x_j} - \epsilon_\rho, \quad (2.32)$$

where the first two terms on the right hand side are molecular and turbulent transport terms, respectively, that decrease in significance with increasing homogeneity of the turbulence. The third term is the production of variance due to the turbulent density flux working against the mean density gradient. The final term is the dissipation of density variance defined by

$$\epsilon_\rho = \kappa_\rho \left\langle \frac{\partial\rho'}{\partial x_j} \frac{\partial\rho'}{\partial x_j} \right\rangle, \quad (2.33)$$

and represents a molecular smoothing of density fluctuations.

Multiplying (2.32) by $N^2(\partial\langle\rho\rangle/\partial z)^{-2}$ gives the equation for turbulent potential energy. Neglecting the transport terms and assuming mean density changes only in the vertical direction (i.e., $\partial\langle\rho\rangle/\partial x = \partial\langle\rho\rangle/\partial y = 0$, where $x \equiv x_1$ and $y \equiv x_2$ are the lateral spatial coordinates), this can be written as

$$\frac{DE_{PE}}{Dt} \approx \frac{g}{\rho_0}\langle u_j\rho'\rangle\delta_{j3} - N^2\epsilon_\rho \left(\frac{\partial\langle\rho\rangle}{\partial z}\right)^{-2} = -B - \epsilon_{PE}, \quad (2.34)$$

where ϵ_{PE} is the irreversible conversion of turbulent potential energy to background potential energy due to molecular diffusion and is given by

$$\epsilon_{PE} = N^2\epsilon_\rho \left(\frac{\partial\langle\rho\rangle}{\partial z}\right)^{-2}. \quad (2.35)$$

In light of equations (2.23) and (2.34), we now explicitly see that the role of the buoyancy flux, B , is to transfer energy between kinetic and potential forms; a negative buoyancy flux (i.e., positive density flux) leads to a temporary decrease in k and a temporary increase in E_{PE} . The decrease in k becomes permanent only if the increase in E_{PE} is subsequently dissipated through ϵ_{PE} and the negative buoyancy flux is sustained. Such a process leads to an increase in the *background* potential energy (i.e., mixing of the mean density field) at the expense of turbulent kinetic energy.

Chapter 3

Literature Review

3.1 Length and Time Scales of Turbulence

Turbulence is often conceptualized as a field of three-dimensional motions known as eddies. Analogous to the two-dimensional swirling motions observed on the surface of a river in the wake of a bridge pier, these motions are considered “semi-coherent” in that they are characterized by an identifiable length scale, l (e.g., the eddy diameter). An eddy of size l is then characterized by a velocity scale, $u(l)$ (e.g., the eddy’s rotational speed), and a time scale, $\tau(l) \equiv l/u(l)$ (see Pope, 2000). The space occupied by a given eddy can also contain smaller eddies, thus giving rise to the chaotic detail that is ubiquitous to turbulent flows. The largest eddies in the turbulent field have scales that are set by the mean flow or physical boundaries, while the smallest scales are influenced by the arresting effects of the fluid’s viscosity. How turbulent kinetic energy is transferred across this spectrum of motion is of fundamental importance to turbulent dynamics so a conceptual framework for this process will be presented first. Common length and time scales constructed through dimensional analysis will then be discussed in the context of this framework for the cases of unforced, sheared, and stratified turbulence.

3.1.1 The Energy Cascade

The traditional framework used to describe the transfer of energy among the various scales of turbulence was put forth by Richardson (1922). Richardson conceptualized that kinetic energy is introduced to the turbulent field at the scales of the largest eddies and is then transferred to successively smaller eddies via inertia as larger eddies breakup. The process is viewed to continue down to the smallest eddies where inertial transfer gives way

to viscous dissipation. At the smallest eddies kinetic energy is converted to internal energy (i.e., heat). Richardson eloquently summarized this “energy cascade” as follows:

Big whorls have little whorls,
Which feed on their velocity;
And little whorls have lessor whorls,
And so on to viscosity
(in the molecular sense).

An important aspect of this framework is that dissipation occurs at the end of the cascade and is, thus, dependent on the rate at which the largest eddies receive kinetic energy from the mean flow. If the kinetic energy of the largest eddies scales with the square of their characteristic velocity, u_0^2 , then the transfer rate should go as u_0^2/τ_0 , where τ_0 is the large eddy time scale. Thus, if the flow is in equilibrium: $\epsilon \sim u_0^2/\tau_0 = u_0^3/l_0$ (see Pope, 2000). For this to be so, the time scale of the smallest eddies (which depend on viscosity) must adjust to, and be less than, that of the larger eddies. In other words, for the cascade to continue uninterrupted small eddies must have transfer rates that at least exceed the rate at which they receive energy from larger scales. But what are these scales, both large and small? How is energy distributed across the length scale spectrum? How do shear and buoyancy effect this process? Classical answers to these questions are addressed in the next sections.

3.1.2 Unforced Turbulence

3.1.2.1 Kolmogorov’s Hypotheses

The foundation of modern turbulence theory may be attributed largely to the hypotheses of Kolmogorov (1941). Kolmogorov reasoned that the largest scales of turbulence are anisotropic due to mean flow and boundary conditions, but directional information is lost as these eddies breakup into successively smaller eddies. The end result is that isotropy is

achieved at sufficiently small scales when Reynolds number is sufficiently high. In this sense, the small scales have universal characteristics in high-Reynolds number flows.

To characterize the smallest scales where dissipation occurs in earnest, Kolmogorov proposed the variables of consideration to be ν and ϵ . Through simple dimensional analysis he reasoned that the smallest eddies have the following characteristic length, velocity, and time scales:

$$\eta \equiv \left(\frac{\nu^3}{\epsilon} \right)^{1/4} \quad (3.1)$$

$$u_\eta \equiv (\epsilon\nu)^{1/4} \quad (3.2)$$

$$\tau_\eta \equiv \left(\frac{\nu}{\epsilon} \right)^{1/2}. \quad (3.3)$$

Interestingly, this reasoning implies that ν and ϵ are independent quantities, despite the obvious dependence of the latter on the former. Here, ϵ is assuming the role of a transfer rate from larger scales as set by the scaling introduced previously (i.e., $\epsilon \sim u_0^3/l_0$). Kolmogorov considered (3.1)-(3.3) to describe the smallest eddies possible. That is, η is the length scale at which an eddy's inertial overturning cannot overcome the arresting effect of viscosity.

Between the large and small scales, Kolmogorov hypothesized that there exists an *inertial subrange* through which kinetic energy is transferred via inertia in accordance with the cascade theory of Richardson (1922). As with the dissipation range, motions of the inertial subrange were also assumed to be universal among flows of high Reynolds number. Unlike the dissipative eddies, however, Kolmogorov hypothesized that eddies of the inertial subrange are dependent only upon ϵ , and are independent of ν . That is, they are small enough to be isotropic but have enough inertia to overwhelm viscosity. With this reasoning, the net transfer rate through the inertial range is constant and equal to ϵ for a flow in equilibrium. Thus, $\epsilon \sim u_0^3/l_0 \sim u(l)^3/l$, for all eddies of size l within the inertial subrange.

Kolmogorov used the notion of a constant transfer rate to investigate the distribution of energy across the scales of the inertial subrange. In essence, he hypothesized that an eddy of size, l , is associated with a specific amount of energy, $k(l) \sim u(l)^2$. Then for the inertial

subrange, the energy of a specific eddy increases with its size according to $k(l) \sim (\epsilon l)^{2/3}$. The distribution of energy is typically discussed in wave-number space where an eddy's wavenumber, κ_l , is the inverse of the eddy's length scale (i.e., $\kappa_l \sim 1/l$)². The energy density (energy per unit wavenumber) for the inertial subrange is then:

$$E(\kappa_l) \sim \frac{k(\kappa_l)}{\kappa_l} \sim \epsilon^{2/3} \kappa_l^{-5/3}. \quad (3.4)$$

This is the famous “ $-5/3$ ” law of Kolmogorov that has been shown to hold for highly turbulent experimental flows (e.g., Saddoughi and Veeravalli, 1994). In logarithmic plots of $E(\kappa_l)$ for data of sufficiently high Reynolds number, the inertial subrange is identifiable as the bandwidth for which the spectrum is linear and of $-5/3$ slope. Typical spectrum plots become non-linear above and below this bandwidth. The bandwidth above the inertial subrange (i.e., small wavenumbers) is known as the *energy-containing range* because the energy density is high. The bandwidth below the inertial subrange (i.e., high wavenumbers) is known as the *dissipative range* because inertial transfer is giving way to viscous loss.

The preceding hypotheses are widely accepted for sufficiently small scales of sufficiently high Reynolds number flows (i.e., those of the inertial subrange and smaller). Now consider the larger scales. Generally, larger scales are assumed to be set by forcing of the mean flow or by boundary conditions and cannot be uniquely determined from ν and ϵ . But what if the flow is unforced? That is, what are the largest scales if the entire field is isotropic? Such a flow could exist if shear, stratification, and boundary effects are absent. The turbulent kinetic energy equation represented in (2.23) then implies that the turbulence freely decays and the only remaining variable to consider for dimensional analysis is the kinetic energy itself, k . Since k represents the total kinetic energy of the turbulence as summed over eddies of all sizes (i.e., $k = \int E(\kappa_l) d\kappa_l$), scales constructed from k are considered “integral scales”.

² κ_l is not to be confused with κ_ρ or κ_T which are molecular diffusivities.

Simple dimensional analysis shows these to be:

$$L_{k\epsilon} \equiv \frac{k^{3/2}}{\epsilon} \quad (3.5)$$

$$u_L \equiv k^{1/2} \quad (3.6)$$

$$T_L \equiv \frac{k}{\epsilon}. \quad (3.7)$$

These are often considered the length, velocity, and time scales of the largest eddies (if mean flow and boundary effects are ignored) due to the integral nature of k (see Pope, 2000; Durbin and Reif, 2001). In-depth physical interpretations of these scales will be given in chapter 4.

3.1.2.2 Taylor Microscale

The Taylor microscale is another, less physically based, length scale of frequent use in studies of isotropic turbulence. Its derivation arises from a scaling of the isotropic simplification of the dissipation rate given in (2.27):

$$\epsilon = 15\nu\langle(\partial u_1/\partial x_1)^2\rangle = 15\nu\langle u_1^2\rangle/\lambda_g^2 = 15\nu u_{rms}^2/\lambda_g^2, \quad (3.8)$$

where $\langle u_1^2\rangle = u_{rms}^2$ in isotropic flow and λ_g is the Taylor microscale. λ_g can be interpreted as the length scale that allows for

$$u_{rms} = \lambda_g \langle \partial u_1 / \partial x_1 \rangle \quad (3.9)$$

(Tennekes and Lumley, 1974). This scale can also be formulated on the basis of the velocity autocorrelation function (see Pope, 2000). Interestingly, λ_g is defined with the assistance of the large-scale velocity, $u_{rms} \sim k^{1/2}$, therefore it does not characterize the small scales where dissipation is actually occurring. Nonetheless, λ_g remains popular due to the frequent use of autocorrelations by observationalists.

3.1.3 Scales of Shear-flow Turbulence

The hypotheses of Kolmogorov are considered strictly valid for sufficiently small scales that can be considered isotropic. The larger scales, on the other hand, are anisotropic due to the influence of external forcing. In general, this forcing can be due to boundary conditions, mean shear, or stratification. Because boundary conditions are flow-specific, the current research will focus on the latter two fundamental mechanisms.

First, consider unstratified flow when mean shear, $S = \partial\langle U_i \rangle / \partial x_j$, is present. With reference to (2.23), the production term is active and the variables available to dimensional analysis are k , ϵ , ν , and S . Again, the inclusion of both ϵ and ν emphasizes the role of ϵ as a down-spectrum transfer rate.

The obvious question is then: over what bandwidth of the energy spectrum is mean shear causing anisotropy? In other words, what determines the upper end (i.e., large-scale extent) of the inertial subrange? In a classical effort to address these questions, Corrsin (1958) viewed the problem in the context of competing time scales. Corrsin, in essence, compared the time scales of inertial transfer and viscous dissipation to that of the mean strain (i.e., shear), S^{-1} . The mean shear time scale can be thought of as an external time scale imposed on the turbulence, while the inertial and viscous dissipation time scales can vary by eddy size. Prior to making any assumptions based on Kolmogorov's hypotheses, Corrsin defined the eddy-wise inertial transfer time scale as

$$\tau_a(\kappa_l) = \frac{k(\kappa_l)}{u(\kappa_l)^3/l} = \frac{\Delta\kappa_l E(\kappa_l)}{(\Delta\kappa_l E(\kappa_l))^{3/2} \kappa_l} = (\kappa_l^3 E(\kappa_l))^{-1/2}, \quad (3.10)$$

where $u(\kappa_l)^2 = k(\kappa_l)$ and $k(\kappa_l) = \Delta\kappa_l E(\kappa_l)$ is the kinetic energy associated with the eddies in the $\Delta\kappa_l$ bandwidth. If a geometric scaling is assumed, $\Delta\kappa_l \approx \kappa_l$, then $k(\kappa_l)$ is the energy of the eddies with size κ_l . Corrsin went on to define the eddy-wise dissipation time scale as

$$\tau_c(\kappa_l) = \frac{k(\kappa_l)}{\nu u(\kappa_l)^2/l^2} = \frac{\Delta\kappa_l E(\kappa_l)}{\nu \Delta\kappa_l E(\kappa_l) \kappa_l^2} = (\nu \kappa_l^2)^{-1}, \quad (3.11)$$

where $\nu u(\kappa_l)^2/l^2$ is the dissipation rate of a given eddy size and dimensionally consistent with (2.27). Again, no assumptions regarding ϵ have been evoked so (3.10) and (3.11) are generally true for the entire spectrum.

Corrsin then proposed local isotropy to be possible only for $\tau_a \ll S^{-1}$ at scales where inertial transfer is relevant (i.e., for $\tau_a \ll \tau_c$), or for $\tau_c \ll S^{-1}$ at scales where viscous dissipation is relevant (i.e., for $\tau_a \gg \tau_c$). The second case pertains to the dissipative region and implies $\kappa_l \gg (S/\nu)^{1/2}$ is needed there for the shear to be of no influence. The corresponding length scale defining this transition is then

$$L_{\nu S} = \left(\frac{\nu}{S}\right)^{1/2}. \quad (3.12)$$

The first case is less straight forward in that it requires specification of $E(\kappa_l)$. For this, Corrsin adopted the Kolmogorovian scaling of (3.4), thus giving the requirement $\kappa_l \gg (S^3/\epsilon)^{1/2}$. The corresponding length scale is often referred to as the ‘‘Corrsin’’ length scale:

$$L_C = \left(\frac{\epsilon}{S^3}\right)^{1/2}. \quad (3.13)$$

Because the scaling of Kolmogorov has been evoked, this scale must be related to the inertial subrange. If the inertial subrange is taken to be isotropic, then L_C may be interpreted as its upper end (i.e., small wavenumber limit). In a study of high-Reynolds number flow in a wind tunnel, Saddoughi and Veeravalli (1994) found that local isotropy, as determined by correlation coefficient spectra, occurs for scales smaller than approximately $0.65L_C$.

In the region where both inertial transfer and viscous dissipation are relevant, Corrsin argued that $\tau_a \approx \tau_c \approx \tau_\eta$ and that local isotropy is, therefore, possible when $\tau_\eta \ll S^{-1} \Rightarrow S(\nu/\epsilon)^{1/2} \ll 1$. In such a case, $L_{\nu S} \ll L_C$, which implies that the requirement $l \ll L_{\nu S}$ for local isotropy is moot. What then is the physical significance of $L_{\nu S}$? Furthermore, what is the physical significance of scales constructed with S and k ? These questions will be addressed in chapter 4.

3.1.4 Scales of Stratified Turbulence

As with mean shear, stratification induces anisotropy at the larger scales of the turbulent field. And like the efforts of Corrsin, classic works by Ozmidov (1965) and Dougherty (1961) sought to determine the largest locally isotropic scales. Dougherty, for example, idealized this to be roughly the scale at which an eddy's contribution to turbulent potential energy balances its turbulent kinetic energy. That is,

$$\frac{1}{2} \frac{g}{\rho_0} \frac{\partial \rho}{\partial z} l^2 \sim \kappa_l E(\kappa_l) \Rightarrow l \sim \left(\frac{\kappa_l E(\kappa_l)}{N^2} \right)^{1/2}. \quad (3.14)$$

As with the formulation of L_C , the $-5/3$ law can be evoked for $E(\kappa_l)$ to yield the so-called ‘‘Ozmidov’’ length scale:

$$L_O = \left(\frac{\epsilon}{N^3} \right)^{1/2}. \quad (3.15)$$

Again, the inclusion of ϵ by way of the Kolomogorov scaling inherently ties this scale to the inertial subrange where ϵ is relevant as a down-spectrum transfer rate. Near and above this scale, however, it is presumed that the tendency for vertical suppression of eddies is realized and (3.4) ceases to hold. In this sense, L_O is the largest isotropic scale and the upper end of the inertial subrange when shear is absent and stratification is the only forcing mechanism.

It is worth noting that (3.15) can also be derived in the fashion shown above for achieving (3.13) with consideration for the time scale of the mean stratification N^{-1} (in place of S^{-1}). Furthermore, a scale formulation analogous to (3.12) is possible, but not frequently referenced in literature. A physical interpretation for this scale will be given in chapter 4.

Due to the well-known anisotropic nature of stratified turbulence, an additional length scale is often formulated using the vertical component of the turbulent velocity, w . This is the buoyancy length scale

$$L_b = \frac{w}{N}, \quad (3.16)$$

which conceptually represents the vertical distance traveled by a fluid particle if its initial kinetic energy, $w^2/2$, is converted to potential, $N^2 L_b^2/2$ (see, e.g., Hopfinger, 1987).

3.1.5 Scales of the Turbulent Scalar Field

The dimensional analysis discussed thus far characterizes turbulent motions using quantities influencing the evolution of turbulent kinetic energy. These being the quantities of (2.23) (i.e., k , ϵ , ν , and S) and the buoyancy frequency, N . While N does not explicitly appear in (2.23), its inclusion in the analysis is intuitive because it represents the external influence of stratification. Because (2.23) is essentially a result of momentum conservation, the scales derived from its quantities describe the mixing of momentum. An alternative is to characterize turbulent eddies through examining how the scalar field is responding to turbulence of the velocity field.

When the scalar of interest is density, there is a coupling of the momentum and scalar dynamics due to buoyancy effects. These effects act in the vertical direction, so particular interest is given to the scales of turbulent overturns, where an overturn can be thought of as the vertical component of an eddy that lifts heavy fluid above light. A commonly accepted measure of overturning is the length scale proposed by Ellison (1957),

$$L_E = \frac{\langle \rho'^2 \rangle^{1/2}}{\partial \bar{\rho} / \partial z}, \quad (3.17)$$

where ρ' is the turbulent density fluctuation about the some mean background density, $\bar{\rho}$, that varies with depth³. L_E may be thought of as a statistical measure of the vertical distance traveled by fluid parcels before returning toward an equilibrium position or irreversibly mixing with surrounding fluid. In a statistical sense, L_E is proportional to the largest eddies of the flow (Stillinger et al., 1983).

³From henceforth, overbar notation will denote a quantity of the mean field, while $\langle \rangle$ will denote a spatial or temporal averaging of turbulent quantities.

A closely related scale used in oceans and lakes is the Thorpe length scale, L_T (Thorpe, 1977). The Thorpe scale can be calculated from an observed instantaneous density profile and is a relatively simple and objective measure of large overturns. Discrete density measurements from the instantaneous profile are monotonically sorted to give a gravitationally stable profile. The vertical distance a sample must be moved adiabatically in this process is its Thorpe displacement, δ_T . For the vertical region of interest (e.g., the vertical extent of a turbulent patch), the Thorpe scale is then calculated as the root-mean-square (rms) δ_T for that region given by

$$L_T = \langle \delta_T^2 \rangle^{1/2}. \quad (3.18)$$

The notable difference between the Thorpe and Ellison scales is the meaning of the $\langle \rangle$ operator. Because L_T is typically based on individual vertical profiles of density, a one-dimensional spatial average is taken over a vertical extent. Whereas, a three-dimensional spatial averaging is typically associated with the Ellison scale. Nonetheless, a strong agreement between L_E and L_T has been confirmed in both experiments (Itsweire, 1984) and numerical simulations (Itsweire et al., 1993) for all but the most strongly stratified flows, where internal wave motions influence L_E but not L_T because of the differences in averaging. This is because a lateral component of ensemble averaging in the presence of internal waves will tend to increase $\langle \rho'^2 \rangle$, and thus L_E , from what would be expected from a vertical ensemble alone. Thus, L_E can be biased toward larger values due to non-overturning wave motions, while L_T truly reflects vertical overturns. The bias increases with stratification as internal waves become more prominent relative to overturns.

It can easily be shown that L_E and L_T are equivalent if vertical averaging is used for both $\langle \rho'^2 \rangle$ and $\langle \delta_T^2 \rangle$, and the background and sorted density profiles are equal and uniform. This is done by substituting the first order approximation, $\rho' = (\partial \bar{\rho} / \partial z) \delta_T$, into (3.17).

3.2 Dimensionless Parameters

Dimensional quantities relevant to turbulence (e.g., characteristic length, velocity, or time scales, molecular viscosity, kinetic energy, etc.) can be grouped into dimensionless parameters that explain some aspect of flow behavior. These parameters represent competing forces or processes within a flow and can be used to delineate regimes in a behavior of interest.

3.2.1 Turbulent Reynolds Number

The Reynolds number, $Re = UL/\nu$, is a widely used parameter expressing the competition of inertial forces, $\rho U^2 L^2$, to viscous forces, μUL . Here, U and L are characteristic velocity and length scales for the motions of interest and $\mu = \rho\nu$ is the fluid's dynamic viscosity. In this sense, motions with $Re \gg 1$ are influenced by their own inertia and are relatively free from the dampening effects of viscosity. This is thus a necessary (although not sufficient, as will be shown) condition for turbulence.

The various choices for the characteristic velocity and length scales lead to an array of Reynolds number formulations. If concerned with the mean flow, for example, U may be a free-stream or average velocity while L is set by bounding geometry. The goal here, however, is to characterize the turbulent field so choices for U and L should be based on turbulent scales. That is, $Re = u(l)l/\nu$, where $u(l)$ decreases with l so that Re decreases toward the smallest dissipative scales. With Kolmogorov's reasoning, $Re_\eta = \eta u_\eta/\nu = 1$ implying a cessation of turbulence for scales smaller than η . This is a rather trivial statement that cannot be used to distinguish different turbulent flows. For this, obvious choices become scales of the largest eddies. In an isotropic sense these are $l = L_{k\epsilon}$ and $u(L_{k\epsilon}) = k^{1/2}$. The turbulent Reynolds number is then

$$Re_L \equiv \frac{k^2}{\epsilon\nu} = \left(\frac{L_{k\epsilon}}{\eta}\right)^{4/3} = \left(\frac{T_L}{T_\eta}\right)^2. \quad (3.19)$$

Here we see that Re_L represents a competition between inertia and viscosity, but also the

ratio of large to small scales (Pope, 2000). It therefore becomes clear that highly turbulent flows (i.e., high Re_L) have dramatic scale ranges. Hence the difficulty in achieving direct numerical solutions of the unfiltered governing equations.

An alternative Reynolds number is that based on the Taylor microscale,

$$Re_\lambda = \frac{u_{rms}\lambda_g}{\nu}, \quad (3.20)$$

which is frequently used to describe isotropic turbulence. If the isotropic approximation of (3.8) is used to estimate ϵ , and the flow is assumed unstratified and stationary (i.e., $P \approx \epsilon$), scaling arguments show that

$$Re_\lambda \approx \left(\frac{20}{3}Re_L\right)^{1/2}. \quad (3.21)$$

Furthermore, the relationships between λ_g and the other isotropic scales are shown by Pope (2000) to be

$$\frac{\lambda_g}{\eta} \approx \sqrt{10}Re_L^{1/4} \quad (3.22)$$

$$\frac{\lambda_g}{L_{k\epsilon}} \approx \sqrt{10}Re_L^{-1/2}. \quad (3.23)$$

3.2.2 Turbulent Shear Parameter

The effects that mean shear has on the turbulence can be characterized with the ratio of an inertial time scale of the turbulence, l/u , to the time scale of mean deformation by shear, S^{-1} :

$$S^* = \frac{l/u}{S^{-1}} = \frac{Sl}{u}. \quad (3.24)$$

A large value of S^* , thus indicates that the rate of deformation exceeds the inertial “turn-over” rate of an eddy of size l . In such a case, the eddy would be expected to be anisotropic. Typically, the inertial scaling of Kolmogorov is assumed (i.e., $\epsilon \sim u^3/l$) and the characteristic

velocity is taken as $u \sim q \equiv \sqrt{2k}$ so that the ratio can be formulated as:

$$S^* = \frac{Sq^2}{\epsilon}. \quad (3.25)$$

With this formulation, $S^* \gg 1$ implies a strong, anisotropic influence at the large scales of the flow. Lee et al. (1990) found this parameter to be useful in describing the highly anisotropic structure of turbulence in both homogeneous and wall-bounded DNS simulations. In wall-bounded turbulence, S^* peaks near the wall in the *buffer layer* where the flow is rapidly sheared and production of turbulent kinetic energy greatly exceeds dissipation. In the *logarithmic-layer*, S^* drops to a constant ($S^* \approx 7$) and production balances dissipation (i.e., $P \approx \epsilon$) so that the flow is locally stationary (for the unstratified case). This was shown by Lee et al. (1990) and later in Pope (2000) with the DNS data of Kim et al. (1987). The wind tunnel data of Saddoughi and Veeravalli (1994) indicate that the stationarity requirement, $S^* \approx 7$, holds even in very high-Reynolds number, homogeneous turbulence.

3.2.3 Turbulent Froude Number

In a fashion analogous to the shear parameter, the turbulent Froude number compares an inertial time scale of the turbulence to the time scale imposed by mean stratification, N^{-1} :

$$Fr = \frac{N^{-1}}{l/u} = \frac{u}{Nl}. \quad (3.26)$$

In a sense, the turbulent Froude number compares an inertial velocity, u , to the velocity of gravity perturbations, Nl . Thus, a large Froude number indicates that the flow is primarily influenced by inertial forces, while a low Froude number characterizes strongly stratified flow in which inertial (i.e., turbulent) motions are suppressed by buoyancy.

Many interpretations of the turbulent Froude number exist given due to various interpretations of u and l . For example, the anisotropy of strongly stratified turbulence has led many to differentiate between horizontal and vertical Froude numbers by specifying l to be

characteristic of horizontal or vertical motions, respectively. Using scaling arguments, Billant and Chomaz (2001) argue that, in the limit of very small horizontal Froude numbers (i.e., $Fr_h \rightarrow 0$; strongly stratification), the vertical Froude number approaches unity and the size of vertical motions scales with U_h/N , where U_h is argued to be a characteristic horizontal velocity.

Lindborg (2006) went on to specify that the turbulent horizontal velocity (defined by the inertial scaling $u_h = (\epsilon l_h)^{1/3}$) can be used so that $Fr_h = \epsilon^{1/3}/Nl_h^{2/3}$. In strongly stratified, stationary, shear-free flow, Lindborg argues that Fr_h is an indicator of the ratio of vertical to horizontal inertial scales in the flow (i.e., $l_v/l_h \sim Fr_h$), and that the relationships between the horizontal inertial scale and the Ozmidov scale is $l_v/L_O \sim Fr_h^{-1/2}$. In turn, this implies $l_h/L_O \sim Fr_h^{-3/2}$. Thus, the ratio of vertical to horizontal scales decreases with increasing stratification, and both inertial scales become larger than L_O as stratification increases.

Ivey and Imberger (1991) also used inertial scaling to specify the velocity scale, but used the three-dimensional rms turbulent velocity so that $u_{rms} \sim (\epsilon l)^{1/3}$, where l is assumed to scale with large overturns observed in density profiles and is similar to L_T . Because l is chosen to be a vertical scale, they formulate a sort of vertical Froude number. Their formulation implies $l_v/L_O \sim Fr^{-3/2}$, where the $-3/2$ dependence is a direct result of using the same length scale in both the scaling of velocity and the denominator of the Froude number definition (c.f. $l_h/L_O \sim Fr_h^{-3/2}$ shown by Lindborg (2006)). The use of a vertical length scale to define the Froude number is intuitively appealing because Fr then represents the competition between kinetic energy, represented generally by $u_{rms}^2/2$, and potential energy, represented by $N^2 l_v^2/2$. However, the scaling of Ivey and Imberger (1991) implies $l_v \sim u^3/\epsilon$, which contradicts the notion that the vertical scale should be influenced by buoyancy through dependence on N (Billant and Chomaz, 2001; Lindborg, 2006). Nonetheless, Ivey and Imberger (1991) measure l_v , N , and ϵ , to calculate Fr and a Reynolds number (i.e., $l_v/\eta \sim Re^{3/4}$). Both parameters are then used to characterize mixing, thus allowing for the explicit consideration of both buoyancy and viscous effects relative to inertia.

Alternatively, the velocity scale can be taken to scale with the turbulent kinetic energy so that $u \sim u_{rms} \sim k^{1/2}$, and l is simply some length scale characteristic of large inertial eddies with no specification of direction (Gregg, 1987). Using the inertial scaling for velocity, one can easily show that the turbulent Froude number can be written as:

$$Fr_k \equiv \frac{\epsilon}{Nk} = \frac{N^{-1}}{T_L}. \quad (3.27)$$

In this sense, l is equivalent to the “isotropic potential” scale, $L_{k\epsilon}$.

3.2.4 Gradient Richardson Number

When dealing with flows subjected to both mean shear and stratification, one’s intuition likely favors a parameter that considers the relative strength of these influences. This is, of course, the gradient Richardson number,

$$Ri = \frac{N^2}{S^2}, \quad (3.28)$$

which can be interpreted as the square of the ratio of mean shear to buoyant timescales. Low Ri indicates that the timescale of buoyancy perturbations is larger than that of mean deformation by shear; in other words, deformation due to shear occurs before buoyancy perturbations can have much influence on the flow as $Ri \rightarrow 0$. Conversely, as $Ri \rightarrow \infty$, stratification becomes strong relative to shear, and buoyancy perturbations are of more influence on the flow than deformation by shear.

Conspicuously missing in (3.28) is any reference to the turbulent flow field. That is, direct reference to any inertial scale internal to the turbulent field is missing, making Ri a “global” or “external” parameter. Nonetheless, Ri is a popular parameter for describing turbulence due to its reliance on mean parameters that are relatively easy to measure (compared to inertial scales) - especially in geophysical settings.

Since S acts to promote turbulence through the production term, (2.25), and N acts to remove turbulence through irreversible mixing of density, (2.35), Ri is often used to parameterize the temporal evolution of stratified turbulence. In homogeneous stratified shear-flow experiments, Rohr et al. (1988) found that a critical gradient Richardson number, $Ri = Ri_c \approx 0.25$, demarks the transition from decaying to growing turbulence (i.e., $\partial k/\partial t \approx 0$). For flows of lesser Ri turbulence was found to grow, while higher Ri indicated decaying turbulence. Interestingly, their numerical value for Ri_c matches the theoretical value for marginal stability of a shear layer between inviscid, non-diffusive fluids of different density (Miles, 1961; Howard, 1961).

However, subsequent studies indicate that Ri_c is not a simple constant. Holt et al. (1992) used scaling arguments to show that Ri_c (for stationarity) depends on a turbulent Reynolds number, Re , turbulent shear parameter, S^* , and the molecular Prandtl number, $Pr = \nu/\kappa\rho$. Using DNS of homogeneous stratified shear-flow they went on to show a weak dependence on Pr , but a significant dependence on Re at low values of S^* . Ri_c was found to increase with increasing Re and approached an asymptotic limit near the inviscid theoretical value of Miles (1961). The reasoning provided being that viscous dissipation is less effective in balancing production at high Re ; therefore, increased stratification (i.e., higher Ri_c) is required to control the growth of turbulent kinetic energy.

For high values of S^* , Holt et al. (1992) effectively claim Ri_c to be an irrelevant concept since rapid distortion of the flow by shear prevents nonlinear interaction (i.e., turbulence). However, Piccirillo and Van Atta (1997) and Jacobitz et al. (1997) found a significant dependence of Ri_c on S^* below this rapid-distortion-theory (RDT) limit using experiments and DNS, respectively. In fact, Piccirillo and Van Atta (1997) indicate Ri_c to be more dependent on S^* than on Re for their range of Re . Both studies highlight that Ri_c is an increasing function of S^* for relatively constant Re when the flow is below the RDT limit. They also highlight that Ri_c reaches an asymptotic limit that is near, but slightly less than 0.25. Piccirillo and Van Atta (1997) argue $S^* \sim P/\epsilon$ and, therefore, an increase in S^* can

be interpreted as production becoming more dominant than dissipation. They presume that an increase in stratification, and thus an increased Ri_c , is needed to balance the excess production (presumably through increased diapycnal mixing) and maintain stationarity.

Shih et al. (2000) extended the simulations of Jacobitz et al. (1997) to slightly higher Reynolds numbers, but still $Re_\lambda \sim O(10^1) - O(10^2)$, and again find dependence on S^* , but indicate that the dependency decreases with increasing Reynolds number. For their highest Reynolds number run of $Re_\lambda \approx 90$, they find $Ri_c \approx 0.17$ despite variation in the initial shear parameter, S_0^* , of up to 12. Furthermore, this finding implies the RDT limit increases with increasing Reynolds number.

More recently, Chung and Matheou (2012) performed even higher Reynolds number simulations ($Re_\lambda \sim O(10^2) - O(10^3)$) of *stationary*, stratified shear-flow turbulence. They too found asymptotic behavior of Ri_c toward a value slightly lower than the inviscid limit. Similar to Shih et al. (2000), they did not report an RDT limit despite maximum values of S^* near 12.

As a final note, the data of Piccirillo and Van Atta (1997) and Chung and Matheou (2012) indicate stationary runs in the unstratified limit (i.e., $Ri_c \rightarrow 0$) are associated with $S^* \approx 7 - 8$. This happens to be in agreement with the stationary value found for high-Reynolds number, unstratified turbulence in the wind tunnel of Saddoughi and Veeravalli (1994) and the log-layer of unstratified channel flow (see Pope, 2000).

3.2.5 Buoyancy Reynolds Number

In studies of stratified flows, a good deal of research has been done in investigating the collapse of turbulence due to the combined dampening effect of buoyancy and viscosity. Seminal work by Gibson (1980) defined a theoretical criterion for collapse of “active” turbulence as the point at which the strain rate of the smallest eddies, $\gamma \sim u_\tau/\eta = \tau_\eta^{-1} = (\epsilon/\nu)^{1/2}$, becomes less than the rate of dampening due to buoyancy, N . Thus, he states that active turbulence in a stratified fluid ceases if the dissipation rate is below some critical value,

i.e., if $\epsilon < 30\nu N^2 = \epsilon_c$, where the particular constant of proportionality is derived from an assumption of local isotropy and $Ri = 0.25$ at the dissipative scales. Gibson argues that when $\epsilon \leq \epsilon_c$ turbulence has collapsed, and fluctuations observed in the scalar field represent “fossilized turbulence” from a past mixing event (Gibson uses a jet contrail as an example of fossil turbulence). The experimental work of Stillinger et al. (1983) and Itsweire et al. (1986), wherein towed grids are used to generate a sudden turbulent event, are in approximate agreement with Gibson’s theory. These studies found $\epsilon_c \approx 25$ and 15, respectively. Interestingly, the grid tow experiments of Rohr et al. (1988) reveal similar results even when shear is present. In light of these findings the intensity of the turbulence is frequently given by:

$$Re_b = \frac{\epsilon}{\nu N^2}. \quad (3.29)$$

This parameter has also been evoked to describe local isotropy. Analogous to Corrsin’s criterion of $S(\nu/\epsilon)^{1/2} \ll 1$ in unstratified shear flow, it can be argued that $N(\nu/\epsilon)^{1/2} \ll 1$, i.e., $Re_b \gg 1$ is needed for local isotropy in stratified turbulence. Since $Re_b = (L_O/\eta)^{4/3}$, local isotropy is seen to depend on a sufficient separation between the smallest scale and the largest scale for which buoyancy effects are minimal. Gargett et al. (1984) used measurements of tidal flows over an estuarine sill to imply that $Re_b > 200$ (i.e., $L_O > 50\eta$) is required for local isotropy at the dissipative scales, while $Re_b > 43000$ (i.e., $L_O > 3000\eta$) is needed for the existence of an inertial subrange. As one would expect, these values are larger than those required for the turbulence to simply be “active”.

As popular as Re_b is among researchers of stratified turbulence, it is a non-unique parameter in that it considers the relationship that inertia has with *both* viscosity and buoyancy. For example, Re_b is often considered a sort of buoyancy Reynolds number because of the reference to inertial and viscous effects (see Gibson, 1987; Smyth and Moum, 2000), while others interpret this parameter as a small-scale Froude number in that it compares a (supposedly) inertial scale in γ^{-1} , to a buoyancy scale in N^{-1} (e.g., Luketina and Imberger, 1989;

Ivey and Imberger, 1991). This non-unique nature is clear by restating the parameter as

$$Re_b = Fr_k^2 Re_L. \quad (3.30)$$

Clearly, high values of Re_b can imply either (1) high Reynolds number (strong turbulence) or (2) high Froude number (weak stratification). The non-uniqueness was pointed out by Gargett (1988) using scaling arguments. She goes on to imply that Re_b scales with the square of a Froude number when Reynolds number is low, but should scale directly with Reynolds number when that parameter is high.

Yamazaki (1990) also highlighted the non-unique nature of Re_b and showed oceanic data that agree with the arguments of Gargett (1988). Specifically, that $Re_b \sim Re_L$ for large values of Re_L (i.e., $Fr_k \rightarrow 1$), while Re_b also depends on Fr_k when Re_L is low. He goes on to conclude that it is the low-Reynolds number case in which Re_L and Fr_k from oceanic data are comparable to the laboratory experiments of Itsweire et al. (1986). He specifically cautions using Re_b to scale laboratory results to oceanic predictions when $Re_b > O(10^2)$. Beyond this limit, high laboratory values of Re_b are likely due to weak stratification (i.e., high Fr_k) rather than strong turbulence; laboratory data is limited to case (2) above, while ocean data may fall under case (1).

As with laboratory experiments, DNS also suffer from practical limitations on Reynolds number. Brethouwer et al. (2007) used artificially forced (i.e., shear-free but stationary) DNS to show that turbulent structures are absent for $Re_b < 1$, but admit that the dynamics of geophysical flows at high Re_b are difficult to simulate because those flows fall into a regime of low Froude number *and* high Reynolds number.

3.2.6 Shear Reynolds Number

Corrsin's criterion of $S(\nu/\epsilon)^{1/2} \ll 1$ for local isotropy in unstratified shear flow was reviewed in section 3.1.3 and mentioned in parallel to Gibson's criterion of $N(\nu/\epsilon)^{1/2} \ll 1$

for stratified flow. In turn, one can formulate a shear Reynolds number as

$$Re_s = \frac{\epsilon}{\nu S^2} \sim S^{*-2} Re_L. \quad (3.31)$$

Since $Re_s = (L_C/\eta)^{4/3}$, the arguments of Corrsin (1958) can be restated. Specifically, local isotropy demands a sufficient separation between the smallest scale, η , and the largest scale for which shear effects are minimal, L_C . While Re_s may be a worthy parameter in this context (assuming stratification is absent), it suffers from a lack of uniqueness as does Re_b because it combines two more fundamental parameters.

3.3 Mixing

3.3.1 Relevance to Numerical Modeling

In numerical modeling of mesoscale flows of the ocean and atmosphere, the turbulent mixing (i.e., fluxes) of momentum and density are considered subgrid-scale process and, as such, often parameterized in terms of eddy diffusivities using equations (2.20) and (2.21). In turn, however, the eddy diffusivities, K_m and K_d , must be specified. In the case of neutral stratification (i.e., density is considered a passive scalar), a multitude of closure models exist to describe K_m . The most common of these being those of two-equation form such as variations of the k - ϵ model (see Durbin and Reif, 2001). Once K_m is estimated, K_d is typically obtained through a turbulent Prandtl number, $Pr_t = K_m/K_d$, that is often considered of order unity for neutral stratification. Stratification, however, complicates matters. Early work of Munk and Anderson (1948) provided empirical corrections for both K_m and K_d when stratification is active using the gradient Richardson number, Ri . The current “industry standard” closure model by Mellor and Yamada (1982) also depends on Ri . Ri -based parameterizations are popular because Ri is composed of external, or grid-scale variables in N and S . However, discrepancies among such works hint at over simplification when

stratification is strong (i.e., high Ri). For example, an Ri -based parameterization of Pr_t by Peters et al. (1988) indicates asymptotic behavior in strongly stratified turbulence, while that of Venayagamoorthy and Stretch (2010) indicates an unbounded increasing of Pr_t with Ri . Understanding how to properly parameterize turbulent mixing remains a gap in the current knowledge base.

3.3.2 Diapycnal Mixing

Apart from their importance to numerical modeling, eddy diffusivities are valuable for characterizing the “state” of geophysical turbulence. In oceanic settings where stable stratification is dominant, vertical eddy diffusivity of density has become a primary diagnostic of turbulent mixing and is key to understanding large-scale ocean circulation (Thorpe, 2005). In essence, the vertical mixing of density by turbulence requires a local vertical flux of fluid across a horizontal density surface, or isopycnal, followed by molecular diffusion of density (i.e., salt and/or heat) between the fluxed fluid and that at the new elevation. Once molecular diffusion has taken place, the mixing is considered “irreversible” or “diapycnal”. This is fundamentally different than advective transport or “stirring” due to non-turbulent internal wave motions; while passage of an internal wave indeed causes a vertical flux of fluid, a lack of turbulence prevents the sharp gradients needed for diffusion of density across an isopycnal. Rather, the isopycnal is locally perturbed but returns to its original elevation without any true mixing.

This processes can be described using the evolution equations for turbulent kinetic (2.23) and potential energy (2.34). The initial flux of otherwise stably-stratified fluid is represented in a negative buoyancy flux, B , that temporarily increases turbulent potential energy at the expense of turbulent kinetic energy. The mixing becomes irreversible if the new turbulent potential energy is then converted to background (i.e., mean) potential energy by way of ϵ_{PE} . If the initial flux is due to non-turbulent internal wave motions, ϵ_{PE} is negligible and buoyancy flux becomes positive as fluid returns to its original position without mixing.

Because the gradient-diffusion hypothesis definition of K_d described by (2.21) involves a density flux that can be either positive or negative, there is no way to distinguish between irreversible and reversible contributions if only the flux, $-\langle w\rho'\rangle$, is measured. As an alternative, vertical diffusivity of density is often referred to in terms an irreversible form derived from the homogeneous, steady state formulation of the density variance equation (2.32):

$$0 = -\langle w\rho'\rangle\frac{\partial\bar{\rho}}{\partial z} - \epsilon_\rho, \quad (3.32)$$

which upon substitution of (2.21) becomes

$$K_d^* = \frac{\epsilon_\rho}{(\partial\bar{\rho}/\partial z)^2}. \quad (3.33)$$

Note that the superscript is used to distinguish K_d^* as an irreversible diapycnal diffusivity that is different from the flux-based formulation. Although (3.33) was derived from a steady state assumption, it remains valid for evolving flows per the arguments of Winters and D'Asaro (1996) and Venayagamoorthy and Stretch (2006).

In many oceanic flows the diffusivity of density, K_d^* , is nearly equal to that of heat, K_T^* , thus

$$K_T^* = \frac{\chi}{2(\partial\bar{T}/\partial z)^2} \quad (3.34)$$

is often used in lieu of (3.33), where $\chi = 2\kappa_T\langle(\partial T'/\partial x_i)^2\rangle$ is the analogue of ϵ_ρ and represents the rate of diffusive smoothing of temperature fluctuations. Here, κ_T is the molecular diffusivity of heat and T' is the turbulent temperature fluctuation. This formulation was originally presented by Osborn and Cox (1972) and is appealing to oceanographers because it consists of conventionally measured quantities.

3.3.3 Mixing Efficiency

One can also arrive at formulations for vertical diffusivities using the steady-state, homogeneous turbulent kinetic energy equation:

$$0 = -\langle ww \rangle \frac{\partial \bar{U}}{\partial z} - \frac{g}{\rho_0} \langle w \rho' \rangle - \epsilon. \quad (3.35)$$

Substitution of the turbulent viscosity hypothesis, (2.20), yields

$$K_m = \left(\frac{1}{1 - R_f} \right) \frac{\epsilon}{S^2}, \quad (3.36)$$

while substitution of the gradient diffusion hypothesis, (2.21), yields

$$K_d = \left(\frac{R_f}{1 - R_f} \right) \frac{\epsilon}{N^2}, \quad (3.37)$$

(Osborn, 1980), where R_f is the flux Richardson number defined by

$$R_f \equiv \frac{-B}{P}. \quad (3.38)$$

The flux Richardson number represents the fraction of turbulent kinetic energy doing work against gravity (i.e., vertical flux of density) versus the total being produced. In this sense, R_f represents the efficiency of mixing. An alternative representation of mixing efficiency is

$$\Gamma \equiv \frac{-B}{\epsilon} = \frac{R_f}{1 - R_f}, \quad (3.39)$$

which effectively compares the two mechanism through which turbulent kinetic energy is lost. High values of Γ indicate that a large amount of the ambient turbulent kinetic energy is being converted into turbulent potential energy versus being lost to heat.

Per the discussion above, it is important to note that the reversible nature of B due to internal wave motions may lead to misleading values of R_f or Γ if one is interpreting these quantities as a mixing efficiencies. These coefficients are truly mixing efficiencies only if the turbulent potential energy created via $-B$ is irreversibly converted to background potential energy via ϵ_{PE} . Alternative irreversible formulations given by Venayagamoorthy and Stretch (2010) are:

$$R_f^* = \frac{\epsilon_{PE}}{\epsilon + \epsilon_{PE}} \quad (3.40)$$

and

$$\Gamma^* = \frac{\epsilon_{PE}}{\epsilon}. \quad (3.41)$$

Substituting (3.40) into (3.37) recovers the irreversible, or diapycnal density diffusivity of (3.33). Thus,

$$K_m^* = \left(\frac{1}{1 - R_f^*} \right) \frac{\epsilon}{S^2} = (1 + \Gamma^*) \frac{\epsilon}{S^2} \quad (3.42)$$

and

$$K_d^* = \left(\frac{R_f^*}{1 - R_f^*} \right) \frac{\epsilon}{N^2} = \Gamma^* \frac{\epsilon}{N^2} \quad (3.43)$$

are irreversible formulations and generally valid for non-stationary flows (Venayagamoorthy and Stretch, 2010), although Gregg (1987) warns that such a formulation for K_m is only valid for large values of mean shear, S . For low shear, equation 3.42 may lead to erroneously high values of K_m^* .

3.4 Parameterizations of Mixing

The mixing of density as embodied in K_d (or alternatively K_T) is of critical importance to understanding and modeling geophysical flows, but upon what does mixing depend? That is, how can this quantity be parameterized? Is it constant or does it depend on dimensionless parameters? If the latter, then which dimensionless parameters are relevant? These questions have been the focus of numerous studies since the early 20th century yet remain relevant and

largely unanswered today. This section presents a brief overview of field studies that have directly observed mixing in the ocean and the laboratory and numerical studies that have sought further insight into the underlying physics. Discrepancies between observed and modeled mixing will be discussed.

3.4.1 Oceanic Observations

Prior to extensive measurements of mixing, Munk (1966) proposed that the vertical eddy diffusivity of heat in the abyssal (i.e., far from boundaries) ocean should be $K_T \approx 10^{-4} m^2 s^{-1}$ based on a simple one-dimensional advection-diffusion equation and global estimates for vertical temperature gradient and upwelling velocity. This value is 1000 times greater than the molecular value, implying that large-scale ocean currents must be driven by mechanical processes of heat transfer, i.e., turbulence. Munk’s work spawned a generation of research investigating the nature and sources of this turbulence.

The advent of “microstructure” (MS) instrumentation in the early 1970’s (e.g., Osborn, 1974) was a major breakthrough in that it allowed observationalists to test Munk’s theory and canonical value of vertical diffusivity. Still widely used today, MS techniques allow for the measurement of small-scale velocity gradients needed for estimation of ϵ required by (3.37) as well as small-scale temperature gradients needed for estimation of χ required by (3.34). Since density is dominantly a function of temperature in the ocean, this gives oceanographers two methods of estimating K_d provided some knowledge of R_f (or Γ) exists⁴.

The behavior of mixing efficiency, frequently represented by R_f or Γ has received a great deal of attention because of its relation to diffusivity, but also because it is a non-dimensional embodiment of a fundamental aspect of mixing. Furthermore, Wunsch and Ferrari (2004) point out that the efficiency at which energy is transfer from large-scale tidal forcing to small-scale turbulence is critical to understanding *global* energy budgets! Early theory of

⁴In theory, one could of course estimate K_T or K_d by directly measuring fluxes; however, this method is not frequently used due to the reversible nature of the fluxes and the inhomogeneous nature, or “patchiness”, of oceanic turbulence (Ivey et al., 2008)

Ellison (1957) suggests that mixing efficiency of turbulence is limited to a maximum value of $R_{f,crit} \approx 0.15$. Subsequently, laboratory measurements by Britter (1974) suggest similar values, $R_{f,crit} \approx 0.18 - 0.2$. A critical value less than unity is quite intuitive if one considers that turbulent kinetic energy can be dissipated to heat via all three directional components but to potential energy (i.e., mixing) only via the vertical component. Values of R_f or Γ beyond critical values may be possible but indicate too much energy is going into buoyancy flux and turbulence must be suppressed (Osborn, 1980).

This early theory has been tested extensively by way of oceanic measurements starting, most notably, with the work of Osborn (1980). Osborn used MS data from various oceanic settings to show that $\Gamma \approx 0.2$ (i.e., $R_f \approx 0.15$) indeed appears to be an upper limit on mixing efficiency and, thus, $K_d \leq 0.2\epsilon/N^2$ seems reasonable. Oakey (1982) went on to explicitly show that a formulation for Γ can be achieved by equating (3.34) and (3.37) to give

$$\Gamma \approx \frac{\chi N^2}{2\epsilon(\partial\bar{T}/\partial z)^2}. \quad (3.44)$$

Using this formulation and MS measurements off the coast of Scotland, Oakey (1982) reported an average mixing efficiency of $\Gamma = 0.24$, but with a rather large standard deviation of 0.14. Similar observations have been made by many others (e.g., Gregg et al., 1986; Peters and Gregg, 1988; Moum, 1996) that all indicate $\Gamma \approx 0.2$ to be a frequently achieved upper bound (see Thorpe, 2005) but that a great deal of variation is possible.

The variation in mixing efficiency below and about its apparent threshold value has garnered much attention. The scaling arguments of Gargett (1988), for example, suggest that Γ should vary inversely with Re_b when the turbulent Reynolds number is low. Ocean observations by Peters and Gregg (1988), however, are in disagreement, showing relatively constant mixing efficiency over a wide range in Re_b ($10^0 < Re_b < 10^5$); however scatter in the data is high and Reynolds numbers may be large. Others suggest that mixing efficiency is a function of the gradient Richardson number. For example, Mellor and Yamada (1982)

use observations to suggest that R_f increases with the Ri and reaches a constant value for sufficiently high Ri . More recently, Pardyjak et al. (2002) provided data from a stably-stratified atmospheric boundary layer that agree with this trend for $Ri < 1$, but suggest that R_f decreases at sufficiently high Ri after reaching a maximum value $R_f \approx 0.4$ at $Ri \approx 1$.

3.4.2 Experimental and Numerical Studies

More detailed and controlled investigations into the behavior of mixing efficiency have been carried out in both physical experiments and numerical studies. Of particular interest has been the validity of $\Gamma \approx 0.2$ as a maximum efficiency and the dependency of mixing efficiency on various dimensionless parameters, most frequently Re_b and Ri .

The gradient Richardson number, Ri , and the buoyancy Reynolds number, Re_b , are popular parameters in oceanography because the former depends only on mean quantities and the latter can be obtained with microstructure techniques that allow estimation of ϵ . Therefore, most studies focus on the variation of mixing efficiency as a function of these parameters. From a practical standpoint, Ri -based parameterizations are appealing because N and S are mean quantities that are resolved at the grid-scale of numerical models. Let us first consider laboratory and numerical studies that have focused on Ri dependency.

Laboratory investigations on the variation of mixing efficiency with Ri are quite numerous (e.g., Linden, 1980; McEwan, 1983; Britter, 1985; Rottman, 1986; Rohr and Van Atta, 1987; Strang and Fernando, 2001b; Rehmann and Koseff, 2004). Due to practical limitations, however, most of these works involve evolving turbulence and not the stationary case implicit in the assumptions of Osborn and Cox (1972) and Osborn (1980). Furthermore, only Rohr and Van Atta (1987) actually induce homogeneous shear to allow for turbulent growth. All of the other studies mentioned involve grid-generated turbulence that freely decays. Because these studies lack mean shear they effectively formulate a gradient Richardson number based

on velocity and length scales set by initial conditions,

$$Ri_0 = \frac{N^2}{(U_0/L_0)^2}, \quad (3.45)$$

where U_0 and L_0 are the velocity and bar spacing of a the grid (note that such a parameter can be loosely interpreted as an inverse Froude number). Despite their limitations, such studies have formed a basis for the current understating of mixing efficiency so select findings will be quickly reviewed here.

Common to all of these studies is the finding that mixing efficiency increases with the gradient Richardson number for low values of that parameter (i.e., strong shear and weak stratification). This is true regardless of the formulation for Ri (compare Linden (1980) and Rohr and Van Atta (1987)) In this regime, efficiency increases with Ri because increased stratification offers an opportunity for increased buoyancy flux while turbulent intensity is not yet inhibited by the stratification. This general trend is in agreement with the oceanic and atmospheric observations cited above.

In the regime of high Ri (i.e., stable stratification), most studies indicate that mixing efficiency achieves an optimal value when $Ri \sim 1$ before decreasing with further increase in Ri . Using DNS of decaying turbulence, Stretch et al. (2010) imply that the optimal value and the subsequent decrease may be due Prandtl number effects (i.e., due to molecular diffusion) that become important when Reynolds number is small - a general characteristic of both laboratory and DNS flows. They find that, when $Ri_0 > 1$, time integrated (i.e., irreversible) mixing efficiency decreases with increasing Pr . This can be explained with the irreversible formulation for mixing efficiency:

$$\Gamma^* = \frac{\epsilon_{PE}}{\epsilon} = f\left(\frac{\kappa_\rho}{\nu}, \dots\right) = f(Pr^{-1}, \dots). \quad (3.46)$$

For example, at low Reynolds numbers, heat ($Pr = 7$) mixes much more efficiently than salt ($Pr = 700$) because turbulent mixing of heat is augmented by a relatively high contribution

from molecular diffusion. For $Ri < 1$ shear is strong enough to generate sufficient turbulent mixing, thus, Pr effects are negligible even if Reynolds number is low. Clearly, a simple Ri -based parameterization for mixing efficiency does not capture the range of behavior due to low Reynolds number.

As an alternative to Ri , Re_b has emerged as an alternative parameter to describe mixing due to its popularity within the oceanography community. Barry et al. (2001), for example, used grid-tow experiments of an un-sheared saltwater bath to investigate the behavior of K_d (based on irreversible mixing) with Re_b , which they interpret as an intensity parameter. Their data suggests that mixing efficiency *decreases* with *increasing* Re_b in an “energetic” regime where $Re_b > 300$. Only for a “weakly energetic” regime of $Re_b < 300$ do they claim mixing efficiency to be constant near the value of Osborn (1980). Here mixing efficiency is seen to depend strongly on Pr as per the discussion above with $\Gamma^* \approx 0.08$ for salt and $\Gamma^* \approx 0.40$ for heat.

Similar result were found by Shih et al. (2005) using DNS that included homogeneous mean shear. They classify a “diffusive” regime for $Re_b < 7$, an “intermediate” regime for $7 < Re_b < 100$, and an “energetic” regime for $Re_b > 100$. They find that diffusivity reaches its molecular value in the diffusive regime, $\Gamma \approx 0.2$ in the intermediate regime, and find that efficiency effectively decreases with increasing Re_b in the energetic regime as did Barry et al. (2001). This remains a puzzling characteristic of both works. Recalling $Re_b = Fr^2 Re$, the reduction in mixing efficiency could be due to either Froude or Reynolds number effects. A lingering question is: what happens in geophysical flows where stratification remains strong (i.e., small Fr) but high Reynolds numbers place the flow in the “energetic” regime of Barry et al. (2001) and Shih et al. (2005)? Does mixing efficiency really decrease in this case?

Ivey and Imberger (1991) investigated the independent effects of turbulent Reynolds and Froude numbers using a compilation of lab data. Their formulations are $Fr = u/NL_C$ and $Re = ul_v/\nu$, where isotropic inertial scaling is used for the velocity scale, $u \sim (\epsilon l_v)^{1/3}$, and l_v is an observed overturning scale. Using a flux-based definition for R_f they show that

this quantity increases with Froude number for $Fr < 1$ and then decreases for $Fr > 1$. An optimal value of $R_f \approx 0.15 - 0.25$ at $Fr \approx 1$ is in agreement with Osborn (1980). The non-monotonic behavior is in agreement with studies involving Ri ; at very low Fr (or high Ri) mixing efficiency is low due to dampening of turbulent flux by stratification, while at high Fr (or low Ri), there is a high capacity for turbulent flux but a lack of density variation to be fluxed. Ivey and Imberger (1991) found that mixing efficiency in the high Froude number regime is independent of Reynolds number provided Re is sufficiently large. For low Froude number, there is considerable scatter in the data that may be due to low Reynolds number effects or internal wave effects since R_f is calculated from buoyancy flux (i.e., reversible). Again, the lingering question is: what happens to mixing efficiency for strong stratification (i.e., small Fr) but high Reynolds number as are found in geophysical flows? Will high Reynolds number flows support $R_f \approx 0.15$ even if stratification is strong? Or, is there some structural mechanism (i.e., Kelvin-Helmholtz billowing discussed next) that prevents Fr from decreasing below unity while the flow remains turbulent?

Specifying mixing efficiency is further complicated by the inhomogeneous and nonstationary nature of natural flows. Such conditions, in fact, violate the popular Osborn-Cox (1972) model of (3.34) and the Osborn (1980) model of (3.37). This shortcoming is pointed out by Ivey et al. (2008) who argue the importance of understanding the “spatial, temporal, and dynamical character of the mixing events themselves” before we can correctly interpret ocean observations. They highlight work by Smyth et al. (2001) who point out that mixing efficiency is function of the specific mechanism driving the turbulence and the temporal evolution of that mechanism. Using DNS, Smyth et al. (2001) focus specifically on the evolution of billow-like structures, known as Kelvin-Helmholtz instabilities, that form on shear layers between fluids of different density. They show that a pre-turbulent phase of $\Gamma \approx 0.8$ precedes a collapse of the billow into three-dimensional turbulence where mixing efficiency falls into agreement with the canonical value of $\Gamma \approx 0.2$. The high efficiency of the pre-turbulent phase is due to a laminar convection. That is, as the billow rolls up, density flux is high, but

ϵ is low because the flow is not yet turbulent. Understanding the signature of such events in microstructure data is key to properly interpreting those data and, thus, understanding mixing in the ocean.

3.5 Overturning

The advent of microstructure techniques to measure ϵ has revolutionized our understanding of oceanic turbulence and the mixing therein via models such as $K_d = \Gamma\epsilon/N^2$ of Osborn (1980). The difficulty and cost of such measurements, however, remains quite high compared to measurements of larger-scale quantities such as N , S , and $\partial\rho/\partial z$. Therefore, there has been considerable effort to indirectly determine ϵ from more easily measurable quantities. The most common method emerged from the work of Dillon (1982) who found apparently linear correlation between the Thorpe overturn scale, L_T , and the fundamental Ozmidov scale, L_O . This apparent agreement implies that the inferred dissipation, ϵ_T , can be determined from

$$\epsilon_T = a^2 L_T^2 N^3, \quad (3.47)$$

where a is an order-one constant of proportionality found empirically to be 0.80 by Dillon (1982). Once a is specified, L_T and N are determined from vertical profiles of density which can be routinely collected from a ship-mounted or bottom-moored conductivity-temperature-density (CTD) profilers. Because $L_T \sim L_O$ has been assumed, (3.47) implies that large scale overturns are fundamentally associated with small scale dissipation. In other words, large overturns are somehow associated with the inertial subrange despite the possibility of large-scale forcing that would violate this condition. Using measurements from the Strait of Gibraltar, Wesson and Gregg (1994) found significant variation in the proportionality constant within the range $0.0625 < a^2 < 16$. This data suggests that a true linear relationship between L_T and L_O may not be universal. Nonetheless, inferring ϵ from overturns remains commonplace in the field of oceanography (e.g., Ferron et al., 1998; Alford et al., 2011).

Using artificially forced (i.e., shear-free but stationary) DNS, Waite and Bartello (2006) suggest that vertical overturns scale more closely with the length scale, u_{rms}/N , than with L_O and that L_O increasingly underestimates overturning with increasing stratification (i.e., decreasing Froude number). This is in qualitative agreement with the scaling arguments of Billant and Chomaz (2001) who also consider strongly stratified, shear-free turbulence. Including the influence of mean shear, Itsweire et al. (1993) performed a DNS study that indicates agreement between the overturning scale, L_E , and L_O occurs for $Ri \approx 0.2$. They too find that L_O underestimates overturning in strong stratification (i.e., large Ri). In weaker stratification (i.e., small Ri) they find the opposite to be true. They do not suggest an alternative predictor of overturning in either regime. Smyth et al. (2001) find that L_O only agrees with the size of overturns shortly after the breakdown of a K-H billow simulated with DNS. They find that overturning, represented by L_T , is in better agreement with $L_b = w/N$, where w is the rms vertical turbulent velocity. The validity of the assumption leading to (3.47) is a major focus of this dissertation and is addressed in chapters 5, 6, and 8.

3.6 Basis for Study

This chapter has presented common length scales, time scales, and dimensionless parameters used to describe geophysical turbulence. Moreover, it has presented a review of relevant literature that references these quantities in descriptions of mixing and mixing efficiency. As such, some knowledge gaps have been revealed. These knowledge gaps correlate strongly with the objectives of chapter 1 and serve as the basis for the current work. More specifically, these gaps are summarized into the following areas:

- An array of length and time scales have been constructed through dimensional analysis; however, physical interpretations of these scales vary. A cohesive presentation of isotropic, sheared, and stratified scales is needed along with meaningful physical interpretations.

- Characterizing large-scale overturning motions in stratified shear flows using fundamental length scales has both fundamental and practical implications, yet agreement between theoretical, experimental, and field studies is lacking. Further investigation into the nature of overturning in both experimental and natural flows is needed.
- Many dimensionless parameters with various formulations have been proposed to explain the phenomena of turbulence under the influence of mean shear and/or stratification; however, no unifying framework exists. A fresh approach at dimensional analysis tempered by physical reasoning is needed to provide a concise, yet comprehensive set of parameters.
- An array of parameterizations for mixing have been proposed based largely on low Reynolds number experiments and numerical simulations. Many of these rely on a single parameter to describe efficiency. In light of the multiple parameters relevant to stratified shear-flow turbulence, a more holistic description of mixing efficiency is needed for the improvement of mixing predictions.

Chapter 4

Dimensional Analysis

This chapter represents a coherent and comprehensive presentation of the fundamental scales and parameters relevant to the rest of the dissertation. Some scales presented in chapter 3 will be revisited and less common scales will be introduced. Dimensionless parameters will be formulated using dimensional analysis. The formulations used here will be related to those already presented in chapter 3. The first section is a thorough discussion of the dimensionless parameters and scales of unstratified shear-flow turbulence that will set the stage for an analogous discussion of shear-free stratified turbulence in the second section. Shear and stratification will be considered separately to provide a basis for the work of chapter 6 that focuses on the combined effects of these two “forcing” mechanisms.

4.1 Unstratified Shear-Flow Turbulence

It is well known that a key characteristic of turbulent flows is the range of length, time, and velocity scales present in the flow. Classically, the quantities employed to define these scales, and thus the “state” of turbulence, are the turbulent kinetic energy, k , the dissipation rate of turbulent kinetic energy, ϵ , and the kinematic viscosity of the fluid, ν . These three quantities can be combined to define the well known length scales, $L_{k\epsilon}$ and η , and the time scales, T_L and T_η , that characterize the canonical case of homogeneous isotropic turbulence (Kolmogorov, 1941). While foundational to our understanding of turbulence, Kolmogorovian theory is incomplete in that it does not consider turbulence’s *raison d’être*: mean shear. Shear acts not only to produce k , via the production term of (2.23), but also to induce anisotropy at the larger scales of the flow. Clearly then, S should be included as a relevant quantity in construction of dimensionless parameters, length, and time scales. Accordingly,

Corrsin (1958) suggests that S should be considered along with the the three classic quantities of isotropic turbulence for a more general characterization that includes the additional length scales L_C and $L_{\nu S}$ and the time scale S^{-1} . In what follows, isotropic and shear scales will be revisited and their physical relevance in the context of the energy cascade process will be discussed. For the interested reader, the physical relevance of the various scales and parameters will be discussed in the context of boundary layer turbulence in appendix A.

4.1.1 Isotropic Scales Revisited

4.1.1.1 Classical large scales, $L_{k\epsilon} = k^{3/2}/\epsilon$ & $T_L = k/\epsilon$

The classic theory of Kolmogorov was strictly intended to describe the smallest scales of the flow where the assumption of isotropy is reasoned to hold. In the absence (or neglect) of other large scale quantities, consideration for total kinetic energy, k , as a fundamental quantity allows for an extension of this theory to large-scale descriptions. Strictly speaking, the large eddy size should scale with bounding geometry or some anisotropic mechanism of the mean flow, but a “backdoor” approach to describe the large eddies would be to first define large velocity, u_0 , and time scales, τ_0 , and then back out a length scales using $l_0 = u_0\tau_0$. A natural velocity scale for the largest motions is $k^{1/2}$. A natural time scale would be the eddy turnover time, but this requires an implicit knowledge of the eddy size. Alternatively, the rate at which that energy is being passed down the cascade, \mathcal{T}_0 , can be evoked to define the time scale from $\mathcal{T}_0 \sim k/\tau_0$. Under the assumption that $\mathcal{T}_0 \sim \epsilon$ as per Kolmogorov’s hypothesis, the time scale and length scales become $\tau_0 \sim T_L = k/\epsilon$ and $l_0 \sim L_{k\epsilon} = k^{3/2}/\epsilon$.

At this point, it is interesting to note that in these formulations, the scales appear to be dependent upon the inertial transfer rate, ϵ . Generally, however, they would be independent variables imposed by boundary or mean flow conditions and would, thus, govern the transfer rate (hence the reference to this being a “backdoor” approach). In this sense, $L_{k\epsilon}$ can be considered an “isotropic potential” length scale that may or may not be realized within

the flow depending on presence of other large scale influences such as boundaries or shear. Because the formulation of $L_{k\epsilon}$ assumes a constant down-spectrum transfer rate that is equal to ϵ , $L_{k\epsilon}$ may also be considered the large-scale cut-off of the inertial subrange if mean forcing and physical confinement are absent. T_L can be interpreted as the time needed to inertially transfer the ambient kinetic energy to smaller scales if anisotropic forcing were to be suddenly shut off. If the characteristic velocity is taken as a rotational speed of the large unforced eddies, and $L_{k\epsilon}$ scales like an eddy diameter, T_L can alternatively be thought of as a “turnover time” of the large unforced eddies. More basically, it can be thought of as an inertial time scale that is “internal” to the flow (i.e., free of the “external” influences of boundaries, shear, or stratification).

4.1.1.2 Classical small scales, $\eta = (\nu^3/\epsilon)^{1/4}$ & $T_\eta = (\nu/\epsilon)^{1/2}$

Under the first similarity hypothesis of Kolmogorov, flows of sufficiently high Reynolds number have small scale motions uniquely determined by ν and the rate at which the small scales receive energy. Equating this latter quantity to the dissipation rate, ϵ , is reasonable under the assumption of a constant down-spectrum transfer rate of kinetic energy to the small-scale end of the inertial region. Assuming ν and ϵ are the most relevant quantities for describing small scale motions, the “Kolmogorov” length, time, and velocity scales can be constructed as was shown in section 3.1.2.

The Kolmogorov length scale, η , can be thought of as the scale in the cascade process, denoted by a wavenumber κ_l , at which the eddy-wise inertial time scale $(\kappa_l^3 E(\kappa_l))^{-1/2}$ equals the eddy-wise viscous time scales $(\nu \kappa_l^2)^{-1}$, where $E(\kappa_l) \sim \epsilon^{2/3} \kappa_l^{-5/3}$ is the eddy-wise kinetic energy density (note that this becomes a questionable assumption outside of the inertial subrange). At scales smaller than η , the viscous time scale is less than the inertial, therefore, energy is dissipated before it can be transferred to smaller scales.

4.1.1.3 New sub-Kolmogorov scales⁵, $L_{k\nu} = (\nu^2/k)^{1/2}$ & $T_{k\nu} = \nu/k$

At this point it is worthwhile to take pause and think about the reasoning behind using ϵ to describe the small scales. Viscous dissipation occurs at small scales, so combining ν and ϵ in the fashion above appeals to one's initial sense of reasoning. However, if one considers that small scales adjust to large scale influences, then dissipation rate could be a function of the turbulent kinetic energy present and the imposed large length scale, i.e., $\epsilon \sim k^{3/2}/l_o$. In this sense, ϵ is *dependent* on k , making k the more fundamental parameter. Dimensionally, additional length and time scales can be constructed by combining k and ν . These being

$$L_{k\nu} = \left(\frac{\nu^2}{k}\right)^{1/2} \quad (4.1)$$

and

$$T_{k\nu} = \frac{\nu}{k}. \quad (4.2)$$

Comparing these scales to the traditional small scales, it is easily shown that $\eta = Re_L^{1/4} L_{k\nu}$ and $T_\eta = Re_L T_{k\nu}$. Thus, $L_{k\nu}$ is indeed the smallest length scale if the flow is turbulent (i.e., $Re_L \gg 1$), and eddies of that scale, if they exist, adjust rapidly (i.e., $T_\eta \gg T_{k\nu}$). The remaining issue is, of course, if these scales have physical relevance. This has yet been established in the literature, however, recent studies do show that fluctuations about η exist and that the range between η and the smallest scales increases with Reynolds number (e.g., Schumacher, 2007). The physical relevancy of these scales may lie in characterizing the intermittency about η .

⁵The ideas presented here were proposed in an unpublished report entitled "A new sub-Kolmogorov length scale in turbulent flows" by S K. Venayagamoorthy and L. P. Dasi (2011).

4.1.2 Shear Scales Revisited

4.1.2.1 Large shear scales, $L_{kS} = (k/S^2)^{1/2}$ & S^{-1}

In deriving the isotropic large length scale, $L_{k\epsilon}$, the choice for a velocity scale was limited to $k^{1/2}$. Acknowledgment of mean shear as a relevant parameter, however, allows the formulation of an alternative velocity scale in $u(l) = Sl$. Sl may be conceptualized as the velocity difference (i.e., fluctuation) across an eddy of diameter l in the presence of a mean velocity gradient that scales like S . Unlike the strictly large-scale velocity, $k^{1/2}$, Sl scales with eddy size and can be thought of as an anisotropic contribution to an eddy's overall velocity scale, $k(l)^{1/2} = \kappa_l E(\kappa_l)$ (note that k is the *total* turbulent kinetic energy integrated over all scales of the flow, while $k(l)$ is an eddy-wise turbulent kinetic energy at some scale, l (or κ_l), in the flow). At the largest scales, a reasonable assumption is that characteristic velocity is wholly of anisotropic nature, and thus, a large eddy's characteristic velocity is fully determined by Sl . Thus, $Sl \sim k^{1/2}$. Solving for the eddy size gives the characteristic length scale of the *largest* shear-driven eddies:

$$L_{kS} = \left(\frac{k}{S^2} \right)^{1/2}. \quad (4.3)$$

It is worth noting that the formulation of L_{kS} avoids making any assumptions about energy transfer rate as was necessary in formulating $L_{k\epsilon}$; the time scale of eddies of size L_{kS} is simply determined by the mean flow to be S^{-1} . Thus, L_{kS} is not tied to a description of the inertial subrange. This scale is not widely referenced in the literature, but the recent work of Venayagamoorthy and Stretch (2010) suggests a correlation with the overturning length scale, L_E , that depends on Ri .

4.1.2.2 Corrsin scale, $L_C = (\epsilon/S^3)^{1/2}$

In formulating L_{kS} , the key assumption was that the large-scale characteristic velocity is *fully* determined by Sl . This assumption is reasonable so long as the rate of shearing is far greater than the rate at which energy is inertially transferred to smaller scales. In other

words, the shear time scale, S^{-1} , should be much less than the eddy-wise inertial time scale, $\tau_a(\kappa_l) = (\kappa_l^3 E(\kappa_l))^{-1/2}$. In the down-scale direction, the scale at which this assumption ceases to hold was shown by Corrsin (1958) to be L_C (see section 3.1.3). Since Corrsin assumed $E(\kappa_l) \sim \epsilon^{2/3} \kappa_l^{-5/3}$, the scale also represents the large-scale extent of the inertial subrange. At scales smaller than L_C , there is a tendency toward isotropy as mean forcing by shear becomes less influential with decreasing eddy size (i.e., increasing κ_l). In this range, $u(l) \sim Sl$ is no longer strictly valid. Rather, Sl should be thought of as the anisotropic contribution to an eddy's characteristic velocity.

4.1.2.3 Small shear scale, $L_{\nu S} = (\nu/S)^{1/2}$

Corrsin (1958) implies that the point in the energy cascade where the eddy-wise dissipation time scale, $\tau_c = (\nu \kappa_l^2)^{-1}$, falls below the mean shear time scale occurs at $L_{\nu S}$. At smaller scales, dissipation occurs before mean shear has the opportunity to have any influence. In this sense, shear remains influential (albeit perhaps minor and diminishing) throughout the inertial subrange. It follows that shear-driven production must cease below $L_{\nu S}$.

Alternatively, $L_{\nu S}$ can be thought of as the scale at which the viscous force (per unit mass) acting across an eddy, $u^{*2}/l = (\tau/\rho)/l = (\nu S)/l$, equals the inertial force (per unit mass) due to shear acting across the eddy $(Sl)^2/l$. In other words, the Reynolds number that considers only the anisotropic contribution to an eddy's velocity, Sl , goes to unity: $(Sl)l/\nu \sim 1 \Rightarrow l \sim (\nu/S)^{1/2}$. Interestingly, this is a condition that occurs regardless of ϵ , so $L_{\nu S}$ is not necessarily tied to the inertial subrange.

4.1.3 Dimensionless Parameters

Unstratified isotropic turbulence involves three independent quantities (i.e., k , ϵ , and ν) with two fundamental dimensions (length and time) so that, according to the Buckingham Pi Theorem, a single dimensionless grouping is needed to characterize the physics of the flow. This is, of course, the turbulent Reynolds number, $Re_L = k^2/\epsilon\nu$, discussed in section

3.2.1. Inclusion of S then necessitates an additional grouping in

$$ST_L = \frac{Sk}{\epsilon}, \quad (4.4)$$

which is the ratio of the “internal” inertial time scale, T_L , to the “external” time scale of the forcing, S^{-1} . ST_L is simply half the shear parameter, S^* , previously discussed; however, the formulation of (4.4) will be used herein because it explicitly uses the variable, k .

Two interesting physical insights can be drawn through consideration of the Reynolds number and shear parameter. (1) Turbulence cannot exist for $Re \ll 1$. Reynolds number less than unity implies that the overall inertial transfer rate of energy down the cascade, T_L^{-1} , is greater than the potential rate at which energy can be dissipated through molecular viscosity, T_η^{-1} . Since small-scale dissipative processes rapidly adjust to match large scale inertial supply, this implies a physically impossible condition in a turbulent flow that is reasonably stationary. (2) Anisotropic turbulence cannot exist for $ST_L \ll 1$. This would imply that the inertial transfer rate is much greater than the mean strain rate of the fluid. For such a condition, fluid motions would be influenced predominately by energy supplied from larger scales and not by energy produced as a direct result of shear. Without significant production, turbulence would decay. Conversely, $ST_L \gg 1$ implies that turbulence decays slower than the fluid is strained and will, therefore, grow.

Figure 4.1 represents an enlightening interpretation of the energy cascade process in terms of the six length scales and two dimensionless parameters considered here to be pertinent to shear-flow turbulence. The range in scales at which shear, and thus production, is proposed to be relevant is shown in red, while the range of expected isotropy is shown in blue. Shear is shown to fade in the down-scale direction through the inertial subrange until $L_{\nu S}$ is reached.

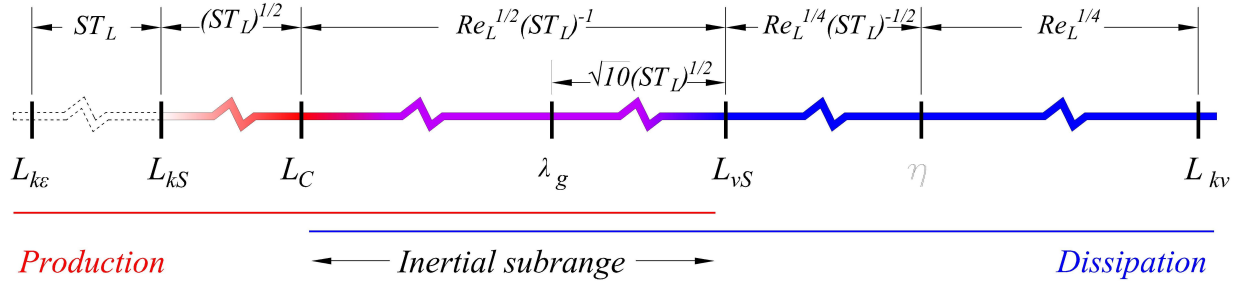


Figure 4.1: Schematic of energy cascade with length scale spectrum for shear-flow. Ratios of subsequent scales are shown in terms of dimensionless parameters. Scale order is shown for the case of all parameters being greater than unity.

Also included in figure 4.1 is the Taylor microscale, λ_g . Placement of this scale is determined from $L_{\nu S}/\eta \sim Re_L^{1/4}(ST_L)^{-1/2}$ and the isotropic relation of (3.22). The exact constant of proportionality in (3.22) is likely influenced by the presence of shear. More importantly, however, is that λ_g is likely larger than $L_{\nu S}$ when shear is relevant.

4.2 Stratified (shear-free) Turbulence

In section 4.1 it was argued that S should be considered along with the classic quantities, k , ϵ , and ν to give a comprehensive description of shear-flow turbulence. When stratification is present, the additional quantity to consider is the buoyancy frequency, N . In this section, scales involving N are interpreted and analyzed in the context of the energy cascade process and overturning motions.

4.2.1 Buoyancy Scales Revisited

4.2.1.1 Large buoyancy scales, $L_{kN} = (k/N^2)^{1/2}$ & N^{-1}

As with inclusion of S , the inclusion of N introduced a new time scale, N^{-1} , and a new velocity scale, Nl . Taking N to be the frequency at which a displaced fluid particle oscillates vertically about its gravitationally-stable position, Nl would scale like the mean vertical

velocity if the particle was displaced vertically some distance l . If l is loosely considered an eddy diameter, Nl is the characteristic velocity of the eddy. This velocity scales with eddy size and can be thought of as the anisotropic component of an eddy's overall velocity scale, $k(l)^{1/2}$. Assuming the largest eddies have characteristic velocities wholly determined by the anisotropic forcing of buoyancy, then $Nl \sim k^{1/2}$. The length scale of these largest eddies of purely stratified turbulence is then

$$L_{kN} = \left(\frac{k}{N^2} \right)^{1/2}. \quad (4.5)$$

As with the formulation of L_{kS} , this formulation makes no assumptions of energy transfer rate. Therefore, L_{kN} is not necessarily tied to the inertial subrange as are $L_{k\epsilon}$ for isotropic turbulence, L_C for sheared turbulence, and L_O of stratified turbulence (discussed next). Using artificially forced (i.e., shear-free but stationary) DNS, Waite and Bartello (2006) suggest that vertical overturns scale closely with the similar length scale, u_{rms}/N .

4.2.1.2 Ozmidov scale, $L_O = (\epsilon/N^3)^{1/2}$

Down-scale of L_{kN} in a fully turbulent flow, Nl no longer fully characterizes eddy velocity below L_O . At L_O , the inertial subrange begins and there is a tendency toward isotropy as large scale forcing due to buoyancy is “forgotten”. In this range Nl is the anisotropic *component* of an eddy's characteristic velocity. L_O is sometimes interpreted as the largest scale possible in a stratified flow instead of L_{kN} . This interpretation is addressed in chapter 5.

4.2.1.3 Small buoyancy scale, $L_{\nu N} = (\nu/N)^{1/2}$

Analogous to $L_{\nu S}$ in shear flow, $L_{\nu N}$ is the length scale at which the viscous time scale, τ_c becomes less than the external forcing time scale. At smaller scales, viscous dissipation occurs too rapidly for buoyancy perturbations to be relevant. This implies that buoyancy

is relevant (albeit minor and diminishing) throughout the inertial subrange. The Reynolds number that considers only the anisotropic component of an eddy’s velocity, Nl , goes to unity at $L_{\nu N}$: $(Nl)l/\nu \sim 1 \Rightarrow l \sim (\nu/N)^{1/2}$.

4.2.2 Dimensionless Parameters

Analogous to shear-flow turbulence, purely stratified turbulence requires Re_L and an additional dimensionless grouping for full description. That additional grouping is typically a turbulent Froude number as discussed in section 3.2.3. The formulation used here is the inverse turbulent Froude number,

$$NT_L = \frac{Nk}{\epsilon}, \quad (4.6)$$

which is the ratio of the internal inertial timescale, T_L , to the external time scale of the forcing N^{-1} . This formulation is used to conform with the formulation of the shear parameter, ST_L . When $NT_L > 1$, anisotropic motions due to gravitational perturbations occur rapidly (i.e., on a short time scale) relative to inertial motions of existing turbulence. Thus, buoyancy effects are strong relative to inertia. Conversely, $NT_L < 1$ characterizes a flow regime where it is inertial motions that are rapid and, thus, act to “smear-out” the motions of slower gravitational perturbations. Anisotropy increases with NT_L .

It can easily be shown that $L_{kN}/L_O = (NT_L)^{1/2}$. Furthermore, NT_L links these two buoyancy scales to the isotropic large scale: $L_{k\epsilon}/L_{kN} = NT_L$, and thus, $L_{k\epsilon}/L_O = (NT_L)^{3/2}$. For strong stratification where $NT_L > 1$, this implies that $L_{k\epsilon} > L_{kN} > L_O$. For the special case of “critical” flow, $NT_L = 1$, all the three length scales equate. The buoyancy length scales are compared in figure 4.2, which also includes the shear scales previously discussed. Each buoyancy scale can be related to its analogous shear scale by some factor of the gradient Richardson number, Ri . It is reasonable to suggest that buoyancy scales assume the roles discussed in this section when Ri is large. Because shear is necessary for sustained turbulence, however, turbulence decays and the energy spectrum collapses if Ri

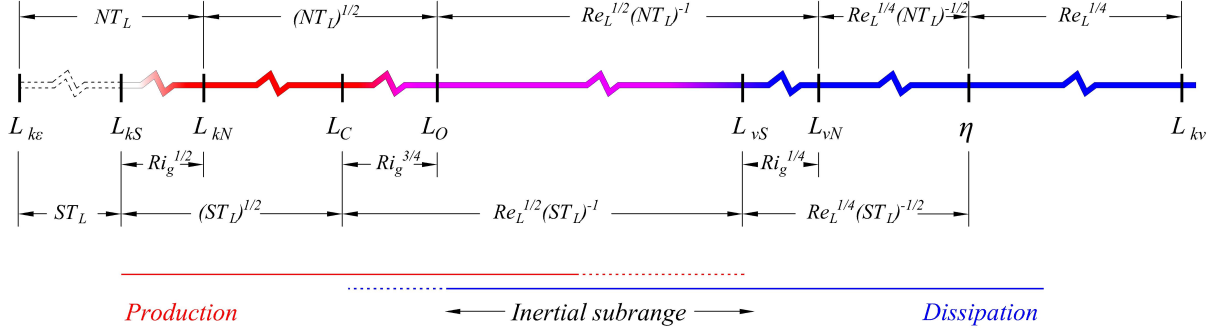


Figure 4.2: Schematic of energy cascade with length scale spectrum for stratified shear-flow. Ratios of subsequent scales are shown in terms of dimensionless parameters. Scale order is shown for the case of all parameters being greater than unity.

becomes much larger than its critical value. When Ri is small, it is the shear scales that are physically relevant to the energy cascade process (e.g., L_O is the upper scale of the inertial subrange for $Ri \gtrsim 1$, while L_C assumes this role for $Ri \lesssim 1$).

The “activity parameter” or buoyancy Reynolds number, $Re_b = \epsilon/\nu N^2$ is another popular dimensionless parameter and was discussed extensively in section 3.2.5. In this discussion, the ambiguity of Re_b is pointed out; it represents the effects of inertia relative to the *combined* dampening effects of buoyancy and viscosity. This becomes clear when formulating the activity parameter in terms of its more fundamental constituents,

$$Re_b = Re_L(NT_L)^{-2}. \quad (4.7)$$

When parameterizing aspects of the flow (e.g., mixing efficiency) on Re_b alone, care should be taken to ensure that observed trends are not dependent on trajectory through an $NT_L - Re_L$ parameter space. Otherwise, Re_b based parameterizations should be qualified with accompanying valid ranges of Re_L and/or NT_L .

4.3 Summary

The scales and parameters formulated in this chapter will be relied upon in those that follow. The next chapter will focus on the scales of overturns in stratified turbulence in the absence of shear so that the role of stratification can be isolated.

Chapter 5

Overturning in Stably-Stratified Turbulence⁶

5.1 Introduction

A relatively simple and objective measure of large-scale vertical overturns in turbulent oceanic flows is the Thorpe length scale, L_T (Thorpe, 1977). Beyond its ability to indicate vertical eddy size from density profiles, however, L_T is of limited use in more fully characterizing turbulence unless some relationship with fundamental quantities of the flow can be determined. In stably-stratified turbulence, these fundamental quantities include turbulent kinetic energy, k , dissipation rate of turbulent kinetic energy, ϵ , buoyancy frequency, N , mean shear rate S , and molecular kinematic viscosity, ν . Dougherty (1961) and Ozmidov (1965) originally suggested the length scale constructed from ϵ and N should indicate the size of the largest eddy unaffected by buoyancy in stratified turbulence — this, of course being the well-known Ozmidov length scale, $L_O = (\epsilon/N^3)^{1/2}$. Subsequent interpretations of this early work popularized L_O as an outer limit on eddy size for a given level of turbulence, as reflected by ϵ , acting against a stably-stratified background density profile, reflected in N , and thus should be related to L_T (e.g., Thorpe, 1977; Dillon, 1982). In this light, L_O has become the preferred fundamental counterpart to the directly measured L_T and, therefore,

⁶The research presented in this chapter has been published in *Physics of Fluids* under the title, “Relevance of the Thorpe length scale in stably stratified turbulence” (Mater et al., 2013). The publication was awarded the 2014 François Frenkiel Award for Fluid Mechanics by the American Physical Society (Division of Fluid Dynamics). Background information and literature relevant to this chapter are presented again so the chapter may be read as a stand-alone work. The chapter is written in a collective “we” voice to acknowledge collaboration with co-authors. Simon M. Schaad contributed substantially to this effort by running the DNS and providing the data considered herein.

often serves as the critical link between a relatively unsophisticated observation and a fundamental aspect of turbulence embodied in ϵ .

Reliance on a common scaling between L_O and L_T is commonplace in the field of oceanography where direct measurement of ϵ with microstructure profilers is far more difficult than that of density profiles from standard Conductivity, Temperature, Depth (CTD) profilers needed for calculation of N and L_T (see Dillon, 1982; Thorpe, 2005). Accurate inferences of ϵ from vertical density profiles, however, inherently require dissipation at small scales to be in phase with the observed large scale motions at the instant of sampling. In other words, the outer scales of the flow must be directly determining the rate of dissipation at the smallest scales. In this study we use direct numerical simulations (DNS) of decaying stably-stratified turbulence and physical reasoning to argue that this commonly held assumption is only valid for the special case when turbulence and buoyancy time scales are approximately equal, i.e., $NT_L \approx 1$, where $T_L = k/\epsilon$ is the turbulence time scale or turbulence decay time. We can refer to this as the critical case since the turbulent Froude number (discussed later) which is simply given by $(NT_L)^{-1}$ is approximately unity. For flows strongly influenced by buoyancy (i.e., $NT_L > 1$), we argue that an overturn size more truly reflects the instantaneous turbulent kinetic energy and show that L_T more generally agrees with a length scale constructed from this quantity, $L_{kN} = (k/N^2)^{1/2}$. In such cases, the outer scales of the flow are larger than the scale of buoyancy control as set by L_O and, instead, are strongly anisotropic and decoupled from ϵ .

In what follows, we provide a brief discussion of the physical interpretations of the fundamental length scales, describe the generation and sampling of numerical data, and explicitly show the performance of various fundamental length scales in predicting L_T under different levels of stratification. We conclude with a discussion of the theoretical and practical implications of predicting k from measured Thorpe scales and consider our results in the context of other DNS, laboratory, and field studies.

5.2 Relevant Length and Time Scales

Here, we discuss the calculation of the Thorpe scale and the physical interpretations of L_O and other fundamental length scales commonly used to describe stratified turbulence. By combining k , ϵ , N , S , and ν two at a time, one can easily construct nine length scales through dimensional analysis. Because we are only concerned with large-scale motions at sufficiently high Reynolds number, we assume that molecular effects are negligible and, thus, consider only those five length scales that exclude ν .

5.2.1 Thorpe Length Scale

The Thorpe scale can be calculated from an observed instantaneous density profile, such as that provided by CTD measurements in the field. Discrete density measurements from the instantaneous profile are monotonically sorted to give a gravitationally stable profile. The vertical distance a sample must be moved adiabatically in this process is its Thorpe displacement, δ_T . For the vertical region of interest (e.g., the vertical extent of the DNS domain or, in an oceanic setting, the depths just encompassing a turbulent patch), the Thorpe scale is then calculated as the root-mean-square (rms) δ_T for that region given by

$$L_T = \langle \delta_T^2 \rangle^{1/2}, \quad (5.1)$$

where $\langle \rangle$ denotes a spatial average in the vertical. For a more thorough explanation of this process see Thorpe (1977). Further details are also given in Section 3.

A closely related measure of overturning is the Ellison length scale, defined as

$$L_E = \frac{\langle \rho'^2 \rangle^{1/2}}{\partial \bar{\rho} / \partial z}, \quad (5.2)$$

where ρ' is the turbulent density fluctuation about some mean background density, $\bar{\rho}$. L_E may be thought of as a statistical measure of the vertical distance traveled by fluid parcels

before returning toward an equilibrium position or irreversibly mixing with surrounding fluid (Ellison, 1957). For the case when the sorted density profile exhibits a uniform gradient and $\langle \rangle$ represents a vertical ensemble averaging applied to both ρ'^2 and δ_T^2 , L_E is exactly equal to L_T . Agreement between L_E and L_T was confirmed in the grid tow experiments of Itsweire (1984) and the DNS of Itsweire et al. (1993) for all but the most strongly stratified flows. In the runs with highest stratification, it was correctly proposed that L_E became larger than L_T due to the effects of internal gravity waves, despite relatively uniform background (i.e., sorted) density gradients. This may be attributed to differences in the averaging schemes used for $\langle \rho'^2 \rangle$ and $\langle \delta_T^2 \rangle$ in the calculation of L_E and L_T , respectively. Specifically, ρ'^2 was averaged over both vertical and lateral (i.e., temporal under Taylor’s hypothesis) extents, while δ_T^2 was averaged only in the vertical. A lateral component of ensemble averaging in the presence of internal waves will tend to increase $\langle \rho'^2 \rangle$, and thus L_E , from what would be expected from a vertical ensemble alone. Thus, L_E can be biased toward larger values due to non-overturning wave motions, while L_T is free of reversible motions and, therefore, truly reflects vertical overturns. The bias increases with stratification as internal waves become more prominent relative to overturns. We use the traditional three-dimensional averaging scheme to calculate L_E , then use the comparison between L_T and L_E as an indicator of internal wave intensity in the present simulations.

5.2.2 Fundamental Scales

Dimensionally, five length scales can be constructed from k , ϵ , N , and S . Those most common in literature include the turbulent length scale, $L_{k\epsilon} = k^{3/2}/\epsilon$ (Pope, 2000), the Ozmidov length scale, $L_O = (\epsilon/N^3)^{1/2}$ (Ozmidov, 1965), and the Corrsin length scale, $L_C = (\epsilon/S^3)^{1/2}$ (Corrsin, 1958). The remaining two link turbulent kinetic energy to buoyancy frequency and mean shear respectively: $L_{kN} = (k/N^2)^{1/2}$ and $L_{kS} = (k/S^2)^{1/2}$.

Physically, the turbulent length scale, $L_{k\epsilon}$, can be thought to represent the largest eddies present in a flow when the effects of shear or buoyancy are negligible (i.e., isotropic turbu-

lence). This interpretation assumes that such eddies are characterized by the velocity scale, $k^{1/2}$, and inertially transfer kinetic energy to smaller scales at a rate equal to ϵ . The latter assumption stems from the second similarity hypothesis of Kolmogorov (Kolmogorov, 1941) and implies that $L_{k\epsilon}$ should be a measure of the large-scale extent of the inertial subrange given truly isotropic flow.

When mean shear or stratification are not negligible, large-scale motions become increasingly anisotropic and have length scales that depart from the isotropic prediction of $L_{k\epsilon}$. The validity of Kolmogorov's hypothesis and the inertial subrange are then relegated to length scales smaller than L_O or L_C for buoyancy or shear-dominated flow, respectively. The largest eddy for which ϵ is a valid estimate of down-scale energy transfer is then L_O when $Ri > Ri_c$ or L_C when $Ri < Ri_c$, where Ri_c is some critical value of the gradient Richardson number, $Ri = N^2/S^2$, that delineates the two regimes. The associated velocity scales are $(\epsilon/N)^{1/2}$ and $(\epsilon/S)^{1/2}$.

Physical interpretations of the final two fundamental length scales need not rely on any assumptions about the transfer rate of turbulent kinetic energy to smaller scales and, therefore, are not concerned with ϵ . Rather, the focus remains on k . The only argument needed to bring physical significance to these scales is that their characteristic velocities are set by $k^{1/2}$ with corresponding time scales given by N^{-1} and S^{-1} , respectively. In this sense, L_{kN} and L_{kS} more generally describe large-scale motions in their respective regimes of buoyancy- and shear-dominated flows than their counterparts L_O and L_C .

In this study we focus on buoyancy-dominated turbulence that is free of shear and, therefore, will emphasize the roles played by L_O and L_{kN} in describing overturning motions. Considering the fundamental quantities of interest, the dimensionless parameters needed to characterize such flows are the turbulent Reynolds number, $Re_L = k^2/\epsilon\nu$, and the turbulent Froude number, $Fr_k = \epsilon/(Nk)$. If one considers the turbulent time scale, T_L , the Froude number may be rewritten as $Fr_k = (NT_L)^{-1}$. This alternative formulation explicitly represents the competition of inertial and buoyancy time scales; therefore, we choose to make

reference to NT_L , rather than Fr_k , throughout this chapter. When $NT_L > 1$, motions due to gravitational perturbations occur rapidly (i.e., on a short time scale) relative to inertial motions of existing turbulence. Thus, we will classify this as a “subcritical” regime (i.e., buoyancy effects are strong). Conversely, flow regimes with $NT_L < 1$ will be classified as “supercritical” (i.e., buoyancy effects are weak). In this state, it is the inertial motions that are rapid and, thus, act to mitigate the motions from the slower gravitational instabilities.

It can easily be shown that $L_{kN}/L_O = (NT_L)^{1/2}$. Furthermore, NT_L links these two buoyancy scales to the isotropic large scale: $L_{k\epsilon}/L_{kN} = NT_L$, and thus, $L_{k\epsilon}/L_O = (NT_L)^{3/2}$. For $NT_L > 1$, this implies that $L_{k\epsilon} > L_{kN} > L_O$. For the special case of “critical” flow, $NT_L = 1$, all the three length scales equate.

The turbulent Reynolds number indicates the competition of inertial and viscous forces in the flow and provides a measure of the range of scales present. The latter interpretation is strictly valid for isotropic flow and follows from $Re_L = k^2/\epsilon\nu = (L_{k\epsilon}/\eta)^{4/3}$, where $\eta = (\nu^3/\epsilon)^{1/4}$ is the Kolmogorov length scale. When buoyancy introduces anisotropy, the large scales are limited to values less than the isotropic potential expressed in $L_{k\epsilon}$. What the actual outer scale is remains to be seen and is the subject of the current work.

While NT_L and Re_L are the only parameters needed to fully characterize a purely stratified flow on dimensional grounds, a third parameter that frequently appears in literature is the buoyancy Reynolds number or “activity parameter”, $Re_b = \epsilon/(\nu N^2)$ (e.g., Gibson, 1980; Shih et al., 2005; Stillinger et al., 1983), which may be interpreted as a relative measure of turbulent stirring (i.e., inertia) to combined stabilizing effects from buoyancy and viscosity (Ivey et al., 2008). The utility of this parameter is limited by the inherent ambiguity elucidated in this interpretation. For example, an increase in Re_b could represent increased inertial effects relative to viscosity (increased Re_L) just as it could represent increased inertial effects relative to buoyancy (decreased NT_L). This becomes clear when formulating the activity parameter in terms of its more fundamental constituents, i.e., $Re_b = Re_L(NT_L)^{-2}$. When parameterizing aspects of the flow (e.g., mixing efficiency) on Re_b alone, care should be

taken to ensure that observed trends are not dependent on trajectory through an $NT_L - Re_L$ parameter space. Otherwise, Re_b -based parameterizations should be qualified with accompanying valid ranges of Re_L and/or NT_L .

The activity parameter may be written as $Re_b = (L_O/\eta)^{4/3}$, and thus also indicates the range of scales free from the anisotropic effects of buoyancy. It follows that Re_b describes the full range of turbulent scales only in the special case that L_O coincides with the largest scale of the flow. Obviously, Re_b loses significance (from a physical standpoint) for weakly stratified turbulence ($N \rightarrow 0$) in which L_O far exceeds outer dimensions of the flow.

5.3 Numerical Approach

5.3.1 Set-up

Direct numerical simulations (DNS) were used to simulate decaying homogeneous stably-stratified turbulence without further production (i.e., shear-free turbulence). This idealized condition is akin to a breaking internal gravity wave or other intermittent disturbance leading to turbulence that is isolated from boundaries and free of sustained mean shear. An isotropic energy spectrum is initially imposed, and the resulting turbulence is allowed to subsequently decay free from any other external sourced of kinetic energy. The laboratory equivalent is the grid-tow experiment in which a bi-lateral mesh is towed through a stratified bath.

The numerical simulations performed for this study were carried out using the pseudo-spectral code developed by Riley et al. (1981). This code simulates a flow field that is periodic in all three spatial directions, with a constant background density gradient (since the flow is homogeneous) with a buoyancy frequency $N^2 = (-g/\rho_0)(\partial\bar{\rho}/\partial z)$ (see Riley et al. (1981) and Venayagamoorthy and Stretch (2006) for further details). The turbulence is initialized as a Gaussian, isotropic, solenoidal field with initial length and velocity scales L_0 and u_0 , respectively. The flow domain is a cube with dimensions $\mathcal{L} = 2\pi$ with a 256^3 grid-point resolution. After the first eddy turnover period, $1L_0/u_0$, the dissipation peaks and begins

to decay. We interpret this as a signature of fully developed turbulence. Prior to this time, the statistics are not representative of decaying stratified turbulence and, thus, these initial transients were ignored in this study. The duration of all simulations was $5L_0/u_0$

5.3.2 Parameter Values

The strength of stratification can be characterized by an initial Richardson number defined as $Ri_0 = (NL_0/u_0)^2$. To more specifically investigate temporal variance in flow characteristics, however, we must turn to NT_L . For this work, seven DNS runs were performed with Ri_0 varying from 0.01 to 158. The Prandtl number $Pr = \nu/\kappa_\rho = 1$ in order to ensure accurate resolution of the smallest scales of the density field. During the runs, Re_L varied narrowly around $O(10^3)$, and NT_L varied from $O(10^{-1})$ to $O(10^2)$. The peak value of Re_b varied from $O(10^0)$ to $O(10^5)$.

Using DNS of slightly lower Re_L values ($O(10^1)$ to $O(10^3)$) and a narrower range in NT_L ($O(10^0)$ to $O(10^1)$), Shih et al. (2005) showed that flows could be categorized into three distinct Re_b -regimes based on the behavior of mixing efficiency: a “diffusive” regime where $\epsilon/(\nu N^2) < 7$, an “intermediate” regime where $7 < \epsilon/(\nu N^2) < 100$, and an “energetic” regime where $\epsilon/(\nu N^2) > 100$. Because of the aforementioned ambiguity in Re_b , the universality of these regime limits remains uncertain (e.g., if mixing efficiency were to become independent of viscosity in high Re_L flows typical of the ocean, the intermediate-energetic transition would shift to higher values of Re_b). Nonetheless, we can conceptualize the turbulent state of the current simulations according to the regimes of Shih et al. (2005) and the stratification parameter NT_L .

Turbulent regimes are illustrated in Figure 5.1 where a line at $NT_L = 1$ has been included to tentatively delineate weak ($NT_L < 1$) and strong ($NT_L > 1$) stratification. Recall, weak stratification implies flows that are not affected by buoyancy forces and in the context of these simulations are more or less isotropic, while the converse is true for strong stratification. Quadrant I represents strongly stratified flows at high values of Re_L . Flows in this quadrant

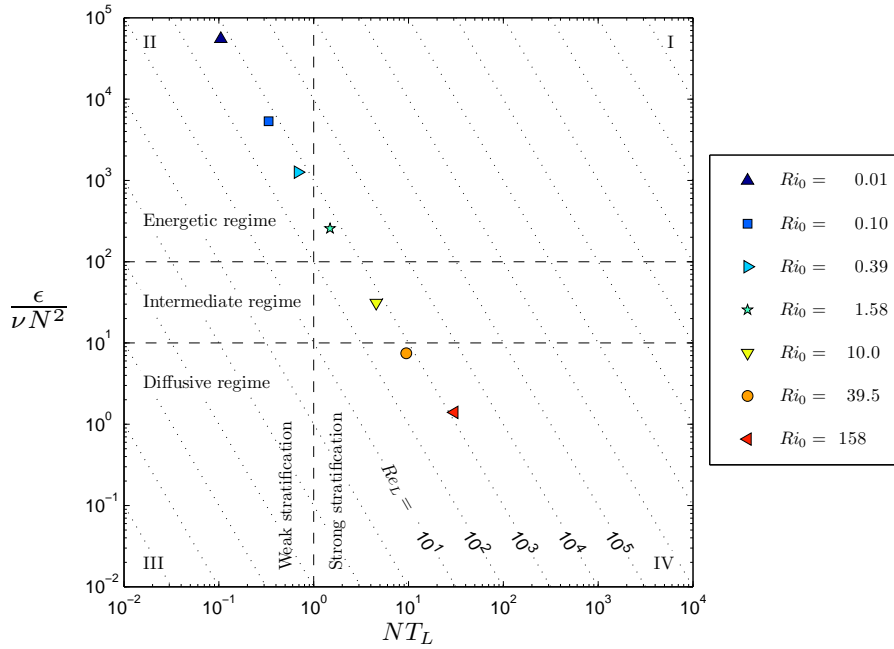


Figure 5.1: Peak Re_b ($\epsilon/(\nu N^2)$) values and corresponding NT_L values plotted over the Re_b regimes defined by Shih *et al.* (2005) and NT_L regimes reported in the current study.

are energetic while at the same time influenced by buoyancy forces. This regime characterizes geophysical flows. Quadrant II represents flows that are energetic but the stratification is weak. In the limit of zero stratification, this regime marks the classical isotropic turbulence limit. Flows in quadrant III are characterized by low Re_L and are considered “diffusive” in that transport of both momentum and scalar occurs dominantly through molecular diffusion as the laminar limit is approached. Flows in quadrant IV are also characterized as “diffusive”, despite higher Re_L values, due to the suppression of turbulence by strong buoyancy effects. The ultimate quest is to understand the physics of strongly stratified energetic flows as denoted by quadrant I. Data points for the current study are barely in the lower end of this range.

5.3.3 Thorpe Sorting

As discussed in Section 5.2.1, the Thorpe scale is calculated by adiabatically sorting density profiles for gravitational stability. Following Smyth and Moum (2000), there are

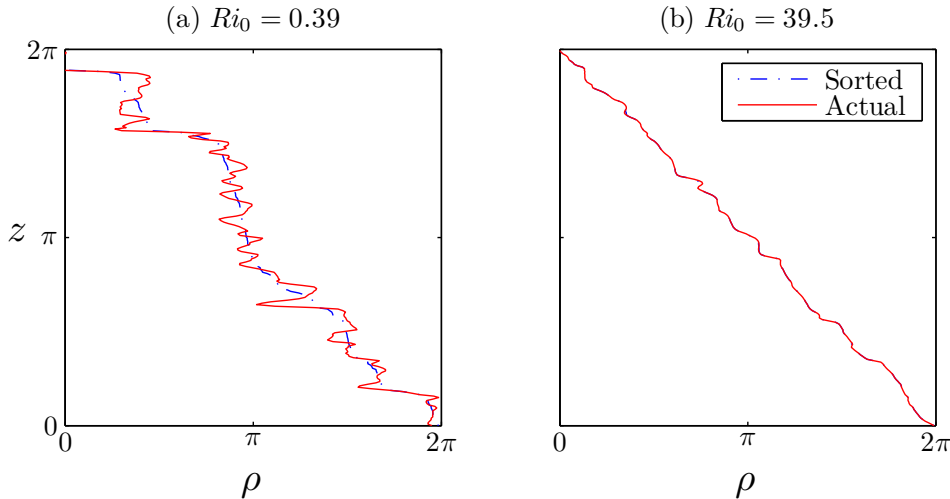


Figure 5.2: Instantaneous and sorted density profiles for; (a) moderate and (b) strong stratification.

two alternative sorting techniques; density is known for all points (x,y,z) in the domain, therefore, we are free to sort values for one-dimensional profiles at each (x,y) or sort the entire domain in a three-dimensional sense as was suggested by Winters et al. (1995).

One-dimensional sorting provides profile-based displacements, $\delta_T = (z - z_{sort})$ for each grid point, where z_{sort} is the depth at which a fluid parcel originating from depth z would be gravitationally stable within a given profile. Typical instantaneous and stable density profiles are plotted in Figure 5.2 for two different strengths of stratification. This figure also illustrates the homogeneous nature of the turbulence and the lack of coherent turbulent patches typical of shear layers, etc. Thus, we are not concerned with identifying vertical regions for Thorpe scale calculations as was done by Smyth et al. (2001). Instead, we treat the entire domain as one turbulent patch. Periodic boundary conditions allow for inclusion of all grid points in these calculations.

In three-dimensional sorting, a fluid parcel is moved to a stable depth relative to all vertical and lateral neighbors and associated with a displacement $\delta_{T3D} = (z - z_{sort3D})$, where z_{sort3D} is the gravitationally stable depth if sorting is also monotonic in the lateral directions (i.e., lateral density gradients are also minimized); thus a parcel's stable position is not

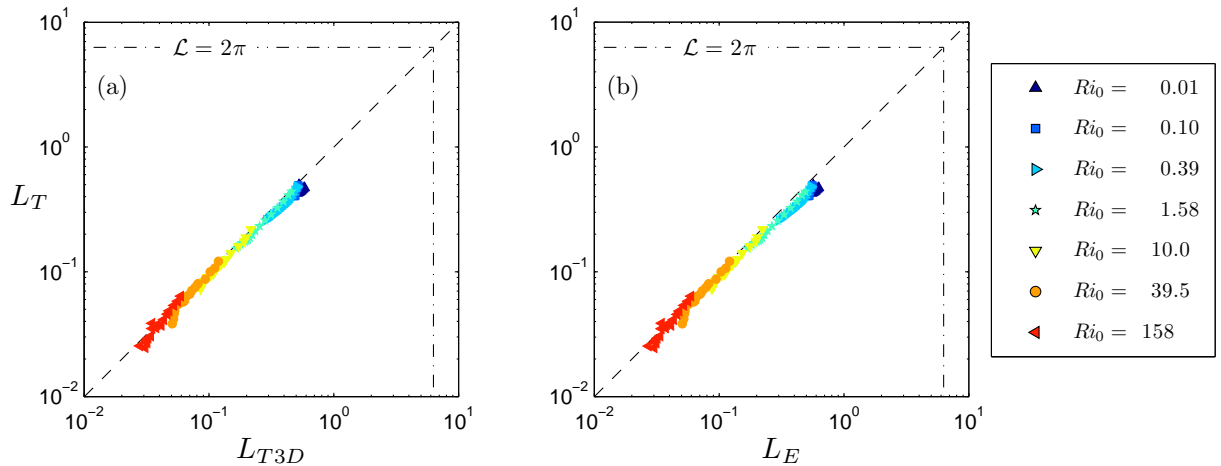


Figure 5.3: One-dimensional Thorpe scale, L_T , versus (a) three-dimensional Thorpe scale, L_{T3D} , and (b) Ellison length scale, L_E . Computational domain extents are indicated by dash-dotted line.

necessarily directly above or below its point of origin. Isopycnal planes of the sorted flow field will be free of internal wave crenulations — the same cannot be said for the isopycnals resulting from one-dimensional sorting.

Once sorting has been performed, the Thorpe scale can be calculated as the rms of either displacement set. Here we distinguish one-dimensional and three-dimensional values as L_T and L_{T3D} , respectively. Because δ_{T3D} can be influenced by non-overturning wave motions (through allowing fluid parcels to be “moved” laterally), L_{T3D} provides a measure of general scalar fluctuations. In contrast, L_T is a specific measure of unstable overturning. As such, $L_T < L_{T3D}$ when internal waves are significant (Smyth and Moum, 2000). The one-dimensional and three-dimensional Thorpe scales are compared in Figure 5.3a. Wave effects appear minimal, even for very stable simulations. An objective of this work is to present practically relevant data to the oceanography community in which field sampling is more analogous to the methods leading to the one-dimensional Thorpe scale. Considering this, and the relatively good agreement between L_T and L_{T3D} , we will refer exclusively to L_T in the rest of this chapter.

5.4 DNS Results

5.4.1 Thorpe vs. Ellison Scales

Prior to investigating fundamental length scales, we first focus on the correlation between the Ellison and Thorpe length scales as a simple check on the nature of the overturns. Figure 5.3b shows excellent agreement between L_E and L_T . The density fluctuations due to non-overturning internal waves appear to be of minimal influence on L_E (see Figure 5.3a).

5.4.2 Thorpe vs. Ozmidov Scales

Following the work of Dillon (1982), the Thorpe scale, L_T , has become a popular predictor of the Ozmidov scale, L_O (or vice versa). Field observations and laboratory experiments imply a linear dependency of the form $L_O = \alpha L_T$ with common estimates of α agreeing with Dillon's value of 0.8 (Itsweire, 1984; Ferron et al., 1998). DNS of stratified turbulence have also revealed correlation between L_O and L_T , but indicate the relationship is nonlinear and perhaps a function of the gradient Richardson number, Ri , (e.g., Itsweire et al., 1993) or a function of overturn age in the case of a shear layer with Kelvin-Helmholtz billows (Smyth and Moum, 2000; Smyth et al., 2001). As shown in Figure 5.4a, we too find a nonlinear dependency between the two length scales for our shear-free simulations. Since the current simulations effectively lack mean shear, the appropriate non-dimensional parameter to further investigate this trend with is NT_L (rather than Ri). Hypothetically, one could also investigate Reynolds number effects; however, the current study is limited to a single order of magnitude range in Re_L (i.e., $O(10^3)$). As such, we implicitly assume Reynolds number independence in the remainder of this discussion.

In Figure 5.4b we see a clear dependence of L_T/L_O on NT_L over possibly two regimes delineated by $NT_L \approx 1$. In the weakly stratified regime ($NT_L < 1$), the size of observed overturns is less than L_O , theoretically indicating negligible influence of buoyancy at the outer scales of the flow. At the regime break L_O becomes smaller than the overturn size,

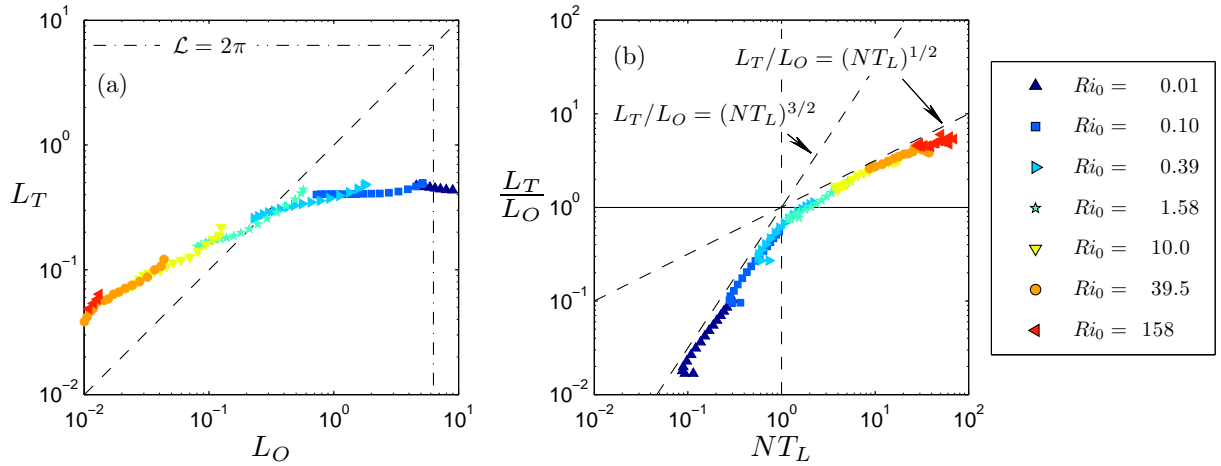


Figure 5.4: Ozmidov length scale, L_O , versus Thorpe scale, L_T : (a) direct comparison, and (b) plotted against the dimensionless stratification parameter, NT_L .

and here we expect an onset of buoyancy control. While the general slope of the data points does decrease in the strongly stratified regime ($NT_L > 1$), it does not completely flatten nor does the ratio of scales go to unity. Thus, contrary to common assertions, the Ozmidov scale does not appear to be the limiting size of overturns in strongly stratified turbulence except for the special case of $NT_L \approx 1$. Beyond this regime break, overturn size continues to increase beyond L_O as a function of NT_L .

5.4.3 Thorpe vs. Turbulent Kinetic Energy Scale

Next, we investigate L_{kN} as an alternative predictor of L_T . Direct comparison is shown in Figure 5.5a. Unlike the Ozmidov scale, L_{kN} shows a strongly linear trend with L_T through all but the three runs with lowest Ri_0 . Further investigation of NT_L dependency is shown in Figure 5.5b. Again, two regimes delineated by $NT_L \approx 1$ are apparent, and L_T is less than the buoyancy-dependent scale in the weakly stratified regime. The ratio, L_T/L_{kN} , however, reaches a constant near unity for the strongly stratified regime. It appears, then, that L_{kN} is a better indicator of overturning events than L_O in buoyancy dominated stratified

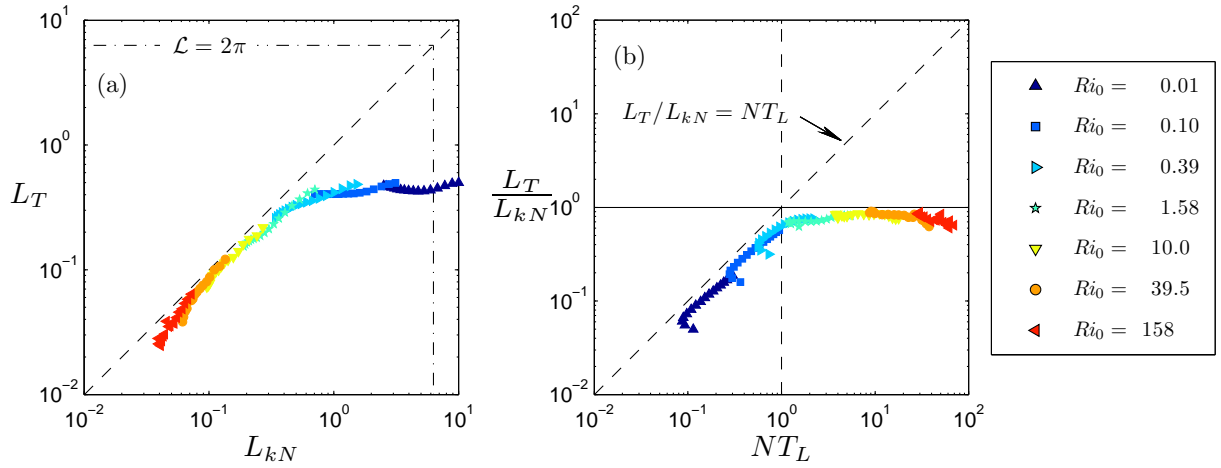


Figure 5.5: Kinetic energy length scale, L_{kN} , versus Thorpe scale, L_T : (a) direct comparison, (b) plotted against the dimensionless stratification parameter, NT_L .

turbulence ($NT_L > 1$). Referring back to Figure 5.4b, this result is reflected in L_T/L_O data closely following the line of $(NT_L)^{1/2}$ for $NT_L > 1$ (cf. $L_{kN}/L_O = (NT_L)^{1/2}$).

5.4.4 Thorpe vs. Isotropic Large Scale

Finally, L_T is compared with the isotropic large scale, $L_{k\epsilon}$, for the main purpose of investigating their relationship in the weakly stratified regime. Direct comparison is given in Figure 5.6a. Clearly, $L_{k\epsilon}$ overestimates L_T in runs of strong stratification, and the discrepancy increases with Ri_0 . In this regime, Figure 5.6b shows that $L_T/L_{k\epsilon}$ data closely follow the line of $(NT_L)^{-1}$. This is a direct result of $L_T \sim L_{kN}$ for $NT_L > 1$ (cf. $L_{k\epsilon}/L_{kN} = NT_L$). Only for weakly stratified runs does there appear to be close correlation. Agreement in the weakly stratified regime is clearly shown in Figure 5.6b, where for $NT_L < 1$, the ratio is near unity.

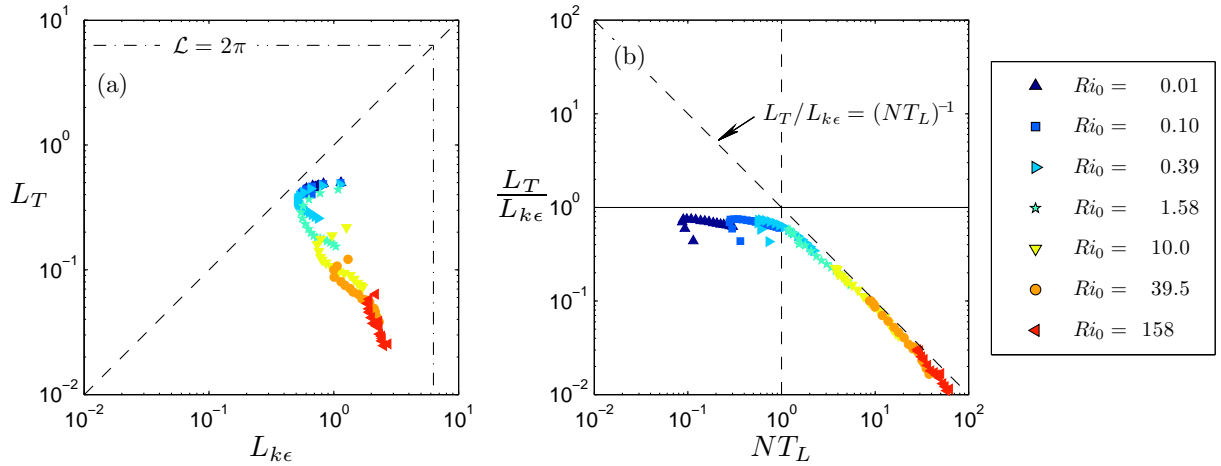


Figure 5.6: Kinetic energy isotropic length scale, $L_{k\epsilon}$, versus Thorpe scale, L_T : (a) direct comparison, (b) plotted against the dimensionless stratification parameter, NT_L .

5.5 Discussion

5.5.1 Physical Interpretations

For strongly stratified turbulence, the lack of correlation between L_T and L_O implies that the rate of dissipation, ϵ , is not fundamental in describing the outer scales of the flow. It should not necessarily come as a surprise that ϵ under-performs in this regard. Recall, the seminal works of Dougherty (1961) and Ozmidov (1965) sought not to determine the outer scale of the flow, but rather to define the largest scale that could remain isotropic in the presence of buoyancy forces (i.e., the large-scale extent of the inertial subrange). This early theory is entirely compatible with the possibility of anisotropic overturns larger than L_O in strongly stratified flows. Such eddies would exist at scales larger than those of the inertial subrange and transfer energy to other scales at rates different than ϵ . In other words, these eddies do not adhere to the second similarity hypothesis of Kolmogorov and, as such, do not have a form determined by ϵ .

Instead, the outer scales of strongly stratified turbulence are more indicative of the total turbulent kinetic energy, k , as implied by the linear relationship between L_T and L_{kN} for $NT_L > 1$. This essentially validates the physical reasoning that the time scale of these eddies scales with N^{-1} , and the velocity goes unequivocally with $k^{1/2}$, not $(\epsilon/N)^{1/2}$. In order for these eddies to exist, N^{-1} must be shorter than the turbulent decay time, T_L (i.e., anisotropic eddies larger than L_O cannot exist if turbulence decays quicker than the eddy can turn over).

In the weakly stratified regime where $NT_L < 1$, the lack of correlation between L_T and L_O is due to the negligible influence of buoyancy. In other words, the flow is nearly isotropic at all scales and the time scale of the largest eddies is much shorter than N^{-1} . Instead, even the large eddies are associated with length and time scales dependent on ϵ — these, of course, being $L_{k\epsilon}$ and T_L , respectively. It is important to note that this would only be the case in flows free of mean shear or the influences of boundaries. The influence of shear or boundaries could induce anisotropic motions even when $NT_L < 1$.

5.5.2 Implications

The linear relationship between L_T and L_{kN} has both practical and theoretical implications. An important theoretical implication of a linear relationship between L_T and L_{kN} is that the ratio of the turbulent potential to the turbulent kinetic energy is likely a constant value in strongly stratified turbulence, where the turbulent potential energy is $E_{PE} = -(g/\rho_0)\langle\rho'^2\rangle/(2\partial\bar{\rho}/\partial z)$. This is a direct implication of $L_E \sim L_T \sim L_{kN}$. From the definition of the Ellison length scale, the turbulent potential energy can be rewritten as $E_{PE} = N^2 L_E^2/2$. Similarly, from the definition of L_{kN} , the turbulent kinetic energy can be written as $k = N^2 L_{kN}^2$. Taking the ratio we see that $E_{PE}/k = (L_E/L_{kN})^2/2$. Assuming the conditions for $L_E \sim L_T$ are valid (i.e., internal wave effects are minimal) and $NT_L > 1$, our results imply that $E_{PE}/k \approx 1/2$. This result is confirmed in Figure 5.7 for the cases of strong stratification.

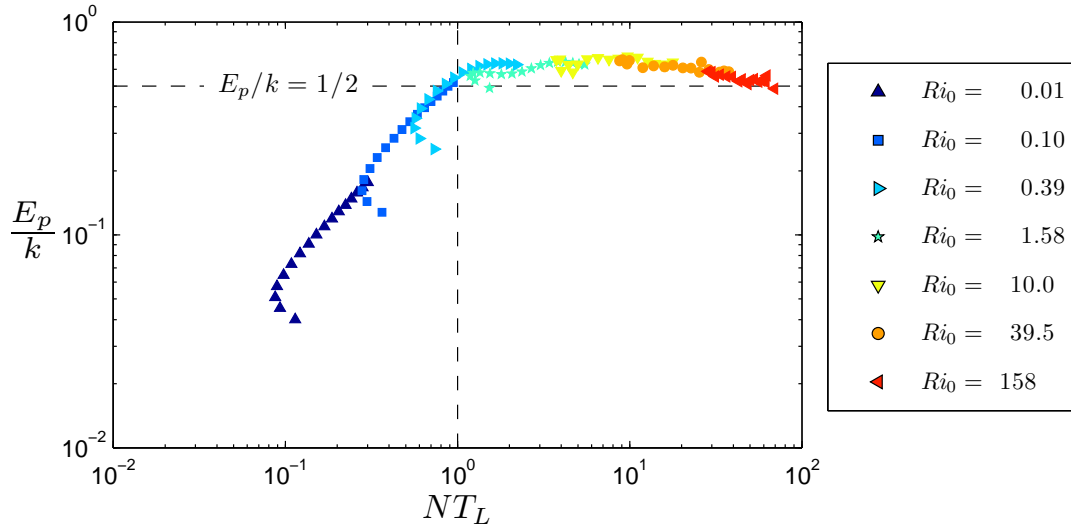


Figure 5.7: Ratio of turbulent potential energy, E_{PE} , to turbulent kinetic energy, k , versus NT_L .

For weak stratification, the relationship, $L_T \sim L_{k\epsilon}$, gives $k \sim (\epsilon L_T)^{2/3}$. This is in agreement with the theory of Luketina and Imberger (1989) and later shown to hold for energetic stages of grid turbulence in various laboratory settings by Ivey and Imberger (1991). In this regime, the ratio of potential to kinetic energy becomes $E_{PE}/k = N^2 \epsilon^{-2/3} (L_E/L_{k\epsilon}^{1/3})^2/2$, or $E_{PE}/k \sim N^2 \epsilon^{-2/3} L_T^{4/3}/2$. Clearly then, energy partitioning is not given by a simple constant when $NT_L < 1$.

The most obvious implication of $L_T \sim L_{kN}$ for $NT_L > 1$ from a practical standpoint is the resulting ability to infer turbulent kinetic energy from observed overturns in a density profile. This would preclude the need for high resolution measurements of three-dimensional velocity fluctuations and, instead, require only the use of a CTD profiler. It is important to note that this fundamentally differs from the common practice of inferring dissipation from density profiles using the assumption of $L_T \sim L_O$ — dissipation must still be measured from microstructure profiling if N and T_L are not equal. If microstructure measurements are available and are collected simultaneously with density measurements, then estimates of both k and ϵ can be obtained. In turn, the dimensionless parameters, NT_L and Re_L , can be calculated. Access to NT_L and Re_L provides a more insightful description of the flow than

that provided by the commonly used “activity parameter”, Re_b , under the reasoning stated in Section 5.2.2.

So far, we have considered shear-free flow. Inclusion of shear would necessitate an additional dimensionless parameter to fully characterize the flow. Through dimensional analysis this parameter can be shown to be $ST_L = Sk/\epsilon$ or, alternatively, Ri . Now, the analysis is no longer cleanly restricted to two regimes based on NT_L , but rather a two-dimensional parameter space involving some paired combination of NT_L , ST_L , and Ri as axes. This could be, for example, an $Ri - NT_L$ parameter space. With this approach, the two previous NT_L regimes can each be subdivided into two Ri -based regimes (assuming a critical value of Ri exists for describing flow behavior and Reynolds number independence). While we find $L_T \sim L_{kN}$ for $NT_L > 1$ when shear is absent, the behavior likely changes for low values of Ri — even if NT_L remains high. Indeed, Venayagamoorthy and Stretch (2010) used the shear-flow DNS of Shih et al. (2005) to show that the overturning scale, as represented by L_E , correlates linearly with L_{kS} , rather than L_{kN} , when $NT_L > 1$ and $Ri < 0.25$.

The applicability of our DNS results to turbulence in the open ocean is yet to be determined. To do so would require simultaneous measurements of density and the fundamental quantities from which the length scales of interest can be calculated. These, of course, being k , ϵ , N , and S . Since non-stationarity and inhomogeneity exist in ocean turbulence, it would be ideal for all these quantities to be measured from a common sampler on a single cast. Herein lies a practical challenge to the technical oceanographic community. If overcoming this challenge were to indeed validate our findings, it would then be up to the investigator in the field to determine in which regime the flow of interest belongs. This, of course, would necessitate the calculation of perhaps NT_L and Ri . While Ri is a mean flow parameter that is relatively easy to obtain, NT_L includes k — the very quantity for which an inferred value is being sought. Because of the difficulty in directly measuring k and ϵ , common values of NT_L — or more specifically the decay time, T_L — are not readily available for ocean turbulence. It is important to note, however, that the common practice of linearly relating

Thorpe and Ozmidov scales implicitly assumes $NT_L \approx 1$. As the strength of stratification relative to T_L and S increases in the ocean, the error of assuming $L_T \sim L_O$ increases, while that of $L_T \sim L_{kN}$ remains valid (given common values in Reynolds number).

5.5.3 Comparisons with Previous Studies

The study of Itsweire et al. (1986) represents a laboratory-based analogue to the current work and, thus, warrants mention. In their experiments, turbulence was generated free of shear using a bilateral mesh and allowed to decay in the presence of stable stratification. As in the current simulations, the density gradient was initially uniform. Their data suggest that the buoyancy parameter, NT_L , is less than unity near the grid where turbulence is intense relative to buoyancy. The parameter then grows monotonically with distance from the grid (i.e., turbulence age) to values greater than unity as turbulence decays while buoyancy effects persist due to incomplete mixing of the ambient density gradient. The growth of NT_L is also observed in the current simulations where N remains fixed. Length scale comparisons from their data are shown in Figure 5.8, where L_E is taken to be an approximation of L_T . In agreement with the current findings, $L_E \sim L_{k\epsilon}$ when $NT_L \lesssim 1$ (young turbulence proximal to grid), and that $L_E \sim L_{kN}$ when $NT_L \gtrsim 1$ (old turbulence distal to grid). The best agreement between L_O and L_E occurs just as the flow is transitioning between these two stages (i.e., $NT_L \approx 1$).

We now briefly compare our results with the shear-layer DNS of Smyth and Moum (2000) and Smyth et al. (2001). In their simulations, gradients in mean velocity and density are isolated to a finite layer within the flow that becomes turbulent via Kelvin-Helmholtz (K-H) instabilities that are thought to be frequent in the deep ocean. Following breakup of the pre-turbulent K-H billow, both scales are shown to decrease, with L_T decreasing most rapidly so that the ratio, L_O/L_T , increases nearly monotonically with time. This leads the authors to suggest that the ratio can be used as an “observational clock” of event age. Smyth et al. (2001) also find that L_T is in fair agreement with the length scale, $L_b = w_{rms}/N$

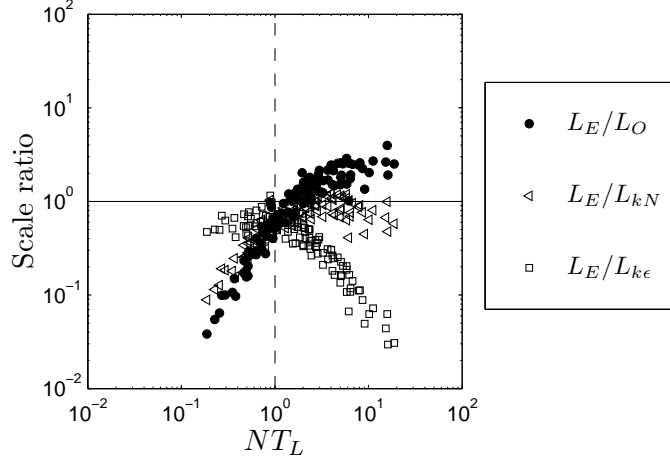


Figure 5.8: Variation of L_E/L_O (circles), L_E/L_{kN} (triangles), and $L_E/L_{k\epsilon}$ (squares) with NT_L for data of Itsweire et al. (1986).

($\approx \sqrt{\frac{2}{3}}L_{kN}$), early and is in excellent agreement with $L_{k\epsilon}$ late. Early correlation between L_T and L_b is also shown by Smyth and Moum (2000) (larger values of their Figure 10b). These findings are suggestive that NT_L decreases with the age of K-H turbulence and, thereby, evolves in the opposite sense of the uniform-gradient case. Apparently, any increase in T_L as K-H turbulence decays is mitigated by reduced N as mixing takes place. Thus, the flow approaches the weakly stratified regime. In the current work and the experiments of Itsweire et al. (1986), N is constant or decreases minimally so that stratification becomes dominant as inertial motions decay. The growth of T_L for K-H turbulence may also be suppressed by some lingering production due to shear.

Smyth et al. (2001) also highlight the effects of variation in Prandtl number. Their data suggest that length scale ratios become dependent on Pr late in the simulation if isotropy is assumed (e.g., if, say, $L_{k\epsilon}$ is approximated by w_{rms}^3/ϵ). Interestingly, however, the dependence on Pr vanishes when the assumption of isotropy is lifted, and data from runs of high Pr collapse upon those for which $Pr = 1$. Runs of high Pr appear most affected by the assumption of isotropy, while the run with $Pr = 1$ is relatively insensitive. This could be a Reynolds number effect; due to practical limitations on grid resolution, the high Pr

runs are limited to low Re . At low Re the vertical turbulent motions are more susceptible to dampening by buoyancy even if buoyancy effects are small (i.e., $NT_L \approx 1$). Hence, the isotropic assumption is less valid for runs of high Pr simply because Re is low.

In oceanic applications, Prandtl number is indeed greater than unity, however, the Reynolds number of these flows is also large so that turbulent advection dominates molecular diffusion of density and Prandtl number effects can often be neglected. The current work sacrifices high Pr for high Re with the hopes that the simulations are more representative of oceanic turbulence. This, of course, remains difficult to prove conclusively due to the practical limitations of DNS.

Finally, the data set of Moum (1996) can be used to compare the current work to actual observations of deep-ocean turbulence. These observations indicate good agreement between L_T , L_O , and L_b over the range of turbulent patches chosen (i.e., $L_T \approx 1.1L_O$ and $L_T \approx 1.0L_b$). The observed oceanic relation $L_T \sim L_b$ is consistent with the present results. Moum's measurements of the ratio L_O/L_T vary by about half an order of magnitude, possibly consistent with our finding that this ratio varies with NT_L . Comparison with our Figure 5.4b suggests that NT_L varies between about 1/2 and 10 in the deep-ocean turbulent events observed in that study.

5.6 Conclusions

The utility of the Thorpe length scale, L_T , in describing the physics of stratified turbulence is dramatically increased when it can be related to a length scale constructed from fundamental quantities of the flow. In light of the findings here, Thorpe scales of decaying, shear-free stratified turbulence exhibit behavior belonging to one of two regimes defined by ranges in the stratification strength parameter, NT_L . This is applicable for the range of Re_L investigated. Our results show that L_T correlates closely with the fundamental length scales, L_{kN} and $L_{k\epsilon}$, in the cases of strong stratification ($NT_L > 1$) and weak stratification

($NT_L < 1$), respectively. In neither regime does L_T have a linear relationship with the Ozmidov scale, L_O ; only for the special case of $NT_L \approx 1$ does L_O describe L_T .

The most obvious implication of the current study is that the utility of the Thorpe scale lies in its ability to indicate the turbulent kinetic energy, rather than the rate of its dissipation when stratification is relevant. This is of practical pertinence from the standpoint that k can be inferred using density profile measurements alone, whereas, accurate estimates of ϵ must be obtained from more direct methods such as microstructure profiling. It should be noted that direct measurement of k is not trivial due to contamination by wave motions and hence the ability to infer k from density profile measurements will be a major breakthrough. When complemented by direct measurements of ϵ , inferred values of k allow for the calculation of Re_L and NT_L — dimensionless parameters upon which aspects of the flow (e.g., mixing efficiency) can be parameterized. Such parameterizations may be more insightful than those based on the activity parameter, Re_b , which ambiguously combines the influences of Re_L and NT_L and is independent of k .

Despite our findings, there exists a long history of studies that find acceptable agreement between L_T and L_O . This is perhaps attributed to measured flows having values of NT_L close to unity. If this is indeed the case, the current findings support the common practice of inferring ϵ . More importantly, the current findings suggest that k can also be inferred since $L_O \sim L_{kN} \sim L_T$ when $NT_L \approx 1$. To verify this assertion and the general findings of this study, independent measurements of k , ϵ , and density profiles are required for high Reynolds number flows. Being able to make these measurements simultaneously and from the same sampler is ideal, yet not widely carried out due to technical challenges.

Finally, the results presented here are for shear-free flows. Inclusion of mean shear would necessitate consideration for an additional dimensionless parameter (ST_L or Ri) to fully characterize the flow. Predicting the behavior of overturning in stratified shear-flow, therefore, requires consideration for regimes additional to those defined by NT_L . Despite this added complication, we predict that the outer scales of the flow will remain more linearly correlated

with length scales constructed from k than those involving ϵ , so long as the outer scales are sufficiently anisotropic. This issue is investigated in the next chapter which broadens the discussion of overturn to include turbulent regimes where mean shear is relevant.

Chapter 6

A Unifying Framework⁷

6.1 Introduction

Turbulent phenomena, such as mixing in the ocean or atmospheric boundary layer, commonly manifest in response to the competing influences of background shear and stratification. Shear in the mean flow acts to promote turbulence while stratification has a dampening effect if stable (i.e., non-convective). In this regard, the parameter of choice for describing such flows is typically the gradient Richardson number, $Ri = N^2/S^2$, in which the role of shearing is represented in the mean shear rate, $S = \partial U/\partial z$ for a uni-directional shear flow, and that of stratification is represented in the buoyancy frequency, $N = \sqrt{(-g/\rho_0)(\partial \bar{\rho}/\partial z)}$. Implicit in Ri -based parameterizations, however, is knowledge of how the turbulence is responding to these background influences. A more comprehensive description would thus entail explicit reference to the inertial timescale of the turbulence, l/u , where u is some measure of the turbulent velocity fluctuations and l is a characteristic length scale whose precise definition varies among researchers. Direct comparisons of this internal time scale to those imposed externally by the mean flow are then embodied in a turbulent Froude number, u/Nl , and an (inversely) analogous shear parameter, Sl/u .

The turbulent Froude number has been widely used in studies of stratified turbulence (e.g., Luketina and Imberger, 1989; Ivey and Imberger, 1991; Brethouwer et al., 2007), while the shear parameter has typically been reserved for studies of unstratified shear flows (e.g., Rogallo, 1981; Lee et al., 1990; Saddoughi and Veeravalli, 1994). Examples of studies evoking

⁷The research presented in this chapter has been published in *Physics of Fluids* under the title, “A unifying framework for parameterizing stably stratified shear-flow turbulence” (Mater and Venayagamoorthy, 2014b). Background information and literature relevant to this chapter are presented again so the chapter may be read as a stand-alone work. The chapter is written in a collective “we” voice to acknowledge collaboration with Dr. S. K. Venayagamoorthy.

the latter in discussions of stratified shear-flow include the direct numerical simulations of Holt et al. (1992), Jacobitz et al. (1997), Shih et al. (2000), and Chung and Matheou (2012) and the experiments of Piccirillo and Van Atta (1997) in which the stationary value of the gradient Richardson number, Ri_s , was found to increase with Sl/u and the Reynolds number. In these studies the inertial velocity and length scales were chosen to be $u \sim k^{1/2}$ and $l \sim k^{3/2}/\epsilon$, respectively, with k being the turbulent kinetic energy and ϵ being the dissipation rate of k .

Recently, the individual effects of shear and stratification were investigated in the context of mixing efficiency by Shimizu (2012). In this reanalysis of laboratory and numerical data sets of homogeneous flows, mixing efficiency was found to vary with both u/Nl and Sl/u where, like other researchers, he chose $u \sim k^{1/2}$ and $l \sim k^{3/2}/\epsilon$ to be used in the definition of both parameters.

In the current work, we seek to broaden the independent consideration for shear and stratification into a unifying framework that allows for a general description of stratified shear-flow turbulence. This will be done with an eye toward oceanic applications in which a behavior of primary importance is diapycnal mixing at high Reynolds number. Since mixing is fundamentally connected to overturning motions and overturns can be readily observed in the field, an investigation of the length scales of these motions will serve as the basis for construction of the conceptual framework.

This approach is practically motivated by the need for accurate inferences of fundamental turbulence quantities, namely k and ϵ , from more easily observed large-scale overturning, the size of which is typically taken to be the Thorpe length scale, L_T , in ocean applications (Thorpe, 1977). This is made possible if L_T is properly scaled with the length scales constructed through dimensional analysis. As the influences of shear and stratification change, so too must the scaling arguments for L_T . Herein lies the practical need for a unifying framework that considers all possible flow regimes.

This work is a direct extension to the shear-free direct numerical simulation (DNS) work of Mater et al. (2013) who show that $L_T \sim L_{k\epsilon} \equiv k^{3/2}/\epsilon$ in a weakly stratified regime (high Froude number) and $L_T \sim L_{kN} \equiv k^{1/2}/N$ in a strongly stratified regime (low Froude number), where $L_{k\epsilon}$ and L_{kN} are constructs of dimensional analysis. They go on to show that L_T approximates the Ozimidov scale, $L_O \equiv (\epsilon/N^3)^{1/2}$, only at the transition between regimes when the Froude number is near unity. The practical implications being that L_T can be used to infer turbulent kinetic energy, k — a notoriously difficult quantity to measure in field studies — and that the common practice of inferring ϵ from $L_T \sim L_O$ made popular by the work of Dillon (1982) is conditioned upon $Fr \approx 1$. Because their study involved shear-free turbulence, however, only regimes in the Froude number space were investigated. With consideration for shear, we now bring the discussion closer to the realm of realistic flows in which turbulence can be decaying or growing and are forced to consider additional regimes using the shear parameter and/or Ri . We now too must consider other fundamental scales involving S , namely $L_{kS} \equiv k^{1/2}/S$ and the Corrsin scale, $L_C \equiv (\epsilon/S^3)^{1/2}$.

As with Mater et al. (2013), the inertial length scale of the turbulence will be defined as $l \sim L_{k\epsilon} \equiv k^{3/2}/\epsilon$ making the inertial time scale $T_L \equiv k/\epsilon$. The parameters of interest then become

$$\begin{aligned}
NT_L &\equiv Nk/\epsilon, \\
ST_L &\equiv Sk/\epsilon, \\
Re_L &\equiv k^2/(\epsilon\nu), \\
Pr &\equiv \nu/\kappa_\rho,
\end{aligned} \tag{6.1}$$

where NT_L is an inverse turbulent Froude number, ST_L is the shear parameter, Re_L is the turbulent Reynolds number, and Pr is the molecular Prandtl number with κ_ρ as the molecular diffusivity of density. For minimal influence of Pr , a three-dimensional parameter space can be conceptualized with each axis representing the strength of stratification, mean

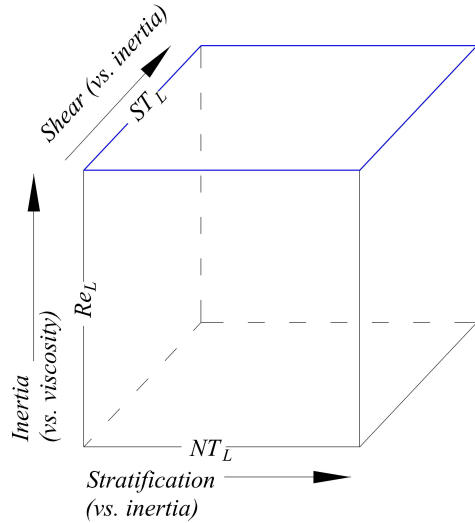


Figure 6.1: Conceptual three-dimensional parameter space for interpreting stratified shear-flow turbulence assuming minimal influence from molecular diffusion.

shear, or viscosity relative to the inertia of the turbulence (figure 6.1). For high Reynolds number flows such as those in most geophysical settings of interest, the space simplifies to an $NT_L - ST_L$ plane. It is with this conceptual framework that the current study seeks to explore stratified shear-flow turbulence with special emphasis on the length scales of overturning and diapycnal mixing. Because field data sets involving all of the fundamental quantities needed to define the parameters in (6.1) are rare, we turn to existing laboratory and numerical data sets for our analysis.

The layout of this chapter is as follows. Section 6.2 revisits the dimensional analysis of stratified shear-flow turbulence. Here, the relevant non-dimensional parameters and fundamental length and time scales will be discussed. In section 6.3, we present the data sets considered and use their plotting positions to begin a discussion of the $NT_L - ST_L$ space and the physical relevance of the regimes within. The dimensionally-constructed scales are compared with the overturning scale to investigate regime-wise scalings in section 6.4. The implications of these results for parameterizations of diapycnal mixing are discussed in section 6.5. In this section, the relevance of our findings to ocean applications where only Ri is available will be discussed. A brief conclusion is presented in section 6.6.

6.2 Dimensional Analysis

6.2.1 A Conceptual Framework

First let us consider the reasoning behind the selection of the parameter set of (6.1). In the absence of mean shear or stratification, turbulence decays and is theoretically isotropic at all scales. The two important mechanisms working in this condition are the inertial transfer of energy from large to small scales and the viscous dissipation of kinetic energy at the smallest scales. Thus, the three quantities setting the state of the turbulence are the total turbulent kinetic energy per mass, $k \equiv \frac{1}{2}\langle u_i u_i \rangle$, the down-spectrum transfer rate, $\epsilon \equiv 2\nu\langle s_{ij}s_{ij} \rangle$, and the viscosity of the fluid, ν . In the definitions above, u_i is the three-dimensional turbulent velocity and $s_{ij} = \frac{1}{2} \left(\frac{\partial u_i}{\partial x_j} + \frac{\partial u_j}{\partial x_i} \right)$ is the fluctuating strain rate tensor. Evoking these three particular quantities assumes the Kolmogorovian reasoning that energy cascades from large to small scales through an isotropic inertial subrange at the same rate as its conversion to internal energy, hence the dual role of ϵ as a both a loss and transfer rate (see Durbin and Reif, 2001). The time scale of the large, purely inertial eddies is then given by T_L and that of the smallest dissipative eddies by $T_\eta \equiv (\nu/\epsilon)^{1/2}$. The ratio of these two time scales is then the only dimensionless grouping needed to describe this kind of flow and is the turbulent Reynolds number, $Re_L = (T_L/T_\eta)^2$.

More generally, turbulence is anisotropic at the largest scales due to background shear and stratification. Therefore, a more comprehensive description of the turbulence depends on the additional “external” time scales, S^{-1} and N^{-1} . Comparison of these time scales to that of the largest inertial eddies gives rise to the shear and buoyancy parameters, $ST_L = T_L/S^{-1}$ and $NT_L = T_L/N^{-1}$.

One may also arrive at Re_L , NT_L , and ST_L upon non-dimensionalizing the evolution equation for k (shown here assuming homogeneous turbulence and one-dimensional shear),

$$\frac{\partial k}{\partial t} = -\langle uw \rangle S - \langle \rho' w \rangle \frac{g}{\rho_0} - 2\nu \langle s_{ij} s_{ij} \rangle, \quad (6.2)$$

with the scaling arguments $t \sim T_L$, $u \sim w \sim k^{1/2}$, $s_{ij} \sim k^{1/2}/\eta$, and $\rho' \sim (\partial\bar{\rho}/\partial z)L_E$, where $\eta \equiv (\nu^3/\epsilon)^{1/4}$ is the Kolmogorov length scale and L_E is the outer scale of the scalar field to be discussed later. The scaled equation becomes

$$\frac{\partial k^+}{\partial t^+} = -\langle u^+ w^+ \rangle ST_L - \langle \rho'^+ w^+ \rangle \frac{L_E}{L_{k\epsilon}} (NT_L)^2 - 2\langle s_{ij}^+ s_{ij}^+ \rangle Re_L^{1/2}, \quad (6.3)$$

where the non-dimensional variables are indicated with + superscripts. Also appearing is the ratio of the scalar length scale, L_E , and the momentum length scale, $L_{k\epsilon}$. If L_E scales with any of the fundamental scales, $L_{k\epsilon}$, L_{kN} , or L_{kS} to be discussed in subsection 6.2.2, this ratio can be cast in terms of NT_L and/or ST_L .

For completeness the Prandtl number has also been included in (6.1), however, the influence of that parameter will not be of particular focus in the current work as we are motivated by geophysical flows at high Reynolds number (i.e., high Peclet number) for which turbulent advection of density occurs on a much shorter time scale than its molecular diffusion. Molecular effects in the laboratory and numerical flows analyzed here are no doubt present but will be of secondary concern in our study of overturning at large-scales where turbulent advection is strong.

Simple dimensional analysis dictates that with the six kinematic quantities considered here, i.e., k , ϵ , ν , κ_ρ , S , and N , four dimensionless groupings are needed for a comprehensive yet non-redundant description of the flow. The set of (6.1) is only one possible description, but chosen here because of explicit reference to T_L . Other popular parameters can be

formulated in terms of those considered here. They include the gradient Richardson number,

$$Ri \equiv N^2/S^2 = (NT_L/ST_L)^2, \quad (6.4)$$

the buoyancy Reynolds number,

$$Re_b \equiv \epsilon/(\nu N^2) = (T_N/T_\eta)^2 = (NT_L)^{-2} Re_L, \quad (6.5)$$

the shear Reynolds number

$$Re_s \equiv \epsilon/(\nu S^2) = (T_S/T_\eta)^2 = (ST_L)^{-2} Re_L, \quad (6.6)$$

and the Peclet number

$$Pe_L \equiv k^2/(\epsilon\kappa_\rho) = Pr Re_L. \quad (6.7)$$

Although Ri lacks an explicit reference to T_L and is not dimensionally required given (6.1), we will retain this popular parameter as an important delineator between regimes of buoyancy dominance and shear dominance when both influences are very strong (i.e., when $T_N \ll T_L$ and $T_S \ll T_L$). Re_b is another popular parameter in oceanic field studies where well established techniques for measurement of N and ϵ exist. This parameter, however, is also non-unique in that it is effectively a comparison of inertial effects to the lumped effects of buoyancy and viscosity. While this characteristic may be useful in predicting the arrest or fossilization of turbulence (Gibson, 1980), high values of Re_b may be misleading. That is, Re_b can be high due to weak stratification (i.e., $NT_L \ll 1$) or strong turbulence (i.e., $Re_L \gg 1$). Because of this ambiguity, we choose not to include this parameter as one of primary significance. This same reasoning is extended to Re_s . Finally, Pe_L , could have been included in (6.1), but is less popular than Pr , hence our selection of the latter in (6.1).

Upon neglecting molecular effects in the limit of high Re_L , our description of the flow reduces to the $NT_L - ST_L$ space represented in Figure 6.2 through which lines of constant

Ri can be constructed. Within this conceptual framework, we have assumed critical values in NT_L , ST_L , and Ri so that the two-dimensional space is delineated into the well-cited regimes of shear and buoyancy dominance, but also a regime in which these background influences are absent or minimal that we entitle the “unforced” regime. In this regime the flow trends toward isotropy in that any sustained “forcing” by shear or stratification is not felt. In such a state, Ri becomes an irrelevant concept. A common example of this kind of flow is unstratified turbulence generated by a grid. Critical values in the parameters are initial estimates informed by classical studies on flow stability and stationarity. The choice of $Ri_c \approx 0.25$ follows from classic shear layer stability analysis (Miles, 1961) and has been shown to be a criterion for stationarity in homogeneous shear flows (e.g., Rohr et al., 1988). Choice of a critical value in the shear parameter follows from findings that $ST_{L,c} \approx 3.3$ in the log layer of unstratified channel flow where production and dissipation are in approximate balance (see Pope, 2000) and at mid-depth in stationary wind tunnel turbulence (Saddoughi and Veeravalli, 1994). Recently, Chung and Matheou (2012) published data suggesting this value is approached in the unstratified limit of stationary homogeneous turbulence. The typical values chosen for Ri_c and $ST_{L,c}$ imply $NT_{L,c} = O(10^0)$ which is in agreement with the findings of Mater et al. (2013) regarding the behavior of the Thorpe scale in the stratified, shear-free limit.

6.2.2 Relevant Length Scales

Dimensionally, nine length scales of the momentum field can be constructed from k , ϵ , ν , N , and S . Since an objective of the current work is to parameterize large scale motions, we will place special attention on the five of those scales that are independent of ν . These “large” scales, mentioned previously, are the turbulent length scale, $L_{k\epsilon} \equiv k^{3/2}/\epsilon$ (Pope, 2000), the Ozmidov length scale, $L_O \equiv (\epsilon/N^3)^{1/2}$ (Dougherty, 1961; Ozmidov, 1965), the Corrsin length scale, $L_C \equiv (\epsilon/S^3)^{1/2}$ (Corrsin, 1958), and two scales linking turbulent kinetic energy to buoyancy frequency and mean shear, $L_{kN} \equiv (k/N^2)^{1/2}$ and $L_{kS} \equiv (k/S^2)^{1/2}$.

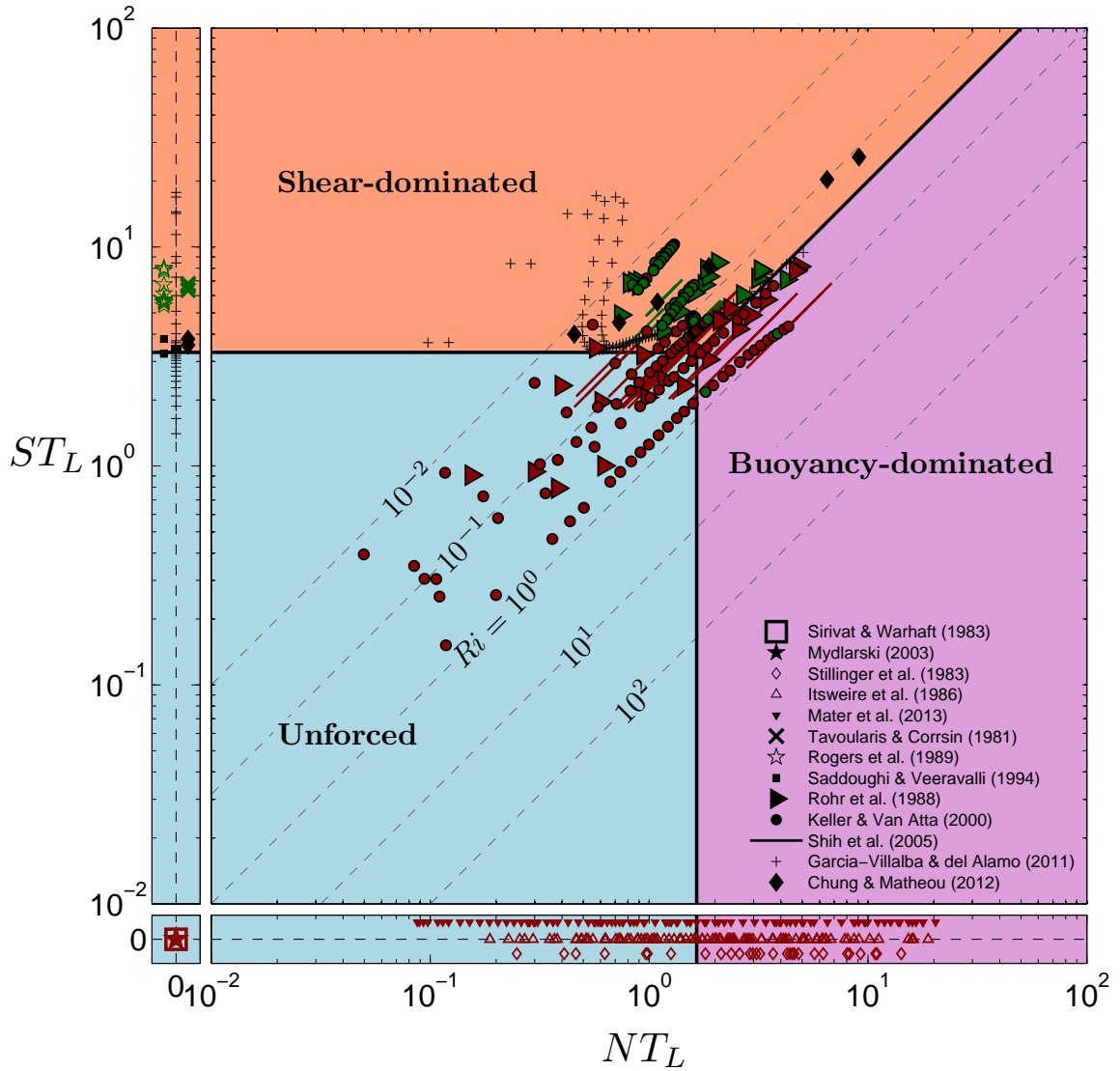


Figure 6.2: Parameter space for interpretation of high-Reynolds number stratified shear-flow turbulence. Growing turbulence ($Dk/Dt > 0$) shown in green, stationary turbulence ($Dk/Dt \approx 0$) shown in black, and decaying turbulence ($Dk/Dt < 0$) shown in red. Select data points have been offset from $NT_L = 0$ or $ST_L = 0$ for clarity. Lines delineating regimes are first order approximations.

Physically, the turbulent length scale, $L_{k\epsilon}$, can be thought to represent the largest eddies present in a flow when the effects of shear or buoyancy are negligible (i.e., isotropic turbulence). Under this assumption, the presence of ϵ indicates that the down-spectrum transfer rate of turbulent kinetic energy is constant at even the largest scales of isotropic turbulence. In other words, the inertial subrange begins at $L_{k\epsilon}$ and ends at the Kolmogorov length scale, η .

When mean shear or stratification are not negligible, the down-spectrum transfer rate of k at large scales should no longer be a constant equal to ϵ since k can be added via shear or subtracted via buoyancy along the way. In other words, the timescale needed for inertial transfer to and from an eddy of wave number κ_l (i.e., “eddy-wise” transfer), given by $\epsilon^{-1/3}\kappa_l^{-2/3}$, is longer than the imposed timescales of either k addition, S^{-1} , or removal, N^{-1} . For increasing wave number (decreasing eddy size) the rate of eddy-wise inertial transfer increases if the turbulence is in approximate equilibrium so that the process becomes dominant at scales smaller than L_C or L_O and the “gross” transfer rate becomes ϵ . In this sense, the upper (i.e., large scale) end of the inertial subrange is theoretically L_C or L_O for small or large values of Ri , respectively.

Given this reasoning, the largest scales in forced flow should be independent of ϵ . On dimensional grounds, the remaining possible predictors are then those that depend on kinetic energy: L_{kN} and L_{kS} . Eddies of this size have the velocity scale, $k^{1/2}$, and a time scale set by the dominant forcing mechanism, N^{-1} or S^{-1} . Because no assumptions about transfer rate are made, L_{kN} and L_{kS} more generally describe large scale motions in their respective regimes of buoyancy- and shear-dominated flows than their counterparts L_O and L_C .

All of the fundamental scales can be related by the three dimensionless parameters highlighted above. This is demonstrated in the schematic energy spectrum of Figure 6.3, where the labeled “spectral gaps” are ratios between a given length scale and its next smallest neighbor. The specific order shown in Figure 6.3 is but one possibility, as all parameters are assumed greater than unity. For example, L_O is shown to be setting the upper end of the

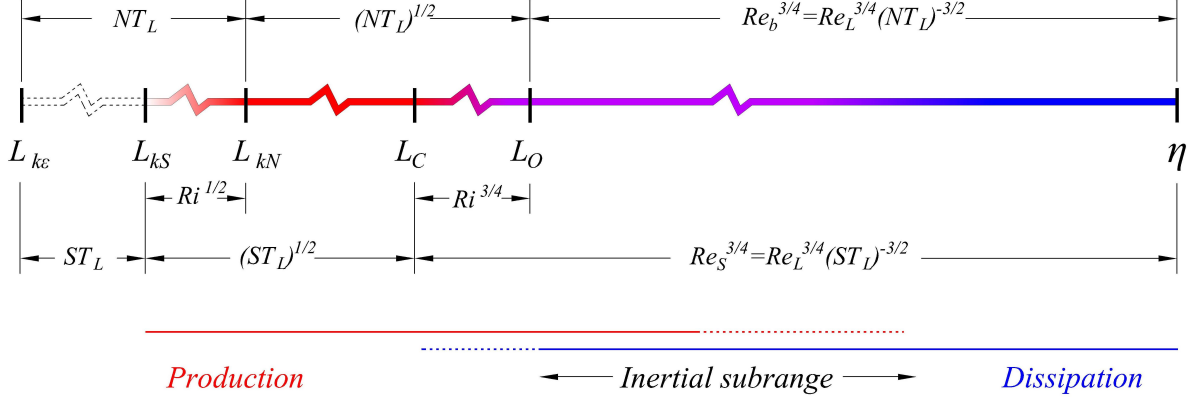


Figure 6.3: Schematic of energy cascade with length scale spectrum. Ratios of subsequent scales are shown in terms of dimensionless parameters. The specific scale order shown is but one possibility since all parameters are assumed greater than unity.

inertial subrange, but a switch to shear dominance (i.e., $Ri \ll 1$) would have L_C assuming this role. Another scenario would be isotropic turbulence where NT_L and $ST_L \rightarrow 0$. In this limit, anisotropic scales would be infinitely large relative to the actual scales of turbulent motion, thus, $L_{k\epsilon}$ would be left as the only reasonable measure of both the largest physical scales and the upper end of the inertial subrange. Note that in the scenario of Figure 6.3, $L_{k\epsilon}$ is the largest of all scales, but likely has no physical analogue in the flow because it does not consider anisotropic effects. For this reason, $L_{k\epsilon}$ can be thought of as the “isotropic potential” large scale in forced flow. Whatever the scenario, we see that the large scales are interrelated through NT_L and ST_L , while Re_L describes the separation of large and small scales. If we reason that the largest overturns in the flow should fall somewhere in the range of large fundamental scales, then we can neglect scales involving ν as well as Re_L in the current analysis. Of course, it may not be acceptable to neglect Re_L when attempting to parameterize behavior other than inviscid overturning (e.g., mixing efficiency) unless the flow is sufficiently turbulent.

6.2.3 A Note on Anisotropy

Thus far, we have taken a simplified approach to dimensional analysis that does not distinguish between vertical and horizontal length scales. This distinction has been made by other researchers of strongly stratified turbulence. Lindborg (2006), for example, uses artificially-forced (i.e., shear-free) DNS to investigate the ratio of an observed characteristic vertical length scale, l_v , to the imposed horizontal scale of forcing, l_h . He found the horizontal energy spectrum to be of the form $\epsilon^{2/3}\kappa_h^{-5/3}$, where κ_h is the horizontal wave number, even at horizontal scales larger than L_O when stratification is strong. It was thus implied that $l_h \sim u_h^3/\epsilon$, where u_h is the horizontal velocity scale and a measure of the horizontal turbulent kinetic energy. Furthermore, Lindborg finds $l_v/l_h \sim Fr_h \equiv \epsilon^{1/3}/(Nl_h^{2/3})$, where Fr_h is a horizontal Froude number, which in turn implies $l_v \sim u_h/N$ in accordance with the scaling arguments of Billant and Chomaz (2001). The first finding implies that $L_{k\epsilon}$ indeed has a physical analogue in the horizontal motions. Since we are currently concerned with overturning, however, we retain the concept that $L_{k\epsilon}$ has no physical analogue in the vertical direction unless the flow is isotropic.

The second finding is more relevant to the current work in that it implies overturns should scale with L_{kN} , which was indeed shown by Mater et al. (2013) when $NT_L \gtrsim 1$. Appealing to the more Lagrangian perspective that the vertical length scale should be a function of the vertical turbulent kinetic energy, other researchers define the proper scaling to be w/N , where w is the vertical turbulent velocity. Moum (1996), for example, finds that such a scale also correlates closely with overturning in the ocean. Interestingly, the choice of velocity scale (i.e., u_h , $k^{1/2}$, or w) appears to be of secondary importance. We therefore have selected $k^{1/2}$ out of generality as well as its applicability to descriptions of unstratified flow.

6.2.4 Observed Length Scales

To test the $NT_L - ST_L$ framework and our physical interpretations of fundamental length scales, these scales will be compared to outer motions of the flow as observed in the scalar field. A commonly accepted measure of overturning is the length scale proposed by Ellison (1957),

$$L_E = \frac{\langle \rho'^2 \rangle^{1/2}}{\partial \bar{\rho} / \partial z}, \quad (6.8)$$

where ρ' is the turbulent density fluctuation about some mean background density, $\bar{\rho}$, and $\langle \rangle$ represents spatial or temporal averaging. L_E may be thought of as a statistical measure of the vertical distance traveled by fluid parcels before returning toward an equilibrium position or irreversibly mixing with surrounding fluid. In a statistical sense, L_E is proportional to the largest eddies of the flow (e.g., Stillinger et al., 1983).

A closely related scale used in oceans and lakes is the Thorpe length scale, L_T (Thorpe, 1977). A relatively simple and objective measure of large overturns, L_T is determined from observed instantaneous vertical density profiles. Agreement between L_E and L_T has been confirmed in both experiments (Itsweire, 1984) and numeric simulations (Itsweire et al., 1993) for all but the most strongly stratified flows, where internal wave motions influence L_E but not L_T . Because L_T is not reported in many of the data sets reported here, we compare fundamental scales to L_E , with the anticipation that results may be applicable to oceanic studies where L_T is more popular.

6.3 Data Sources

Our objective is to explore the $NT_L - ST_L$ space to the greatest extent possible using available numerical and laboratory data. Accordingly, consideration is given to data sets that include both mean shear and stratification, but also those in which one or both influences are absent. In the flows considered, stratification and mean velocity are of uniform gradient with the exception of the channel flow data of Garcia-Villalba and del Alamo (2011) (GVA)

where the presence of a wall results in inhomogeneous shear. In unstratified cases, overturns are observed in a passive scalar field. Basic information on all of the chosen data sets is provided in Table 6.1. Only records with $Re_b > 1$ will be considered if stratification is present. Admittedly, this rather low threshold and the relatively low Reynolds numbers do not ensure a lack of viscous effects, making our exclusion of Re_L in the subsequent analysis an undoubted oversimplification. However, because highly turbulent geophysical data sets rarely, if ever, include k , we are limited to the data of less turbulent numerical and laboratory flows. With this limitation, we proceed under the assumption that overturning at the outer scales is only minimally influenced by viscosity and that the parameters most descriptive of this behavior are NT_L and ST_L .

In Figure 6.2 we see the data sets plotted within the $NT_L - ST_L$ space. Given these plotting positions and knowledge of experimental setups, we can begin to interpret the physical relevance of the three regimes. Perhaps most evident is the relevance of the regimes as they relate to growth and decay of turbulence. For turbulence to be stationary there must be some balance between the time scale driving production, S^{-1} , and those driving its loss rate - either through transfer to smaller scales, T_L , conversion to potential energy, N^{-1} , or both. In the unstratified limit, ST_L is the ratio of relevance, and as expected, stationary data falls at the transition between “unforced” and “shear-dominated” regimes where $T_L \approx 3.3S^{-1}$. This is clearly demonstrated by the mid-depth wind tunnel data of Saddoughi and Veeravalli (1994) and the homogeneous DNS of Chung and Matheou (2012). For higher values of ST_L , shear forcing occurs on a shorter time scale than that of inertial energy transfer to smaller scales so that energy essentially accumulates at the largest scales and turbulence grows. This is demonstrated in the DNS data of Rogers et al. (1989) and the wind tunnel data of Tavoularis and Corrsin (1981) where $ST_L > ST_{L,c}$. For lower values of ST_L of the unforced regime, production cannot maintain pace with inertial transfer and turbulence freely decays as is demonstrated in the data of Sirivat and Warhaft (1983) and Mydlarski (2003) with $ST_L = 0$.

For the unstratified stationary channel flow simulation of GVA, data from the log-region clusters near $ST_{L,c}$ due to the approximate balance between production and dissipation and negligible net transport of k there. Above and below the log-region, however, the inhomogeneous nature of the flow results in significant net transport of turbulent kinetic energy k so that $ST_L \neq ST_{L,c}$ yet local stationarity is maintained. Near the wall, strong shear results in production exceeding dissipation so the flow is locally shear-dominated (i.e., $T_L \gg S^{-1}$), however, “excess” k is transported away from the wall so that local stationarity is maintained. Far from the wall, dissipation outpaces shear-driven production so the flow locally trends toward an “unforced” state (i.e., $T_L \ll S^{-1}$), however, local stationarity is maintained due the supply of k originating from the near wall region.

Now consider stratified shear flow where the evolution of turbulence is a function of ST_L but also NT_L as in (6.3). When the flow is approximately homogeneous, the particular balance between S^{-1} and T_L needed for stationarity is regulated by the time scale at which k is lost to potential energy, N^{-1} , in such a way that Ri becomes an approximate constant. We denote this constant value as Ri_s and note the subtle distinction between Ri_s , which denotes stationarity, and Ri_c , which denotes the canonical critical value we have used to delineate between shear- and buoyancy-dominated regimes. So long as $Ri = Ri_s$, stationarity can exist for $ST_L > ST_{L,c}$ because any additional production of kinetic energy is negated by a conversion to potential energy. As pointed out by others (e.g., Holt et al., 1992; Piccirillo and Van Atta, 1997; Jacobitz et al., 1997; Shih et al., 2000), however, Ri_s is only an approximate constant and is likely an increasing function of Re_L and ST_L for low Re_L . With this reasoning and a given value of Re_L , stationarity should occur along a curve within the shear-dominated region of the $NT_L - ST_L$ space that approaches the horizontal line, $ST_L = ST_{L,c}$, in the unstratified limit (small NT_L) and the inclined line, $Ri = Ri_c$, in the strongly stratified limit (large NT_L). As Re_L increases, the curve likely converges upon these asymptotes more rapidly until it becomes effectively coincidental with $ST_{L,c}$ and Ri_c . The notion of a “stationary curve” is supported by the data of Chung and Matheou (2012) and

the log-region data of GVA (densely spaced points). Furthermore, the remaining data sets indicate that the transition between growth and decay occurs along a similar curve that is in apparent agreement with the curve set by the log-region channel data.

In general, turbulence can occupy more than one regime during the course of its evolution. For the non-stationary stratified cases considered here, turbulence moves from the unforced regime into one of the other two. For example, consider the stratified shear-flow experiments of Rohr and Van Atta (1987) and Keller and Van Atta (2000) (KV) in which turbulence was initialized by a grid while mean shear and stratification (i.e., Ri) remained approximately constant with distance downstream. The sudden pulse of grid-generated turbulence results in rapid inertial motions (i.e., $T_L \ll N^{-1}$ and $T_L \ll S^{-1}$) immediately downstream of the grid so that the influence of ambient stratification and shear are minimal and, thus, Ri is effectively an irrelevant concept. Indeed, turbulence initially decayed for all runs irrespective of Ri . In Figure 6.2 we see that only as the flow transitions out of the unforced regime does Ri become relevant to the long term growth or decay of k . This occurs at sufficient distance downstream of the grid where T_L becomes comparable to N^{-1} and/or S^{-1} . The trend is reflected in the DNS of Shih et al. (2005) (SKIF) where the initial conditions are analogous to an initial grid disturbance.

It is also reasonable that flows with different initial conditions could have different trajectories through the space. Although unavailable to the current study, turbulence generated by Kelvin-Helmholtz (K-H) instabilities (e.g., Smyth et al., 2001) may very well evolve in the opposite sense to homogeneous grid turbulence. That is, such a flow may begin near the interface between shear- and buoyancy-dominated regimes and then move toward the unforced regime as N and S decrease due to thickening of the shear layer. Indeed, Smyth et al. (2001) use DNS to show that the overturning in late-stage K-H turbulence scales with $L_{k\epsilon}$. As will be shown here, this is a key characteristic of turbulence in the unforced regime.

Table 6.1: Data from wind tunnel (WT), saltwater flume (SWF), and direct numerical simulation (DNS) studies. Turbulence is categorized as sheared (S) or shear-free (SF) with passive (PS) or active scalar (AS).

Researcher	Re_L	NT_L	ST_L	Ri	Re_b	Model	Turbulence
Sirivat & Warhaft (1983)	97	0	0	-	∞	WT	SF;PS
Mydlarski (2003)	1000-4200	0	0	-	∞	WT	SF;PS
Stillinger et al. (1983)	53-1070	0.2-14	0	∞	3-2600	SWF	SF;AS
Itsweire (1986)	29-4200	0.2-19	0	∞	2-1450	SWF	SF;AS
Mater et al. (2013)	93-700	0.1-20	0	∞	1-54450	DNS	SF;AS
Tavoularis & Corrsin (1981)	2700-4200	0	6.3-6.8	0	∞	WT	S;PS
Rogers et al. (1989)	140-740	0	5.4-8.0	0	∞	DNS	S;PS
Saddoughi & Veeravalli (1994) ^a	135000	0	3.8	0	∞	WT	S;PS
Rohr et al. (1988) ^b	100-2500	0.2-5	0.8-8.5	0.01-0.38	14-5900	SWF	S;AS
Keller & Van Atta (2000)	50-975	0.05-4	0.15-10.3	0.02-1	4-51400	WT	S;AS
Shih et al. (2005)	29-830	0.5-7	1.8-7.0	0.04-1	1-7700	DNS	S;AS
Garcia-Villalba & del Alamo (2011) ^c	184-535	0-5	0.6-5.0 ^d	0-0.40	5-880, ∞	DNS	S;AS
Chung & Matheou (2012) ^{a,e}	1000-8000	0-9	3.6-26	0-0.13	100-10000, ∞	DNS	S;AS

^aNot used in scale calculations

^bAs presented in Rohr (1985).

^cData from log-law region ($0.05 < y/h < 0.9$) of their cases B1-B3.

^dValues increase to 17.0 in buffer region (plotted in Figure 6.2).

^eExcluding their R10 cases.

6.4 Observed vs. Fundamental Length Scales

Each fundamental length scale is compared to the overturn scale, L_E , in Figures 6.4-6.6 for the noted data sets of Table 6.1. Data points have been color-coded in accordance with their plotting positions of Figure 6.2.

First, consider the shear scales L_{kS} and L_C . Linear correlations of the form $L_{kS} = \beta_{kS}L_E$ and $L_C = \beta_C L_E$ are apparent in Figures 6.4 (a)-(d) and (e)-(h), respectively, when flow is in the shear-dominated region (salmon colored points). Generally, the linear nature of the relationship with L_E is stronger and the constant of proportionality closer to unity with L_{kS} than with L_C . Noting that $L_{kS}/L_C = \beta_{kS}/\beta_C = (ST_L)^{1/2}$ and $L_{kS} \approx L_E$ leads to $\beta_C \approx (ST_L)^{-1/2}$. Thus, variation in ST_L within and among the data sets is seen to be the reason for $L_C \sim L_E$ being slightly weaker than $L_{kS} \sim L_E$. However, the variation in ST_L is slight and indicates that there is a relatively consistent range of scales, $L_C < l < L_{kS} \approx L_E$, that occurs above the inertial subrange in shear-dominated flow.

Next, consider the buoyancy scales L_{kN} and L_O shown in Figure 6.5. For points in the buoyancy-dominated region (purple), the DNS data of SKIF and Mater et al. (2013) most clearly indicate that L_E is linearly related to L_{kN} with a constant of proportionality that is approximately one (Figures 6.5 (a) and (c)), i.e., $L_{kN} = \beta_{kN}L_E$ with $\beta_{kN} \approx 1$. The same data indicate a non-linear relationship with L_O (Figures 6.5 (e) and (g)). As discussed in Mater et al. (2013), agreement between L_O and L_E is limited to the transition between the buoyancy-dominated and isotropic regimes (blue-purple) in their data. The same trend is observable in the data of SKIF. In the buoyancy-dominated regime, L_O becomes less than L_E as the inertial subrange becomes truncated to scales smaller than those of the overturning motions. In the other regions, both L_{kN} and L_O become large as N decreases. In the right panels of Figure 6.5 we see the trend replicated, albeit with more scatter, by the laboratory data. Note that β_{kN} appears to vary between data sets.

Finally, consider the fundamental isotropic scale, $L_{k\epsilon}$, shown in Figure 6.6. For nearly all data points in all regimes, we find $L_{k\epsilon}$ to be larger than the overturning length scale, L_E , thus supporting the notion that $L_{k\epsilon}$ is an isotropic potential that is not physically realized in the vertical motions when anisotropy is present. Only for points in the unforced regime (blue), is there a trend toward agreement. Taken as a whole these points represent a weak linear correlation of the form $L_{k\epsilon} = \beta_{k\epsilon} L_E$. Interestingly, the same could be said for points from the shear-dominated regime (salmon colored) in Figure 6.6 with a relation of the form $L_{k\epsilon} = \alpha L_E$, where α is an apparent constant that is larger than $\beta_{k\epsilon}$. This is especially apparent in the data of SKIF and GVA. Again assuming $L_{kS} \approx L_E$ in the shear-dominated regime, we see that the apparent linear relationship (i.e., the consistency of α) is due to the narrow range in ST_L for such flows; for the shear-dominated points, $L_{k\epsilon} = \alpha L_E \approx \alpha L_{kS}$ so that $\alpha \approx L_{k\epsilon}/L_{kS} = ST_L$.

6.5 Discussion

6.5.1 Relevancy to Conceptual Interpretations of Length Scales

From the qualitative analysis of section 6.4, we see that the concept of an $NT_L - ST_L$ space is indeed useful for interpreting large scale turbulent overturning, and that frequently cited critical values in Ri and ST_L appear to be good first order approximations of regime thresholds. Furthermore, it appears that scales involving turbulent kinetic energy generally appear to be better predictors of overturns than those without. In other words, the magnitude of k appears fundamental to overturn size in all regimes, while the relevance of ϵ is less general. In shear-dominated flow, $L_{kS} \sim L_E > L_C$ supports the suggestion that the Corrsin scale defines an upper limit of the inertial subrange that is somewhat smaller than the largest scales of the flow. Likewise, $L_{kN} \sim L_E > L_O$ supports the same assertion regarding the Ozmidov scale in buoyancy-dominated flow. These findings are in accord with the original arguments leading to the derivation of L_C (Corrsin, 1958) and L_O (Dougherty,

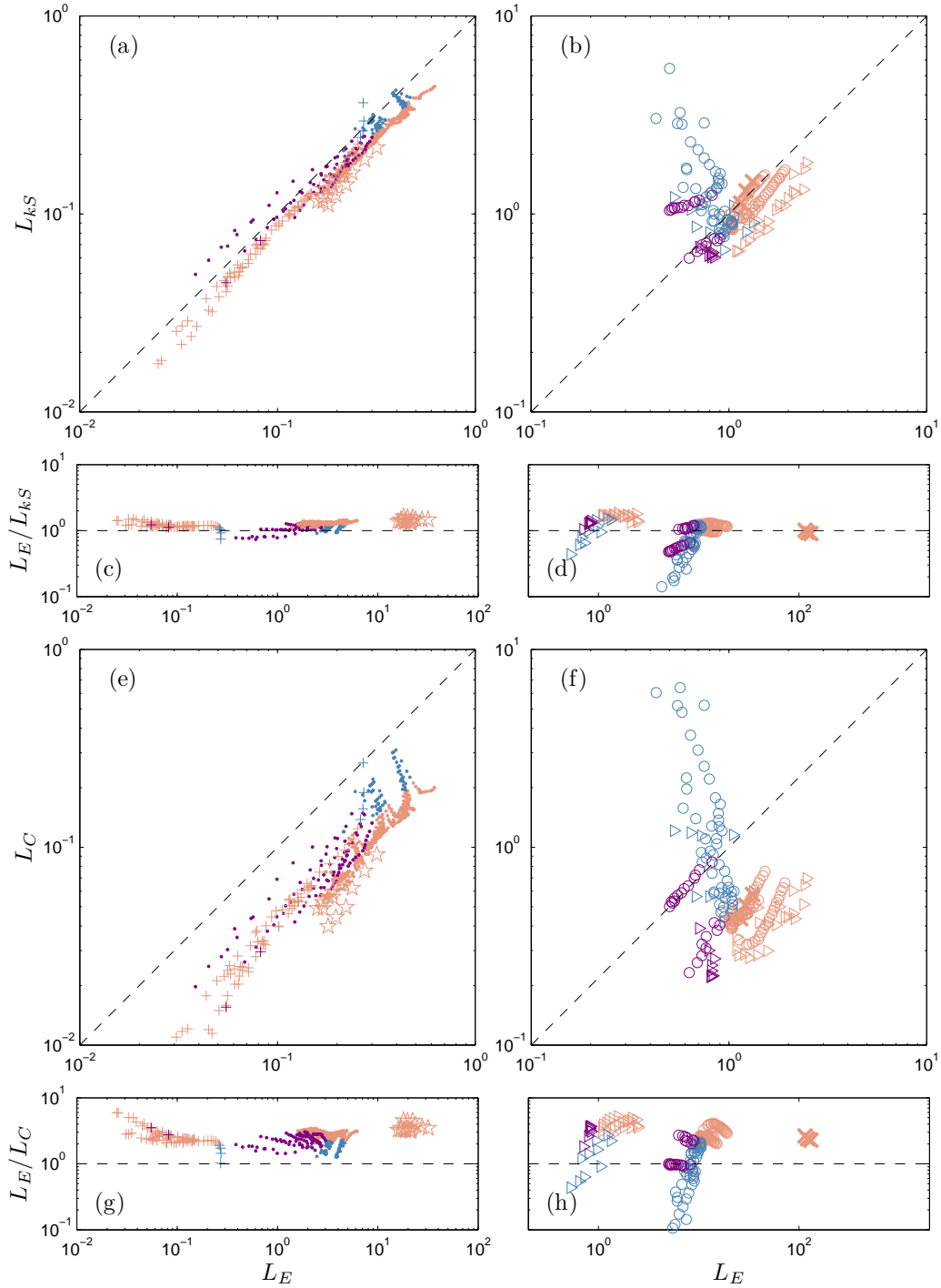


Figure 6.4: Comparisons of the fundamental shear length scales, L_{kS} and L_C , to L_E . Left panels show DNS data in normalized units (a,c,e,g); right panels show experimental data in cm (b,d,f,h). Data of SKIF and Rogers et al. (1989) have been shifted to the right by 10^1 and 10^2 , respectively in (c) and (g). Data of KV and Tavoularis and Corrsin (1981) have been shifted to the right by 10^1 and 10^2 , respectively in (d) and (h). Shifts were done for clarity. Symbols are noted in Figure 6.2 with the exception of SKIF which are shown as dots.

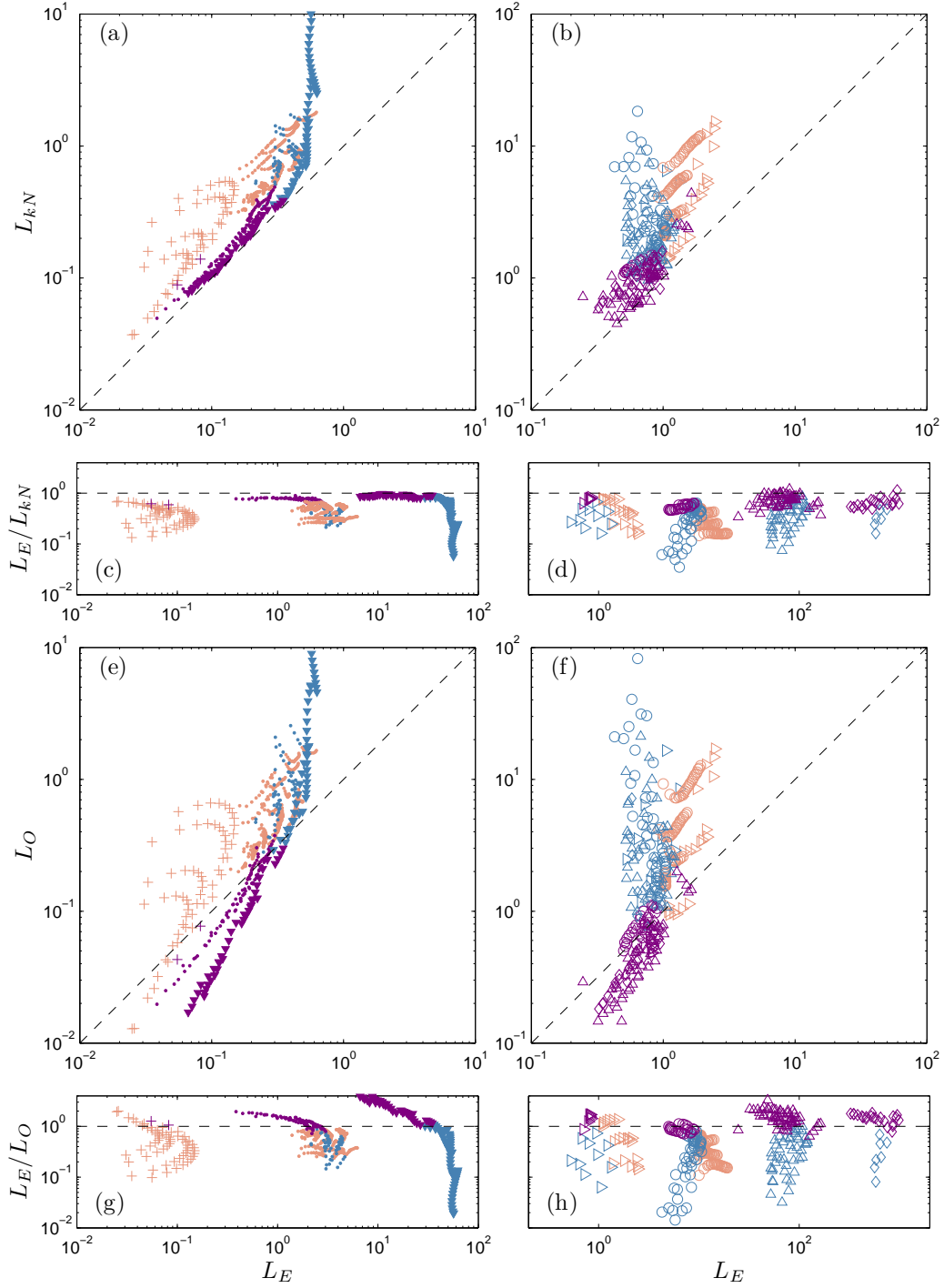


Figure 6.5: Comparisons of the fundamental buoyancy length scales, L_{kN} and L_O , to L_E . Left panels show DNS data in normalized units (a,c,e,g); right panels show experimental data in cm (b,d,f,h). Data of SKIF and Mater et al. (2013) have been shifted to the right by 10^1 and 10^2 , respectively in (c) and (g). Data of KV Itsweire et al. (1986), and Stillinger et al. (1983) have been shifted to the right by 10^1 , 10^2 , and 10^3 , respectively in (d) and (h). Shifts were done for clarity. Symbols are noted in Figure 6.2 with the exception of SKIF which are shown as dots.

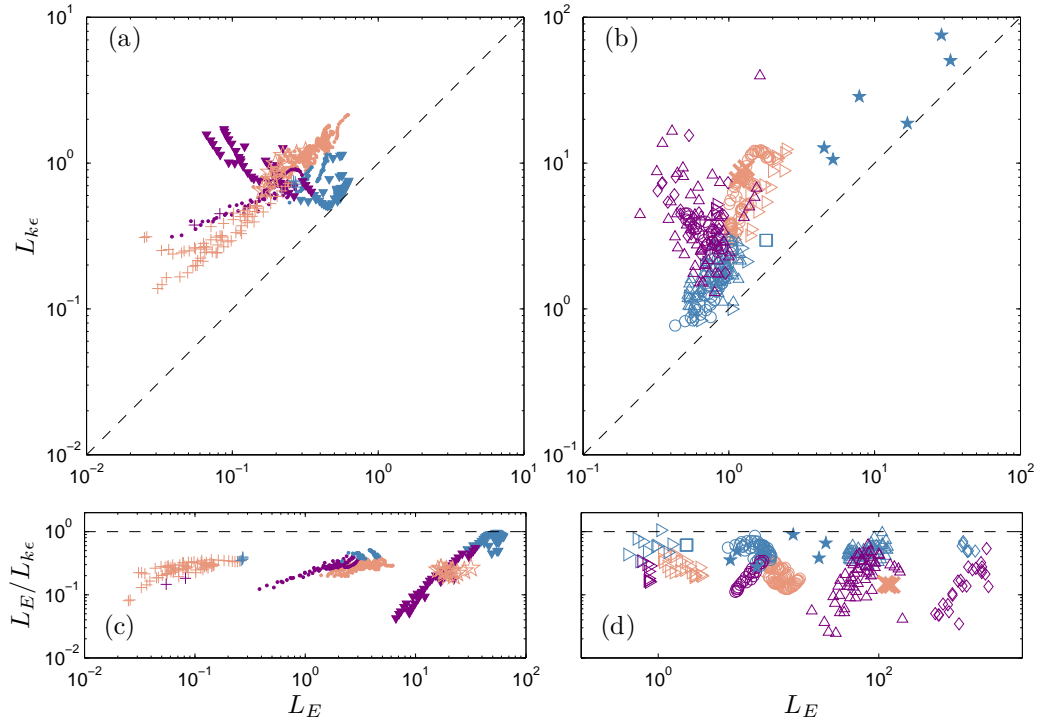


Figure 6.6: Comparisons of the fundamental isotropic length scale, $L_{k\epsilon}$, to L_E . Left panels show DNS data in normalized units (a,c); right panels show experimental data in cm (b,d). Data of SKIF, Mater et al. (2013), and Rogers et al. (1989) have been shifted to the right by 10^1 , 10^2 , and 10^2 , respectively in (c). Data of KV, Itsweire et al. (1986), Tavoularis and Corrsin (1981), and Stillinger et al. (1983) have been shifted to the right by 10^1 , 10^2 , 10^2 , and 10^3 , respectively in (d). Shifts were done for clarity. Symbols are noted in Figure 6.2 with the exception of SKIF which are shown as dots.

1961; Ozmidov, 1965) that sought not to determine the outer scale of the flow, but to define the largest scale that could remain isotropic in the presence of shear or stratification. These early theories are entirely compatible with the possibility of anisotropic overturns larger than L_C or L_O as realized in the current data. In the unforced regime, where $S, N \rightarrow 0$ and $L_E \sim L_{k\epsilon}$, all scales involving forcing approach infinity, and thus lack any physical analogue in the flow.

6.5.2 Relevancy to Oceanic Measurements

A main implication of the current findings is that inferences of turbulent kinetic energy and its dissipation rate can be made from observations of overturning. Specifically,

$$k \sim \begin{cases} (\epsilon L_T)^{2/3} & \text{if } ST_L < ST_{L,c} \text{ and } NT_L < NT_{L,c} \text{ (unforced)} \\ (SL_T)^2 & \text{if } ST_L \geq ST_{L,c} \text{ and } Ri \leq Ri_c \text{ (shear-dominated)} \\ (NL_T)^2 & \text{if } NT_L \geq NT_{L,c} \text{ and } Ri \geq Ri_c \text{ (buoyancy-dominated)} \end{cases} \quad (6.9)$$

and

$$\epsilon \sim \begin{cases} N^3 L_T^2 & \text{if } ST_L < ST_{L,c} \text{ and } NT_L \approx NT_{L,c} \text{ (unforced/buoyancy-dominated)} \\ N^3 L_T^2 & \text{if } ST_L \geq ST_{L,c}, Ri \leq Ri_c \text{ and } ST_L \approx (NT_L)^{3/2} \text{ (shear-dominated)} \\ S^3 L_T^2 & \text{if } NT_L \geq ST_{L,c}, Ri \geq Ri_c \text{ and } ST_L \approx (NT_L)^{2/3} \text{ (buoyancy-dominated)} , \end{cases} \quad (6.10)$$

where we have assumed $L_T \approx L_E$. Note that the second line of relation (6.10) results from the possibility of $L_T \sim L_{kS} = L_O$ in the shear-dominated regime despite, as claimed here, that L_O is of less physical relevance than L_{kS} or its analogue, L_C , in this regime; theoretically, it is L_C , instead of L_O , that determines the upper end of the inertial subrange while L_{kS} determines the largest scale of the flow. As Ri decreases below Ri_c in the shear-dominated regime, L_O grows relative to L_C and will thus become coincident with L_T when

$Ri \approx (NT_L)^{-1}$, or $ST_L \approx (NT_L)^{3/2}$, despite becoming an irrelevant concept physically. Analogously, the third line of relation (6.10) results from the possibility of $L_T \sim L_{kN} = L_C$ in the buoyancy-dominated regime; as Ri increases, L_C grows relative to the more physically relevant L_O and becomes coincident with L_T when $Ri \approx ST_L \approx (NT_L)^{2/3}$.

Selection of the proper relation from (6.9) or (6.10) requires determination of flow regime — a not so trivial task in practice since T_L is not known *a priori*. One possible solution is an iterative approach to determine k if microstructure measurements of ϵ are available. Specifically, the flow can be initially assumed to be shear- or buoyancy-dominated depending on the value of Ri made available through mean measurements of N and S . Next, a preliminary value for k can be inferred from either the second or third condition of (6.9). With measurements of ϵ , corresponding values of NT_L and ST_L can then be determined along with the suggested regime. If the suggested regime agrees with that guessed initially, the preliminary value for k can be considered an accurate inference. Otherwise, the flow is likely in the unforced regime and the first relation of (6.9) is needed to infer k . If validated, a method such as this stands to be a major breakthrough in the field of observational oceanography due to the practical difficulties in directly measuring all three components of the fluctuating velocity that define k . Moreover, by inferring k from a purely overturning scale in L_T , the kinetic energy due to non-overturning internal waves is effectively filtered out making the inferred value representative of purely turbulent kinetic energy.

Beyond providing access to elusive quantities, the current findings have implications for estimates of diapycnal mixing of density and momentum in the open ocean. In the absence of microstructure measurements, accurate inference of ϵ is especially relevant to estimations of density diffusivity based on the popular formulation of Osborn (1980),

$$K_d = \Gamma \frac{\epsilon}{N^2}, \quad (6.11)$$

and to estimations of momentum diffusivity using an analogous formulation,

$$K_m = (1 + \Gamma) \frac{\epsilon}{S^2}, \quad (6.12)$$

(see Gregg, 1987) where $\Gamma \equiv -B/\epsilon$ is the mixing efficiency defined in terms of the buoyancy flux, $B \equiv -\langle \rho' w \rangle g / \rho_0$. The diffusivities above are typically estimated using some assumed value or parameterization for Γ and an inferred value of ϵ obtained under the assumption of $L_T \sim L_O$ without explicit knowledge of the flow regimes outlined here. In light of the current findings, we see that this may lead to over-estimations of mixing in buoyancy-dominated flow or under-estimations in the weakly stratified regimes (not considering errors in estimating Γ).

Now consider an alternative approach where (6.11) and (6.12) are re-cast in terms of k which, according to a comparison of (6.9) and (6.10), can be more generally inferred than ϵ . Without loss of generality, the equations become

$$K_d = \Gamma \frac{L_{kN}^2}{T_L} = \left(\frac{\Gamma}{ST_L} \right) Ri^{-1/2} \frac{k}{N}, \quad (6.13)$$

and

$$K_m = (1 + \Gamma) \frac{L_{kS}^2}{T_L} = \left(\frac{1 + \Gamma}{ST_L} \right) Ri^{1/2} \frac{k}{N}. \quad (6.14)$$

In the present data we see that ST_L rarely exceeds about 10 with most of the stratified shear-flow data falling near or slightly above $ST_{L,c}$. This is in accordance with the discussion of Jacobitz et al. (1997), who indicated that there exists a maximum value of ST_L above which rapid distortion of the flow reduces nonlinear interactions, thereby limiting the production of turbulence. The lack of data with $ST_L \ll ST_{L,c}$ is likely due to the rapid rate at which such turbulence would decay. If it is assumed that oceanic turbulence exhibits a similarly narrow range in ST_L , then that parameter can be replaced in (6.13) and (6.14) by some average constant in the interest of practicality. Let this constant be defined as \widehat{ST}_L . Furthermore, if

ocean turbulence is assumed to be predominately shear- and/or buoyancy-dominated, then k can be inferred upon knowing solely Ri and using the latter two relations of (6.9) so that the inferred value, \hat{k} , is given by

$$\hat{k} = \begin{cases} (\beta_{kS}L_T S)^2 & \text{if } Ri < Ri_c \\ (\beta_{kN}L_T N)^2 & \text{if } Ri > Ri_c. \end{cases} \quad (6.15)$$

where β_{kS} and β_{kN} are constants of order $O(10^0)$ from the relations $L_{kS} = \beta_{kS}L_T$ and $L_{kN} = \beta_{kN}L_T$. With this simplification, (6.13) and (6.14) can be approximated as simple functions of the readily measurable L_T , N , and S , and a parameterized mixing efficiency, $\hat{\Gamma}$:

$$\widehat{K}_d = \begin{cases} \frac{\hat{\Gamma}}{ST_L} N(\beta_{kS}L_T)^2 Ri^{-3/2} & \text{if } Ri < Ri_c \\ \frac{\hat{\Gamma}}{ST_L} N(\beta_{kN}L_T)^2 Ri^{-1/2} & \text{if } Ri > Ri_c \end{cases} \quad (6.16)$$

$$\widehat{K}_m = \begin{cases} \frac{1+\hat{\Gamma}}{ST_L} N(\beta_{kS}L_T)^2 Ri^{-1/2} & \text{if } Ri < Ri_c \\ \frac{1+\hat{\Gamma}}{ST_L} N(\beta_{kN}L_T)^2 Ri^{1/2} & \text{if } Ri > Ri_c \end{cases} \quad (6.17)$$

where hat notation ($\hat{}$) has been used to denote parameterized or assumed values. Presently, we will leave a discussion of mixing efficiency within the context of the current framework for chapter 7 but note that, in practice, this quantity is typically assumed to be an increasing function of Ri (e.g., Mellor and Yamada, 1982) or simply a constant of approximately 0.20 (e.g., Ferron et al., 1998). The advantage of (6.16) and (6.17) is that the diffusivities are approximated with a more robust interpretation of L_T .

To employ the simplified models of (6.16) and (6.17), we can assume $\widehat{ST}_L = 4$ based on the central tendency of the considered data. Also, we will approximate mixing efficiency with the simple exponential that mimics the fit of Mellor and Yamada (1982). However, because counter-gradient buoyancy fluxes are present in some data sets, we carefully redefine the

mixing efficiency to be

$$\Gamma^* = \epsilon_{PE}/\epsilon \quad (6.18)$$

where $\epsilon_{PE} \equiv N^2 \epsilon_\rho / (\partial \bar{\rho} / \partial z)^2$ is the irreversible dissipation of available (turbulent) potential energy (i.e., the rate at which background potential energy is irreversibly increased) with $\epsilon_\rho \equiv \kappa_\rho \langle \frac{\partial \rho'}{\partial x_j} \frac{\partial \rho'}{\partial x_j} \rangle$ representing the dissipation of scalar variance. In using Γ^* , instead of the traditional Γ , reversible stirring effects are avoided. In (6.18) and elsewhere, the superscript $*$ indicates the irreversible (i.e., diapycnal) nature of the term. We note that the two forms, Γ and Γ^* , are equal for stationary, homogeneous flows and that an irreversible flux Richardson number can be defined as $R_f^* \equiv \epsilon_{PE} / (\epsilon_{PE} + \epsilon) = \Gamma^* / (1 + \Gamma^*)$. In lieu of a more formal parameterization of R_f^* or Γ^* we use a simple exponential form,

$$\widehat{R}_f^* = 0.17(1 - \exp(-7.5 Ri)), \quad (6.19)$$

where we have assumed the asymptotic value of the flux Richardson number to be 0.17 (Osborn, 1980). For subsequent calculations, \widehat{K}_d^* and \widehat{K}_m^* denote the values from (6.16) and (6.17) when mixing efficiency is defined by (6.18). Our choice for (6.19) as a parameterization for R_f^* is no doubt an oversimplification, but is used here as a simple demonstration that provides an acceptable fit to the data (not shown) and is practically relevant. The proportionality constants needed for determining \hat{k} , namely β_{kS} and β_{kN} , were determined for each data set and are order one. To determine β_{kS} for a given data set, only points within the shear-dominated regime were considered. Likewise, β_{kN} is determined only using points within the buoyancy-dominated regime.

The new models can be compared to the actual diapycnal diffusivities. Assuming approximately stationary, homogeneous turbulence, these are

$$K_d^* = \frac{\epsilon_{PE}}{N^2}, \quad (6.20)$$

and

$$K_m^* = (\epsilon + \epsilon_{PE}) \frac{\epsilon}{S^2}, \quad (6.21)$$

which result from substitution of (6.18) into (6.11) and (6.12), respectively. We note that (6.20) is simply the Osborn-Cox formulation (Osborn and Cox, 1972) and (6.21) is its analogue for momentum diffusivity. The comparisons are shown in Figures 6.7(a) and 6.8(a) for the data sets which include ϵ_{PE} .

For comparison, conventional diffusivity estimates that rely on $L_O = L_E \Rightarrow \epsilon = N^3 L_E^2$ for use in (6.11) and (6.12) are plotted against the actual values in Figures 6.7(b) and 6.8(b). Since we are not currently concerned with the best method for parameterizing mixing efficiency, we use (6.19) in both new and conventional estimates for consistency. Clearly, the lack of a linear relationship between L_O and L_E leads to weaker performance of the conventional method when compared to that of the proposed alternative.

The relative agreement between actual and inferred diffusivities under the proposed method is quite encouraging. The scatter in the data is primarily due to ST_L values that differ from the assumed constant and departures in R_f^* from the simple prediction of (6.19). This can be examined further upon inspection of the ratios

$$\frac{\widehat{K}_d^*}{K_d^*} = \left(\frac{\widehat{\Gamma}^*}{\Gamma^*} \right) \frac{S\hat{k}/\epsilon}{\widehat{ST}_L} \quad (6.22)$$

and

$$\frac{\widehat{K}_m^*}{K_m^*} = \left(\frac{1 + \widehat{\Gamma}^*}{1 + \Gamma^*} \right) \frac{S\hat{k}/\epsilon}{\widehat{ST}_L}, \quad (6.23)$$

where the approximated or assumed quantities are again differentiated with hats. It can be seen from the factors in parentheses that the performance of \widehat{K}_d^* is more sensitive to the parameterization of mixing efficiency than is \widehat{K}_m^* . Evoking β_{kS} and β_{kN} leads to $\hat{k} \approx k$ so that the second factor is essentially the ratio of actual ST_L to its assumed value.

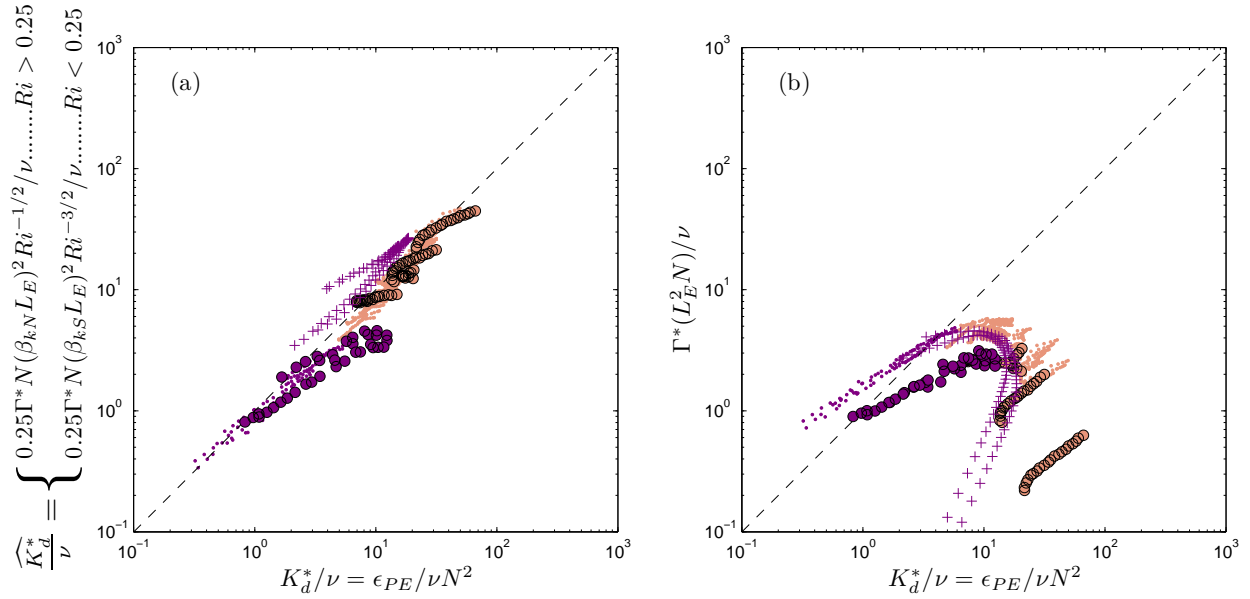


Figure 6.7: Comparisons of estimated and actual density diffusivity, K_d^* , normalized by ν . In (a), the estimated diffusivity, \widehat{K}_d^* , is calculated from (6.16) with Γ^* from (6.19), $\widehat{ST}_L = 4$, and $\beta_{kS} = 0.76, 0.83, 0.88$ and $\beta_{kN} = 1.37, 1.65, 1.90$ for the data of SKIF, GVA, and KV, respectively. In (b), the estimate $\Gamma^*(L_E^2 N)$ is based on the conventional assumption, $L_E \approx L_O$. Symbols are as indicated in Figure 6.2 with the exception of the SKIF data which are shown as dots. Points are colored according to the regimes of Figure 6.2. For the evolving turbulence of SKIF and KV, only data after the shear-normalized time of $St = 6$ (for SKIF) or the grid-normalized distance of $x/M = 50$ (for KV) were considered to lessen the influence of initial conditions (i.e., the flow is no longer in the unforced regime).

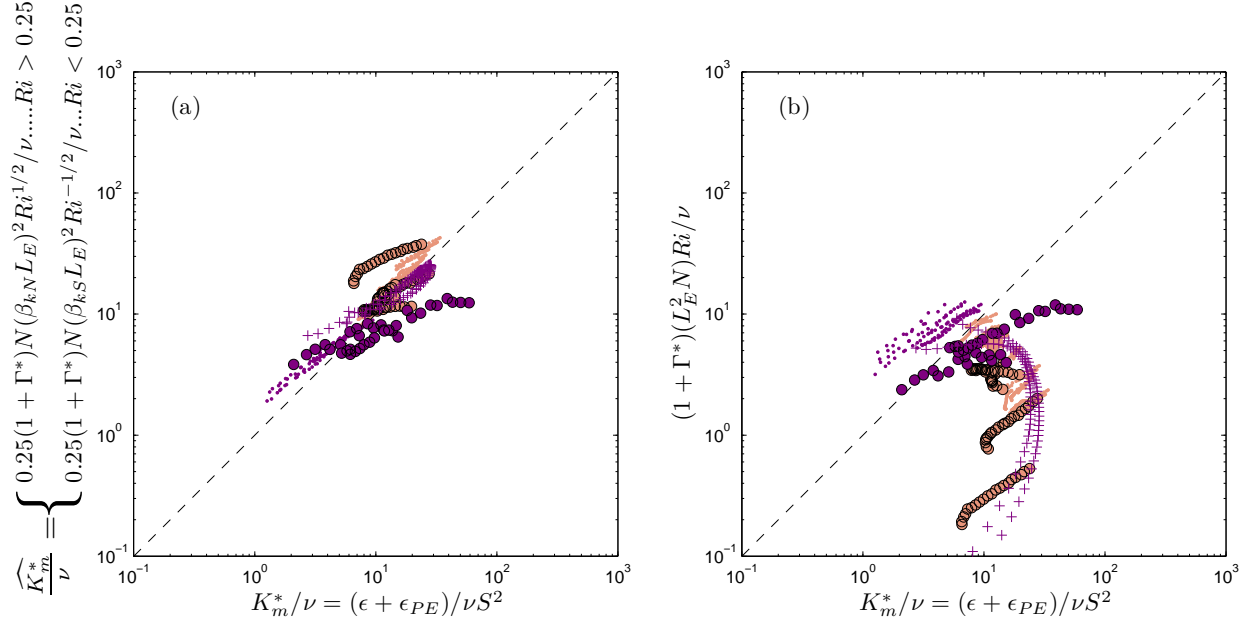


Figure 6.8: Comparisons of estimated and actual momentum diffusivity, K_m^* , normalized by ν . In (a), the estimated diffusivity, $\widehat{K_m^*}$, is calculated from (6.17) with Γ^* from (6.19), $\widehat{ST}_L = 4$, and $\beta_{kS} = 0.76, 0.83, 0.88$ and $\beta_{kN} = 1.37, 1.65, 1.90$ for the data of SKIF, GVA, and KV, respectively. In (b), the estimate $(1 + \Gamma^*)(L_E^2 N) Ri$ is based on the conventional assumption, $L_E \approx L_O$. Symbols are as indicated in Figure 6.2 with the exception of SKIF data which are shown as dots. Points are colored according to the regimes of Figure 6.2. For the evolving turbulence of SKIF and KV, only data after the shear-normalized time of $St = 6$ (for SKIF) or the grid-normalized distance of $x/M = 50$ (for KV) were considered to lessen the influence of initial conditions (i.e., the flow is no longer in the unforced regime).

6.6 Conclusions

Using dimensional analysis and physical reasoning we have argued that NT_L , ST_L , Re_L , and Pr form a comprehensive set of dimensionless parameters that generally describes stably-stratified shear-flow turbulence. In the interest of geophysical applications where molecular effects are minimal, we have proposed that the description simplifies to a two-dimensional parameter space defined by NT_L and ST_L . While not needed from a strictly dimensional analysis standpoint, we have also evoked the popular mean parameter, Ri . With these three parameters we see that the flow can potentially occupy three conceptual regimes of “shear-dominated”, “buoyancy-dominated”, and “unforced” turbulence. While the first two regimes are commonly cited and delineated using Ri , consideration for the third regime allows for the unifying framework presented here. Foundational to the framework is that knowledge of the time scale of the turbulence, T_L , is needed along with the imposed timescales, S^{-1} and N^{-1} , for a complete description of the turbulence. Using DNS and experimental data, we have shown such a description to be particularly enlightening with regard to the growth of turbulence and the length scale of overturning. In the shear-dominated regime, turbulence grows and the size of the overturns is determined by L_{kS} , while turbulence decays in the buoyancy-dominated and unforced regimes where the overturns are determined by L_{kN} and $L_{k\epsilon}$, respectively. These insights would not be possible using a single parameter such as Ri .

These findings have several implications for oceanic studies. Most obviously, they imply that turbulent kinetic energy can be inferred from observed overturns and mean quantities if some idea of flow regime exists. Due to the notorious difficulties involved in measuring k , oceanic data have not been plotted within the $NT_L - ST_L$ space and, therefore, generalities of oceanic flow regimes are lacking. However, it is reasonable that oceanic flows are strongly influenced by both mean shear and stratification so that Ri becomes the only parameter needed for inference of k . In this sense, inference of k becomes more general than inference of ϵ since the latter also requires knowledge of NT_L . This has serious implications for field

estimations of diapycnal mixing when only Ri is typically available. Because inference of ϵ without knowledge of NT_L is apparently less robust than inference of k , we have re-cast the traditional Osborn formulations for density and momentum diffusivity in terms of k . Upon exploiting the apparently narrow range in ST_L so that this parameter is assumed to be some constant value, the diffusivities become approximate functions of L_T , Ri , and Γ^* . A simple Ri -based parameterization for Γ^* is employed to allow evaluation of this new model. A comparison of the model to the quasi-stationary prediction of the Osborn-Cox formulation yields encouraging results and shows improved performance over the traditional method of inferring ϵ from L_T . The next step toward verifying and applying this unifying framework to oceanic (and atmospheric) turbulence will require independent but concurrent measurements of k , ϵ , S , and N for high Reynolds number flows.

In the next chapter, we will employ the multi-dimensional framework in a study of mixing efficiency. The Ri -based description used in this chapter (equation 6.19) will be evaluated along with several others commonly used in defining turbulent diffusivities. Both DNS and field data will be relied upon.

Chapter 7

Parameterizations of Mixing Efficiency⁸

7.1 Introduction

The efficiency at which turbulent kinetic energy is irreversibly converted to background potential energy in a stratified fluid is of fundamental importance to estimates of diapycnal mixing in geophysical settings. In both observational studies and numerical models of oceanic and atmospheric flows, diapycnal mixing is typically represented using the turbulent diffusivity formulation of Osborn (1980) for stationary, homogeneous turbulence,

$$K_d = \left(\frac{R_f}{1 - R_f} \right) \frac{\epsilon}{N^2}, \quad (7.1)$$

where ϵ is the dissipation rate of turbulent kinetic energy, $N = \sqrt{(g/\rho_0)\partial\bar{\rho}/\partial z}$ is the buoyancy frequency, and the mixing efficiency is represented as the flux Richardson number,

$$R_f = \frac{-B}{P} \approx \frac{-B}{-B + \epsilon}, \quad (7.2)$$

where $B = -(g/\rho_0)\langle u_i \rho' \rangle \delta_{i3}$ is the vertical buoyancy flux and $P = -\langle u_i u_j \rangle S$ is the production of turbulent kinetic energy (TKE) that is a function of the Reynolds stress tensor, $\langle u_i u_j \rangle$, and the mean shear, $S = \partial\bar{U}_i/\partial x_j$. The approximate equivalence in equation 7.2 arises from the same assumptions underpinning the formulation of equation 7.1 (see Gregg, 1987). A

⁸This chapter constitutes a manuscript that has been published in *Geophysical Research Letters* under the title, “The quest for an unambiguous parameterization of mixing efficiency in stably stratified geophysical flows” (Mater and Venayagamoorthy, 2014a). Background information and literature relevant to this chapter are presented again so the chapter may be read as a stand-alone work. The chapter is written in a collective “we” voice to acknowledge collaboration with Dr. S. K. Venayagamoorthy.

related representation of the mixing efficiency is the flux coefficient $\Gamma = -B/\epsilon = R_f/(1-R_f)$, however, the current work will refer exclusively to R_f as the “mixing efficiency”.

The widespread use of equation 7.1 in both modeling and observational campaigns has promoted a great deal of research on understanding the variability of R_f about the canonical maximum value of $R_f \approx 0.17$ ($\Gamma \approx 0.2$) theorized by Ellison (1957), shown experimentally by Britter (1974), and inferred in the ocean by Osborn (1980). Because of the difficulties in directly measuring R_f in the field (i.e., non-stationarity, counter-gradient buoyancy fluxes, poor spatial resolution, etc.) and the general complexity of geophysical flows, our current understanding of mixing efficiency is primarily founded upon well-controlled laboratory experiments and direct numerical simulations (DNS). However, even within the context of these simple flows, no single parameterization for R_f in terms of broadly relevant non-dimensional parameters has received widespread acceptance. This lack of a unified description of mixing efficiency is largely due to certain ambiguities that arise when only a single non-dimensional parameter is employed to describe R_f . The goal of this chapter is to explain key ambiguities that plague three popular single-parameter approaches. We will generally consider approaches based on the gradient Richardson number, $Ri = N^2/S^2$, the turbulent Froude number, $Fr = u/(Nl)$, and the buoyancy Reynolds number, $Re_b = \epsilon/(\nu N^2)$, where u and l are the velocity and length scales that characterize the inertial motions (i.e., energy-containing eddies) of the turbulence and ν is the kinematic viscosity of the fluid.

Because we wish to examine the efficiency at which turbulent kinetic energy is being irreversibly converted to background potential energy, we will only consider the down-gradient component of the buoyancy flux that leads to mixing. Therefore, we will consider an alternative measure of irreversible mixing efficiency that is defined using the positive-definite dissipation rate of available (turbulent) potential energy, $\epsilon_{PE} = N^2\epsilon_\rho(\partial\bar{\rho}/\partial z)^{-2}$, where $\epsilon_\rho = \kappa_\rho\langle\frac{\partial\rho'}{\partial x_j}\frac{\partial\rho'}{\partial x_j}\rangle$ is the molecular smoothing of density fluctuations and κ_ρ is the molecular diffusivity of density. Similar to other investigations of evolving flows (e.g., Peltier and Caulfield, 2003; Venayagamoorthy and Stretch, 2010), we define the irreversible mixing

efficiency to be

$$R_f^* = \frac{\epsilon_{PE}}{\epsilon_{PE} + \epsilon}, \quad (7.3)$$

where the superscript indicates the diapycnal (irreversible) nature of the term.

7.2 A Unifying Framework

Ambiguities that arise using solely Ri , Fr , or Re_b to describe R_f^* will be highlighted using the multiple-parameter approach of Mater and Venayagamoorthy (2014b). They present a conceptual framework which explicitly considers the independent influences that shear, stratification, and viscosity have on the inertial scales of the turbulence using a shear strength parameter,

$$ST_L = \frac{Sk}{\epsilon}, \quad (7.4)$$

a buoyancy strength parameter,

$$NT_L = \frac{Nk}{\epsilon}, \quad (7.5)$$

and the turbulent Reynolds number,

$$Re_L = \frac{k^2}{\nu\epsilon} = \left(\frac{T_L}{T_\eta}\right)^2, \quad (7.6)$$

where $k = \frac{1}{2}\langle u_i u_i \rangle$ is the turbulent kinetic energy, $T_L = k/\epsilon$ is the time scale of the inertial motions (i.e., largest eddies in an isotropic sense), and $T_\eta = (\nu/\epsilon)^{1/2}$ is the Kolmogorov time scale (i.e., that of the smallest eddies). We note that $NT_L = Fr_k^{-1}$, where Fr_k is a Froude number with $u \sim k^{1/2}$ and $l \sim k^{3/2}/\epsilon$. In the interest of geophysical flows, an assumption of Reynolds number independence allows the framework to be simplified to a two-dimensional parameter space based on NT_L and ST_L that, with consideration for the gradient Richardson number, is divided into “unforced”, “shear-dominated”, and “buoyancy-dominated” regimes. The $NT_L - ST_L$ parameter space is represented here in figure 7.1 in which we have re-named

the “unforced” regime to be the “inertia-dominated” regime due to the possibility of decaying turbulence generated by un-sustained forcing mechanisms (i.e., external forcing by a sudden disturbance not related to mean shear). Turbulence generally grows in the shear-dominated regime and decays in the buoyancy-dominated regime. Mater and Venayagamoorthy (2014b) find the regimes to be relevant for scaling the vertical overturns observed in a large database of numerical and laboratory flows. In the current chapter, we wish to extend the discussion to include mixing efficiency of low Reynolds number flows and, as such, complement the $NT_L - ST_L$ plane with the $Re_L - NT_L$ plane that frequently appears (in related forms) in studies of stratified turbulence (figure 7.2). We explore the behavior of mixing efficiency within the framework of figures 7.1 and 7.2 using the the homogeneously-stratified shear-flow DNS data of Shih et al. (2005). Select comparisons with the atmospheric boundary layer data collected during the Vertical Transport and Mixing Experiment (VTMX) (Monti et al., 2002; Princevac et al., 2008) will also be made. Particular focus will be on the subset of the VTMX data presented in Lozovatsky and Fernando (2013). Because turbulent kinetic energy, k , is rarely measured in field studies such as the VTMX experiment, only the DNS data of Shih et al. (2005) are plotted in figures 7.1 and 7.2.

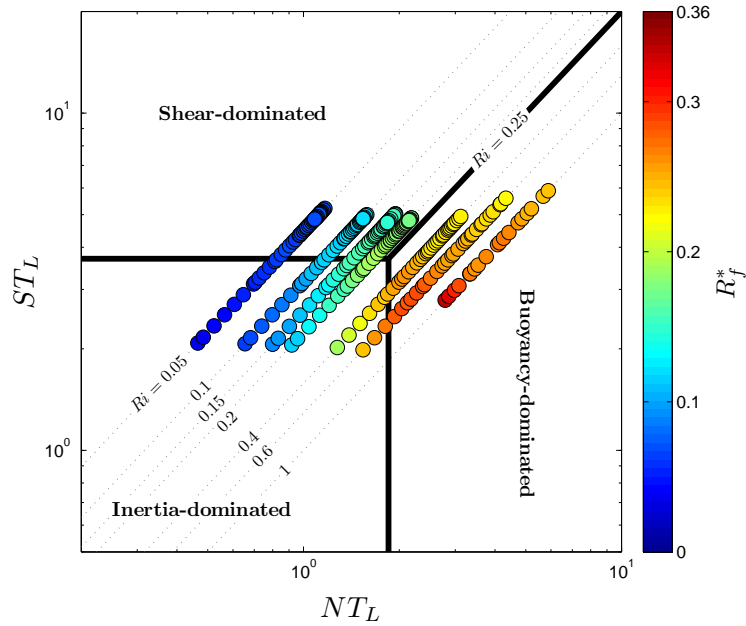


Figure 7.1: Parameter space for interpretation of high-Reynolds number turbulence from Mater and Venayagamoorthy (2014b) with data from Shih et al. (2005). Lines delineating regimes are first order approximations.

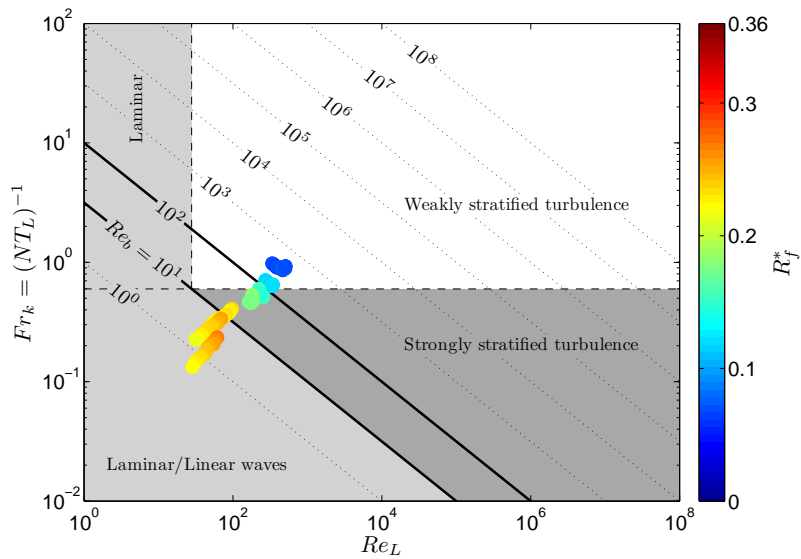


Figure 7.2: Parameter space for interpretation of stratified turbulence assuming minimal influence from shear. Data from Shih et al. (2005). Lines delineating regimes are first order approximations. Lines of $Re_b = 10$ and $Re_b = 100$ are shown in bold to delineate the “diffusive” ($Re_b < 10$), “intermediate” ($10 < Re_b < 100$), and “energetic” ($Re_b > 100$) regimes of Shih et al. (2005)

7.3 Ambiguities of Single-Parameter Approaches

7.3.1 Ri -based Approaches

Ri -based approaches characteristically assume that the mean time scales, N^{-1} and S^{-1} , are relevant to the small-scale turbulent dynamics that lead to mixing. We can generally represent such descriptions using the simplified scheme of Karimpour and Venayagamoorthy (2014) that mimics the popular parameterization of Yamada (1975) and Mellor and Yamada (1982) (as presented in Pardyjak et al. (2002)) given by,

$$R_f = R_f^\infty \{1 - \exp(-7.5Ri)\}, \quad (7.7)$$

where R_f^∞ is the maximum, asymptotic value of the flux Richardson number that is approached in strongly stratified turbulence ($Ri \gg Ri_c \approx 0.25$).

The irreversible mixing efficiency for the DNS data is plotted against Ri in figure 7.3 along with the simple parameterization of equation 7.7 using $R_f^\infty \approx 0.25$. Also plotted are the VTMX boundary layer data from Lozovatsky and Fernando (2013) along with their fit, $\Gamma = 0.005 + 1.7Ri - 1.1Ri^2$, under the assumption $\Gamma \approx R_f^*/(1 - R_f^*)$.

7.3.1.1 $Ri < 0.25$

First consider the behavior at low Ri where both the field-based fit and the Ri -based parameterization of equation 7.7 are in approximate agreement. The agreement between the predictions and the two data sets is encouraging, however, a systematic deviation from the Ri -based parameterizations is observable in the DNS data when points are identified by their respective regimes in figure 7.1. Specifically, equation 7.7 shows excellent agreement with the DNS data when the flow is in the shear-dominated regime, but over-predicts R_f^* in the inertia-dominated regime. Turbulence is inertia-dominated early in the simulations due to the sudden, shear-independent, injection of energy specified by the initial conditions

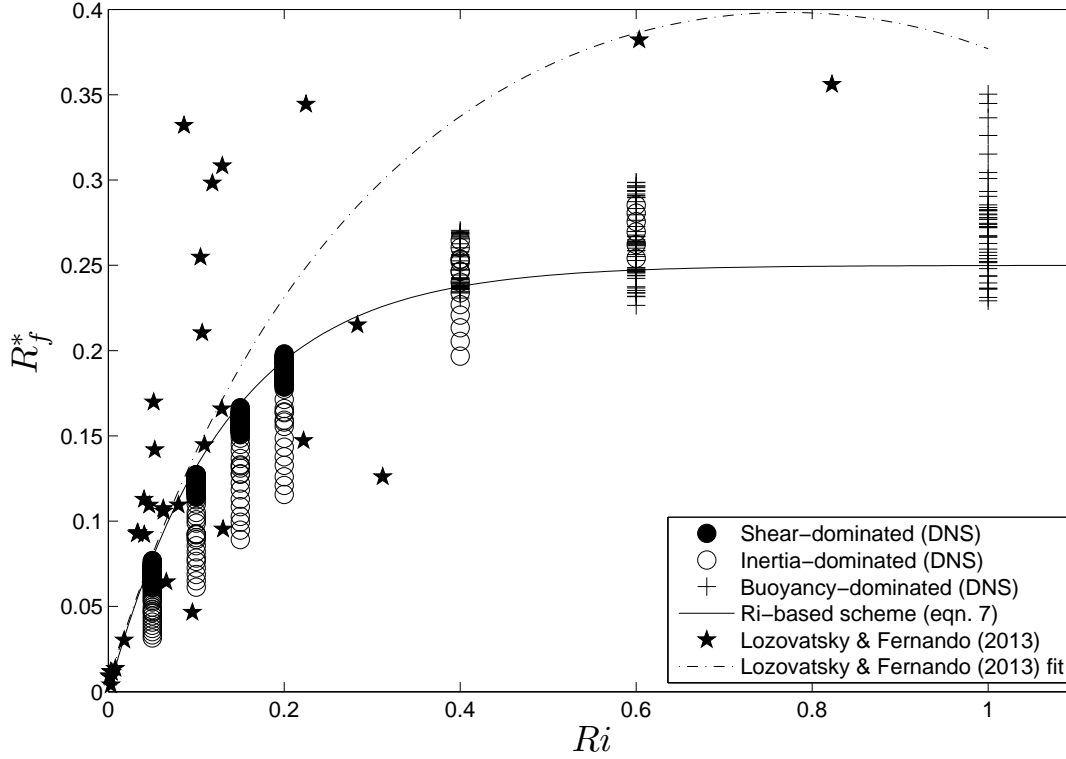


Figure 7.3: Diapycnal mixing efficiency, R_f^* , versus the gradient Richardson number, Ri , for the DNS data of Shih et al. (2005) and the geophysical data of Lozovatsky and Fernando (2013).

which leads to $T_L \ll S^{-1}$ and $T_L \ll N^{-1}$. Only after the initial disturbance decays and T_L grows do the ambient shear and stratification take over in determining the efficiency. This phenomenon is analogous to low-efficiency mixing that occurs immediately downstream of a grid (e.g., observed by Keller and Van Atta (2000)) or immediately following a sudden introduction of non-local energy into an otherwise homogeneously-sheared flow, say by a breaking internal wave. In such cases of external forcing, Ri is not the proper diagnostic because the turbulent kinetic energy present in the flow has been generated by mechanisms other than mean shear. The ambiguity of Ri in this regard has been discussed by Chang et al. (2005) and Xu et al. (2006) in the context of turbulent diffusivity, with Zaron and Moum (2009) finding that consideration for the mean kinetic energy gives an improved parameterization.

It is important to note that the temporal evolution of R_f^* demonstrated by grid-like turbulence is likely different from other mechanisms such as K-H billows in which R_f^* *decreases* with time (Smyth et al., 2001; Mashayek et al., 2013). It is conceivable that K-H turbulence evolves in the opposite sense of grid turbulence, with a transition into the inertia-dominated regime occurring later as rapid homogenization of the flow causes S , N , and R_f^* to decrease.

7.3.1.2 $Ri > 0.25$

Next consider R_f^* at high Ri where the field data exhibits a higher efficiency than the DNS data and there is considerably more scatter about equation 7.7. If weak turbulence is possible in this regime, the additional parameters to logically consider are the turbulent Reynolds number, Re_L , and the molecular Prandtl number, $Pr = \nu/\kappa_\rho$ (if comparing flows of different fluids). Unfortunately, a quantitative analysis of Reynolds number dependence is precluded because k is not available from the field data. However, physical reasoning suggests that for strong stratification, efficiency may be increased by increasing the molecular diffusion rate of the scalar (via decreasing Pr) or by increasing the small-scale gradients across which the molecular diffusion acts (via increasing Re_L). Because the DNS and field data have similar Prandtl numbers ($Pr \approx 0.7$), the increased Reynolds number of the field data is a likely explanation for the higher efficiency.

As Ri increases for a given flow, the importance of Re_L and Pr in describing mixing efficiency should become more pronounced. Likewise, the efficiency at a high value of Ri should change with Re_L (and/or Pr), thus implying that the oft-observed non-monotonic decrease in efficiency at high Ri (e.g., Phillips, 1972; Strang and Fernando, 2001a; Mashayek et al., 2013) is intimately related with the Reynolds number of the flow. Physical reasoning suggests that the decrease in efficiency in strongly stratified flow could be forestalled to higher values of Ri by increasing the Reynolds number so that the small-scale overturning structure responsible for mixing (e.g., richness of secondary instabilities with K-H billows discussed by Mashayek and Peltier (2013)) is maintained. From observations of high Reynolds number

shear instabilities in a strongly stratified estuary, Geyer et al. (2010) suggest the efficiency should maintain its optimal value for sufficiently high Reynolds number. Clearly then, a description of R_f^* at high Ri without consideration for Re_L (and Pr if comparing different fluids) is likely ambiguous. Furthermore, it is quite possible that Re_L and Ri are not totally independent and that the precise relationship between the two parameters at high Ri likely depends on the mechanism which drives the turbulence.

7.3.2 Fr -based Approaches

Whereas Ri is restricted to descriptions of shear-driven turbulence in which the mean shear is easily defined, the turbulent Froude number, generically defined as $Fr = u/(Nl)$, is more broad in its applicability so long as the inertial scales u and l — or alternatively the time scale of the turbulence, l/u — can be identified. Identification of l/u is, however, a nontrivial matter. Most generally, $l/u \sim T_L \equiv k/\epsilon$ so that $Fr = Fr_k = (NT_L)^{-1}$ in line with the approach of Mater and Venayagamoorthy (2014b). However, because k is not easily obtained in the field a more practical approach is to assume $l \sim L_T$ and $u \sim (\epsilon L_T)^{1/3}$ so that $Fr = Fr_T \equiv (L_O/L_T)^{2/3}$ as was proposed by Luketina and Imberger (1989), where L_T is the observed overturning scale (see Thorpe, 1977) and $L_O = (\epsilon/N^3)^{1/2}$ is the Ozmidov scale which may be interpreted as the large-scale bound on the inertial subrange (Ozmidov, 1965).

7.3.2.1 $Fr_T > 1$

For weakly stratified sheared and shear-free laboratory turbulence with $Fr_T > 1$, Ivey and Imberger (1991) show that the simple scheme,

$$R_f = (1 + R_{\rho w}^{-1} Fr_T^{-2})^{-1}, \quad (7.8)$$

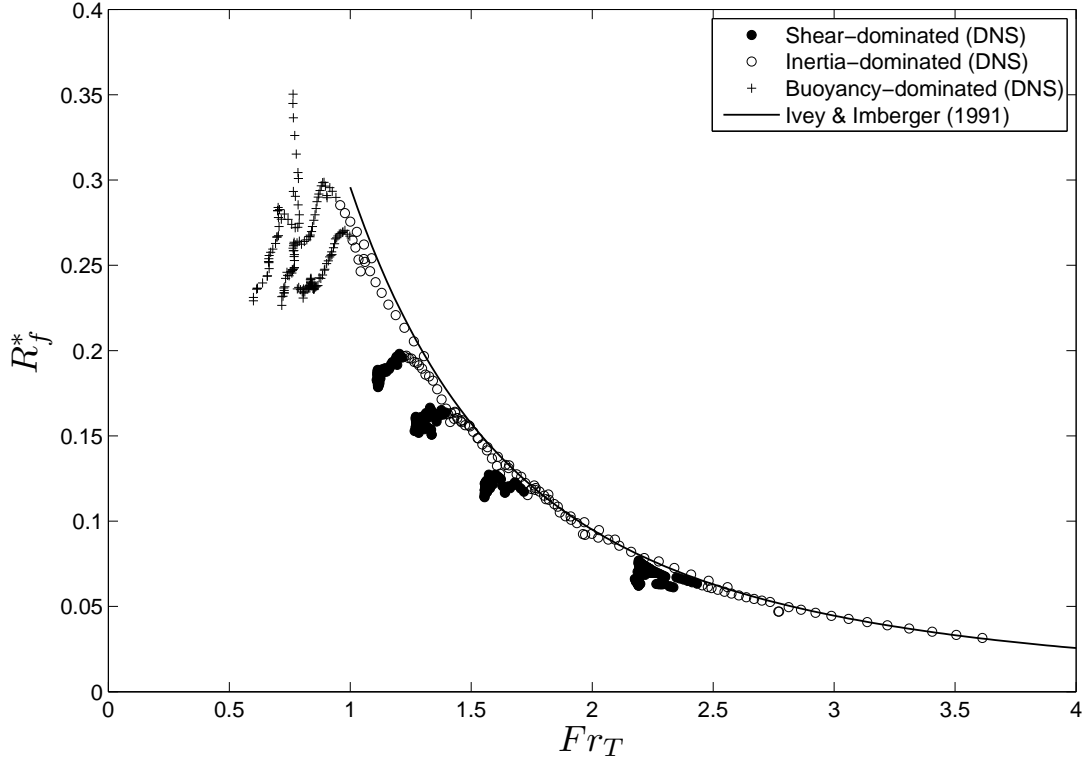


Figure 7.4: Diapycnal mixing efficiency, R_f^* , versus the overturn Froude number, Fr_T , for the DNS data of Shih et al. (2005). The parameterization of Ivey and Imberger (1991) for $Fr_T > 1$ (equation 7.8) is plotted using $R_{\rho w} = 0.42$.

provides for an excellent description of the decrease in R_f that occurs with increasing Fr_T , where $R_{\rho w} = \langle \rho' w' \rangle / (\langle \rho' \rangle \langle w' \rangle)$ is the density flux correlation coefficient which is assumed constant for a given Prandtl number. We too find that equation 7.8 accurately represents R_f^* in the weakly stratified (i.e., $Fr_T > 1$) data of Shih et al. (2005) when a representative value of $R_{\rho w} \approx 0.4$ is chosen (figure 7.4). These data correspond to the inertia- and shear-dominated regimes of figure 7.1. In contrast with the performance of the Ri -based scheme of equation 7.7, equation 7.8 is able to capture the inertia-dominated behavior, while slightly overestimating R_f^* in the shear-dominated regime where shear-induced anisotropy leads to a departure from the assumed scaling, $u \sim (\epsilon L_T)^{1/3}$ (Mater and Venayagamoorthy, 2014b). As such, Fr_T appears as the proper diagnostic in the inertia-dominated regime, while Ri properly diagnoses shear-dominated turbulence.

7.3.2.2 $Fr_T < 1$

Analogous to the decrease in R_f at high Ri , Ivey and Imberger (1991) show R_f to decrease with decreasing Fr_T for $Fr_T < 1$. In agreement with the discussion of section 7.3.1.2, they suggest R_f to be additionally dependent on the Reynolds number of the turbulence, which they define as $Re_T = (L_T/\eta)^{4/3}$, where $\eta = (\nu^3/\epsilon)^{1/4}$ is the Kolmogorov length scale. Their proposed parameterization for $Fr_T < 1$ (not plotted) employs both Re_T and Fr_T in an empirical fit to laboratory data. Unfortunately, the empirical nature of the fit limits its general applicability to other flows. Piccirillo and Van Atta (1997) for example show a large amount of scatter about the parameterization in their wind tunnel data, which they attribute to intermittent turbulent events. More recently, Dunckley et al. (2012) tested the parameterization using oceanic data with similarly discouraging results. In light of these findings, the Ivey and Imberger parameterization for $Fr_T < 1$ is conceptually promising, but perhaps lacks universality due to the variety of turbulent mechanisms that can affect the $Fr_T - Re_T$ interdependence as well as the intermittent nature of strongly stratified geophysical flows.

7.3.3 Re_b -based Approaches

As a parameter that includes an explicit, measurable quantification of the turbulence in ϵ , Re_b is a dynamic alternative to Ri that is available from field-based microstructure measurements. Furthermore, Re_b is unequivocally defined unlike the Froude number which has various definitions depending on the choice of u and l . Given these apparent advantages, recent efforts have attempted to employ Re_b as a diagnostic of mixing efficiency. A well-cited example is the work of Shih et al. (2005) who find R_f to agree with the canonical value (≈ 0.17) for a so-called “intermediate” regime of $7 < Re_b < 100$, before decreasing in an “energetic” regime of $Re_b > 100$ according to the empirical fit,

$$R_f = 1.5Re_b^{-1/2}. \tag{7.9}$$

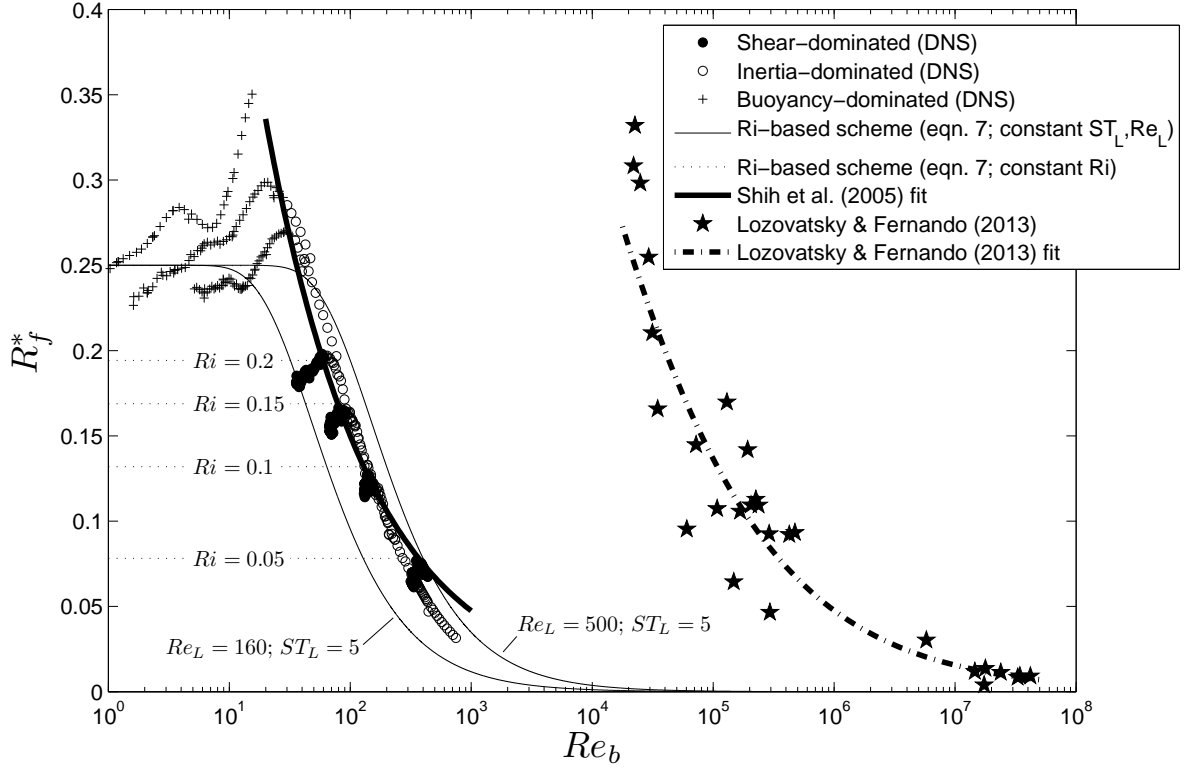


Figure 7.5: Diapycnal mixing efficiency, R_f^* , versus the buoyancy Reynolds number, Re_b , for the DNS data of Shih et al. (2005) and the geophysical data of Lozovatsky and Fernando (2013). The Ri -based scheme has been plotted assuming different values of ST_L and Re_L (solid lines) or Ri (dotted lines).

Recently, Lozovatsky and Fernando (2013) show an alternative fit for the VTMX field data given by $\Gamma = 50Re_b^{-1/2}$ or

$$R_f = (1 + 0.02Re_b^{1/2})^{-1}. \quad (7.10)$$

Equations 7.9 and 7.10 are plotted in figure 7.5 along with R_f^* for the DNS and field data. The Ri -based scheme considered in section 7.3.1 is also projected in noting that equation 7.7 may be re-written as

$$R_f = R_f^\infty \{1 - \exp(-7.5Re_L(ST_L)^{-2}Re_b^{-1})\}. \quad (7.11)$$

The curves shown are projected for different values of Re_L with ST_L held constant.

First consider the DNS data. Immediately obvious is that the roll-off limb (i.e., the “energetic regime” of Shih et al. (2005)) is composed of points from the shear-dominated or inertia-dominated regimes. Thus, mixing efficiency apparently decreases with Re_b primarily because of decreasing Ri as shown in figure 7.3 or decreasing NT_L (i.e., increasing Fr_T beyond $Fr_T = 1$ as shown in figure 7.4). This is shown quite clearly by superimposing the Ri -based scheme for constant Re_L and ST_L . Re_L for data constituting the falling limb ranges from approximately 160 late in the run with $Ri \approx 0.2$ to approximately 500 late in the run with $Ri \approx 0.05$ (Re_L plot not shown). In both runs, $ST_L \approx 5$ late in the run (see figure 7.1). Substituting these values into equation 7.11 gives two curves that bracket the falling limb data, thus reiterating that the data are well explained with the simple Ri -based description.

The ability of inviscid parameters (Ri and NT_L) to describe high- Re_b data raises an interesting and important question regarding the universality of the proposed fit of Shih et al. (2005) and Re_b -based parameterizations in general. Specifically, is there a universal relationship between the intensity of turbulence (Re_L) and the strength of the stratification (Ri or NT_L) that supports an unambiguous description of mixing efficiency based on Re_b ? This is a particularly important question to consider when employing DNS-based parameterizations to describe geophysical turbulence. In the former, high Re_b is most easily achieved with weak stratification due to computational limitations on Re_L . In the latter, however, turbulence can be sustained in the presence of strong stratification due to high Reynolds numbers. For example, consider the geophysical data of Lozovatsky and Fernando (2013) plotted in figure 7.5. In contrast to the prediction of Shih et al. (2005), the field data suggests that the trend of decreasing mixing efficiency may shift toward higher Re_b (into the “energetic regime”) by least three orders of magnitude. High mixing efficiency despite high Re_b implies that geophysical flows occupy a high Re_L , high NT_L regime not achieved in the DNS simulations.

Brethouwer et al. (2007) highlight the strongly stratified, high-Reynolds number regime that characterizes geophysical flows using a two-dimensional parameter space similar to figure 7.2 that features their formulations for the turbulent Reynolds and Froude numbers. An analogous figure is presented in Ivey and Imberger (1991). Assuming minimal influence from shear, figure 7.2 further demonstrates that the transition from “intermediate” to “energetic” turbulence proposed by Shih et al. (2005) based on their data coincides with the transition from buoyancy-dominated (strongly stratified) to weakly stratified flow (either shear- or inertia-dominated) that occurs at $NT_L \approx 1.7$ (see figure 7.1). It is likely that the particular $Re_L - NT_L$ relationship, and thus the intermediate-energetic regime transition, is unique to the trajectory of their data through the $Re_L - NT_L$ space. In comparing the DNS and field data in figure 7.5, it is likely that different trajectories are possible for geophysical flows that shift the falling limb to higher values of Re_b . To validate this hypothesis, reliable estimates of Re_L and NT_L in geophysical flows are needed.

7.4 Relevance to Field Observations

As discussed by Mater and Venayagamoorthy (2014b), a major gap remains in validating and extending the multi-parameter space used here to geophysical flows due to the current inability to accurately quantify the time scale of the turbulence, T_L , in the field. This is due mainly to difficulties associated with isolating the turbulent contribution to the three-dimensional velocity field used to quantify k . Mater and Venayagamoorthy (2014b), however, suggest a possible method for estimating k from observable quantities, N , S , and ϵ and L_T . They suggest making an initial estimate of flow regime based on Ri (i.e., either buoyancy-dominated or shear-dominated) followed by an estimation of k from either $k \sim (NL_T)^2$ (for $Ri > 0.25$) or $k \sim (SL_T)^2$ (for $Ri < 0.25$). Concurrent microstructure measurements of ϵ then allow for estimation of NT_L and ST_L which, in turn, are to be used to check

that the flow is indeed in the regime initially guessed. If the flow is found to fall into the inertia-dominated regime, the estimate of k , and thus NT_L and ST_L , are to be revised using $k \sim (\epsilon L_T)^{2/3}$. Such an approach likely works best for well-developed stratified turbulence forced by shear, in which Ri is a calculable and relevant quantity (i.e. flows near the shear-buoyancy-dominated transition). These flows may occur in the thermocline (Moum, 1996) and a specific example may be “marginally stable” turbulence of the equatorial undercurrent recently studied by Smyth and Moum (2013).

When turbulence is forced by mechanisms other than mean shear, say by convective collapse of topographically induced lee waves, the flow likely falls into either the buoyancy-dominated or inertia-dominated regime, implying that k should be inferred from $k \sim (L_T N)^2$ or $k \sim (\epsilon L_T)^{2/3}$, respectively. Noting $NT_L \approx Fr_T^{-1}$ in the former regime and $NT_L \approx Fr_T^{-3}$ in the latter, Fr_T provides a practical means of determining which scaling is most relevant. In the case of a breaking wave, it is likely that the first scaling applies for youthful turbulence ($Fr_T < 1$) and the latter applies in older turbulence where mixing has sufficiently reduced the stratification ($Fr_T > 1$). It is important to note, however, that such mechanisms quite possibly demonstrate a pre-turbulent period similar to that found for K-H billows (Smyth et al., 2001) where the available potential energy, $E_{PE} = -(g/\rho_0)\langle\rho'^2\rangle/(2\partial\bar{\rho}/\partial z) \approx N^2 L_T^2/2$, exceeds k . Instantaneous observations of L_T in youthful turbulence may then lead to overestimation of k . It remains unclear if temporal averaging in convectively-generated turbulence, say that of the Luzon Strait observed by Alford et al. (2011), leads to $\langle E_{PE} \rangle \sim \langle k \rangle$ as is suggested by the findings of (Moum, 1996) for small shear-driven overturns of the thermocline.

7.5 Concluding Remarks

The inherent complexity of stratified shear-flow turbulence necessitates a multi-parameter description of mixing efficiency. Because of this complexity, single parameter schemes are

afflicted by certain ambiguities that limit their general application to numerical models or field estimations of diapycnal mixing. Using the simple example of turbulence in the presence of homogeneous shear and stratification, we have identified several ambiguities associated with descriptions based solely upon the gradient Richardson number (Ri), the turbulent Froude number (Fr_T), and the buoyancy Reynolds number (Re_b) using a multi-parameter framework. For weakly stratified turbulence (i.e., shear-dominated or inertia-dominated), our findings suggest that an Ri -based description of mixing efficiency, such as equation 7.7, may be highly effective if complemented with a Froude number-based scheme such as equation 7.8 to account for forcing mechanisms other than mean shear (i.e., those leading to $T_L \ll S^{-1}$). For the DNS considered here, Ri governs when $ST_L > 3.3$ while Fr_T governs for $ST_L < 3.3$. Neither scheme, however, is sufficient when stratification is strong and turbulence is weak, with the decrease in mixing efficiency at high Ri or low Fr_T (high NT_L) likely being dependent the Reynolds number and the nature of the dominant turbulent mechanism. The tendency of R_f^* to increase with increasing Reynolds numbers at high Ri or low Fr_T is an important concept that remains an open area of research due to the practical restraints of numerical and laboratory flows. Finally, parameterizations based on Re_b should be viewed with caution since the interdependence of the constituent parameters, Re_L and NT_L , is not likely universal.

Extension of the multi-dimensional framework to the interpretation of turbulence in the field remains a challenge due to the lack of reliable estimates of k . While promising, the indirect estimates of k discussed in section 7.4 for either shear-driven or convectively-driven turbulence, will remain unvalidated until direct quantification of k in the field becomes a reality. As such the quest for an unambiguous parameterization of mixing efficiency in geophysical flows persists due to an incomplete set of calculable parameters.

Nonetheless, the current work provides motivation and direction for this quest in the context of observational oceanography. Furthermore, the ambiguities pointed out here have immediate implications for numerical models in which both k and ϵ are calculated as part

of turbulence closure routines, thus allowing access to the framing parameters of figures 7.1 and 7.2.

The next chapter switches our focus back to the relevancy of overturning, but in the context of observed flows and measurable quantities. The concepts embodied in the framework of this chapter and last are relied upon to help explain the observed results.

Chapter 8

Oceanic Observations of Overturning and Dissipation⁹

8.1 Introduction

Vertical density overturns are commonly used to indirectly determine the dissipation rate of turbulent kinetic energy, ϵ , and in turn diapycnal diffusivity in the ocean following the seminal works of Thorpe (1977) and Dillon (1982). In an investigation of turbulence within the thermocline, Dillon (1982) provides observational evidence suggesting a linear relationship between the size of observed overturns as quantified by the Thorpe length scale, L_T (Thorpe, 1977), and the dimensionally-constructed Ozmidov length scale, $L_O \equiv (\epsilon/N^3)^{1/2}$ (Dougherty, 1961; Ozmidov, 1965), where $N \equiv \sqrt{-(g/\rho_0)\partial\bar{\rho}/\partial z}$ is the ambient buoyancy frequency determined from the background density gradient, $\partial\bar{\rho}/\partial z$. Subsequent observations in the ocean thermocline (Moum, 1996) and in topographically-driven turbulence (Wesson and Gregg, 1994; Ferron et al., 1998) seem to agree with Dillon’s findings and have largely popularized the use of

$$\overline{\epsilon_T} = a^2 \overline{L_T^2 N^3} \quad (8.1)$$

as a method for inferring the mean dissipation rate from a given set of conventionally-measured density profiles, where the overbar represents an ensemble average in time and/or space. If valid for the flow and sample set of interest, equation 8.1 serves as a measure of

⁹A manuscript based on the work of this chapter has been submitted to the *Journal of Physical Oceanography*. The title of the work is, “Biases in Thorpe scale estimation of turbulence dissipation from large overturns in the ocean.” Background information and literature relevant to this chapter are presented again so the chapter may be read as a stand-alone work. The chapter is written in a collective “we” voice to acknowledge collaboration with Dr. S. K. Venayagamoorthy, Dr. Lou St. Laurent of Woods Hole Oceanographic Institution, and Dr. James N. Moum of Oregon State University

dissipation that is more simple and accessible than direct measurements using microstructure shear profilers. The constant of proportionality, a , is determined from an arithmetic mean of L_O/L_T (Dillon, 1982) or $\log(L_O/L_T)$ (Ferron et al., 1998) and is generally suggested to be close to unity. Widespread appeal of equation 8.1 has naturally led to its use in the study of flows characterized by large overturns. For example, Alford et al. (2011) employ the method to investigate temporal and spatial evolution of turbulence driven by topographically-influenced overturns in Luzon Strait of the South China Sea where overturns over 100 m in height have been observed. The method has also been employed in a numerical sub-grid routine to parameterize diapycnal mixing due to large overturning lee waves by Klymak and Legg (2010). Approaches such as these apply equation 8.1 to instantaneous realizations of the density field (i.e., a given profile or time step), and as such, are susceptible to error incurred from temporal variability from the physical conditions supporting $L_T \sim L_O$. Perhaps more importantly, it remains unclear if the fundamental arguments supporting $L_T \sim L_O$ even hold on average for such flows, given that the work of Thorpe (1977) and Dillon (1982) focused on relatively weak turbulence and small overturns ($< 10\text{m}$) driven by different processes. If the fundamental arguments do not hold, equation 8.1 may be unreliable regardless of the amount of averaging in time and space.

The goal of this chapter is to evaluate the relationship between L_T and L_O , and thus the appropriateness of equation 8.1, in environments where intense turbulence is driven by the collapse of large overturns. Both sampling issues and fundamental arguments will be discussed in an analysis of the results. Of particular interest are observations from Luzon Strait in the South China Sea and those from the Brazil Basin in the southern Atlantic Ocean. Common to such environments is the tidally-driven accumulation of available potential energy (APE) in large amplitude, topographically-influenced overturns that convectively destabilize into turbulent kinetic energy (TKE). The TKE is then dissipated to heat and/or is converted to mean potential energy via diapycnal mixing. Henceforth, the turbulence associated with this process will be referred to as “convectively-driven.” A third data set

from the northern Atlantic Ocean will be featured to examine overturning where dissipation rates are more representative of the relatively quiescent ocean interior.

8.2 Fundamentals of the Thorpe-Ozmidov relation

Fundamentally, L_T is related to the APE that is stored in a patch of turbulence at the instant of sampling. This can be shown in defining the APE in terms of the Ellison length scale, $L_E \equiv \langle \rho'^2 \rangle^{1/2} (\partial \bar{\rho} / \partial z)^{-1}$, such that

$$APE \equiv \frac{1}{2} N^2 L_E^2 \approx \frac{1}{2} N^2 L_T^2. \quad (8.2)$$

In a strict sense, the definition proposed in equation 8.2 is valid if the rms density fluctuation, $\langle \rho'^2 \rangle^{1/2}$, is calculated using perturbations from the stable reference state that is obtained by three-dimensionally re-sorting the density field to a state of minimum potential energy as proposed by Winters et al. (1995). The reference state should also be that which defines N . In the one-dimensional limit represented by a single profile, L_T then approximates L_E and the two length scales are equivalent if the reference density profile is linear. Given equation 8.2, the arguments needed to support $L_T \sim L_O$ are (i) that APE within an overturn scales with the total turbulent kinetic energy, k , so that $L_T \sim k^{1/2} N^{-1}$ and (ii) that the overturns inertially transfer their kinetic energy down-spectrum at a rate equal to ϵ so that $k \sim (\epsilon L_T)^{2/3}$. Combining these two assumptions gives

$$\frac{1}{2} N^2 L_T^2 \sim (\epsilon L_T)^{2/3} \Rightarrow L_T \sim L_O, \quad (8.3)$$

In other words, the turbulent Froude number defined by $Fr_k \equiv \epsilon / (kN)$ is assumed to be $O(1)$.

There is considerable evidence from laboratory experiments and direct numerical simulations (DNS) to suggest that these assumptions should not hold on an instantaneous, or sample-wise basis for well-developed, shear-driven turbulence. For example, Rohr et al. (1988) demonstrate L_T/L_O to be an increasing function of the gradient Richardson number, $Ri \equiv N^2/S^2$, in laboratory flows where the mean shear, S , and stratification are uniform. In their experiments, they find $L_T/L_O \approx 1$ only when $Ri \approx 0.25$. Mater and Venayagamoorthy (2014b) who, using a large database of homogeneous DNS and laboratory results, suggest additional dependence on the inverse Froude number, Fr_k^{-1} , and the shear strength parameter, Sk/ϵ . Specifically, they find $L_T/L_O \approx 1$ at $Ri \approx 0.25$ only when the time scales of the shear and buoyancy fluctuations are comparable to those of the inertial motions (i.e., $Sk/\epsilon = O(1)$ and $Fr_k^{-1} = Nk/\epsilon = O(1)$). When shear is absent or of limited influence (i.e., $Sk/\epsilon \ll 1$), they find L_T/L_O to be an increasing function of Fr_k^{-1} , and that $L_T/L_O \approx 1$ only when $Fr_k^{-1} = O(1)$ as suggested by the arguments above. Only at this transition from a buoyancy-dominated to a well-mixed, inertia-dominated (quasi-isotropic) regime are assumptions (i) and (ii) simultaneously satisfied so that the outer motions of the flow scale with both ϵ and N . Unfortunately, the exact dependence of L_T/L_O on Ri , Fr_k or Sk/ϵ in the ocean has not been widely reported; however, the recent findings of Smyth and Moum (2013) that strongly stratified turbulence of the equatorial undercurrent demonstrates marginal stability on average, i.e., $\langle Ri \rangle \approx 0.25$, seems to support the use of equation 8.1, in an average sense, for long time series observations of well-developed, shear driven turbulence.

Oceanic turbulence, however, is driven by both mean shear and the intermittent, convective collapse of large overturns. Use of equation 8.1 — in even an average sense — with regard to the latter mechanism is largely unvalidated. This additional mechanism brings additional possibilities for violation of assumptions (i) and (ii), with assumption (i) being particularly dubious on a sample-wise basis because APE and TKE may be strongly out of phase. In an investigation of Kelvin Helmholtz (K-H) billows, Smyth et al. (2001) clearly demonstrate that L_T/L_O should monotonically decrease over time as a billow collapses into

turbulence. They find $L_T > L_O$ for young turbulence characterized by $APE > TKE$ and $L_T < L_O$ for older, well-developed turbulence that has effectively drained the APE stored in the initial overturn. Qualitatively, the phase difference between APE and TKE in K-H turbulence is similar to what occurs during intermittent convectively-unstable overturning that characterizes regions such as Luzon Strait and the Brazil Basin.

8.3 Data Sets

This section describes some basic and pertinent details of each of the three data sets considered. All data sets have been provided complements of Dr. Lou St. Laurent of Woods Hole Oceanographic Institution. Study site locations are shown in figure 8.1.

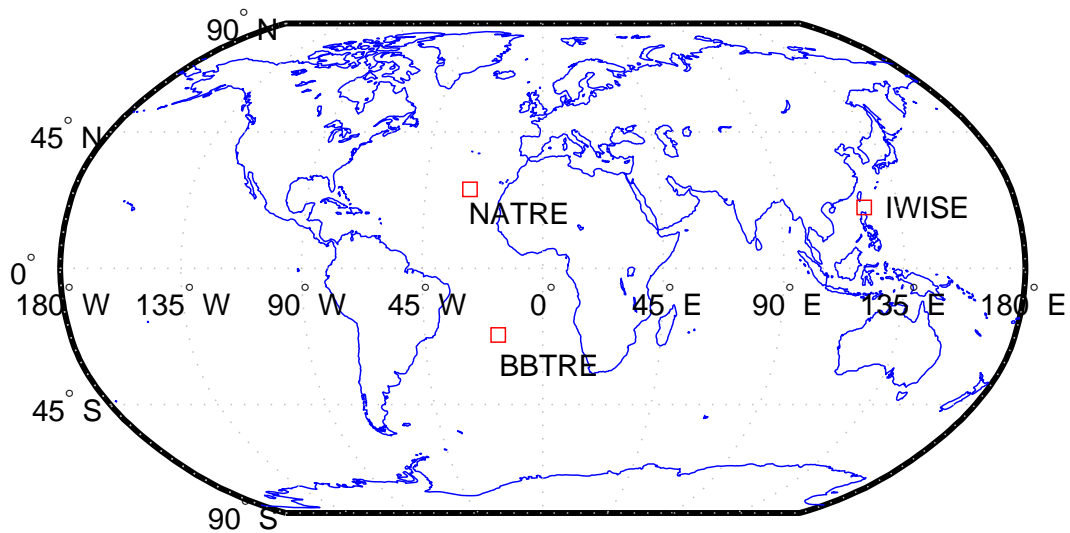


Figure 8.1: Study site locations.

8.3.1 Luzon Strait (IWISE)

Luzon Strait, separating Taiwan to the north and the Philippines to the south, is characterized by strong tidal currents and relatively strong stratification that interact with dramatic seafloor topography in the form of approximately parallel ridges running north-south across the strait (figure 8.2). These features make the area unique in its ability to convert

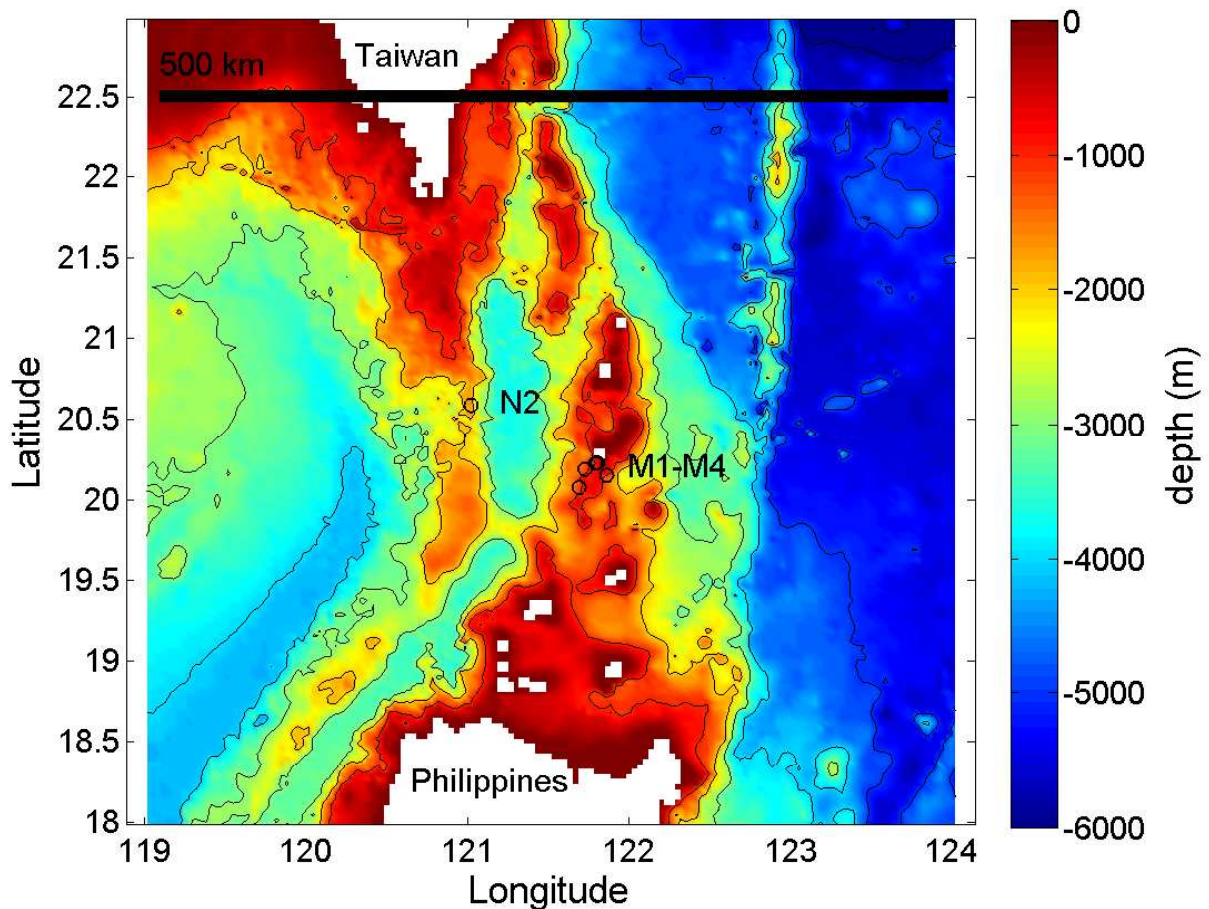


Figure 8.2: Bathymetry and profile locations for IWISE. Profiles were taken directly over each of the parallel ridges spanning the strait. Contours are shown at 1000 m intervals. Bathymetric data is from Smith and Sandwell (1997).

barotropic energy (that of the surface tide) to baroclinic energy in the form of large amplitude internal waves that propagate into the South China Sea as well as break locally in the form of large overturns (Alford et al., 2011). In 2011, ship-based surveys were conducted at

sites along both ridges as part of the Internal Waves In Straits Experiment (IWISE) funded by the U.S. Office of Naval Research to study the generation, propagation, and dissipation of internal waves in Luzon Strait. Hydrographic (i.e., temperature, salinity) and turbulence data (i.e., microstructure shear for calculation of dissipation) were collected at the station locations shown in figure 8.2. Details of the survey are reported in St Laurent (2012). “M” stations are clustered at the crest of the east ridge at roughly the 1000 m isobath. These four stations (M1-M4) were each occupied twice ($\sim 36hr$ intervals) during opposite phases of the spring-neap cycle of the tide. The first occupations were during the neap tidal period, while the second occupations were during the spring tidal period when tidal currents are relatively high. The N2 station is on the western ridge at the 1800 m isobath and was occupied during the spring tidal period. Turbulence profiling was conducted at each site using a free-falling vertical microstructure profiler (VMP) that is capable of measuring horizontal shear at the scales of the turbulence, thus allowing for direct estimates of ϵ . The VMP was also equipped with conductivity and temperature probes that allow for vertical descriptions of the density field needed for calculation of L_T and N through an equation of state. Most casts of the VMP were accompanied by a quasi-simultaneously lowered Conductivity-Temperature-Depth (CTD) profiler for high resolution vertical density profiles. However, we only consider data from the VMP platform in the current study to avoid possible errors associated with spatial and temporal variability between density profiles from the CTD and dissipation profiles from the VMP. VMP data considered here has been previously filtered to a resolution of 1 db so that the minimum Thorpe scale resolved is $L_{T,min} \approx 1$ m. Following elimination of certain profiles due to dubious temperature data, a total of 71 out of 78 profiles were used in the current study. These profiles extend to within ~ 75 m of the seafloor. Henceforth, we will refer to this data set as “IWISE”.

8.3.2 Brazil Basin (BBTRE)

The Brazil Basin is a region of the southern Atlantic Ocean bordered by the Mid-Atlantic Ridge (MAR) to the east and the South American continent to the west (figure 8.3). Near

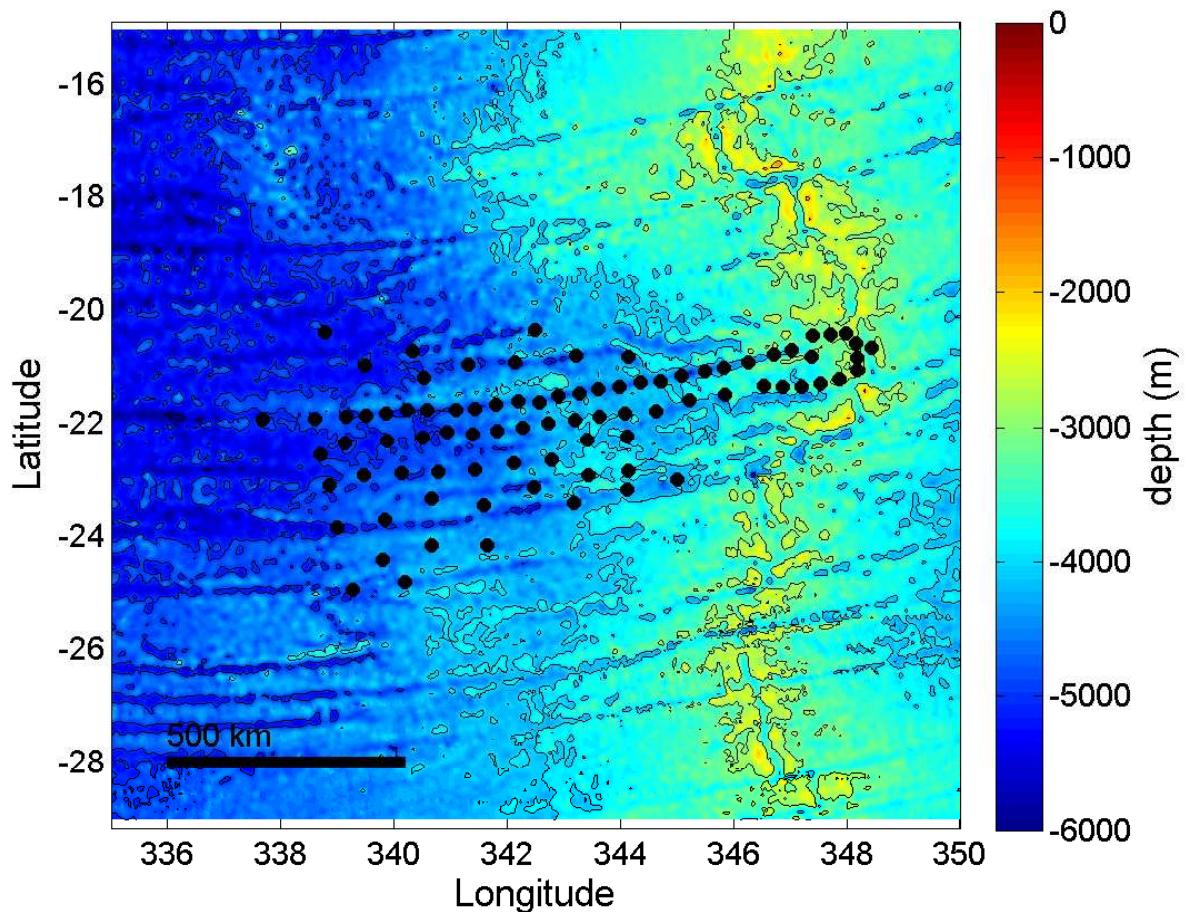


Figure 8.3: Bathymetry and profile locations for BBTRE. The Mid Atlantic Ridge runs north-south to the east of the profile locations which are located over latitudinally-oriented ridges and canyons leading to the MAR. Contours are shown at 1000 m intervals. Bathymetric data is from Smith and Sandwell (1997).

the MAR, the seafloor is dissected by a large number of east-west oriented fracture zones with ridge-canyon bathymetry. Bathymetric relief is dramatic, with ridge crests rising up to 1 km above canyon floors. As such, turbulence is greatly enhanced near the bottom (St Laurent et al., 2001). The Brazil Basin Tracer Release Experiment (BBTRE), funded by the U.S. National Science Foundation (NSF), was initiated in 1996 with the release of

110 kg of sulfur hexafluoride near $21.7^{\circ}S$, $18.4^{\circ}W$ on the western flank of the MAR to study mixing and stirring over the rough bathymetry of the Brazil Basin. Accompanying hydrographic/turbulence surveys were conducted in 1996 and 1997 (for details see Polzin et al., 1997; Ledwell et al., 2000). In the current study, we will analyze a subset of data collected in 1997 that is featured in St Laurent et al. (2001). A total of 89 vertical profiles of temperature, salinity, and microstructure dissipation will be used. All profiles extend to within ~ 20 m of the seafloor. As with IWISE, all variables considered were collected from a single profiler so that hydrographic and dissipation measurements are contemporaneous in time and space. The vertical resolution of the data is 0.5 db, however, only $L_T > 1$ db ≈ 1 m will be considered to be consistent with the IWISE analysis. Henceforth, we will refer to this data set as “BBTRE”.

8.3.3 North Atlantic (NATRE)

To contrast with the enhanced turbulence of Luzon Strait and the fracture zone of the Brazil Basin, we will consider data collected as part of the North Atlantic Tracer Release Experiment (NATRE) in the Canary Basin where the seafloor is relatively smooth and turbulence is generated from the background internal wave field (figure 8.4). Here, dissipation rates are more representative of the relatively quiescent ocean interior (Toole et al., 1994) and convectively-driven turbulence due to large overturns is absent. In the absence of significant turbulence, molecular effects become increasingly important in the diffusion of heat and salinity. Given these scalars diffuse at different rates, this process is known as “double diffusion” and can result in the formation of vertical “salt fingers” (Schmitt, 1994; St. Laurent and Schmitt, 1999). This has serious implications for estimates of L_T which will be discussed in section 8.4. To characterize the hydrographic and turbulent properties of the experiment area, 155 vertical profiles using a VMP were collected (for details see St. Laurent and Schmitt, 1999). Sample locations are mapped in figure 8.4. Of these profiles, 150 were available to the current study. Most profiles terminate at ~ 2000 m, with 25 shallower profiles terminating

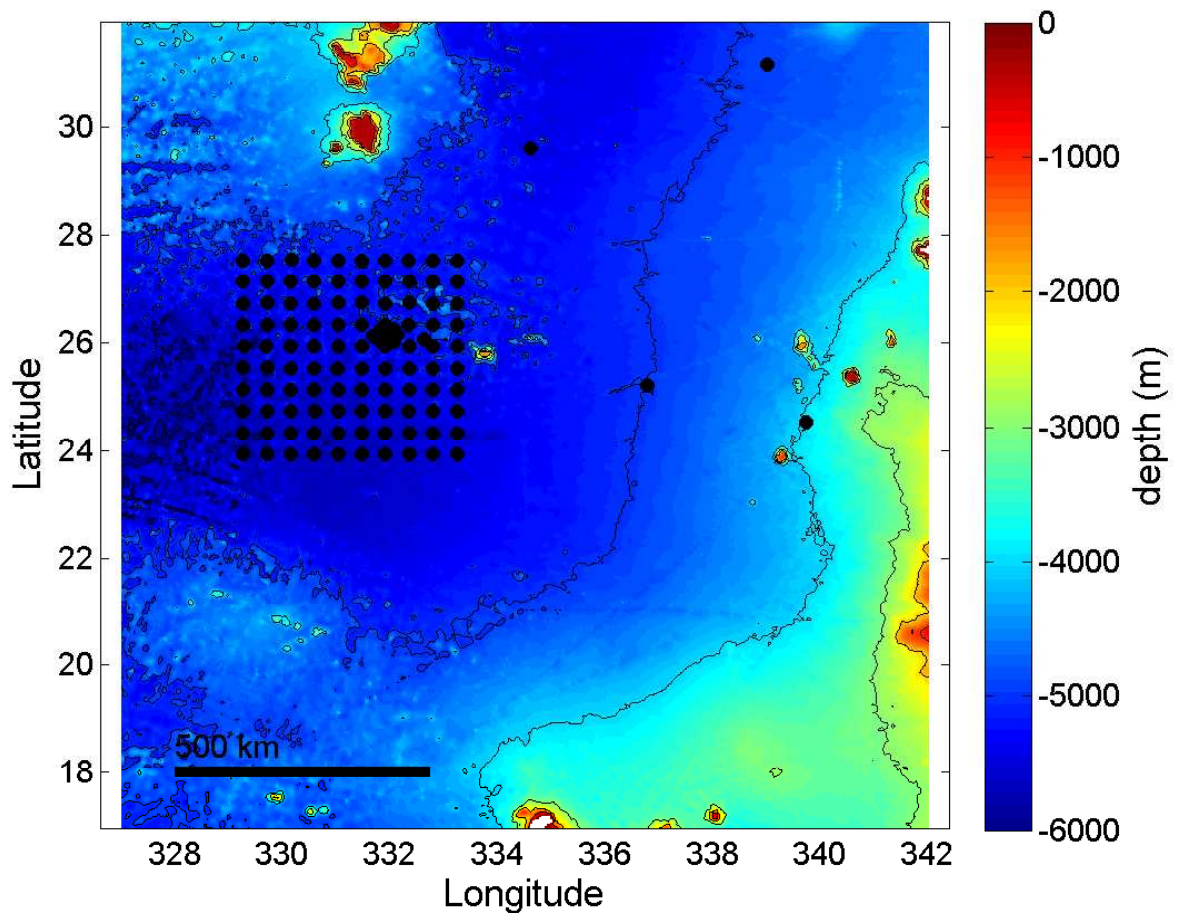


Figure 8.4: Bathymetry and profile locations for NATRE. Profiles were taken over mildly sloping topography of the West African Shelf in a roughly 500km by 500km rectilinear pattern. Additional profiles were taken near the dye injection point. Contours are shown at 1000 m intervals. Bathymetric data is from Smith and Sandwell (1997).

at ~ 1000 m, 10 deeper profiles extending to ~ 3000 m, and 3 very deep profiles extending to ~ 4000 m. The deeper profiles do not reveal bottom enhanced dissipation rates as is seen in the BBTRE data. The vertical resolution of the data is 0.5 db, yet we will only consider $L_T > 1$ db ≈ 1 m for consistency among data sets.

8.4 Methods

8.4.1 Thorpe scale calculations for turbulent patches

The process proposed by Thorpe (1977) for determining L_T involves re-sorting an instantaneously observed vertical profile of potential density, σ , such that the profile is monotonically increasing with depth (i.e., gravitationally stable). This is done while keeping track of the displacement required of each data point. For a given depth, z_i , this displacement is calculated as $\delta T_i = z_i - z_{sorted}$, where z_{sorted} is the depth to which the sample taken at z_i must be moved to achieve a stable profile. In this sense δT reflects the displacements needed of samples in the original profile. For an individual overturn in quiescent fluid, δT is large and negative at the upper boundary, increases with depth, and is large and positive at the lower boundary so that a “reverse Z” signature appears in the profile of δT (assuming z_i is positive and increases with depth). The root mean square of δT for the depth range exhibiting this signature then determines L_T of the overturn:

$$L_T = \langle (\delta T)^2 \rangle^{1/2}. \quad (8.4)$$

Because overturns are observed at various stages of development, and thus coherency, the reverse Z pattern is not always easy to distinguish. As such, we objectively identify “turbulent patches” for Thorpe scale calculations as vertical segments of the profile over which δT values sum to zero. Patch boundaries are determined using a top-down cumulative sum, $\sum_{j=1}^n \delta T_j$, where $j = 1$ corresponds to a beginning value at the top of the profile and $j = n$ corresponds to the end value near the bottom of the profile. For most of the water column the density profile is stable so that $\sum \delta T = 0$ because $\delta T = 0$. Over an overturning patch, however, $\sum \delta T$ decreases from zero as a function of depth in the uplifted heavy fluid before increasing back to zero as a function of depth in the down-welled light fluid. The depths where $\sum \delta T = 0$ on either side of the overturning fluid delineate the patch. It is over these

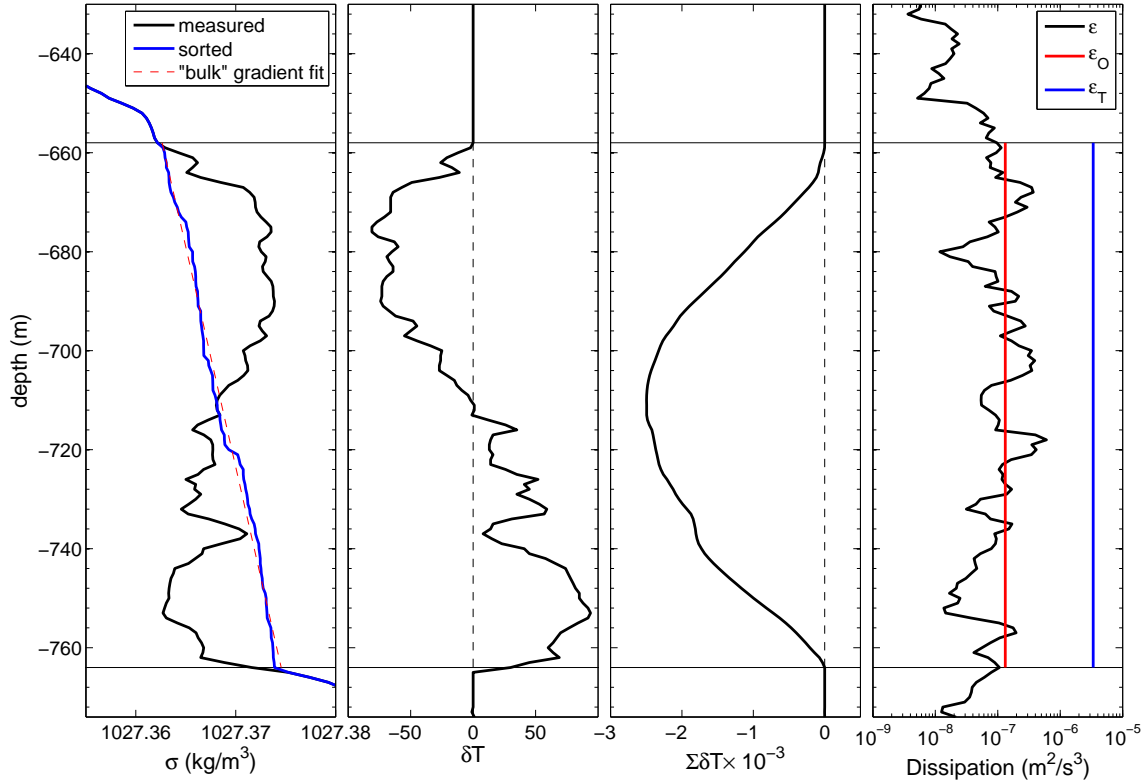


Figure 8.5: Example of density (first panel), Thorpe displacement (second panel), top-down cumulative sum of Thorpe displacements (third panel), and dissipation (fourth panel) profiles for a turbulent patch. The patch is objectively delineated using the bounds on non-zero $\Sigma\delta T$.

delineated vertical segments that corresponding averages of buoyancy frequency and dissipation rate are taken for calculation of L_O . The process of identifying a turbulent patch is shown in figure 8.5.

8.4.2 Temperature-salinity relationships

Because of concern over the reliability of salinity measurements, we use potential temperature, Θ , as a surrogate for potential density. We note, however, that in weakly energetic (low Reynolds number) flows such as those sampled in NATRE, inversions in $\Theta(z)$ may not be true overturns in that they are compensated by salinity in such as way that the water column is stable. Such conditions favor double diffusive transport through salt fingering rather

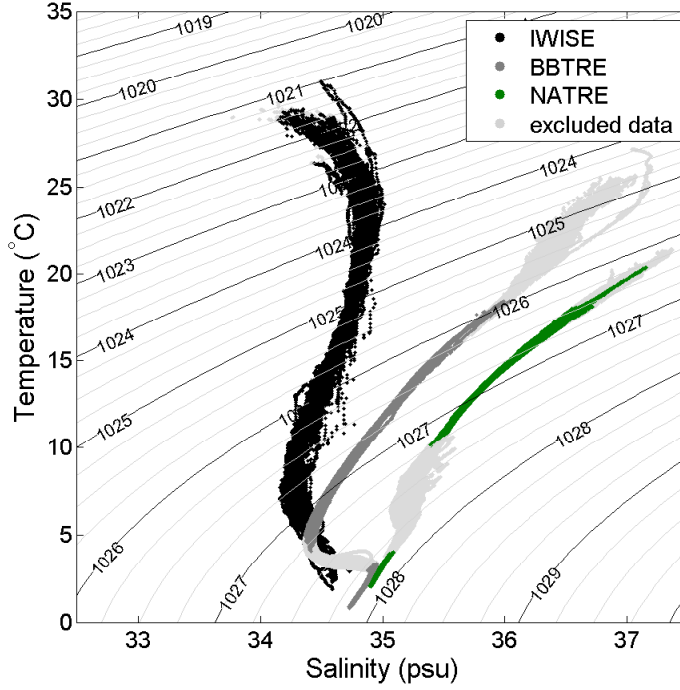


Figure 8.6: Temperature-salinity (T-S) diagram for IWISE, BBTRE, and NATRE data.

than turbulent mixing (Schmitt, 1994; St. Laurent and Schmitt, 1999). Data susceptible to salt fingering appears as spread along a line of constant σ in a temperature-salinity (T-S) diagram (Schmitt, 1999). Figure 8.6 shows a T-S diagram for the data considered here. Spread in the T-S relationship, typically referred to as “spice”, can be seen for $\sigma < 1026 \text{ kg m}^{-3}$ in the BBTRE data which correspond to the upper 200 m of near-surface water that is susceptible to atmospheric influence. Some spice is also seen for $\sigma \lesssim 1026.5 \text{ kg m}^{-3}$ in the NATRE data which also roughly corresponds to the upper 200 m. Spice can also be seen for $1027.25 \lesssim \sigma \lesssim 1027.75 \text{ kg m}^{-3}$ in both BBTRE and NATRE, which corresponds to water from approximately 750 – 2000 m in BBTRE and from 600 – 2000 m in NATRE. Data from these depth ranges, lightly shaded in figure 8.6, are omitted from our calculations. In contrast, IWISE data exhibits less spice due to more intense turbulent mixing throughout the water column. The T-S relationship for IWISE suggests that density is strongly a function of temperature for most of the water column.

8.4.3 Calculation of buoyancy frequency

In accordance with the arguments of section 8.2, the buoyancy frequency, N , should be that which characterizes the background stratification against which a particular overturn is working; that is, the density profile used to calculate $\partial\bar{\rho}/\partial z$ (or more strictly, $\partial\bar{\sigma}/\partial z$) should characterize the *background* potential energy so that perturbations from $\bar{\rho}(z)$ (or $\bar{\sigma}(z)$) characterize the potential energy *available* for conversion to turbulence. Unfortunately, the limitations of field sampling and the non-stationary, inhomogeneous nature of natural flows make determination of a background N nontrivial. Most commonly, the Thorpe-sorted density profile is used as a surrogate for that of the background state, and the gradient of the profile across a turbulent patch is calculated in some fashion. In the current work, a “bulk” density gradient is calculated from the Thorpe-sorted profile using the method of Smyth et al. (2001), wherein the approximate equivalence of the Thorpe and Ellison scales is exploited to yield:

$$\left(\frac{\partial\bar{\sigma}}{\partial z}\right)_{bulk} \equiv \frac{\langle\sigma'^2\rangle^{1/2}}{L_T}. \quad (8.5)$$

The density perturbation, σ' , is determined as the difference between the instantaneous and sorted values at a given depth, the square of which is averaged over the vertical extent of the event (see figure 8.5). Since we use potential temperature as a surrogate for potential density, a “pseudo” potential density profile is used to determine σ' . The pseudo potential density profile is computed directly from the temperature profile using a constant arbitrary salinity and an approximation to the non-linear equation of state (see Gill, 1982). As such, the profile effectively provides accurate values of the temperature-sorted equivalent density gradient needed for N , but not true values of density.

8.4.4 Estimation of dissipation

To allow a straight-forward comparison between data sets, we assume $a = 1$ in calculating the inferred dissipation rate, ϵ_T , from equation 8.1. The actual value of a (in a statistical

Table 8.1: Patch-wise statistics

Data set	$\langle \log \frac{L_T}{L_O} \rangle$	$std(\log \frac{L_T}{L_O})$	$10^{\langle \log(L_T/L_O) \rangle}$	a
IWISE	-0.12	0.49	0.77	[0.42, 4.03]
BBTRE	-0.03	0.35	0.93	[0.48, 2.38]
NATRE	0.26	0.54	1.84	[0.16, 1.88]
Ferron et al. (1998)	0.04	0.30	1.10	[0.46, 1.82]

sense) for each data set will be given separately in section 8.5. The dissipation rate used in calculation of L_O for a given patch is an arithmetic average of the VMP measurements over the vertical extent of the patch (see figure 8.5). This patch-averaged dissipation will be denoted as ϵ_O , while the un-averaged VMP measurements will simply be denoted as ϵ . Select profiles of Θ , N , L_T , L_O , ϵ_O , ϵ_T , and ϵ are included in appendix B for each study site.

8.5 Direct comparisons

First, consider the direct comparison of L_T and L_O for the ensemble of turbulent patches as identified by the criteria of section 8.4. The relationship is portrayed as a two-dimensional histogram of observations from individual patches (figure 8.7).

As do Wesson and Gregg (1994), we find that the data cluster near $L_T \approx L_O$ but with considerably more scatter than reported by Dillon (1982). L_T/L_O is lognormally distributed with statistics for each data set reported in table 8.1 along with those from Ferron et al. (1998) who also report lognormal behavior. With the exception of NATRE, the statistics compare well across data sets and the constant of proportionality is comparable to that found by Ferron et al. (1998). For NATRE, L_T is roughly twice as large as L_O on average — a finding that we elaborate on below. ϵ_T and ϵ_O are compared in figure 8.8.

To further investigate scatter in the Thorpe-Ozmidov relationship, L_T/L_O and ϵ_T/ϵ_O are plotted in figure 8.9 and 8.10, respectively, against the normalized overturn size, $\widehat{L}_T \equiv L_T/L_{\nu N}$, where $L_{\nu N} \equiv (\nu/N)^{1/2}$ is a dimensionally-constructed small scale that is indepen-

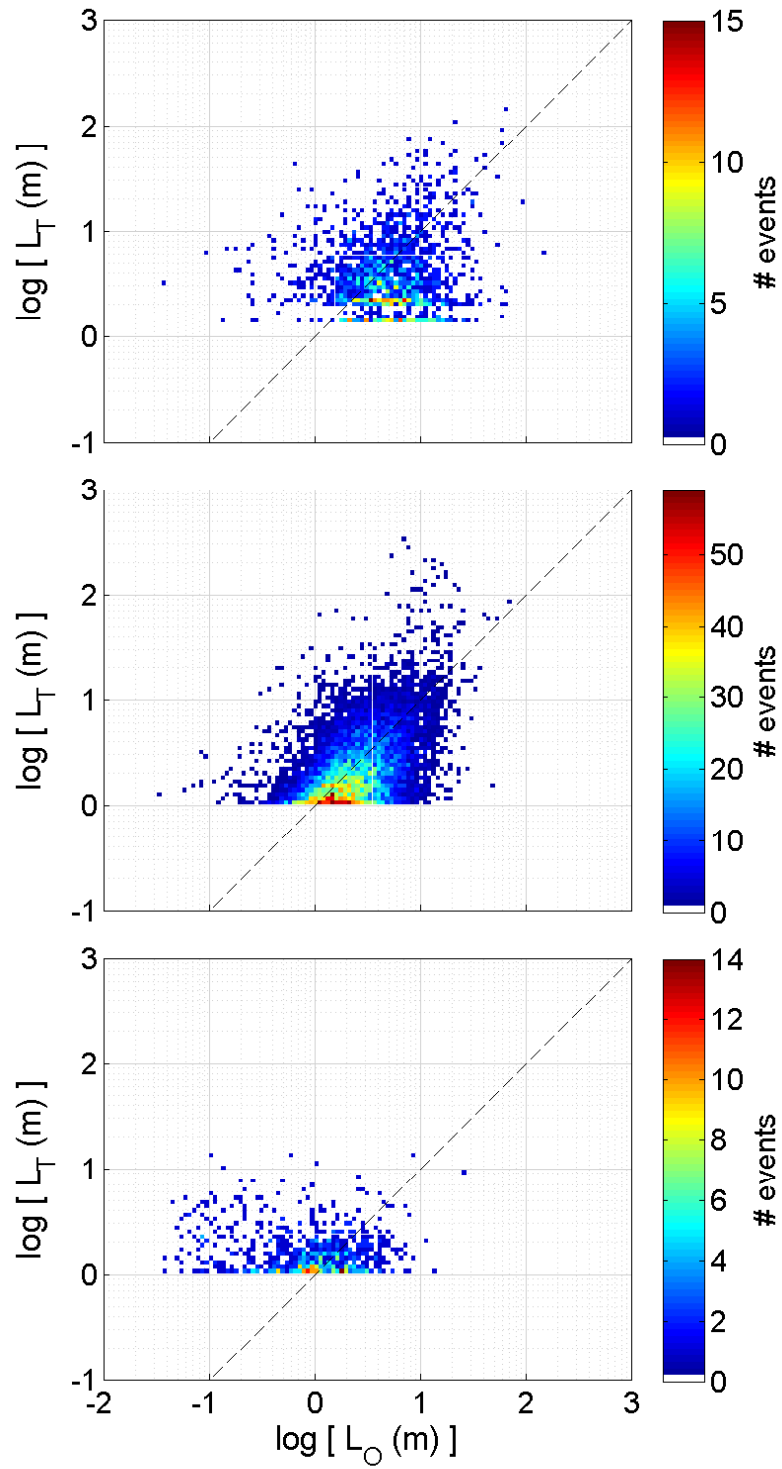


Figure 8.7: Scatter plot comparisons of the Thorpe (L_T) and Ozmidov (L_O) scales calculated from turbulent patches for IWISE (top), BBTRE (middle), and NATRE (bottom). Point density is represented by colorbars.

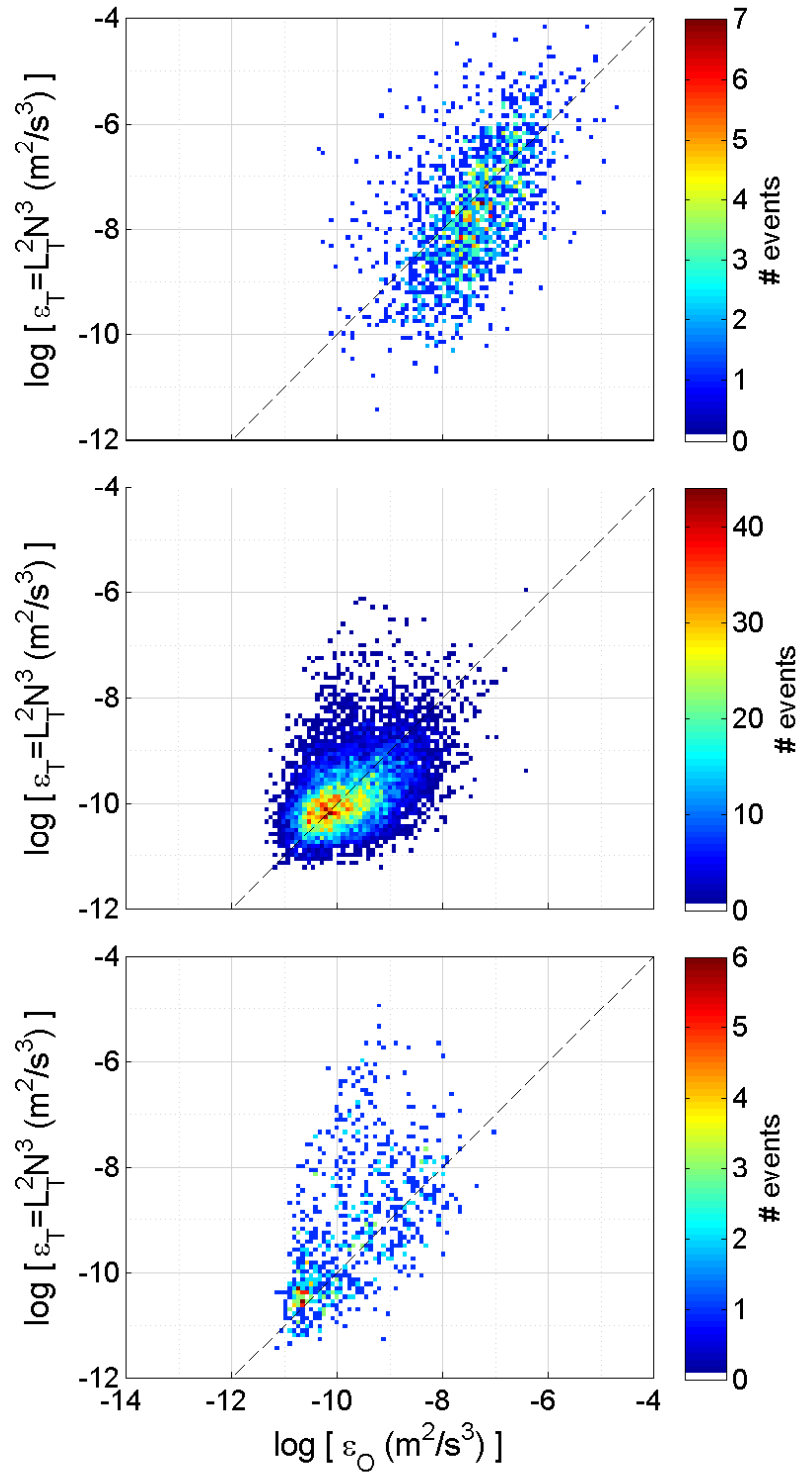


Figure 8.8: Scatter plot comparison of the Thorpe-inferred dissipation (ϵ_T) and the patch-averaged measured dissipation (ϵ_O) from turbulent patches for IWISE (top), BBTRE (middle), and NATRE (bottom). Point density is represented by colorbars.

dent of the turbulence. $L_{\nu N}$ physically represents the length scale over which the viscous diffusion of momentum occurs on time scale N^{-1} . Given constant viscosity, \widehat{L}_T expresses the size of an overturn with respect to the background stratification and allows for the conceptual distinction between young overturns that have yet to mix the fluid (i.e., high N , large \widehat{L}_T) from those occurring in older turbulence where significant mixing has already occurred (i.e., low N , small \widehat{L}_T). That is, \widehat{L}_T is conceptually a surrogate for the (inverse) age of the turbulence. Under this reasoning, all three data sets suggest L_T/L_O should decrease with event age in apparent agreement with the K-H turbulence studied by Smyth et al. (2001). This trend appears as a positive correlation between L_T/L_O and \widehat{L}_T in figure 8.9. It is important to note, however, that the data sets do not collapse upon one another; \widehat{L}_T seems to indicate relative age *for a given set of observations*, but does not allow for comparison of event age between data sets. Segregation of the data is likely due to forcing by the mean flow, with data from strong forcing (e.g., IWISE) shifting to higher values of \widehat{L}_T . This apparent shift suggests \widehat{L}_T is also a general indicator of mean forcing.

Distributions of L_T/L_O and ϵ_T/ϵ_O are shown as histograms in the right panels of figure 8.9 and 8.10, respectively, for quartiles of the data delineated by \widehat{L}_T . Quartile delineations are indicated in the left panels with the first quartile starting at $\widehat{L}_T = 24$ to avoid resolution errors (discussed later). These results may be encouraging for use of equation 8.1 in a highly averaged sense, however, the skewness toward large ϵ_T/ϵ_O when \widehat{L}_T is large hints that bias is possible if sampling includes large overturns in strongly forced flows.

Further interpretation of the data is possible considering various physical regimes present in figure 8.9. First note that

$$\frac{L_T}{L_O} = Re_b^{-1/2} \widehat{L}_T \quad (8.6)$$

so that lines of constant buoyancy Reynolds number, $Re_b \equiv \epsilon/(\nu N^2)$, may be constructed through the space. Following the suggestion of Gibson (1980), a line corresponding to $Re_b = 30$ has been drawn to approximately delineate “active” turbulence ($Re_b > 30$; below line) from “fossil” turbulence ($Re_b < 30$; above line). A number of overturns observed in NATRE

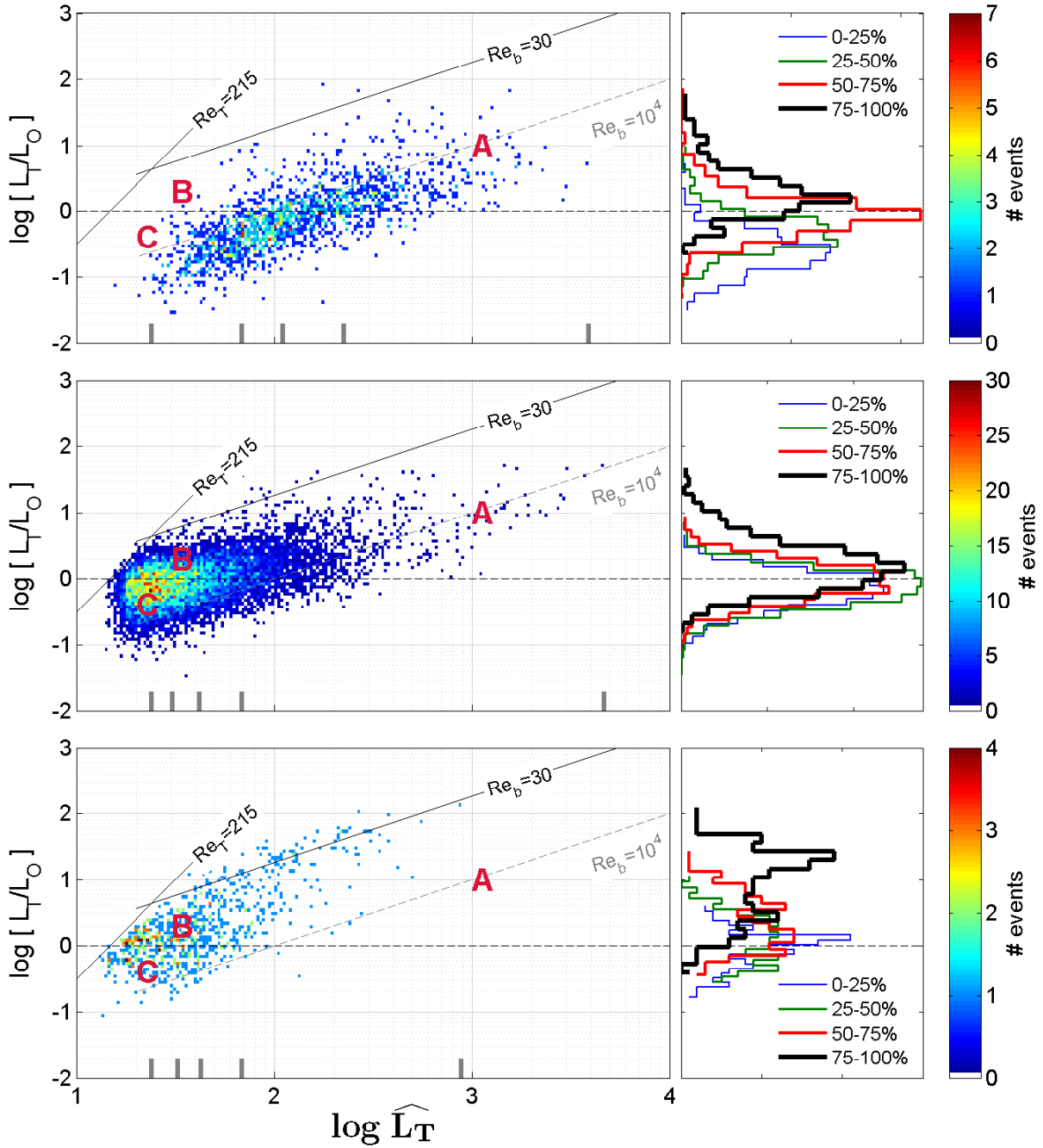


Figure 8.9: Comparison of L_T/L_O with the normalized overturn scale, $\widehat{L}_T = L_T/L_{\nu N}$, for IWISSE (top), BBTRE (middle), and NATRE (bottom). Conceptual regimes are labeled A (strongly forced, presumably young turbulence and large overturns), B (weakly forced, strongly stratified turbulence and small overturns) and C (weakly forced, weakly stratified turbulence and small overturns; old convectively-driven turbulence). Point density is represented by colorbars. Quartile distributions of the data are shown in the right panels.

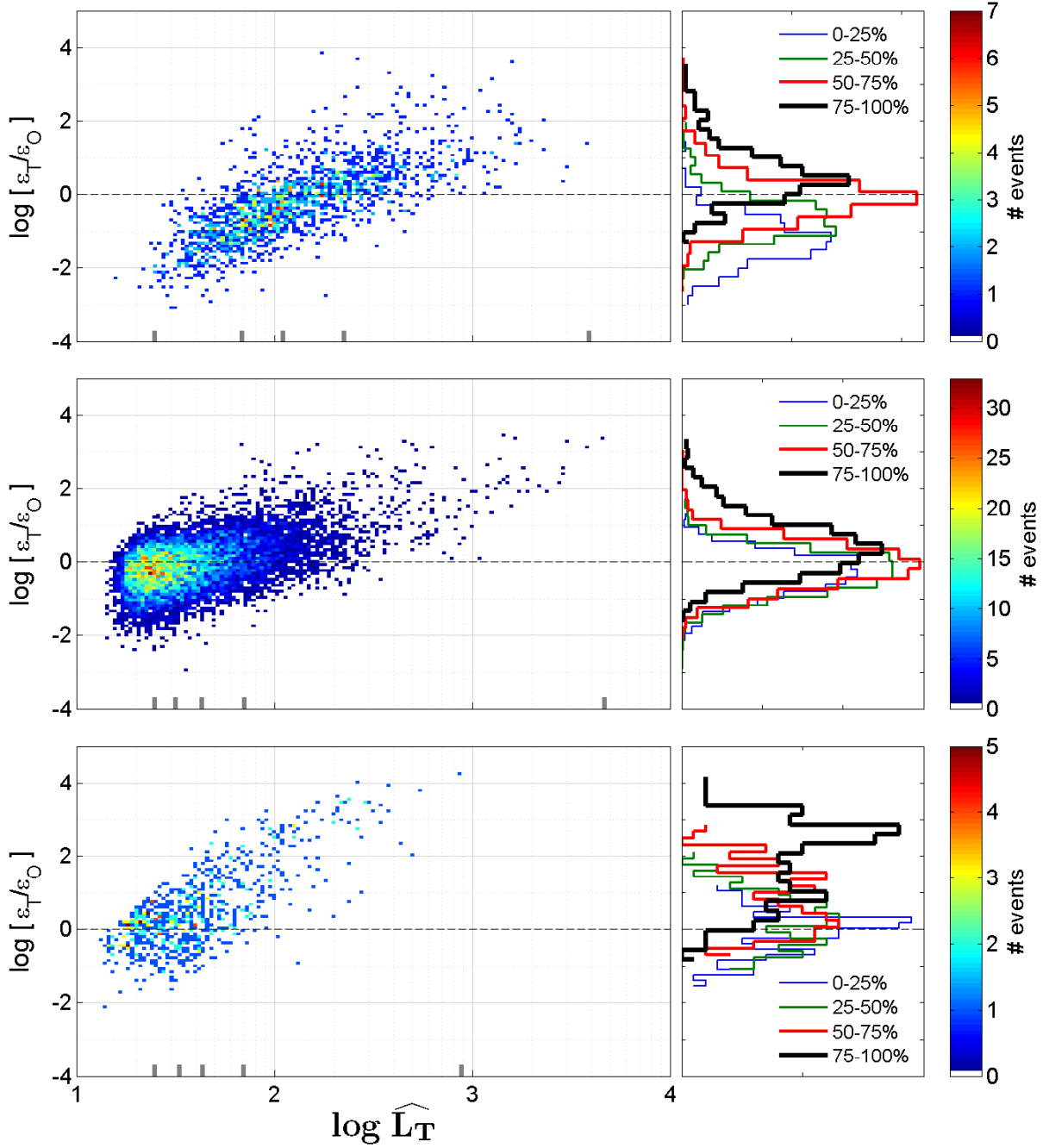


Figure 8.10: Comparison of ϵ_T/ϵ_O with the normalized overturn scale, $\widehat{L}_T = L_T/L_{\nu N}$, for IWISSE (top), BBTRE (middle), and NATRE (bottom). Point density is represented by color-bars. Quartile distributions of the data are shown in the right panels.

fall into the fossil regime, possibly due to non-turbulent salt fingering that persists despite our elimination of depths characterized by obvious spice in the T-S relationship. Furthermore, equation 8.6 shows that the data segregation seen by comparing the left panels of figure 8.9 (discussed above) is due to differences in Re_b between the study sites; strongly turbulent IWISE data clusters along $Re_b \sim O(10^4)$ while weakly turbulent NATRE data clusters closer to the fossil-active transition. BBTRE, which features weak dissipation rates high in the water column and strong dissipation rates near bottom topography, spans a wider range in Re_b and overlaps with both NATRE and IWISE data. The apparent consistency of Re_b for a given data set suggests that this parameter is not particularly useful in describing L_T/L_O .

Next, note that

$$\frac{L_T}{L_O} = Re_T^{-3/2} \widehat{L}_T^3, \quad (8.7)$$

where $Re_T \equiv (L_T/\eta)^{4/3}$ is the Reynolds number of the overturns presented by Luketina and Imberger (1989) and $\eta \equiv (\nu^3/\epsilon)^{1/4}$ is the Kolmogorov length scale. Since the minimum resolved Thorpe scale is approximately 1 m and the approximate shear probe noise level is $O(10^{-11} \text{ m}^2\text{s}^{-3})$, we cannot hope to resolve turbulence with $Re_T \lesssim 215$. Using this value, equation 8.7 is plotted in figure 8.9 to indicate where the data has been truncated due to these restrictions. There may well be some weakly turbulent overturns above this line that are not resolved. In recognition of this truncation, the quartile distributions do not consider data with $\widehat{L}_T < 24$ which results from equations 8.6 and 8.7 given $Re_{b,min} = 30$ and $Re_{T,min} = 215$; for $\widehat{L}_T \gtrsim 24$, L_T/L_O is limited physically by the stratification rather than artificially by measurement resolution.

Now consider the three regimes loosely labeled A-C in figure 8.9. The labels are positioned to aid in a qualitative discussion of data and are not intended to quantitatively delineate regimes. In regime A, forcing is strong with respect to the stratification (large \widehat{L}_T) and $L_T > L_O$ suggests that stratification is strong with respect to the turbulence. This regime is populated by large, presumably young overturns of the IWISE and BBTRE data sets. The

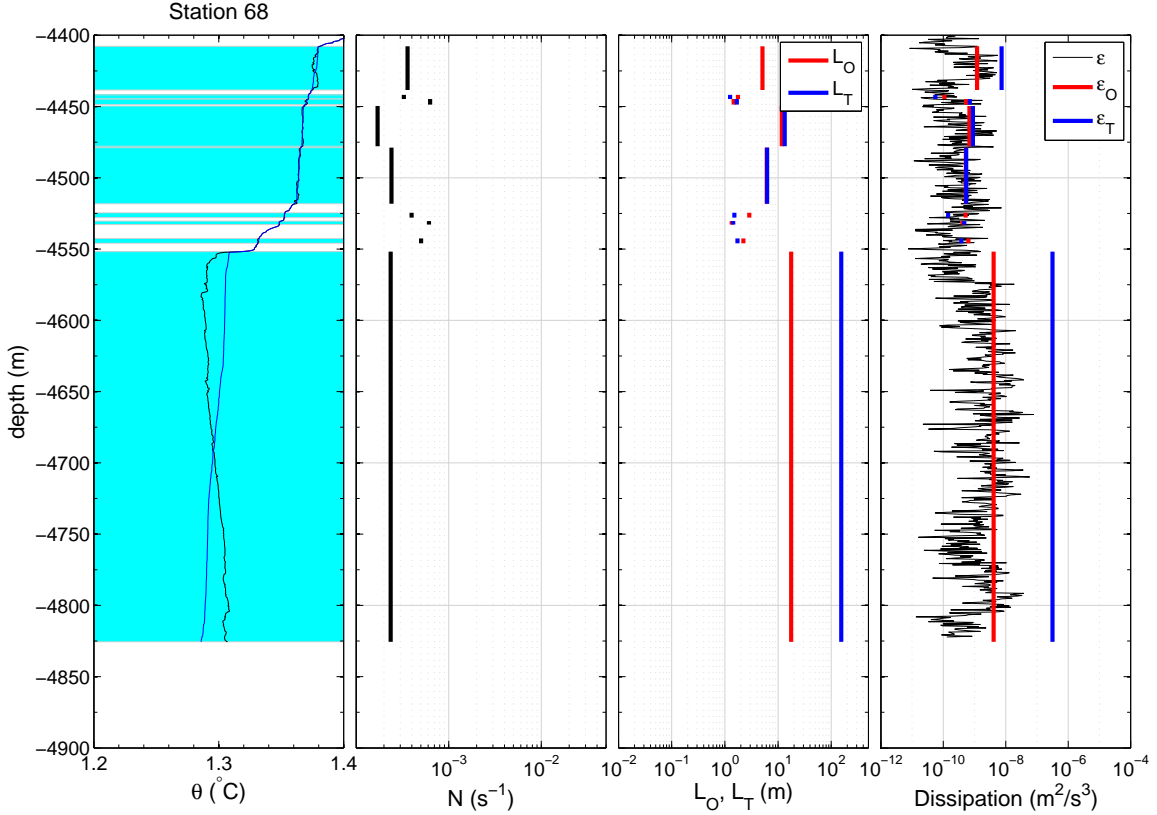


Figure 8.11: Example turbulent patch from BBTRE. The patch falls within regime A ($\widehat{L}_T = 2400$ and $L_T/L_O = 8.8$) and demonstrates a large coherent overturn suggestive of a youthful billow. The bottom of the overturn was not measured by the VMP cast, likely resulting in a somewhat smaller L_T than actual existed.

convective nature of these overturns suggests $L_T > L_O$ in regime A is likely due to $APE > k$, i.e., violation of assumption (i). Assumption (ii) is also expected to be violated because the turbulence is, presumably, not yet fully developed and is strongly anisotropic at the outer scales. The near-bottom patch from BBTRE shown in figure 8.11 is exemplary of an event from regime A. The patch demonstrates a coherent overturn shape suggestive of a young overturn. In contrast, a less coherent and presumably older overturn from a nearby station is shown in figure 8.12. This patch is representative of the transition from regime A to C.

IWISE and BBTRE data extend from regime A into regime C where overturns are presumably due to older, developed turbulence that has mixed the flow and reduced the

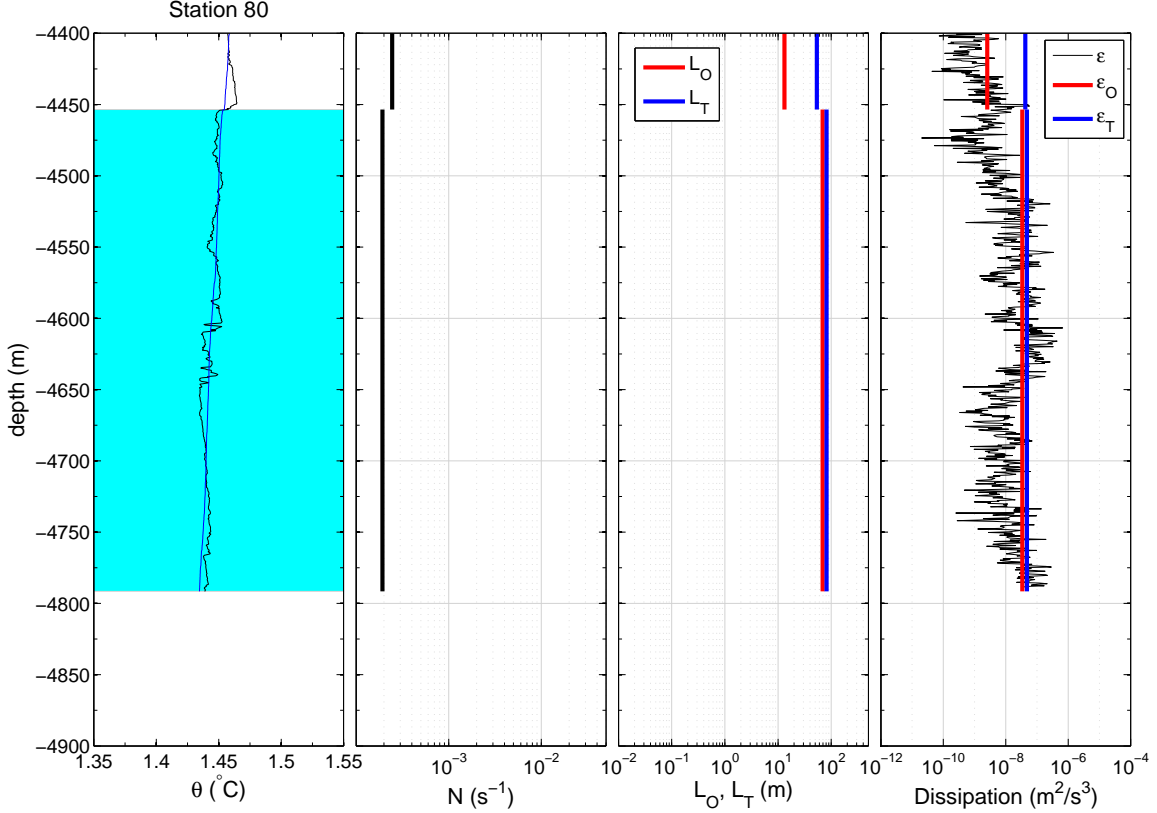


Figure 8.12: Example turbulent patch from BBTRE. The patch represents a transitional regime between regimes A and C ($\overline{L_T} = 1100$ and $L_T/L_O = 1.2$) and demonstrates an incoherent structure and higher dissipation rates. These characteristics are suggestive of older, more developed turbulence.

stratification such that $L_T < L_O$. This regime likely corresponds with either the “unforced/isotropic” or “shear-dominated” regimes of Mater and Venayagamoorthy (2014b) who investigated well-developed homogeneous turbulence. They find L_T to be better correlated with $L_{k\epsilon} \equiv k^{3/2}\epsilon^{-1}$ for unforced/isotropic flow or $L_{kS} \equiv k^{1/2}S^{-1}$ for shear-dominated flow. The former finding suggests possible adherence to assumption (ii) in regime C. $L_T < L_O$ in regime C is then due to a breakdown in assumption (i) as stratification becomes weak. The DNS results of Mater et al. (2013) support this, showing $APE \ll k$ in the weakly stratified limit (i.e., $Fr_k \gg 1$), as might be expected.

Regime B is populated with the weakly forced, small overturns of NATRE and BBTRE data. This regime is perhaps analogous to the “buoyancy-dominated” regime of Mater and Venayagamoorthy (2014b) who show the regime to be characterized by $L_T \sim k^{1/2}N^{-1}$ in support of assumption (i) but also $L_T > L_O$ — a finding they suggest is due to buoyancy-induced anisotropy at the outer scales that effectively truncates the inertial subrange¹⁰ to smaller scales, i.e., violation of assumption (ii). Along with possible fossil overturns or compensation of temperature inversions by salinity, the violation of assumption (ii) due to strong stratification and weak turbulence is a possible explanation for relatively large values of $\langle L_T/L_O \rangle$ (i.e., small values of a) reported for NATRE (see table 8.1). Nonetheless, taken together, weakly forced data of regimes B and C indicate a central tendency of $L_T \approx L_O$ in agreement with Dillon (1982) and Moum (1996) who examined data from the thermocline where mean forcing is relatively weak and turbulence is due to mean shear or low amplitude internal waves rather than large convective instabilities.

8.6 Mean profiles

Comparisons of the previous section indicate that there is perhaps a central tendency for $L_T/L_O \approx 1$ when all data sets are considered despite an obvious dependency on the normalized overturn size, \widehat{L}_T . Next, consider the use of equation 8.1 to determine the average vertical distribution of dissipation rate, which is an important consideration for ocean circulation models (Melet et al., 2013). For all data sets, patch-wise length scales, buoyancy frequency, and dissipation rates were averaged in 100 m vertical bins across profile ensembles. These ensemble-averaged values are denoted with angled brackets $\langle \rangle$ and are shown as a function of depth in figures 8.13, 8.14, 8.15, and 8.16 for IWISE M stations, IWISE station N2, BBTRE data, and NATRE data, respectively. Turbulence at BBTRE is bottom-enhanced, therefore, average values are shown as a function of distance above the local bottom.

¹⁰In stratified turbulence, the inertial subrange is the range of eddy sizes, $L_O \gtrsim l \gtrsim \eta$, for which the inertial scaling $l \sim k(l)^{3/2}\epsilon^{-1}$ is valid, with $k(l)$ being the eddy-wise kinetic energy.

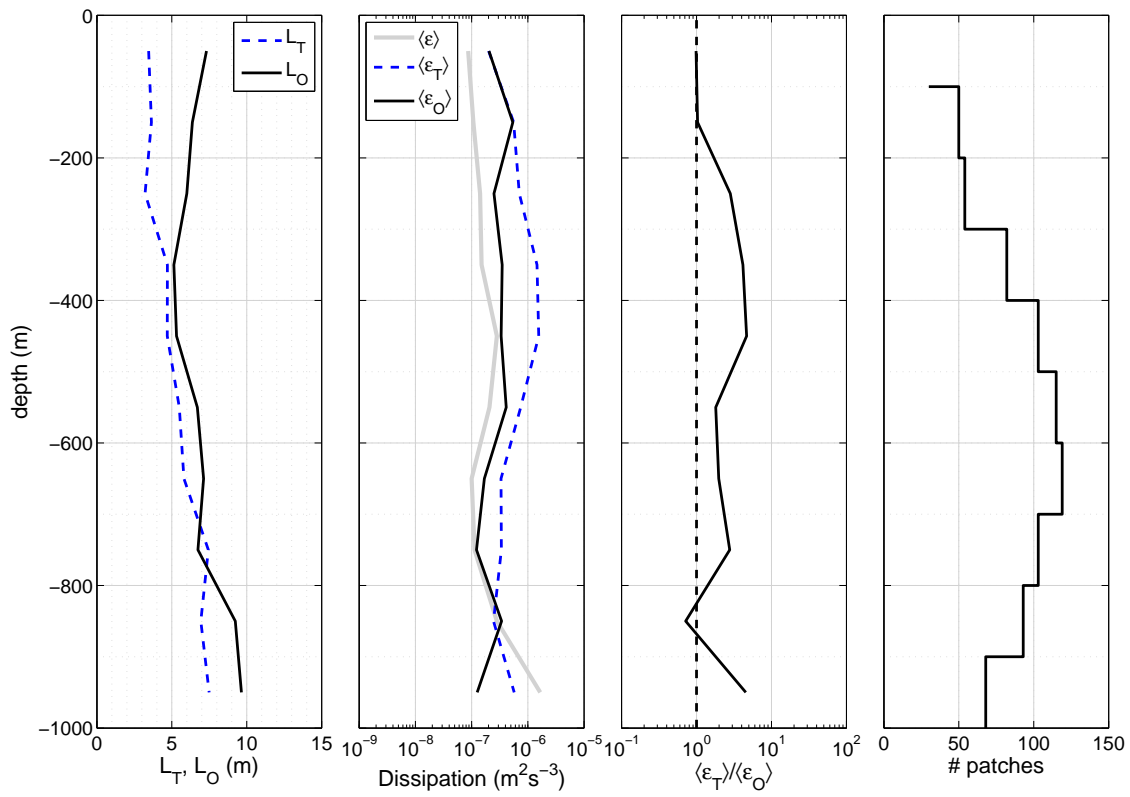


Figure 8.13: Mean values as a function of depth for IWISE M stations during spring tide.

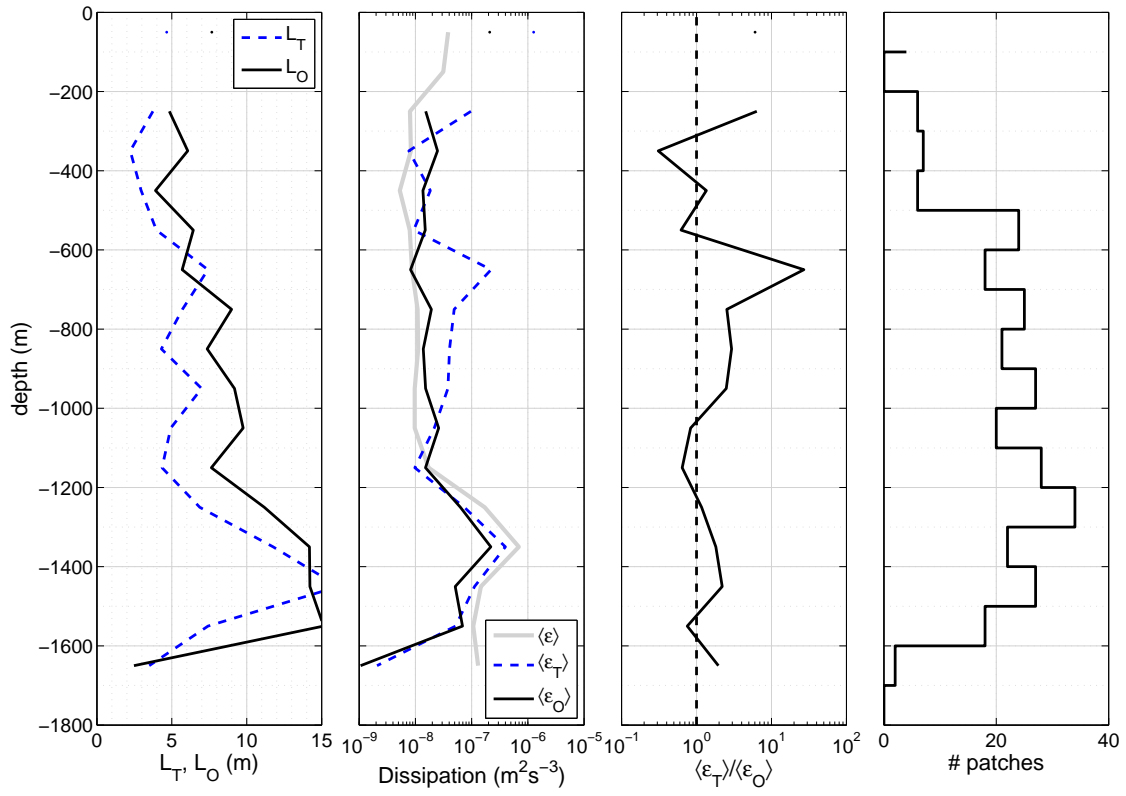


Figure 8.14: Mean values as a function of depth for IWISE station N2.

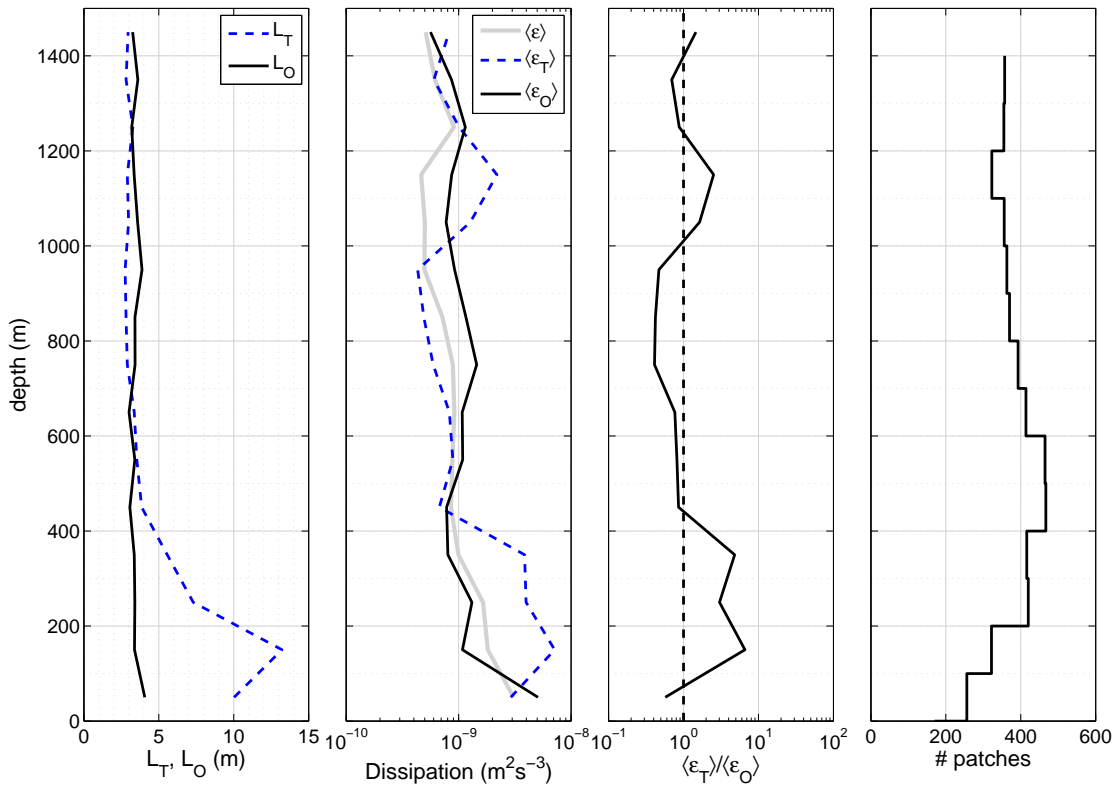


Figure 8.15: Mean values as a function of height above bottom for BBTRE.

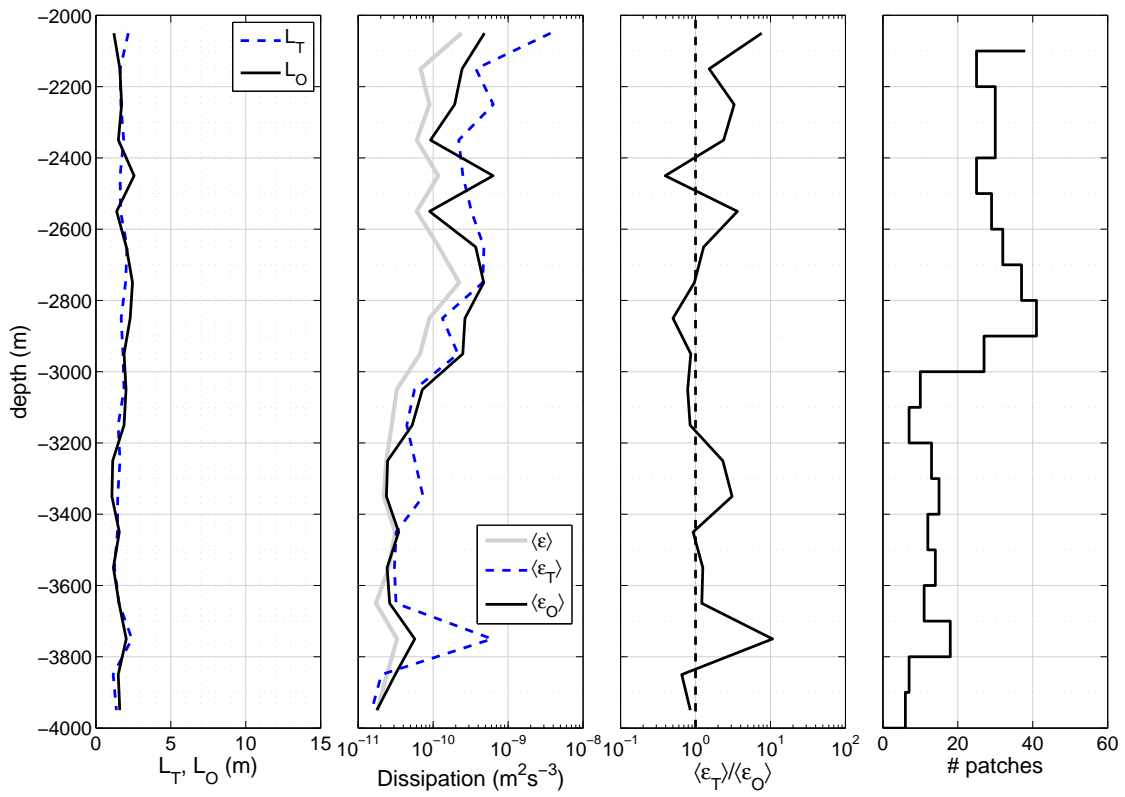


Figure 8.16: Mean values as a function of depth for NATRE.

In qualitative agreement with Ferron et al. (1998), the average inferred dissipation rate, $\langle \epsilon_T \rangle$, is generally larger than, but within an order of magnitude of the average measured dissipation rate, $\langle \epsilon_O \rangle$. Agreement is relatively poor for BBTRE close to the bottom where $\langle L_T \rangle > \langle L_O \rangle$ and $\langle \epsilon_T \rangle > \langle \epsilon_O \rangle$ may be due to the presence of large, young overturns associated with bathymetric ridges (regime A of figure 8.9).

$\langle \epsilon_T \rangle > \langle \epsilon_O \rangle$ also characterizes the mid-depths of the IWISE data. This may be due to the occurrence of large overturns and strong advection near the base of the Kuroshio Current (see St Laurent, 2012). Interestingly, however, near-bottom agreement at IWISE N2 is better than what is observed for near-bottom data of BBTRE despite a strong influence from bottom roughness. This difference may be due to the fact that IWISE stations were occupied over the course of at least a single tidal cycle so that both young ($\langle \epsilon_T \rangle > \langle \epsilon_O \rangle$) and old ($\langle \epsilon_T \rangle < \langle \epsilon_O \rangle$) turbulence could be sampled with repeated VMP casts. Another possible explanation is that bottom-induced drag at IWISE N2 is also leading to high dissipation as a result of strong near-bottom mean shear. Spatial variability may also be reduced at this station due to the fact that turbulent fluid near the bottom is advected back and forth across the ridge during the course of a tidal cycle rather than being swept downstream. In contrast, the flow over topography observed in BBTRE is predominately unidirectional.

Agreement is relatively good in the NATRE data set. Interestingly, the bias toward $\epsilon_T > \epsilon_O$ observed in figure 8.10 is not reflected in the mean profile due to the scarcity of large overturns.

Because dissipation is not necessarily zero outside of identified patches, ensemble averaging was also done for continuous (as opposed to patch-wise) VMP measurements of ϵ . Profiles of $\langle \epsilon \rangle$ are shown as a light gray line in the second panel of figures 8.13 - 8.16. In general, $\langle \epsilon_O \rangle \gtrsim \langle \epsilon \rangle$ which indicates that dissipation is concentrated in overturns. A notable exception to this is the near-bottom data from IWISE N2 where, as discussed above, bottom-enhanced shear or non-local turbulence due to flow reversal may be playing a role in increasing the dissipation occurring outside of overturns.

The results of this section generally support the use of equation 8.1 in an ensemble averaged sense, but indicate a potential bias toward $\langle \epsilon_T \rangle > \langle \epsilon_O \rangle$ in portions of the water column characterized by large overturns and when temporal averaging is limited (e.g., near-bottom BBTRE). This has important implications for time series (e.g., see Alford et al., 2011) or time-integrated estimates of dissipation (discussed next) in which contributions by individual overturns are important.

8.7 Time integration: energy budgets

Of particular importance to ocean circulation models is the correct budgeting of kinetic energy between various sources and sinks so that models are energetically consistent. The two important sinks are, of course, viscous dissipation and conversion to mean potential energy via diapycnal buoyancy flux. Commonly, the latter is related to the former using a prescribed mixing efficiency (see Osborn, 1980). As such, time integration of ϵ in turbulent regions of the ocean provides a means for estimating the total energy consumed by the turbulence during a given period of time. Therefore, time integrated values provide valuable information for the calibration and validation of numerical models. In this section we consider the possibility of using ϵ_T for this purpose and evaluate the effectiveness of time integration in smoothing over the phase difference between APE of the large overturns and TKE of the subsequent turbulence. Data from IWISE M sites during the spring tidal period are considered (direct comparison of L_T and L_O is shown in figure B.9 of appendix B). A time series of the true dissipation rate measured by the VMP, ϵ , is shown as a function of depth for each profile in figure 8.17.

Integration of measured dissipation values with respect to depth for each profile gives a time series of the the power lost to viscous dissipation per unit surface area of the ocean. Time integration then gives the unit energy dissipated. With the assumption of constant density¹¹, ρ_0 , the vertically, time-integrated dissipation (i.e., unit energy) is estimated from

¹¹The change in density across the depth is at most $(1028 - 1021)\text{kgm}^{-3}/1021\text{kgm}^{-3} \times 100\% = 0.7\%$,

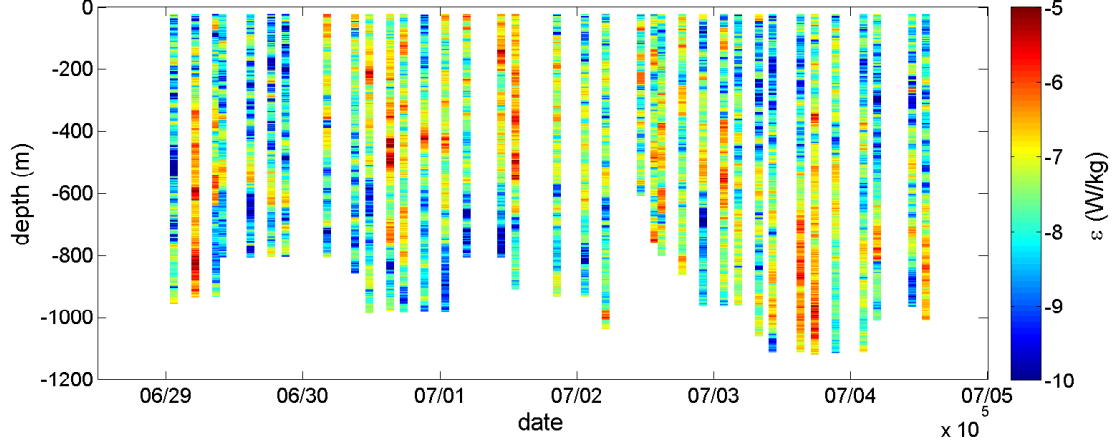


Figure 8.17: Time series of dissipation rates for profiles taken during the spring tidal cycle at IWISE M stations.

VMP measurements using

$$Unit\ Energy\ (patches) \approx \rho_0 \sum_{i=1}^n \sum_{j=1}^m (\epsilon_O \Delta z_{patch})_{j,i} \Delta t_i, \quad (8.8)$$

where n is the total number of profiles ($n = 36$ for IWISE M during the spring tidal period), m is the total number of patches with $L_T > 1$ m in a given profile, $\Delta z_{patch,j}$ is the vertical extent of a given patch, and Δt_i is the central differenced time increment allotted to each profile ($\Delta t \approx 4$ hr for IWISE M). Analogously, Thorpe-inferred unit energy is estimated using

$$Unit\ Energy\ (Thorpe) \approx \rho_0 \sum_{i=1}^n \sum_{j=1}^m (\epsilon_T \Delta z_{patch})_{j,i} \Delta t_i. \quad (8.9)$$

Depth and time integrated values of ϵ_O and ϵ_T are shown in figure 8.18. Measured unit power (shown as green bars) demonstrates high temporal variability and is extremely high by ocean interior standards¹², with some values approaching or exceeding $0.5\ \text{Wm}^{-2}$. While roughly in phase with measured values, the Thorpe-inferred unit power (shown as blue bars) exceeds direct measurements by over an order of magnitude for several of the profiles and

whereas ϵ can vary by several orders of magnitude. Therefore, the error in assuming constant density is considered small.

¹²For comparison, the mean power for NATRE for similar depths and over a comparable time period is $\approx 2.2 \times 10^{-4}\ \text{Wm}^{-2}$. A time series plot of ϵ from NATRE profiles is included as figure B.10 in appendix B.

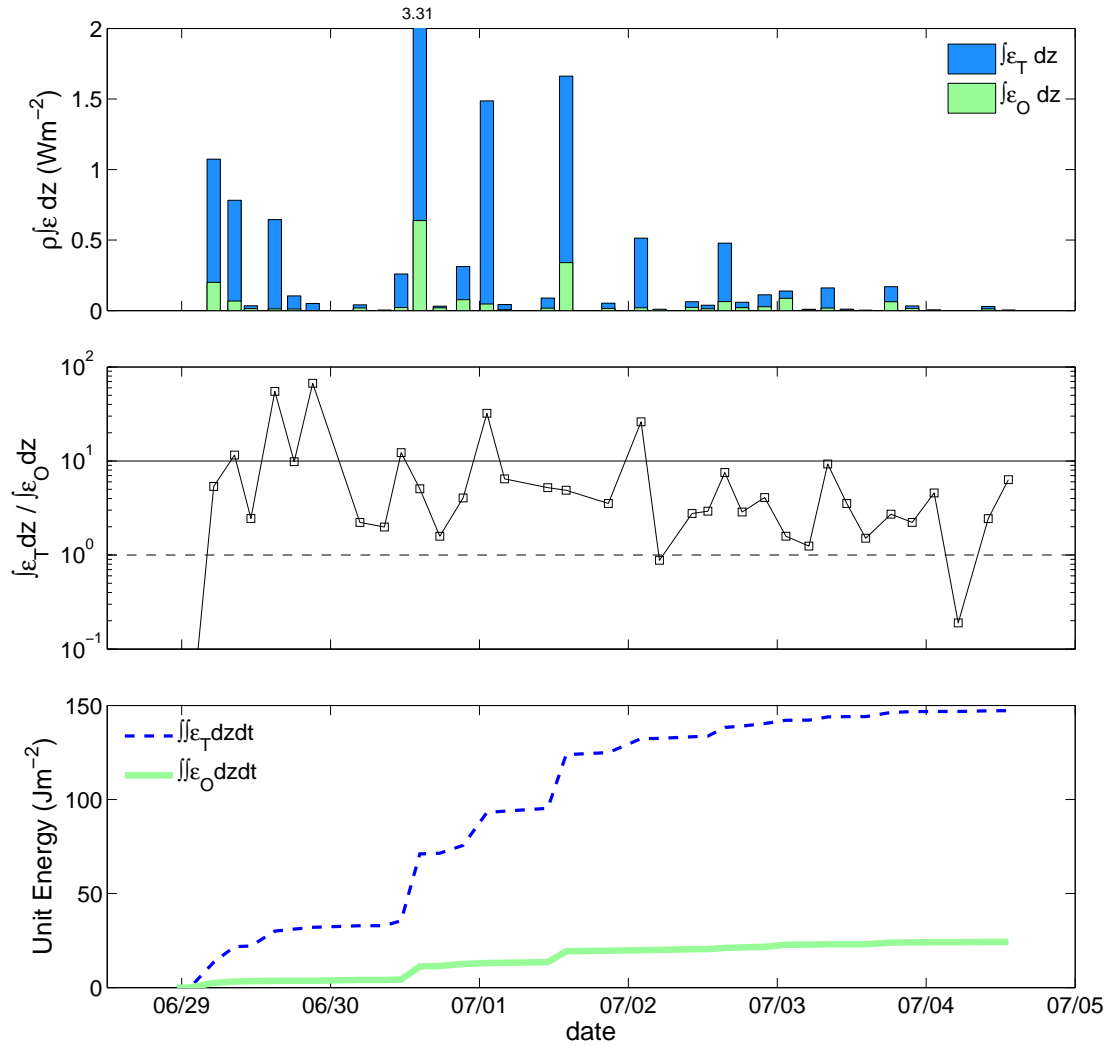


Figure 8.18: Unit power from depth integration of measured and Thorpe-inferred dissipation rates (top), ratio of inferred to measured unit power (middle), and unit energy dissipated determined by time integration of unit powers (bottom) for profiles taken at IWISE M stations over a spring tidal period.

is greater than the measured power for all but three profiles (middle panel). This dramatic overestimation occurs partly because of the lognormal nature of L_T/L_O which allows for rare but large overturns for which $\epsilon_T \gg \epsilon_O$ (see figure 8.10) to heavily weight estimates of power for an individual profile. The bias is further magnified as a result of effectively weighting ϵ_T by patch size; since Δz_{patch} correlates with L_T (not shown), the bias toward $\epsilon_T > \epsilon_O$ that occurs at large L_T is magnified in the estimates of power from $\sum_{j=1}^m (\epsilon_T \Delta z_{patch})_j$. Consistent overestimation of unit power by the Thorpe-based method results in a time-increasing overestimation of the dissipated energy shown in the bottom panel. Over the course of the spring tidal period, the energy inferred to have dissipated (147 Jm^{-2}) is approximately six times greater than that which was directly measured within turbulent patches (24 Jm^{-2}) and approximately four times greater than that which was measured over the total depth (39 Jm^{-2} ; not plotted)¹³.

Apparently, the large overestimation by the Thorpe-based method seen in some profiles is not balanced by underestimation in others. A possible explanation for this may be that lateral advection of turbulent fluid away from the M sites prevents temporal integration from capturing both young and old turbulence. Perhaps more concerning, however, may be that temporal integration smooths over the lag between APE and TKE, but assumption (ii) remains invalid in the mean. That is, while L_T quite possibly indicates the TKE present in the flow on average — as suggested by the results of Moum (1996) and Mater and Venayagamoorthy (2014b) — it remains unclear whether it is also representative of the *dissipation* of TKE, even in a time-integrated sense.

8.8 Conclusion

Using data sets from three different oceanic settings, we have shown that L_T increases with respect to L_O as a function of overturn size. In drawing an analogy with the DNS

¹³For perspective, the M sites collectively represent about 10 km^2 of ocean so that the total energy consumed during the site occupation is roughly $4 \times 10^5 \text{ kJ}$ or 100 kWhr — this is enough energy to run a laptop operating at 100 W for over 40 days!

findings of Smyth et al. (2001) which focused specifically on K-H billows, we suggest that this trend reflects the temporal evolution of the large overturns that have been observed at sites such as Luzon Strait and the fracture zone of the Brazil Basin. The dependencies indicated here suggest that equation 8.1 is significantly biased by the state and/or age of the observed overturns. Hence, incomplete sampling (a particularly vexing problem in observing naturally-occurring geophysical flows) leads to biases in dissipation estimates from Thorpe scales.

While it may be tempting to employ equation 8.1 when overturns are an obvious feature of the turbulence, the apparent bias shown here has serious implications for estimations of energy budgets based on profile-wise use of the equation and may lead to field-based inferences and numerical models that are too dissipative. A much needed next step in the evaluation of equation 8.1 is a campaign focused on sampling the full cycle of several turbulent events in a manner that tracks the turbulent fluid in space so that temporal and spatial variability can be separated from variability due to violation of the physical arguments. Until such resolution is achieved, the findings of this chapter suggest that the use of equation 8.1 in regions characterized by large overturns that convectively drive the turbulence should be approached with caution, especially for small sample sizes.

Chapter 9

Summary & Conclusions

9.1 Summary of Investigation

This dissertation represents a three-pronged approach to studying the dynamics of stably-stratified shear-flow turbulence using (1) dimensional analysis, (2) direct numerical simulations and laboratory data, and (3) field observations. Of particular focus has been the link between the basic physical quantities that characterize turbulent mixing (i.e., k , ϵ , ν , N , and S) and the length scale of overturning motions that can be readily quantified from observations, L_T .

Using dimensional analysis, the basic quantities were combined in chapter 4 to form a suite of fundamental length scales, time scales, and dimensionless parameters of physical relevance.

In chapter 5, the relationships between L_T and the fundamental length scales were determined using DNS for the simple case of homogeneously-stratified turbulence that decays in the absence of shear.

In chapter 6, the relationships between L_T and the fundamental length scales were determined using a large database of DNS and laboratory results for the general case of stably-stratified shear-flow turbulence. For the first time, L_T was shown to correlate with specific fundamental length scales in specific regimes of a multi-parameter, multi-regime framework that independently considers the strength of both shear and stratification with respect to the inertia of the turbulence. Independent consideration for shear and stratification was made possible by comparing the time scales S^{-1} and N^{-1} to that of the inertial motions, $T_L = k/\epsilon$, using the dimensionless parameters ST_L and NT_L . These parameters were considered along with Ri to form a unifying description of high Reynolds number turbulence.

Inclusion of the turbulent Reynolds number, Re_L , allowed the multi-parameter framework to be used in chapter 7 in an evaluation of common single-parameter descriptions of diapycnal mixing efficiency. Single-parameter schemes based on based on Ri , the turbulent Froude number, Fr_T , and the buoyancy Reynolds number, Re_b , were generally considered. The multi-parameter framework was used to explain specific shortcomings of these schemes.

Finally, the commonly assumed scaling, $L_T \sim (\epsilon/N^3)^{1/2}$, was tested in chapter 8 using various oceanic data sets. Emphasis was placed on observations from Luzon Strait and the Brazil Basin where turbulence is driven by overturns that are very large by open ocean standards. An alternative forcing mechanism, convective destabilization of overturning billows, was considered in recognition that not all turbulence in the ocean is produced simply by mean shear.

9.2 Conclusions on Key Findings

The following is a brief description of the main outcomes of this study:

- The Thorpe length scale, L_T , is a simple and objective measure of overturning whose fundamental relevance changes with the relative strengths of shear and stratification. The DNS of homogeneously-stratified turbulence in the absence of shear revealed $L_T \sim k^{1/2}N^{-1}$ in a strongly stratified regime characterized by $NT_L \gtrsim 1$ and $L_T \sim k^{3/2}\epsilon^{-1}$ in a weakly stratified regime characterized by $NT_L \lesssim 1$, where $NT_L = Nk/\epsilon$ is the buoyancy strength parameter (i.e., inverse Froude number). Only for $NT_L \approx 1$ was L_T found to agree with the Ozmidov scale, $L_O = (\epsilon/N^3)^{1/2}$.
- Consideration for both stratification and mean shear motivated the construction of an $Re_L - NT_L - ST_L$ parameter space, where $Re_L = k^2/(\epsilon\nu)$ and $ST_L = Sk/\epsilon$ are the turbulent Reynolds number and shear strength parameter, respectively. The space was simplified to a $NT_L - ST_L$ plane in the interest of intense geophysical turbulence where observable overturns are minimally influenced by viscosity. A buoyancy-dominated

regime ($NT_L \gtrsim 1.7$, $Ri \gtrsim 0.25$), a shear-dominated regime ($ST_L \gtrsim 3.3$, $Ri \lesssim 0.25$), and an inertia-dominated regime ($NT_L \lesssim 1.7$, $ST_L \lesssim 3.3$) were first conceptualized and then found to be relevant in scaling L_T for a large database of DNS and laboratory flows. Specifically, it was found that $L_T \sim k^{1/2}N^{-1}$, $L_T \sim k^{1/2}S^{-1}$, and $L_T \sim k^{3/2}\epsilon^{-1}$ in the buoyancy-, shear-, and inertia-dominated regimes, respectively. $L_T \sim L_O$ was found only for the case of $NT_L = O(10^0)$ and $ST_L \lesssim 3.3$, or for $NT_L = O(10^0)$, $ST_L \approx 3.3$ and $Ri \approx 0.25$ when shear is present.

- The various scalings for L_T indicate that the common practice of inferring dissipation from $L_T \sim L_O \Rightarrow \epsilon \sim L_T^2 N^3$ is not strictly valid. Instead, it is generally more appropriate to infer k so long as the turbulence is well-developed as it is in the experimental flows considered here. Inference of k is practical for stratified flows in which Ri is an effective diagnostic (i.e., turbulence is due to well-defined mean shear). In such flows, k can be inferred from easily observed quantities using $k \sim (L_T S)^2$ for $Ri \lesssim 0.25$ and $k \sim (L_T N)^2$ for $Ri \gtrsim 0.25$. Recasting the Osborn formulation for diapycnal diffusivity in terms of k and Ri makes inferred values of k relevant to mixing. The new model was shown to be more accurate than estimates of diffusivity based on inferred values of ϵ when tested with select DNS and laboratory data.
- An investigation of diapycnal mixing efficiency in stratified shear-flow turbulence revealed that the accuracy of a given single-parameter description of R_f^* depends on the regime to which the flow belongs. Ri is an accurate diagnostic in the shear-dominated regime but fails in the inertia-dominated regime where turbulence is generated by external forcing (rather than mean shear). On the other hand, Fr_T , is an accurate diagnostic in the inertia-dominated regime where $l \sim L_T$ and $u \sim (\epsilon L_T)^{1/3}$ are the correct characteristic length and velocity scales, respectively, that can account for external forcing. Fr_T loses accuracy, however, in the shear-dominated regime where $u \sim S L_T$ is more appropriate. Neither Ri or Fr_T sufficiently describe R_f^* in the buoyancy-dominated

regime where additional consideration for Re_L , Pr , and the turbulent mechanism are needed. This remains an important area of research in the quest for an unambiguous description of mixing efficiency.

- The investigation of diapycnal mixing efficiency also showed that the buoyancy Reynolds number, $Re_b = Re_L(NT_L)^{-2}$, is a misleading parameter for describing R_f^* because it fails to distinguish between (i) a low-Reynolds number, weakly stratified regime of low efficiency (low Re_L , low NT_L , low R_f^*) and (ii) a high-Reynolds number, strongly stratified regime of high efficiency (high Re_L , high NT_L , high R_f^*). In case (i), efficiency is low at high Re_b due to weak stratification (i.e., there is nothing to mix). In case (ii), efficiency is high at high Re_b because strong stratification and strong turbulence coexist to allow for sustained mixing. DNS and laboratory turbulence is restricted to case (i) due to computational limitations on Re_L , while geophysical turbulence falls under case (ii). The clear implication of this finding is that Re_b -based parameterizations developed for low-Reynolds number experimental flows are not universal or appropriate for geophysical flows. This is confirmed through comparison of the DNS results of Shih et al. (2005) with the atmospheric boundary layer observations of Lozovatsky and Fernando (2013). The decrease in R_f^* that occurs at $Re_b \approx 100$ in the DNS data is not observed in the observations. Rather, the observations demonstrate R_f^* values well above the canonical value of 0.17 up to $Re_b \approx 10^5$.
- For the two oceanic data sets exhibiting large overturns, L_T is found to increase with respect to L_O as a function of the normalized overturn size, $\widehat{L}_T = L_T N^{1/2} \nu^{-1/2}$. This was presumed to be a function of age of turbulent patches, with younger patches exhibiting larger \widehat{L}_T and $L_T \gg L_O$. When sampling favors large overturns, overestimation of turbulent diffusivity will occur if $\epsilon \sim L_T^2 N^3$ is assumed. This bias is especially relevant to time series representations of inferred mixing. The bias persists despite spatio-temporal averaging of the data considered here. The bias is quantified over a

spring tidal period at Luzon Strait where depth- and time-integration of inferred and measured values of ϵ show that inferred energy dissipation is four times too large.

9.3 Suggestions for Further Research

The multi-dimensional framework that is at the heart of this research remains to be validated using high-Reynolds number geophysical data. This is primarily because direct quantification of k in the field is hindered by the current inability to accurately filter non-turbulent motions of internal waves from those of the turbulence which actually lead to diapycnal mixing. This is a fundamental issue that remains to be solved for the benefit of, not just the current work, but for the small-scale physical oceanography community in general given the fundamental relevance of k . A promising device for approaching this problem is a Pitot tube capable of measuring microscale velocity fluctuations in three dimensions that is current being deployed on ocean moorings and profiling bodies by the Ocean Mixing Group at Oregon State University. The response frequency of this device is sufficiently high as to allow for the construction of energy spectra which represent the energy-containing scales and most of the inertial subrange for typical ocean turbulence (J. Moum, personal communication, December 2013). Filtering issues aside, deployment of the Pitot tube on a platform that affords contemporaneous measurement of ϵ , N , S , and $\rho(z)$ is a possible means of validating the findings of this dissertation regarding the scaling of L_T .

Additionally, the current work has focused primarily on well-developed turbulence and has emphasized the productive role of an imposed homogeneous mean shear. While this viewpoint has guided many classic studies, geophysical turbulence is often generated intermittently by mechanisms such as Kelvin-Helmholtz billows where the mean shear is dynamically linked to the turbulence and evolves with time. It would be greatly interesting and informative to examine such flows using the proposed framework to see if scalings of L_T are consistent with the homogeneous case. This could be done using data from K-H DNS such as that of Smyth and Moum (2000).

Furthermore, chapter 8 of this dissertation has highlighted that geophysical turbulence can be generated by mechanisms other than mean shear, with special focus on the convective destabilization of large overturning billows. Until these motions become fully turbulent, they may be difficult to classify within the context of the proposed framework. As such, overturns in environments such as the Luzon Strait demand further attention in line with the work of chapter 8. Specifically, a sampling campaign aimed at capturing the full evolution of a turbulent billow in time and space would reveal whether the apparent bias of $L_T > L_O$ is physically based (as proposed here) or is a result of insufficient sampling.

References

- Alford, M. H., MacKinnon, J. A., Nash, J. D., Simmons, H., Pickering, A., Klymak, J. M., Pinkel, R., Sun, O., Rainville, L., Musgrave, R., et al. (2011). Energy flux and dissipation in Luzon Strait: Two tales of two ridges. *Journal of Physical Oceanography*, 41(11):2211–2222.
- Barry, M. E., Ivey, G. N., Winters, K. B., and Imberger, J. (2001). Measurements of diapycnal diffusivities in stratified fluids. *Journal of Fluid Mechanics*, 442:267–291.
- Billant, P. and Chomaz, J. (2001). Self-similarity of strongly stratified inviscid flows. *Physics of Fluids*, 13(6):1645–1651.
- Brethouwer, G., Billant, P., Lindborg, E., and Chomaz, J. (2007). Scaling analysis and simulation of strongly stratified turbulent flows. *Journal of Fluid Mechanics*, 585:343–368.
- Britter, R. E. (1974). *An experiment on turbulence in a density stratified fluid*. PhD thesis, Monash University, Victoria, Australia.
- Britter, R. E. (1985). Diffusion and decay in stably-stratified turbulent flows. In *Turbulence and Diffusion in Stable Environments*, pages 3–13. Oxford Univ Press.
- Chang, Y. S., Xu, X., Özgökmen, T. M., Chassignet, E. P., Peters, H., and Fischer, P. F. (2005). Comparison of gravity current mixing parameterizations and calibration using a high-resolution 3D nonhydrostatic spectral element model. *Ocean Modelling*, 10(3):342–368.
- Chung, D. and Matheou, G. (2012). Direct numerical simulation of stationary homogeneous stratified sheared turbulence. *Journal of Fluid Mechanics*, 696:434–467.
- Corrsin, S. (1958). Local isotropy in turbulent shear flow. NACA research memorandum 58B11, National Advisory Committee for Aeronautics, Washington D.C., USA.
- Dillon, T. M. (1982). Vertical overturns: a comparison of Thorpe and Ozmidov length scales. *Journal of Geophysical Research-Oceans*, 87(C12):9601–9613.
- Dougherty, J. (1961). The anisotropy of turbulence at the meteor level. *Journal of Atmospheric and Terrestrial Physics*, 21(2):210 – 213.
- Dunckley, J., Koseff, J., Steinbuck, J., Monismith, S., and Genin, A. (2012). Comparison of mixing efficiency and vertical diffusivity models from temperature microstructure. *Journal of Geophysical Research-Oceans*, 117(C10).

- Durbin, P. and Reif, B. (2001). *Statistical Theory and Modeling for Turbulent Flows*. Wiley.
- Ellison, T. H. (1957). Turbulent transport of heat and momentum from an infinite rough plane. *Journal of Fluid Mechanics*, 2:456–466.
- Ferron, B., Mercier, H., Speer, K., Gargett, A., and Polzin, K. (1998). Mixing in the Romanche fracture zone. *Journal of Physical Oceanography*, 28(10):1929–1945.
- Garcia-Villalba, M. and del Alamo, J. C. (2011). Turbulence modification by stable stratification in channel flow. *Physics of Fluids*, 23(4):1–22.
- Gargett, A. E. (1988). The scaling of turbulence in the presence of stable stratification. *Journal of Geophysical Research-Oceans*, 93(C5):5021–5036.
- Gargett, A. E., Osborn, T. R., and Nasmyth, P. W. (1984). Local isotropy and the decay of turbulence in a stratified fluid. *Journal of Fluid Mechanics*, 144:231–280.
- Geyer, W. R., Lavery, A. C., Scully, M. E., and Trowbridge, J. H. (2010). Mixing by shear instability at high Reynolds number. *Geophysical Research Letters*, 37(22).
- Gibson, C. H. (1980). Fossil temperature, salinity, and vorticity turbulence in the ocean. In Nihoul, J. C., editor, *Marine Turbulence Proceedings of The 11th International Lige Colloquium on Ocean Hydrodynamics*, volume 28 of *Elsevier Oceanography Series*, pages 221 – 257. Elsevier.
- Gibson, C. H. (1987). Fossil turbulence and intermittency in sampling oceanic mixing processes. *Journal of Geophysical Research-Oceans*, 92(C5):5383–5404.
- Gill, A. E. (1982). *Atmosphere-Ocean Dynamics*, volume 30. Academic press.
- Gregg, M. C. (1987). Diapycnal mixing in the thermocline: Review. *Journal of Geophysical Research*, 92(C5):5249–5286.
- Gregg, M. C., D’Asaro, E. A., Shay, T. J., and Larson, N. (1986). Observations of persistent mixing and near-inertial internal waves. *Journal of Physical Oceanography*, 16(5):856–885.
- Holt, S. E., Koseff, J. R., and Ferziger, J. H. (1992). A numerical study of the evolution and structure of homogeneous stably stratified sheared turbulence. *Journal of Fluid Mechanics*, 237:499–539.
- Hopfinger, E. J. (1987). Turbulence in stratified fluids - a review. *Journal of Geophysical Research-Oceans*, 92(C5):5287–5303.
- Howard, L. N. (1961). Note on a paper of John W. Miles. *Journal of Fluid Mechanics*, 10:509–512.

- Hoyas, S. and Jiménez, J. (2006). Scaling of the velocity fluctuations in turbulent channels up to $Re = 2003$. *Physics of fluids*, 18:011702.
- Itsweire, E. C. (1984). Measurements of vertical overturns in a stably stratified turbulent-flow. *Physics of Fluids*, 27(4):764–766.
- Itsweire, E. C., Helland, K. N., and Van Atta, C. W. (1986). The evolution of grid-generated turbulence in a stably stratified fluid. *Journal of Fluid Mechanics*, 162:299–338.
- Itsweire, E. C., Koseff, J. R., Briggs, D. A., and Ferziger, J. H. (1993). Turbulence in stratified shear flows - implications for interpreting shear-induced mixing in the ocean. *Journal of Physical Oceanography*, 23(7):1508–1522.
- Ivey, G. N. and Imberger, J. (1991). On the nature of turbulence in a stratified fluid part 1: The energetics of mixing. *Journal of Physical Oceanography*, 21(5):650–658.
- Ivey, G. N., Winters, K. B., and Koseff, J. R. (2008). Density stratification, turbulence, but how much mixing? *Annual Review of Fluid Mechanics*, 40(1):169.
- Jacobitz, F. G., Sarkar, S., and Van Atta, C. W. (1997). Direct numerical simulations of the turbulence evolution in a uniformly sheared and stably stratified flow. *Journal of Fluid Mechanics*, 342:231–261.
- Karimpour, F. and Venayagamoorthy, S. K. (2014). A simple turbulence model for stably stratified wall-bounded flows. *Journal of Geophysical Research-Oceans*, 119(2):870–880.
- Keller, K. H. and Van Atta, C. W. (2000). An experimental investigation of the vertical temperature structure of homogeneous stratified shear turbulence. *Journal of Fluid Mechanics*, 425:1–29.
- Kim, J., Moin, P., and Moser, R. (1987). Turbulence statistics in fully developed channel flow at low Reynolds number. *Journal of Fluid Mechanics*, 177:133–166.
- Klymak, J. M. and Legg, S. M. (2010). A simple mixing scheme for models that resolve breaking internal waves. *Ocean Modelling*, 33(3):224–234.
- Kolmogorov, A. N. (1941). The local structure of turbulence in incompressible viscous fluid for very large Reynolds number. *Dokl. Akad. Nauk SSSR*, 30:299–303.
- Kundu, P. K. (1990). *Fluid Mechanics*. Acad. Press.
- Ledwell, J. R., Montgomery, E. T., Polzin, K. L., St. Laurent, L. C., Schmitt, R. W., and Toole, J. M. (2000). Evidence for enhanced mixing over rough topography in the abyssal ocean. *Nature*, 403(6766):179–182.

- Lee, M., Kim, J., and Moin, P. (1990). Structure of turbulence at high shear rate. *Journal of Fluid Mechanics*, 216:561–583.
- Lindborg, E. (2006). The energy cascade in a strongly stratified fluid. *Journal of Fluid Mechanics*, 550:207–242.
- Linden, P. (1980). Mixing across a density interface produced by grid turbulence. *Journal of Fluid Mechanics*, 100(04):691–703.
- Lozovatsky, I. and Fernando, H. (2013). Mixing efficiency in natural flows. *Philosophical Transactions of the Royal Society A: Mathematical, Physical and Engineering Sciences*, 371(1982):20120213.
- Luketina, D. A. and Imberger, J. (1989). Turbulence and entrainment in a buoyant surface plume. *Journal of Geophysical Research-Oceans*, 94(C9):12619–12636.
- Mashayek, A., Caulfield, C. P., and Peltier, W. R. (2013). Time-dependent, non-monotonic mixing in stratified turbulent shear flows: Implications for oceanographic estimates of buoyancy flux. *Journal of Fluid Mechanics*, 736:570–593.
- Mashayek, A. and Peltier, W. R. (2013). Shear-induced mixing in geophysical flows: Does the route to turbulence matter to its efficiency? *Journal of Fluid Mechanics*, 725:216–261.
- Mater, B. D., Schaad, S. M., and Venayagamoorthy, S. K. (2013). Relevance of the Thorpe length scale in stably stratified turbulence. *Physics of Fluids*, 25(7):076604.
- Mater, B. D. and Venayagamoorthy, S. K. (2014a). The quest for an unambiguous parameterization of mixing efficiency in stably stratified geophysical flows. *Geophysical Research Letters*, 41(TBD,doi=10.1029/2010GL045272).
- Mater, B. D. and Venayagamoorthy, S. K. (2014b). A unifying framework for parameterizing stably stratified shear-flow turbulence. *Physics of Fluids*, 26(3).
- Mater, B. D., Venayagamoorthy, S. K., St. Laurent, L., and Moum, J. N. (submitted). Biases in Thorpe scale estimation of turbulence dissipation from large overturns in the ocean. *Journal of Physical Oceanography*.
- McEwan, A. (1983). Internal mixing in stratified fluids. *Journal of Fluid Mechanics*, 128:59–80.
- Melet, A., Hallberg, R., Legg, S., and Polzin, K. (2013). Sensitivity of the ocean state to the vertical distribution of internal-tide-driven mixing. *Journal of Physical Oceanography*, 43(3):602–615.
- Mellor, G. L. and Yamada, T. (1982). Development of a turbulence closure model for geophysical fluid problems. *Reviews of Geophysics*, 20(4):851–875.

- Miles, J. W. (1961). On the stability of heterogeneous shear flows. *Journal of Fluid Mechanics*, 10:496–508.
- Monti, P., Fernando, H., Princevac, M., Chan, W., Kowalewski, T., and Pardyjak, E. (2002). Observations of flow and turbulence in the nocturnal boundary layer over a slope. *Journal of the Atmospheric Sciences*, 59(17).
- Moum, J. N. (1996). Energy-containing scales of turbulence in the ocean thermocline. *Journal of Geophysical Research-Oceans*, 101(C6):14095–14109.
- Munk, W. H. (1966). Abyssal recipes. In *Deep Sea Research and Oceanographic Abstracts*, volume 13, pages 707–730. Elsevier.
- Munk, W. H. and Anderson, E. R. (1948). Notes on a theory of the thermocline. *Journal of Marine Research*, 7:276–295.
- Mydlarski, L. (2003). Mixed velocity-passive scalar statistics in high-Reynolds-number turbulence. *Journal of Fluid Mechanics*, 475:173–203.
- Oakey, N. S. (1982). Determination of the rate of dissipation of turbulent energy from simultaneous temperature and velocity shear microstructure measurements. *Journal of Physical Oceanography*, 12(3):256–271.
- Osborn, T. R. (1974). Vertical profiling of velocity microstructure. *Journal of Physical Oceanography*, 4(1):109–115.
- Osborn, T. R. (1980). Estimates of the local rate of vertical diffusion from dissipation measurements. *Journal of Physical Oceanography*, 10(1):83–89.
- Osborn, T. R. and Cox, C. S. (1972). Oceanic fine structure. *Geophysical & Astrophysical Fluid Dynamics*, 3(1):321–345.
- Ozmidov, R. V. (1965). On the turbulent exchange in a stably stratified ocean, engl. transl. *Izv. Acad. Sci. USSR Atmos. Oceanic Phys.*, 1:853–860.
- Pardyjak, E. R., Monti, P., and Fernando, H. J. S. (2002). Flux Richardson number measurements in stable atmospheric shear flows. *Journal of Fluid Mechanics*, 459:307–316.
- Peltier, W. and Caulfield, C. (2003). Mixing efficiency in stratified shear flows. *Annual Review of Fluid Mechanics*, 35(1):135–167.
- Peters, H., Gregg, M., and Toole, J. (1988). On the parameterization of equatorial turbulence. *Journal of Geophysical Research-Oceans*, 93(C2):1199–1218.

- Peters, H. and Gregg, M. C. (1988). Some dynamical and statistical properties of equatorial turbulence. *Elsevier Oceanography Series*, 46:185–200.
- Phillips, O. M. (1972). Turbulence in a strongly stratified fluid is it unstable? *Deep Sea Research and Oceanographic Abstracts*, 19(1):79 – 81.
- Piccirillo, P. and Van Atta, C. W. (1997). The evolution of a uniformly sheared thermally stratified turbulent flow. *Journal of Fluid Mechanics*, 334:61–86.
- Polzin, K., Toole, J., Ledwell, J., and Schmitt, R. (1997). Spatial variability of turbulent mixing in the abyssal ocean. *Science*, 276(5309):93–96.
- Pope, S. B. (2000). *Turbulent Flows*. Cambridge University Press.
- Princevac, M., Hunt, J., and Fernando, H. (2008). Quasi-steady katabatic winds on slopes in wide valleys: Hydraulic theory and observations. *Journal of the Atmospheric Sciences*, 65(2).
- Rehmann, C. R. and Koseff, J. R. (2004). Mean potential energy change in stratified grid turbulence. *Dynamics of Atmospheres and Oceans*, 37(4):271–294.
- Richardson, L. F. (1922). *Weather Prediction by Numerical Process*. Cambridge University Press.
- Riley, J. J., Metcalfe, R. W., and Weissman, M. A. (1981). Direct numerical simulations of homogeneous turbulence in density-stratified fluids. In *AIP Conference Proceedings*, volume 76, pages 79–112.
- Rogallo, R. S. (1981). *Numerical Experiments in Homogeneous Turbulence*, volume 81315. National Aeronautics and Space Administration.
- Rogers, M. M., Mansour, N. N., and Reynolds, W. C. (1989). An algebraic model for the turbulent flux of a passive scalar. *Journal of Fluid Mechanics*, 203:77–101.
- Rohr, J. J. (1985). *An Experimental Study of Evolving Turbulence in Uniform Mean Shear Flows with and without Stable Stratification*. PhD thesis, University of California, San Diego.
- Rohr, J. J., Itsweire, E. C., Helland, K. N., and Van Atta, C. W. (1988). Growth and decay of turbulence in a stably stratified shear flow. *Journal of Fluid Mechanics*, 195:77–111.
- Rohr, J. J. and Van Atta, C. W. (1987). Mixing efficiency in stably stratified growing turbulence. *Journal of Geophysical Research-Oceans*, 92(C5):5481–5488.
- Rottman, J. W., B. R. E. (1986). The mixing efficiency and decay of grid-generated turbulence in stably stratified fluids. In *Proceedings of the 9th Australasian Fluid Mechanics Conference, University of Auckland, Auckland, New Zealand*.

- Saddoughi, S. G. and Veeravalli, S. V. (1994). Local isotropy in turbulent boundary layers at high Reynolds number. *Journal of Fluid Mechanics*, 268:333–372.
- Schmitt, R. W. (1994). Double diffusion in oceanography. *Annual Review of Fluid Mechanics*, 26(1):255–285.
- Schmitt, R. W. (1999). Spice and the demon. *Science*, 283(5401):498–499.
- Schumacher, J. (2007). Sub-Kolmogorov-scale fluctuations in fluid turbulence. *Europhysics Letters*, 80(5):54001.
- Shih, L. H., Koseff, J. R., Ferziger, J. H., and Rehmann, C. R. (2000). Scaling and parameterization of stratified homogeneous turbulent shear flow. *Journal of Fluid Mechanics*, 412:1–20.
- Shih, L. H., Koseff, J. R., Ivey, G. N., and Ferziger, J. H. (2005). Parameterization of turbulent fluxes and scales using homogeneous sheared stably stratified turbulence simulations. *Journal of Fluid Mechanics*, 525:193–214.
- Shimizu, K. (2012). Parameterizing individual effects of shear and stratification on mixing in stably stratified shear flows. *Journal of Geophysical Research-Oceans*, 117(C3):C03030.
- Sirivat, A. and Warhaft, Z. (1983). The effect of a passive cross-stream temperature gradient on the evolution of temperature variance and heat flux in grid turbulence. *Journal of Fluid Mechanics*, 128:323–346.
- Smith, W. H. and Sandwell, D. T. (1997). Global sea floor topography from satellite altimetry and ship depth soundings. *Science*, 277(5334):1956–1962.
- Smyth, W. D. and Moum, J. N. (2000). Length scales of turbulence in stably stratified mixing layers. *Physics of Fluids*, 12(6):1327–1342.
- Smyth, W. D. and Moum, J. N. (2013). Marginal instability and deep cycle turbulence in the eastern equatorial Pacific Ocean. *Geophysical Research Letters*, 40(23):6181–6185.
- Smyth, W. D., Moum, J. N., and Caldwell, D. R. (2001). The efficiency of mixing in turbulent patches: Inferences from direct simulations and microstructure observations. *Journal of Physical Oceanography*, 31(8):1969–1992.
- St Laurent, L. C. (2012). Internal wave generation processes at deep-sills in the Luzon Passage Region of the South China Sea. Technical report, U.S. Office of Naval Research.
- St. Laurent, L. C. and Schmitt, R. W. (1999). The contribution of salt fingers to vertical mixing in the North Atlantic Tracer Release Experiment. *Journal of Physical Oceanography*, 29(7):1404–1424.

- St Laurent, L. C., Toole, J. M., and Schmitt, R. W. (2001). Buoyancy forcing by turbulence above rough topography in the abyssal Brazil Basin. *Journal of Physical Oceanography*, 31(12):3476–3495.
- Stillinger, D. C., Helland, K. N., and Van Atta, C. W. (1983). Experiments on the transition of homogeneous turbulence to internal waves in a stratified fluid. *Journal of Fluid Mechanics*, 131:91–122.
- Strang, E. and Fernando, H. (2001a). Vertical mixing and transports through a stratified shear layer. *Journal of Physical Oceanography*, 31(8):2026–2048.
- Strang, E. J. and Fernando, H. J. S. (2001b). Entrainment and mixing in stratified shear flows. *Journal of Fluid Mechanics*, 428(1):349–386.
- Stretch, D. D., Rottman, J. W., Venayagamoorthy, S. K., Nomura, K. K., and Rehmann, C. R. (2010). Mixing efficiency in decaying stably stratified turbulence. *Dynamics of Atmospheres and Oceans*, 49(1):25–36.
- Tavoularis, S. and Corrsin, S. (1981). Experiments in nearly homogenous turbulent shear flow with a uniform mean temperature gradient. Part 1. *Journal of Fluid Mechanics*, 104:311–347.
- Tennekes, H. and Lumley, J. L. (1974). *A First Course in Turbulence*. MIT Press.
- Thorpe, S. A. (1977). Turbulence and mixing in a Scottish loch. *Philosophical Transactions of the Royal Society A-Mathematical Physical and Engineering Sciences*, 286(1334):125–181.
- Thorpe, S. A. (2005). *The Turbulent Ocean*. Cambridge University Press.
- Toole, J. M., Schmitt, R. W., and Polzin, K. L. (1994). Estimates of diapycnal mixing in the abyssal ocean. *Science*, 264(5162):1120–1123.
- Venayagamoorthy, S. K. and Stretch, D. D. (2006). Lagrangian mixing in decaying stably stratified turbulence. *Journal of Fluid Mechanics*, 564:197–226.
- Venayagamoorthy, S. K. and Stretch, D. D. (2010). On the turbulent Prandtl number in homogeneous stably stratified turbulence. *Journal of Fluid Mechanics*, 644:359–369.
- Von Karman, T. (1930). Mechanische Ähnlichkeit und turbulenz. *Nachrichten von der Gesellschaft der Wissenschaften zu Göttingen, Mathematisch-Physikalische Klasse*, 1930:58–76.
- Waite, M. L. and Bartello, P. (2006). Stratified turbulence generated by internal gravity waves. *Journal of fluid Mechanics*, 546:313–340.
- Wesson, J. C. and Gregg, M. C. (1994). Mixing at Camarinal sill in the Strait of Gibraltar. *Journal of Geophysical Research-Oceans*, 99(C5):9847–9878.

- Winters, K. B. and D'Asaro, E. A. (1996). Diascalar flux and the rate of fluid mixing. *Journal of Fluid Mechanics*, 317(1):179–193.
- Winters, K. B., Lombard, P. N., Riley, J. J., and D'Asaro, E. A. (1995). Available potential energy and mixing in density-stratified fluids. *Journal of Fluid Mechanics*, 289:115–128.
- Wunsch, C. and Ferrari, R. (2004). Vertical mixing, energy, and the general circulation of the oceans. *Annual Review of Fluid Mechanics*, 36:281–314.
- Xu, X., Chang, Y. S., Peters, H., Özgökmen, T. M., and Chassignet, E. P. (2006). Parameterization of gravity current entrainment for ocean circulation models using a high-order 3D nonhydrostatic spectral element model. *Ocean Modelling*, 14(1):19–44.
- Yamada, T. (1975). The critical Richardson number and the ratio of the eddy transport coefficients obtained from a turbulence closure model. *Journal of the Atmospheric Sciences*, 32(5):926–933.
- Yamazaki, H. (1990). Stratified turbulence near a critical dissipation rate. *Journal of Physical Oceanography*, 20(10):1583–1598.
- Zaron, E. D. and Moum, J. N. (2009). A new look at Richardson number mixing schemes for equatorial ocean modeling. *Journal of Physical Oceanography*, 39(10):2652–2664.

Appendix A

Length Scales of the Unstratified Boundary Layer¹⁴

In chapter 4, the scales and energy spectrum of unstratified shear-flow turbulence were discussed in the context of homogeneous shear (i.e., ST_L and Re_L do not vary with location). In natural flows, however, the presence of boundaries induces heterogeneity in the flow as mean velocity decreases rapidly toward the bounding surface. Very near the surface, or “wall”, shear is high but so too are viscous effects so that local values of ST_L and Re_L vary dramatically with position. The interaction of these two counteracting influences gives rise to complex turbulent dynamics that have received much attention. The famous Prandtl mixing length hypothesis supposes that the turbulent velocity fluctuations near the wall scale with the anisotropic velocity scale: $v \sim u \sim Sl_{mix}$, where l_{mix} is a mixing length that Von Karman (1930) suggested should increase in a linear fashion away from the wall (i.e., $l_{mix} = \kappa z$, where $\kappa \approx 0.41$ is a constant and z is the wall-normal distance). These suggestions combine to give the famous “log-law”, or logarithmic profile of mean velocity that empirically holds for $z^+ \gtrsim 30$, where $z^+ = z/\delta_\nu$ is the wall-normal coordinate normalized by the viscous length scale, $\delta_\nu = \nu/u^*$. This viscous length scale is essentially $L_{\nu S}$ at the wall (i.e., $\delta_\nu = \nu/u^* = \nu/\sqrt{\tau_0/\rho} = \nu/\sqrt{\nu S_0} = (\nu/S_0)^{1/2}$, where $u^* = \sqrt{\tau_0/\rho}$ is the shear velocity and $\tau_0 = \rho\nu S_0$ is the shear stress at the wall). Closer to the wall, the “log-law” breaks down. $5 < z^+ < 30$ is often characterized as a “buffer layer” where both ST_L and turbulent production peaks, relative to dissipation. $z^+ < 5$ is typically considered the “viscous sublayer” where Reynolds stress (i.e., turbulence) is negligible compared to viscous

¹⁴Many of the ideas presented here were initially proposed in an unpublished report entitled “Relevant length scales in wall-bounded turbulent flows” by L. P. Dasi and S. K. Venayagamoorthy (2010).

stress and the mean velocity profile is linear. In these regions, the “log-law” breaks down because $l_{mix} \sim z$ is no longer valid.

What then is the behavior of l_{mix} and can this behavior be explained using the fundamental length scales? Moreover, what do the fundamental scales tell us about the boundary layer regions based on the physical interpretations of section 4.1.2? The unstratified channel-flow DNS of Hoyas and Jiménez (2006) provides an excellent data set for such an investigation. They simulated uni-directional flow over a smooth wall for $Re_\tau = 180, 550, 950, \text{ and } 2003$, where $Re_\tau = u^*\delta/\nu$ is the “friction” Reynolds number and δ is the half depth of the channel (full depth if free surface). In what follows, this data set is examined to determine the behavior of the fundamental length scales. Hopefully, this will provide a new framework for interpreting near wall dynamics.

The six fundamental length scales are plotted in figure A.1 as they vary from the wall. Both the length scales and the wall normal distance have been normalized by the viscous length scale at the wall, δ_ν . The boundary layer can be delineated into regions based on length scale “cross-over” points. The physical significance of these regions is proposed below.

- $z^+ < 1.3$: Very near the wall $L_{k\nu} > \eta > L_{\nu S} > L_C > L_{kS} > L_{k\epsilon}$. Taking $L_{k\nu}$ to be the smallest possible scale as per the reasoning of section 4.1.1 (or alternatively η in the classical sense), this implies that turbulence is not possible and the flow is laminar. As shown in figure A.2, the local Reynolds number based on L_{kS} is much less than unity (i.e., $k^{1/2}L_{kS}/\nu = L_{kS}/L_{k\nu} \ll 1$), as is the traditional Reynolds number (i.e., $Re_L = (L_{k\epsilon}/\eta)^{4/3} \ll 1$). Also, $ST_L < 1$, however, this parameter is not of much use since the flow is laminar (i.e., small T_L is more indicative of $k \rightarrow 0$ than rapid turbulence). In this region, the mean velocity profile is linear as to be expected in the viscous sublayer (see figure A.3). Also note that $L_{k\nu} = \delta_\nu$ as expected.
- $1.3 \leq z^+ < 3$: At $z^+ \approx 1.3$, L_{kS} becomes larger than L_C , i.e., $ST_L > 1$. The decay time of the turbulence, T_L , has increased, indicating an increased presence of turbulence; however, the Reynolds number, $k^{1/2}L_{kS}/\nu$, remains less than unity. Moreover, L_{kS}

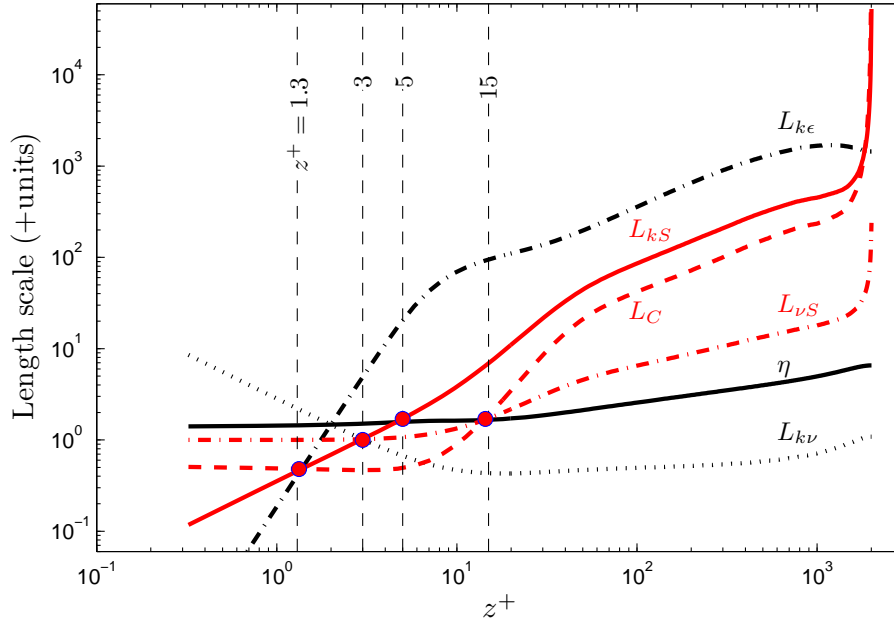


Figure A.1: Wall normal profiles of the fundamental length scales computed from DNS of unstratified channel flow. Data for the computations has been provided by Hoyas and Jiménez (2006). Only $Re_\tau = 2003$ case shown for clarity.

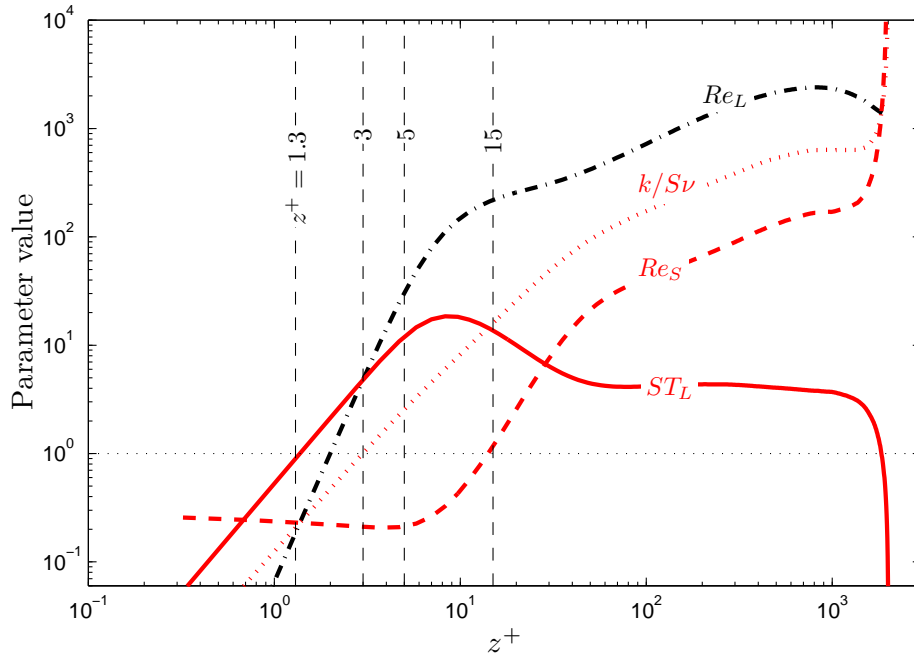


Figure A.2: Wall normal profiles of dimensionless parameters computed from DNS of unstratified channel flow. Data for the computations has been provided by Hoyas and Jiménez (2006). Only $Re_\tau = 2003$ case shown for clarity.

remains less than $L_{\nu S}$; if L_{kS} is the largest eddy in the flow, and $L_{\nu S}$ is the smallest scale for which production is possible (as argued in section 4.1.2), then no production is possible in this region. Without sufficient Reynolds number or local production, it is likely that turbulent kinetic energy is being transported from more distal regions due to heterogeneity of the flow.

- $3 \leq z^+ < 5$: At $z^+ \approx 3$, L_{kS} becomes larger than $L_{k\nu}$ and $L_{\nu S}$. If $L_{k\nu}$ is taken as the smallest scale possible, this signifies the possibility of the existence of locally shear-driven turbulence. That is, the local turbulent Reynolds number based on L_{kS} exceeds unity $k^{1/2}L_{kS}/\nu = L_{kS}/L_{k\nu} > 1$ (so too does Re_L). If $L_{\nu S}$ is taken as the small-scale bound on production, this point also indicates the onset of local production. The range of scales available for production, $L_{kS} > l > L_{\nu S}$, increases monotonically with distance from the wall. L_{kS} remains less than η , however, so no down-spectrum cascade of energy is possible; rather, turbulence is immediately arrested at the scale it is produced. It is also interesting to note that the velocity profile is no longer linear for $3 \lesssim z^+$, which is well inside the conventional outer limit of the viscous sublayer, $z^+ = 5$ (see figure A.3). This may be due to the increasing presence of locally produced turbulence.
- $5 \leq z^+ < 15$: At $z^+ \approx 5$, L_{kS} becomes larger than η signifying that a down-spectrum cascade of energy is possible. Since $\eta > L_{\nu S}$, however, there is essentially an overlap of production and dissipative ranges, so cascading energy does not do so in a purely inertial fashion as envisaged in the theory of Kolmogorov. Also note that η is classically considered the smallest possible scale, not $L_{k\nu}$. Taking L_{kS} to be the largest scale, classic theory then implies turbulence can only exist for $z^+ \gtrsim 5$, not $z^+ \gtrsim 3$. This aligns with the classic view that the viscous sublayer extends to $z^+ \approx 5$. With the new interpretation, however, the viscous sublayer ends and the buffer layer begins at $z^+ \approx 3$, not $z^+ \approx 5$.

- $z^+ \geq 15$: At $z^+ \approx 15$, $L_{\nu S}$ becomes larger than η , indicating that a purely inertial (free of shear) cascade of energy is possible from $L_{\nu S}$ to η . Also, L_C becomes larger than η (i.e., $Re_s = (L_C/\eta)^{4/3} = (L_C/L_{\nu S})^2 > 1$), indicating that the classic inertial subrange becomes possible down-scale of L_C . Beyond $z^+ \approx 15$, the order of scales agrees with that conceptualized for homogeneous shear-flow turbulence in figure 4.1.
- “Log-law” region: If it is assumed that the turbulent velocity fluctuations scale with the square root of the turbulent kinetic energy (i.e., $v \sim u \sim k^{1/2}$), a good guess for a predictor of l_{mix} is L_{kS} . Then, taking $L_{kS} \sim l_{mix} \sim z$ to be a necessary condition for a logarithmic mean velocity profile, the profile of L_{kS} can be examined to predict where the “log-law” might fail. The profile for $Re_\tau = 2003$ is shown in figure A.4. While a large portion of the profile is indeed linear, the lower extent of the linear portion is at $z^+ \approx 60$ rather than $z^+ \approx 30$ as shown in the profile of mean velocity of figure A.3. Furthermore, the slope of this portion is 0.68, which is somewhat higher than the classic value of 0.41. It appears, then, that $l_{mix} \sim L_{kS}$ is not strictly valid; while L_{kS} may correlate with the largest eddies, it is not exactly the mixing length as defined by Prandtl.

If it is instead assumed that the turbulent velocity fluctuations scale with the Corrsin velocity scale, $(\epsilon/S)^{1/2}$, then L_C becomes an alternate candidate for predicting l_{mix} . The profile of this scale is also shown in figure A.4 and has a slope of 0.32, which is slightly *less* than the classic value of 0.41. Clearly, l_{mix} is underestimated by L_C , but overestimated by L_{kS} . The failure of both scales to predict l_{mix} is likely due to complex anisotropic nature of the flow (i.e., deviation from $v \sim u$).

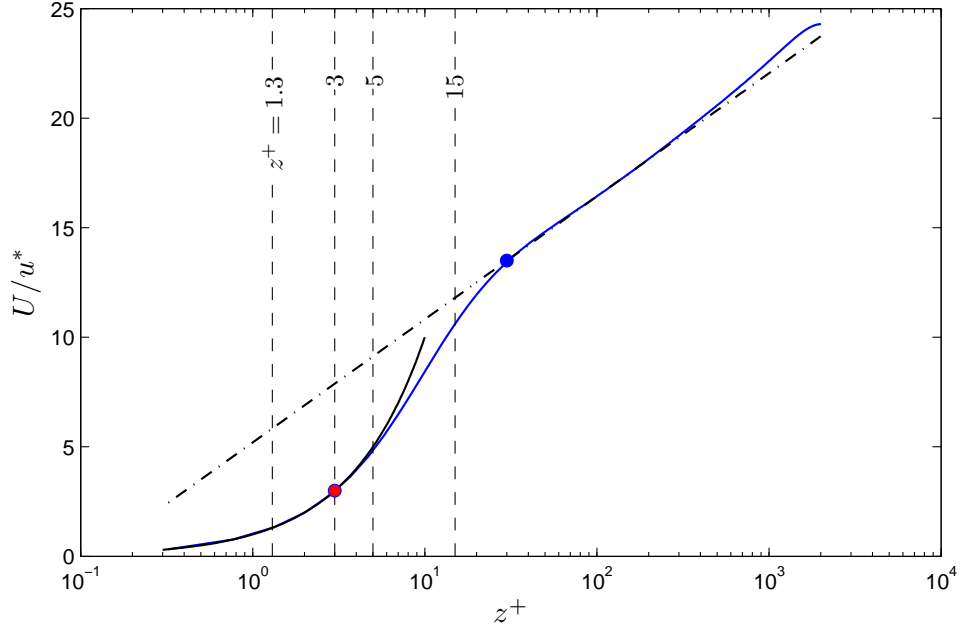


Figure A.3: Mean velocity profile from DNS of unstratified channel flow. Linear viscous law, $U = z$ (solid black line), departs from the velocity profile at $z^+ \approx 3$ (red dot). This corresponds to the first appearance of locally produced eddies as implied by $L_{kS} > L_{k\nu}$ and the beginning of shear-driven production as implied by $L_{kS} > L_{\nu S}$. The log law (dashed line) agrees with the velocity profile beginning from $z^+ \approx 30$ as expected. Data for the computations has been provided by Hoyas and Jiménez (2006). Only $Re_\tau = 2003$ case shown for clarity.

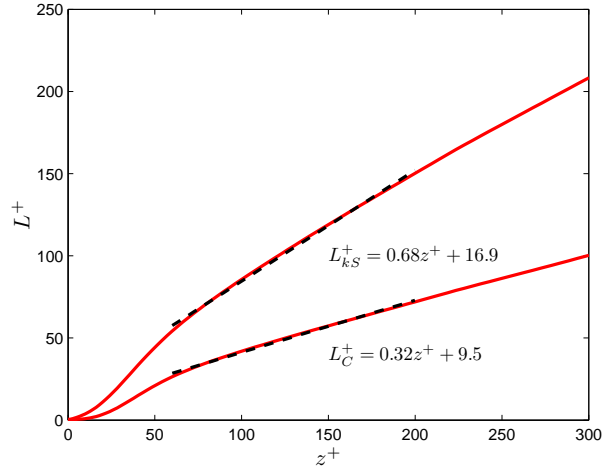


Figure A.4: Wall normal profile of the proposed largest scale, L_{kS} , and the Corrsin scale, L_C . Scale is shown to grow linearly with distance from the wall as expected of Prandtl's mixing length l_{mix} for the log-law region; however linearity does not occur until well beyond the expected start of the this region and the proportionality constant is higher than the von Karman value. Data for the computations has been provided by Hoyas and Jiménez (2006). Only $Re_\tau = 2003$ case shown for clarity.

Appendix B

Select Field Observations

B.1 IWISE M profiles (spring tidal period)

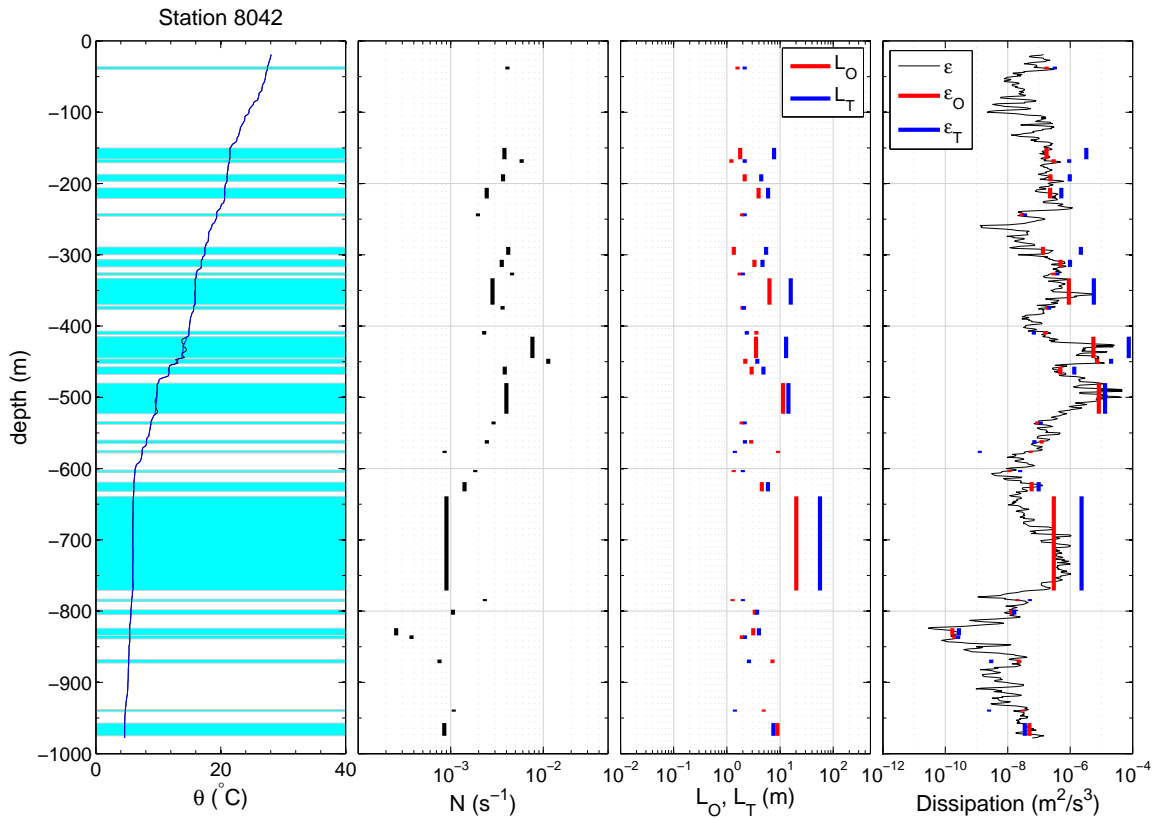


Figure B.1: IWISE profile 8042 from station M2 during the spring tidal period. Turbulent patches with $L_T \geq 1$ m are identified in the left panel. Four events with $L_T > 10$ m and $\epsilon_T > \epsilon_O$ are observed at 350 m, 425 m, 500 m and 700 m. The two most energetic events, occurring at 425 m and 500 m, are comparable in size but are occurring in different density gradients. The overturn at 425 m is associated with a larger N value, a more coherent shape (left panel), and a larger overestimation by ϵ_T . This overturn is likely younger than the less coherent weakly stratified overturn at 500 m.

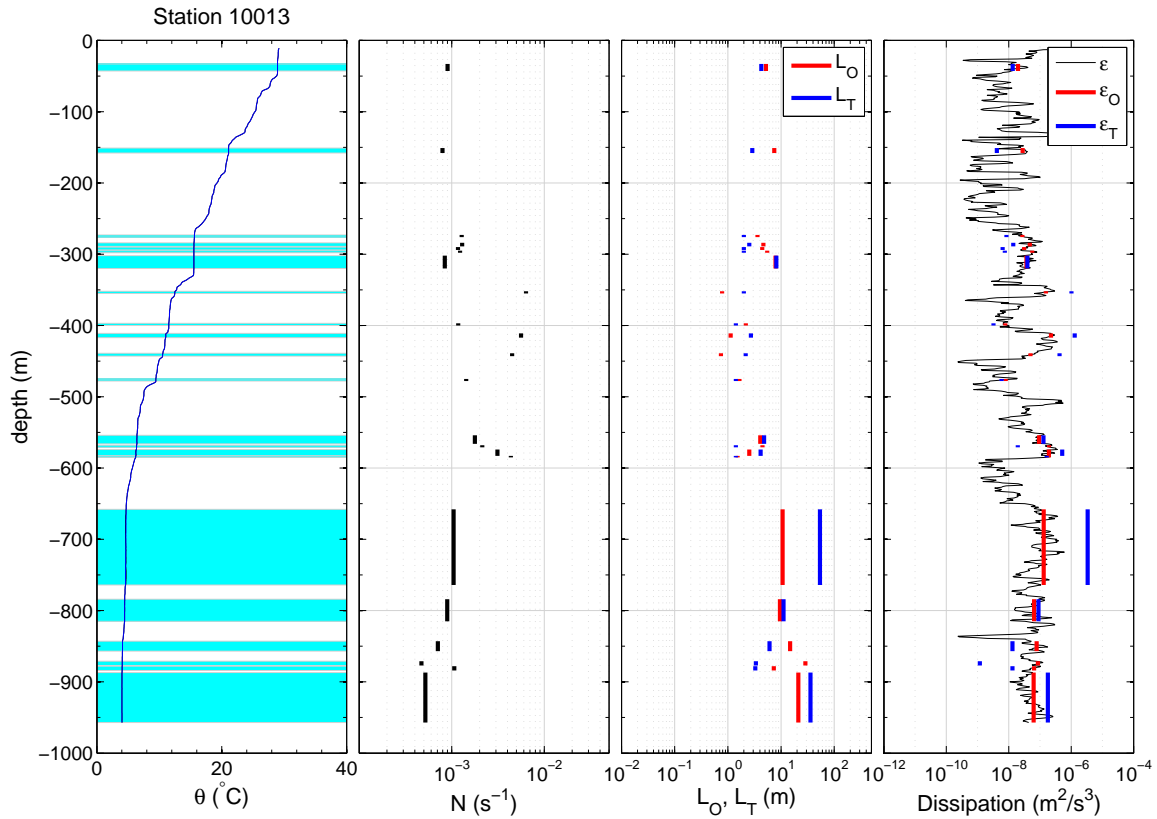


Figure B.2: IWISE profile 10013 from station M4 during the spring tidal period. Turbulent patches with $L_T \geq 1$ m are identified in the left panel. Three events with $L_T > 10$ m are observed below 600 m. $\epsilon_T > \epsilon_O$ for all three overturns, and the magnitude of overestimation is seen to be a function of patch size and L_T .

B.2 IWISE N2 profiles (spring tidal period)

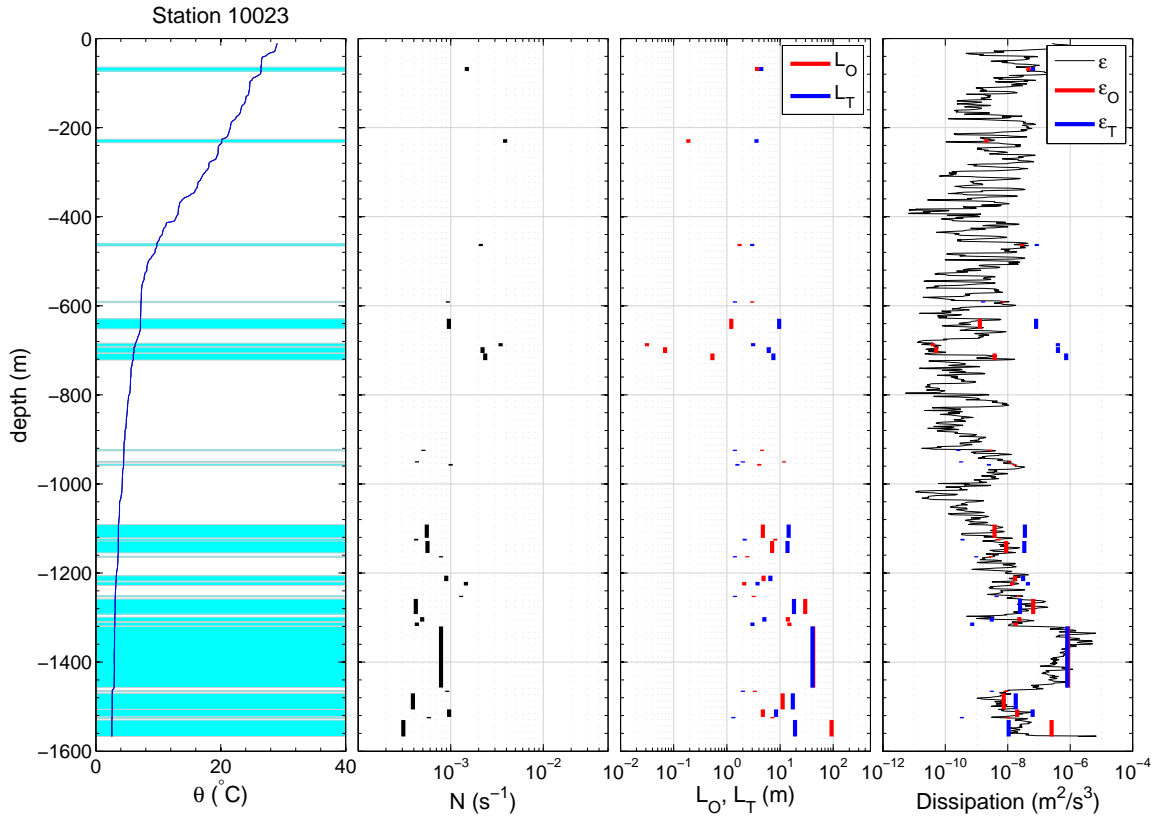


Figure B.3: IWISE profile 10023 from station N2 during the spring tidal period. Bottom enhanced turbulence is demonstrated in the right panel. A large turbulent patch demonstrating $\epsilon_T \approx \epsilon_O$ is observed at 1400m. This agreement occurs despite relatively large L_T due to intense near-bottom dissipation. This phenomena is unique to station N2 and may be the result of increased shear near the bottom.

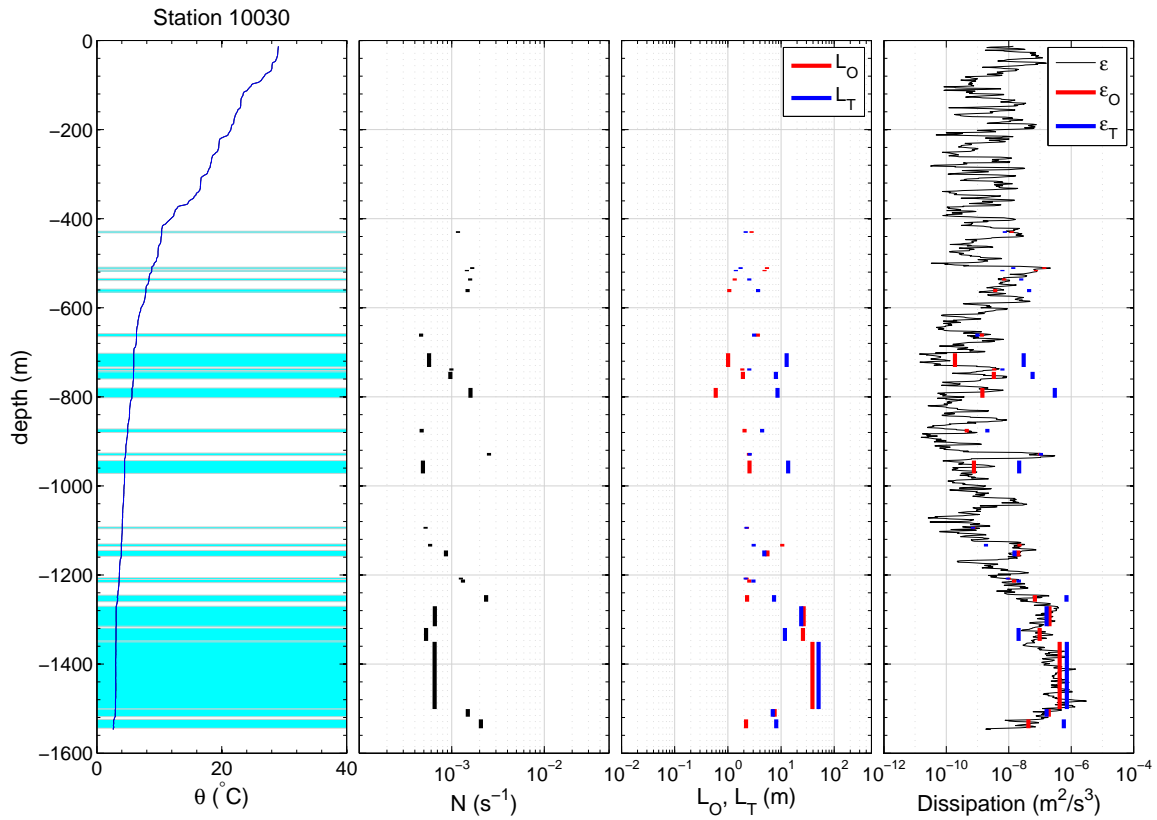


Figure B.4: IWISE profile 10030 from station N2 during the spring tidal period. As with profile 10023 from station N2 (figure B.3), dissipation is enhanced near the bottom and a large turbulent patch demonstrating $\epsilon_T \approx \epsilon_O$ is observed near 1400 m.

B.3 BBTRE profiles

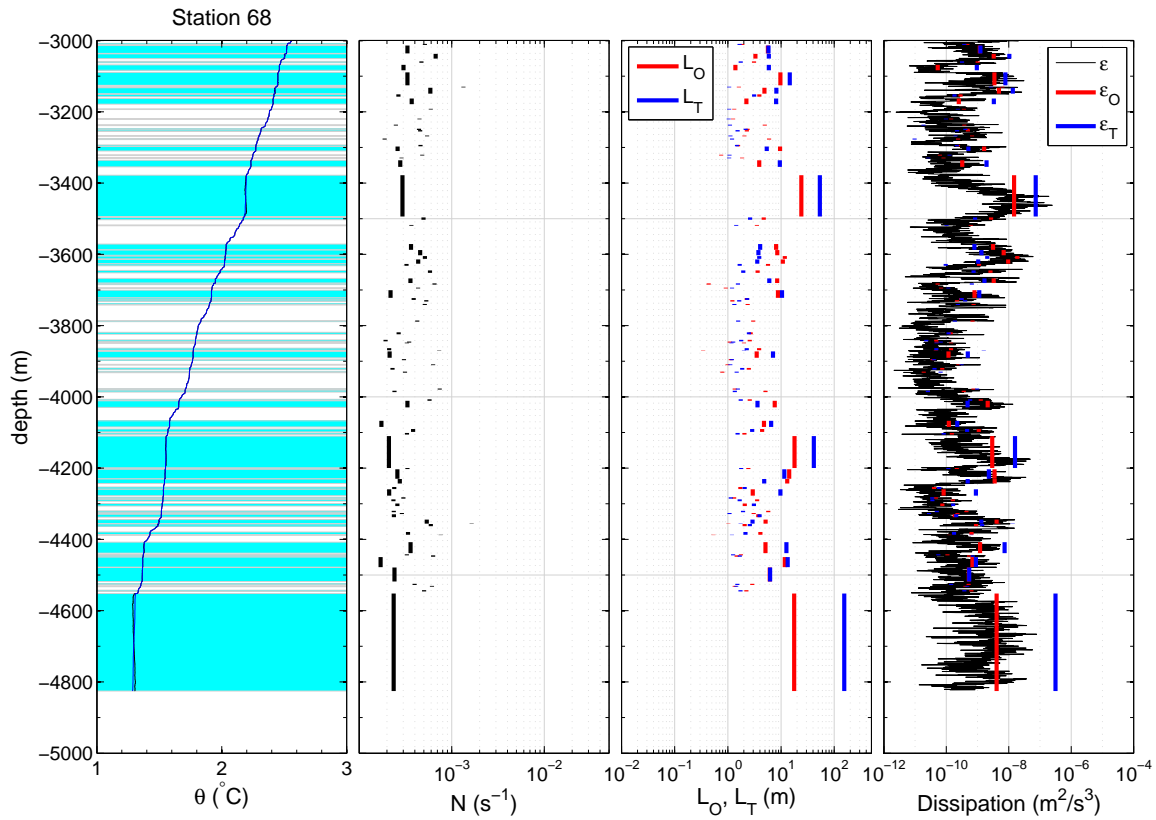


Figure B.5: BBTRE profile 68 for the lower ≈ 2000 m where the fluid is predominately temperature-stratified. Dissipation is enhanced near the bottom and a large turbulent patch demonstrating $\epsilon_T \gg \epsilon_O$ is observed near 4700 m. The patch demonstrates a the shape of a coherent overturn (see figure 8.11), thus suggesting a young overturn.

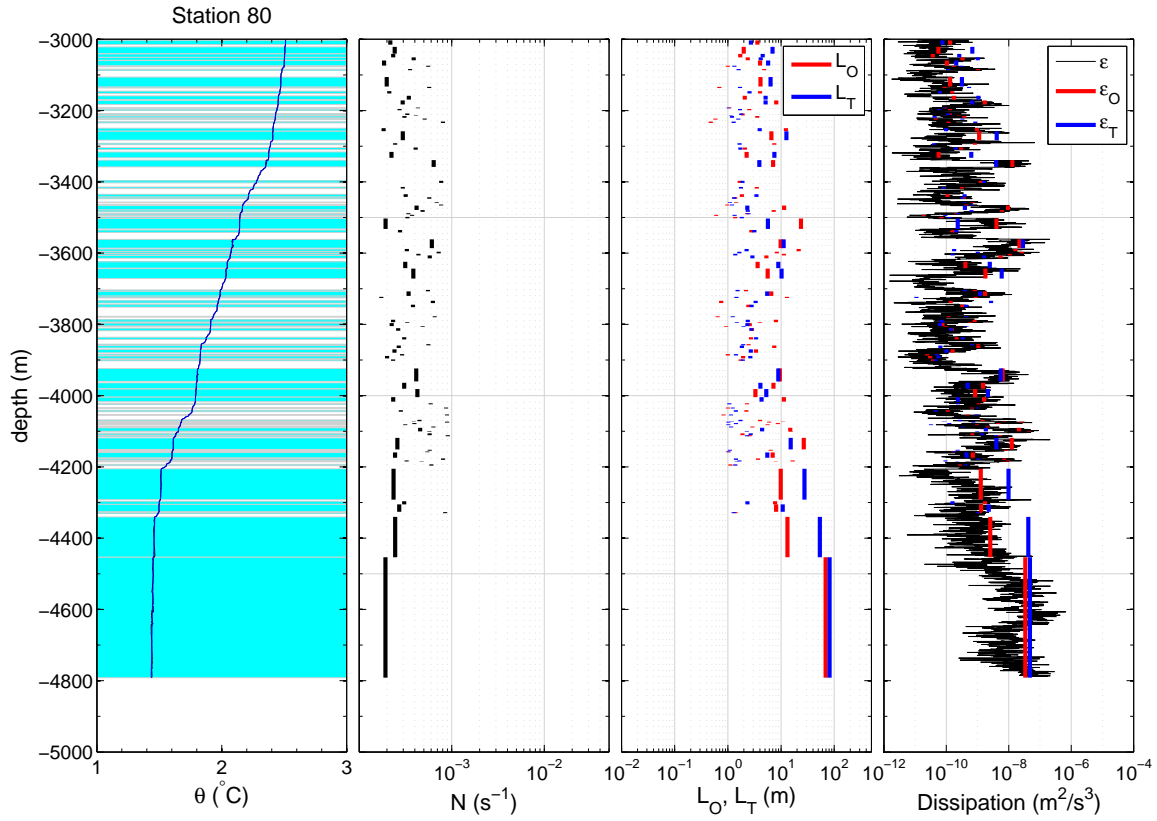


Figure B.6: BBTRE profile 80 for the lower ≈ 2000 m where the fluid is predominately temperature-stratified. Like profile 68 (see figure B.5), dissipation is enhanced near the bottom and a large turbulent patch is observed. However, unlike the near-bottom patch of profile 68, this patch demonstrates $\epsilon_T \approx \epsilon_O$ due to higher ϵ . This, along with the lack of a coherent overturn-shape (see figure 8.12), suggests the patch is more developed and older than that observed near the bottom in profile 68.

B.4 NATRE profiles

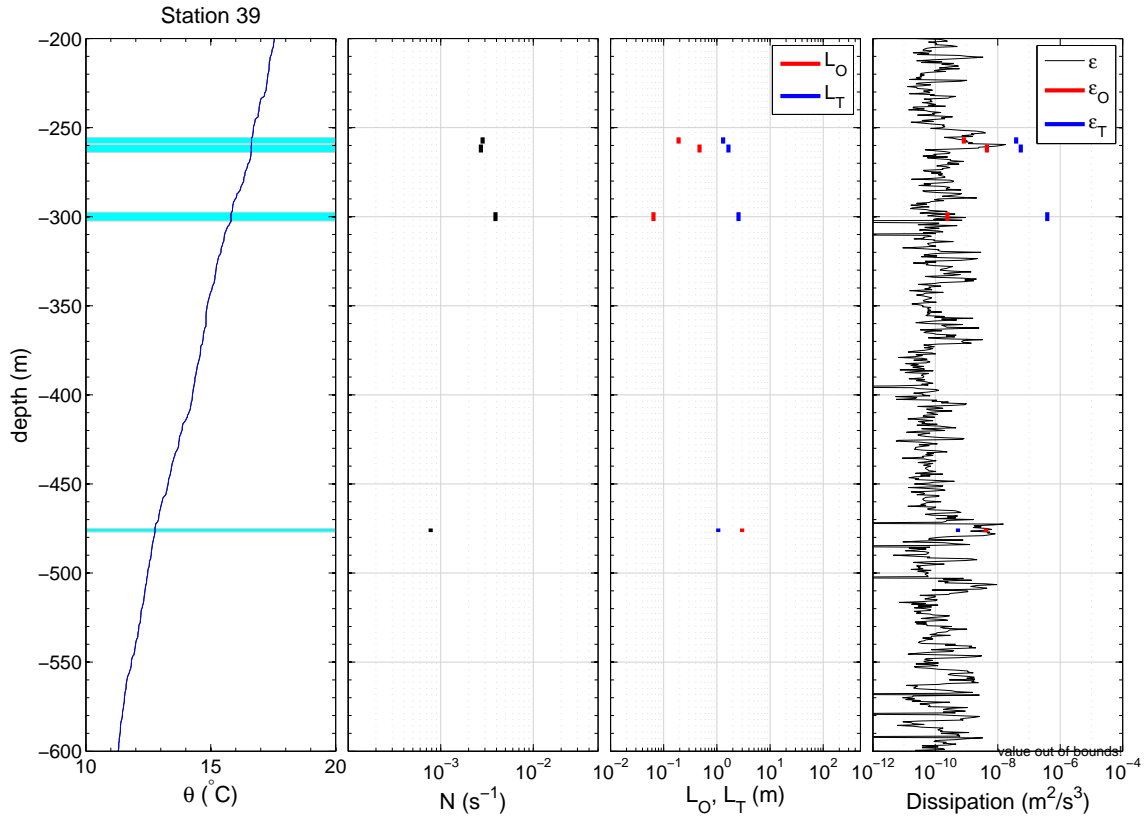


Figure B.7: NATRE profile 39 from 200 m to 600 m where salinity compensation of temperature inversions is expected to be minimal. Dissipation, overturn size, and the number of overturns are far less than for IWISE or BBTRE, while N is comparable or larger. This suggests the observed tendency for $\epsilon_T \gg \epsilon_O$ is due to strong anisotropy which is preventing the inertial transfer of energy to smaller scales from matching ϵ (i.e. violation of assumption (ii)).

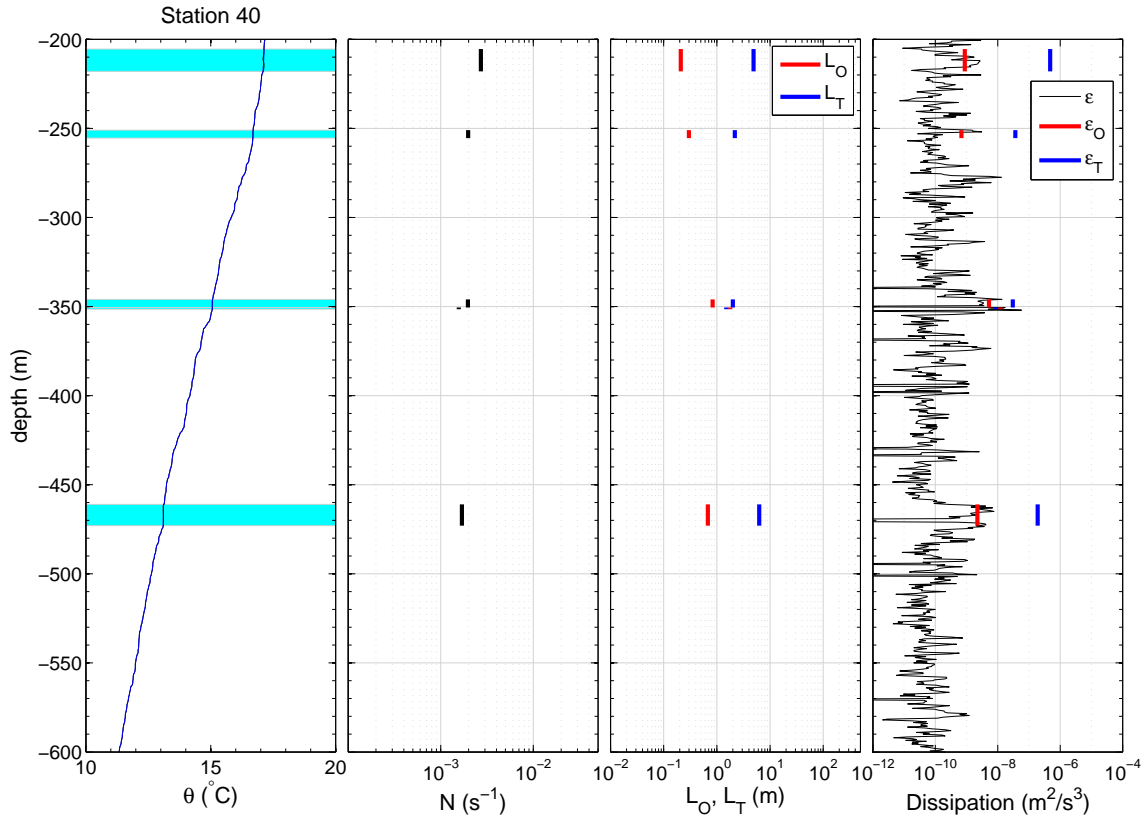


Figure B.8: NATRE profile 40 from 200 m to 600 m where salinity compensation of temperature inversions is expected to be minimal. Again, NATRE data is characteristically weakly turbulent with small and few overturns. Like the overturns in profile 39 (see figure B.7), the overturns in this profile demonstrate $\epsilon_T \gg \epsilon_O$ despite their relatively small size. These overturns fall into the strongly stratified, weakly forced regime B of figure 8.9 where overturns likely scale better with k than with ϵ due to strong anisotropy.

B.5 Additional figures

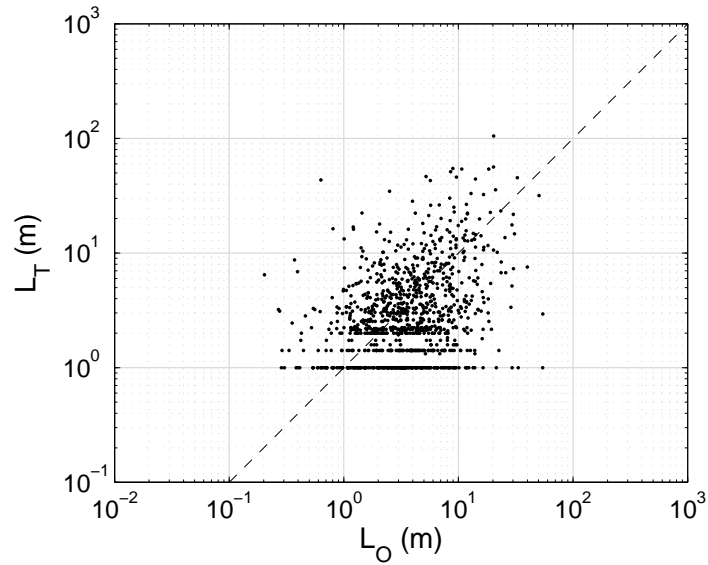


Figure B.9: Comparison of Thorpe, L_T , and Ozmidov, L_O , scales for IWISE M stations during the spring tidal period.

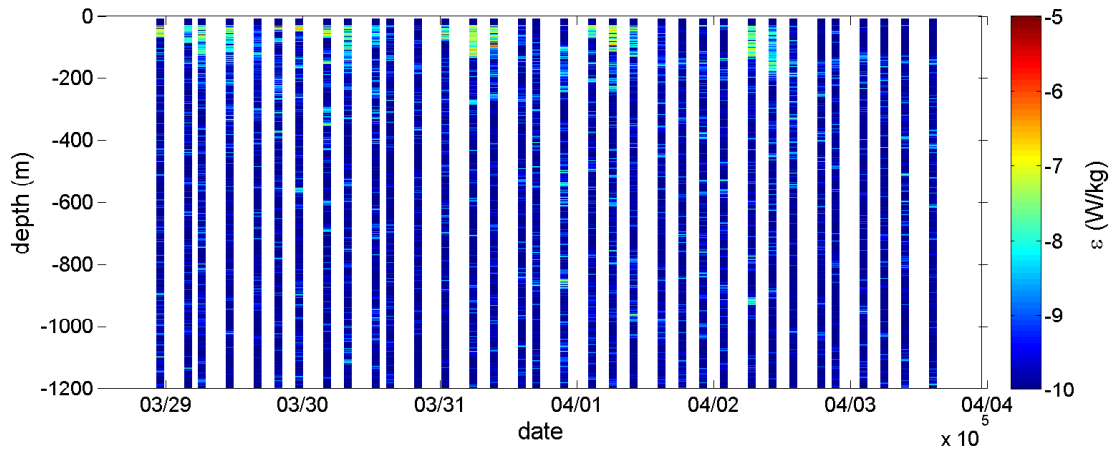


Figure B.10: Time series of dissipation rates for NATRE profiles taken near the dye injection location. Dissipation rates are more typical of those of the open ocean than the high rates observed at Luzon Strait (see figure 8.17).